UNIVERSIDADE DE LISBOA

FACULDADE DE CIÊNCIAS

Personalised Therapies for All: Targeting Alternative Chloride Channels in Cystic Fibrosis

"Documento Definitivo"

Doutoramento em Biologia

Especialidade de Biologia de Sistemas

Madalena do Carmo Fragoso Pinto

Tese orientada por:

Prof. Dr. Margarida D. Amaral e Prof. Dr. Karl Kunzelmann

Documento especialmente elaborado para a obtenção do grau de doutor

2021

UNIVERSIDADE DE LISBOA

FACULDADE DE CIÊNCIAS

Ciências
ULisboa

Personalised Therapies for All: Targeting Alternative Chloride Channels in Cystic Fibrosis

Doutoramento em Biologia

Especialidade de Biologia de Sistemas

Madalena do Carmo Fragoso Pinto

Tese orientada por:

Prof. Dr. Margarida D. Amaral e Prof. Dr. Karl Kunzelmann

Júri:
Presidente:

- Doutor Rui Manuel dos Santos Malhó, Professor Catedrático e Presidente do Departamento de Biologia Vegetal da Faculdade de Ciências da Universidade de Lisboa

Vogais:

- Doutor Henry L. Danahay, Head of Biology, Enterprise Therapeutics (Reino Unido), na qualidade de individualidade de reconhecida competência na área científica;
- Doutora Deborah Baines, Professor, St George's University of London (Reino Unido);
- Doutor Martin J. Hug, Direktor, Klinikumsapotheke da Universitäts klinikum Freiburg (Alemanha);
- Doutora Margarida Sofia Pereira Duarte Amaral, Professora Catedrática, Faculdade de Ciências da Universidade de Lisboa (orientadora)

Documento especialmente elaborado para a obtenção do grau de doutor

Fundação para a Ciência e Tecnologia do Ministério da Educação e Ciência (FCT/PD/BD/114393/2016)

2021

Madalena do Carmo Fragoso Pinto foi bolseira de doutoramento no âmbito do programa doutoral BioSys – Sistemas Biológicos, Genómica Funcional & Integrativa (FCT/PD/00065/2012) da Faculdade de Ciências da Universidade de Lisboa, financiada pela Fundação para a Ciência e Tecnologia do Ministério da Educação e Ciência, Bolsa PD/BD/114393/2016.

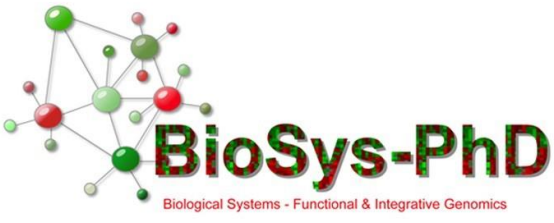

De acordo com o disposto no artigo 24º do Regulamento de Estudos de Pós-Graduação da Universidade de Lisboa, Despacho nº 7024/2017, publicado no Diário da República – 2ª Série – nº 155 – 11 de Agosto de 2017, foram utilizados nesta dissertação resultados incluídos nos seguintes artigos:

1. Lérias JR*, **Pinto MC***, Botelho HM, Awatade NT, Quaresma MC, Silva IAL, Wanitchakool P, Schreiber R, Pepperkok R, Kunzelmann K, Amaral MD. A novel microscopy-based assay identifies extended synaptotagmin-1 (ESYT1) as a positive regulator of anoctamin 1 traffic. *Biochim. Biophys. Acta - Mol. Cell Res.* **2018**, *1865*, 421–431, doi:10.1016/j.bbamcr.2017.11.009 [*Shared first authorship]

2. Lérias JR*, **Pinto MC***, Benedetto R, Schreiber R, Amaral MD, Aureli M, Kunzelmann K. Compartmentalized crosstalk of CFTR and TMEM16A (ANO1) through EPAC1 and ADCY1. *Cell. Signal.* **2018**, *44*, 10–19, doi:10.1016/j.cellsig.2018.01.008. [*Shared first authorship]

3. Benedetto R, Ousingsawat J, Cabrita I, **Pinto MC**, Lérias JR, Wanitchakool P, Schreiber R, Kunzelmann K. Plasma membrane–localized TMEM16 proteins are indispensable for expression of CFTR. *J. Mol. Med.* **2019**, 97(5):711-722, doi:10.1007/s00109-019-01770-4.

4. **Pinto MC**, Schreiber R, Lérias JR, Ousingsawat J, Duarte A, Amaral MD, Kunzelmann K. Regulation of TMEM16A by CK2 and Its Role in Cellular Proliferation. *Cells* **2020**, *9*, doi:10.3390/cells9051138.

5. **Pinto MC**, Quaresma MC, Silva IAL, Railean V, Ramalho SS, Amaral MD. Synergy in Cystic Fibrosis Therapies: Targeting SLC26A9. *Int. J. Mol. Sci.* **2021**, *22*(23), 13064, doi:10.3390/ijms222313064.

6. **Pinto MC**, Botelho HM, Silva IAL, Railean V, Neumann B, Pepperkok R, Schreiber R, Kunzelmann K, Amaral MD. Systems Approaches to Unravel Molecular Function: High-content siRNA Screen Identifies TMEM16A Traffic Regulators as Potential Drug Targets for Cystic Fibrosis. *Journal of Molecular Biology* **2022**, *434*, 167436, doi:10.1016/j.jmb.2021.167436.

7. **Pinto MC**, Botelho HM, Silva IAL, Railean V, Amaral MD. Identification of SLC26A9 traffic regulators as novel targets for Cystic Fibrosis therapies. In preparation. **2022**

Durante a realização do presente trabalho, foram também publicados ou estão em preparação os seguintes artigos, não incluídos nesta dissertação:

8. **Pinto MC***, Silva IAL*, Figueira MF, Amaral MD, Lopes-Pacheco M. Pharmacological Modulation of Ion Channels for the Treatment of Cystic Fibrosis. *J. Exp. Pharmacol.* **2021**, *13*, 693–723, doi:10.2147/JEP.S255377. [*Shared first authorship]

9. Lim SH, Snider J, Birimberg-Schwartz L, Ip W, Serralha JC, Botelho HM, Lopes-Pacheco M, **Pinto MC**, Moutaoufik MT, Zilocchi M, Laselva O, Esmaeili M, Kotlyar M, Lyakisheva A, Tang P, Vázquez LL, Akula I, Aboualizadeh F, Wong V, Grozavu I, Opacak-Bernardi T, Yao Z, Mendoza M, Babu M, Jurisica I, Gonska T, Bear C, Amaral MD, Stagljar I. CFTR Interactome Mapping Using the Mammalian Membrane Two-hybrid High-throughput Screening System. *Mol Syst Biol.* **2022**, *18*: e10629, doi:10.15252/msb.202110629.

10. Quaresma MC, Botelho HM, Pankonien I, Rodrigues CS, **Pinto MC**, Costa PR, Duarte A, Amaral MD. Exploring YAP1-centered networks linking dysfunctional CFTR to epithelial–mesenchymal transition. *Life Sci. Alliance* **2022**, 5(9):e202101326, doi.org/10.26508/lsa.202101326.

11. Botelho HM, Lopes-Pacheco M, **Pinto MC**, Silva IAL, Clarke L, Cachatra V, Neumann B, Tischer C, Moiteiro C, Kunzelmann K, Pepperkok K, Amaral MD. Functional Genomics Reveals Global Genes Rescuing F508del-CFTR Traffic and Potential Drug Targets for Cystic Fibrosis. In preparation. **2022**

No cumprimento do disposto da referida deliberação, a autora esclarece serem da sua responsabilidade, exceto quando referido o contrário, a execução das experiências que permitiram a elaboração dos resultados apresentados, assim como da interpretação e discussão dos mesmos. Os resultados obtidos por outros autores foram incluídos com a autorização dos mesmos para facilitar a compreensão dos trabalhos e estão assinalados nas respetivas figuras e metodologias.

“There is nothing noble in being superior to your fellow man; true nobility is being superior to your former self.”

- Ernest Hemingway

Acknowledgments

As these 5 years come to an end, I want to thank all the people that somehow contributed to the success of this work.

Firstly, I would like to thank my supervisors Prof. Margarida Amaral and Prof. Karl Kunzelmann, not only for allowing me to develop my research in their labs, but most importantly for all the knowledge, guidance, and support over the years.

I would also like to thank Dr. Rainer Pepperkok, the ALMF, and the Pepperkok group at EMBL, for the opportunity to work with state-of-the-art technologies, and for always being so friendly and making me feel welcome.

I would like to thank the two SRC groups (CF trust) I had the pleasure to be a part of, and, in particular, Dr. Mike Gray, for the knowledge, the shared experiences, and the possibility of presenting my work around the world.

I am truly thankful to the Kunzelmann group, Inês, Roberta, Raquel, and Ji, for making me feel at home and as part of the group. To Dr. Rainer Schreiber, Patricia, and Silvia for always being so helpful. Inês and Robi, thank you for being there for me, in the fun and the hard moments, for making my life so much easier, for your patience, your support, and most importantly, your friendship.

To the Amaral lab, and all the amazing friends I made here. Thank you for the constant scientific input, for the long talks, and for listening to my (very frequent) complaints. I especially want to thank Violeta and the incredible postdocs Hugo, Ines, Susana, Iris, and Miqueias, for all your help, advice, mentorship, and friendship.

To my dear friends and “montaditos buddies” Aires, André, Filipa, and Luís, and all my BioSys colleagues. Thank you for making these years more fun!

To Sofia C (the best lab manager in the world!) and Sofia R, I cannot stress enough how critical your friendship and support have been during this Ph.D., and especially in the last few years. To the best of the best, Margarida. For always being by my side. For being my number one fan and the first to point out my mistakes. My “oldest sister”, “thank you for being my friend”.

To my long-time friends Bárbara, Gonçalo and Mafalda, for your unconditional support and friendship.

To the best friends in the whole world, my “migos” – Catarina, Coelho, Fred, Gui, João, and Nuno – for bringing me joy, for all the incredible experiences, for motivating

me and at the same time taking my mind off work. A very special thanks to Ana, Leonor, and Silvia, you are a true blessing, and I am so lucky to have you in my life!

Finally, I would like to thank my family. Aos meus primos João e Bernardo, à Inês e à Gigi (e à nossa casa feita de palmier), e especialmente à minha mãe, ao meu pai, ao meu irmão Diogo, Ana, à pequenina Ana Leonor, e à minha irmã Marta. O vosso apoio, paciência, orgulho e amor incondicional foram uma grande motivação para atingir os meus objetivos. Por fim, ao João, a melhor pessoa que podia ter a meu lado. Isto não seria possível sem ti.

Thank you all for being part of this amazing journey. New challenges await!

Summary

Cystic Fibrosis (CF) is a life-shortening genetic disorder caused by mutations in the CF Transmembrane Conductance Regulator (*CFTR*) gene, which encodes a cAMP-regulated chloride (Cl^-) and bicarbonate (HCO_3^-) channel expressed at the apical membrane of epithelial cells. Faulty CFTR causes unbalanced salt and fluid transport, resulting in dehydrated lung secretions, enhanced mucus viscosity, and impaired mucociliary clearance, culminating in progressive obstruction of the airways. Other organs such as the intestine, reproductive tissues, and pancreas are also affected in CF.

Despite recent progress in the development of therapies targeting the root cause of the disease, several people with CF, namely the ones with rare or "unrescuable" mutations, still lack effective treatments. An alternative would be to develop "mutation-agnostic" therapies, namely through the modulation of other (non-CFTR) anion channels/transporters. The main goal of this work was to understand if and how these alternative channels can be used as therapeutic targets in CF.

TMEM16A is the major contributor to Ca^{2+}-activated Cl^- secretion in the airways and has the potential to bypass defective CFTR-dependent Cl^- secretion. Here we developed a screening platform that was used to identify novel modulators of TMEM16A trafficking and function (**Chapter 1**). We have also demonstrated an overlap between Ca^{2+} and cAMP-induced currents, implying an intimate relationship between TMEM16A and CFTR (**Chapter 2**). Furthermore, another member of the TMEM16 family, TMEM16F, was also shown to regulate CFTR trafficking and function (**Chapter 2**).

Another interesting alternative target is SLC26A9, a constitutively active Cl^- transporter. We showed that CFTR expression, function, and rescue by modulators are dependent on SLC26A9 expression levels (**Chapter 3**). Finally, we have also identified regulators of SLC26A9 trafficking, that can potentially be used as novel therapeutic targets in CF therapies (**Chapter 3**).

Taken together, our findings support a role for TMEM16A and SLC26A9 as clinically relevant disease modifiers and promising therapeutic targets to circumvent deficient Cl^- secretion in CF.

Keywords: Cystic Fibrosis; CFTR; Cystic Fibrosis Transmembrane Conductance Regulator; TMEM16A; anoctamin 1; Ca^{2+}-activated Cl^- channel; SLC26A9; solute carrier family 26, member 9; Cl^- transporter; intracellular traffic.

Resumo

A Fibrose Quística (FQ) é a doença autossómica recessiva letal mais comum na população caucasiana, com uma prevalência de 1 em cada 2500-6000 nascimentos. A FQ é causada por mutações no gene ***C****ystic* ***F****ibrosis* ***T****ransmembrane Conductance* ***R****egulator* (*CFTR*), que codifica para uma proteína regulada por AMP cíclico (cAMP) localizada na membrana apical de células epiteliais, onde transporta cloreto (Cl^-) e bicarbonato (HCO_3^-).

Entre as mais de 2100 variações genéticas conhecidas no gene *CFTR*, a mutação mais comum consiste na deleção de três pares de bases, que resulta na remoção de uma fenilalanina na posição 508 (F508del) da proteína. Esta mutação afeta o processamento da proteína que, devido a um *folding* incorreto, fica retida no retículo endoplasmático e é rapidamente enviada para degradação proteassomal. Assim sendo, a proteína CFTR não chega à membrana plasmática (MP), onde exerce a sua função de canal aniónico.

A disfunção ou ausência da CFTR na MP causa um desequilíbrio no transporte de iões e água, que resulta em secreções pulmonares desidratadas, aumento da viscosidade do muco e numa função mucociliar deficiente, que culmina na obstrução progressiva das vias respiratórias. Outros órgãos como o intestino, sistema reprodutor, e pâncreas são também afetados em pessoas com FQ.

O desenvolvimento de novas terapias para a FQ tem evoluído significativamente ao longo dos últimos anos, incluindo a terapia tripla recentemente aprovada (Kaftrio®) para pessoas que possuam pelo menos uma cópia da mutação F508del na CFTR (~80-85% das pessoas com FQ). No entanto, muitas pessoas com FQ, nomeadamente as que têm mutações raras ou grandes inserções e deleções genéticas que não são possíveis de corrigir, não dispõem ainda de terapias eficientes. Para além disso, há ainda uma grande incerteza na eficiência do tratamento a longo prazo, nem todas as pessoas com FQ respondem da mesma forma aos fármacos disponíveis, e o custo dos mesmos é muito elevado. É, portanto, fundamental encontrar novas terapias para a FQ, nomeadamente que possam ser usadas para tratar todos os pacientes, independentemente das suas mutações no gene CFTR. Uma alternativa possível é o desenvolvimento de terapias independentes da mutação da CFTR, particularmente através da modulação da atividade de outros canais/transportadores de aniões.

O principal objetivo deste trabalho foi o estudo destes canais/transportadores de aniões alternativos para compreender se e como podem ser usados como alvos terapêuticos para a FQ.

A proteína TMEM16A é a maior contribuinte para a secreção de Cl^- dependente de cálcio (Ca^{2+}) – CaCC (do inglês ***C**alcium **A**ctivated **C**l⁻ **C**hannel*) – e tem o potencial de compensar a secreção de Cl^- deficiente na FQ. A TMEM16A pertence à família de proteínas TMEM16/anoctaminas, que apenas é expressa em organismos eucariotas. Em mamíferos esta família contém 10 membros (TMEM16A-H, J e K), com sequências conservadas, particularmente na zona que forma o poro. Apesar da relação próxima entre os membros da família, estes apresentam diferentes funções que incluem transporte de iões, *scrambling* de fosfolípidos, regulação do volume celular, proliferação, apoptose, etc. Entre os vários membros, apenas a TMEM16A e a TMEM16B aparentam ser CaCCs, mas só a TMEM16A é expressa no trato respiratório. Surpreendentemente, foi reportado que a TMEM16F é necessária para o *scrambling* de fosfolípidos dependente de Ca^{2+}, facilitando o seu movimento entre os dois lados da bicamada lipídica. Esta proteína apresenta ainda a função de transporte de Cl^-. Os restantes membros da família são todos *scramblases*.

Neste trabalho estudámos o tráfego e função da TMEM16A, começando por desenvolver uma plataforma de *screening* para identificar novos reguladores de tráfego e função da mesma (**Capítulo 1**).

No entanto, os benefícios de ativar ou inibir a TMEM16A são ainda discutíveis. Estudos em pacientes com asma mostram um aumento da expressão da TMEM16A, particularmente em células secretoras de muco, após estimulação com citocinas pró-inflamatórias. Outros estudos reportam uma diminuição significativa da secreção de muco em células epiteliais pulmonares primárias quando a TMEM16A é inibida. Neste caso, inibidores da TMEM16A teriam um impacto positivo nos pacientes. Da mesma forma, pacientes com vários tipos de cancro, onde foi observada um aumento de expressão da TMEM16A, podem beneficiar de inibidores da mesma. Os nossos dados corroboram esta hipótese já que, em células cancerígenas, o *knockdown* e/ou inibição da TMEM16A, diminui a proliferação celular (**Capítulo 1**).

Pelo contrário, ratinhos que não expressam TMEM16A (TMEM16A *knockout*) apresentam sintomas semelhantes aos da FQ, como secreção de Cl^- reduzida e acumulação de muco nas vias respiratórias. Para além disto, o *knockout* de TMEM16A nos pulmões e intestino de ratinho, diminui não só as correntes de Cl^- ativadas por Ca^{2+}, mas também as correntes ativadas por cAMP, o que sugere que a presença e ativação

da TMEM16A é fundamental para a secreção de Cl^-. Ainda neste tópico, demonstrámos que, na ausência de CFTR na MP, uma porção da corrente de Cl^- ativada por cAMP se deve à TMEM16A, o que apoia a necessidade de procurar ativadores da TMEM16A para aumentar a secreção de Cl^- na FQ (**Capítulo 2**). Observámos também que, em células humanas, a ausência de TMEM16A (e também de TMEM16F) reduzem drasticamente a expressão da CFTR na MP e a sua função de secreção de Cl^- (**Capítulo 2**).

Não obstante, sem um estímulo farmacológico, a TMEM16A pode não ser suficiente para compensar a falta de secreção de aniões mediada pela CFTR na FQ, dada a pequena contribuição de CaCCs para a secreção de Cl^- no epitélio pulmonar e a sua ativação transitória, em contraste com a secreção permanente de Cl^- pela CFTR. Contudo, a TMEM16A pode ser estimulada através da regulação dos níveis dos seus interatores, idealmente também potenciando a atividade do canal sem alterar a sua expressão nem a concentração de Ca^{2+} intracelular (**Capítulo 1**).

Para além da TMEM16A, a SLC26A9 é outro potencial alvo terapêutico para a FQ. Esta proteína transporta Cl^- e é expressa em células epiteliais dos órgãos afetados na FQ, e por isso mantém a possibilidade de poder compensar pela falta de função da CFTR.

A SLC26A9 de ratinho, muito semelhante à proteína humana, forma homodímeros com N- e C-terminais citoplasmáticos e 14 domínios transmembranares. O C-terminal contém um domínio *sulfate transporter and anti-sigma factor antagonist* (STAS), responsável pela interação entre as duas subunidades do dímero.

Apesar de estar localizada predominantemente no citosol das células, foi proposta uma interação entre a SLC26A9 e a CFTR, através do domínio STAS da SLC26A9 e do domínio R da CFTR. Há ainda dados que apontam para uma interação através dos domínios PDZ de ambas.

O número de estudos da SLC26A9 no contexto da FQ aumentou recentemente devido aos seus efeitos na patologia dos órgãos afetados na FQ e em outras doenças respiratórias. A SLC26A9 atua como modificadora da função pulmonar e da resposta a terapias para a FQ. Além disso, polimorfismos no gene *SLC26A9* estão associados ao agravamento de outras complicações associadas à FQ, como obstrução intestinal e doença pancreática. A SLC26A9 contribui ainda para o transporte de Cl^- epitelial e previne a acumulação de muco em condições inflamatórias.

Neste trabalho mostrámos uma forte relação entre a função da CFTR e a expressão da SLC26A9, evidenciando ainda o papel da SLC26A9 na eficácia dos corretores da CFTR (**Capítulo 3**). Por fim, identificámos também reguladores do tráfego da SLC26A9, que podem ser utilizados como novos alvos terapêuticos na FQ (**Capítulo 3**).

Em resumo, os nossos resultados apoiam a hipótese de que canais/transportadores de Cl^- alternativos, como a TMEM16A e a SLC26A9, são modificadores relevantes da FQ, e que aumentar a expressão destes na MP, e, consequentemente, a sua função, pode compensar a secreção de Cl^- deficiente na FQ. O estudo destes canais de Cl^- pode levar à identificação de novos alvos terapêuticos não só para a FQ, mas também para outras doenças muco-obstrutivas como a asma e a doença pulmonar obstrutiva crónica (DPOC).

Palavras-chave: Anoctamina 1/TMEM16A; canal de cloreto ativado por cálcio; CFTR; Fibrose Quística; SLC26A9; transportador de cloreto; tráfego intracelular.

Table of Contents

List of figures

List of tables

List of appendices

Abbreviations

007-AM	8-pCPT-2-O-Me-cAMP
ABC	ATP-binding cassette
ADCY	Adenylyl cyclase
ADRA2C	Adrenergic receptor 2C
Ani9	(4-Chloro-2-methylphenoxy)-acetic acid [(2-methoxyphenyl) methylene]hydrazide
ANO	Anoctamin
AP2M1	Adaptor Related Protein Complex 2 Subunit μ
ASL	Airway surface liquid
ATP	Adenosine triphosphate
BFA	Brefeldin A
BHY	Human oral squamous cell carcinoma cells
bp	Base pair
BSA	Bovine serum albumin
Ca^{2+}	Calcium ion
CaCC	Calcium-activated chloride channel
CaCCinh-A01	6-(1,1-dimethylethyl)-2-[(2-furanylcarbonyl)amino]-4,5,6,7-tetrahydro-benzo[b]thiophene-3-carboxylic acid
Cal-33	Head and neck squamous carcinoma cells
cAMP	Cyclic adenosine monophosphate
CBAVD	Congenital bilateral absence of the vas deferens
CCH	Carbachol
cDNA	Complementary DNA
CF	Cystic Fibrosis
CFBE41o-/CFBE	Cystic Fibrosis bronchial epithelial cells
CFRD	CF-related diabetes
CFTR	Cystic fibrosis transmembrane conductance regulator
Cl^-	Chloride ion
CK2/CSNK2	Casein kinase 2
CO_2	Carbon dioxide
COPB1	Coatomer subunit beta

COPZ1	Coatomer subunit zeta-1
CX4945	Silmitasertib
CXCR3	Chemokine receptor 3
DAG	Diacylglycerol
DMEM	Dulbecco's Modified Eagle Medium
DMSO	Dimethylsulfoxide
Dox	Doxycycline
eGFP	Enhanced green fluorescent protein
EMT	Epithelial-mesenchymal transition
ENaC	Epithelial sodium channel
EPAC1	Exchange protein directly activated by cAMP 1
ER	Endoplasmic reticulum
ERES	Endoplasmic reticulum exit sites
ERQC	Endoplasmic reticulum quality control
ESI09	α-[(2-(3-Chlorophenyl)hydrazinylidene]-5-(1,1-dimethylethyl)-β-oxo-3-isoxazolepropanenitrile
ESYT	Extended synaptotagmin
FBS	Fetal bovine serum
Fsk	Forskolin
Gen	Genistein
GOI	Gene of interest
GPCR	G-protein coupled receptor
HA	Hemagglutinin
HCO_3^-	Bicarbonate ion
HBE	Human bronchial epithelial cells
HEK	Human embryonic kidney cells
HNE	Human nasal epithelial cells
I^-	Iodide ion
IBMX	3-isobutyl-1-methylxanthine
I/F	IBMX/Forskolin
Iono	Ionomycin
IP_3	Inositol 1,4,5-triphosphate

IP_3R	Inositol 1,4,5-triphosphate receptor
I/V	Current/voltage
K^+	Potassium ion
KD	Knockdown
kDa	KiloDalton
LLI	Liquid-liquid interface
LRRK1	Leucine Rich Repeat Kinase 1
MCC	Mucociliary clearance
$MgCl_2$	Magnesium Chloride
mRNA	Messenger ribonucleic acid
Na^+	Sodium ion
NBD	Nucleotide binding domain
NFM	Non-fat milk
Niclo	Niclosamide
NMD	Nonsense-mediated mRNA decay
P2RY2	Purinergic receptor P2Y2
PAGE	Polyacrylamide gel electrophoresis
PBS	Phosphate buffered saline
PBS-T	Phosphate buffered saline with Tween20
PCR	Polymerase chain reaction
PDE	Phosphodiesterase
PDZ	PSD-95, Disc-large, and ZO-1
PFA	Paraformaldehyde
PIP_2	Phosphatidylinositol 4,5-biphosphate
PKA	Protein kinase A
PKC	Protein kinase C
PLC	Phospholipase C
PM	Plasma membrane
PTC	Premature termination codon
PVDF	Polyvinylidene Fluoride
R domain	Regulatory domain
RNA	Ribonucleic acid

SD	Standard deviation
SDS	Sodium dodecyl sulphate
SEM	Standard error of mean
siRNA	Small interfering ribonucleic acid
SLC26	Solute carrier family 26
STAS domain	Sulfate transporter and anti-sigma factor antagonist
TBB	4,5,6,7-Tetrabromo-2-azabenzimidazole,4,5,6,7-Tetrabromobenzotriazole
TBS	Tris-buffered saline
TMEM16	Transmembrane protein 16
TRAM34/T34	1-[(2-Chlorophenyl)diphenylmethyl]-1H-pyrazole
UTP	Uridine triphosphate
% v/v	Percentage expressed in volume per volume
wt	Wild type
% w/v	Percentage expressed in weight per volume

I. Introduction

1. Cystic Fibrosis

1.1 General Introduction

Cystic Fibrosis (CF) is the most common life-shortening autosomal recessive disorder in Caucasians[1], affecting more than 90,000 individuals worldwide and almost 50,000 in Europe[2]. The frequency of CF varies among different ethnic groups, the highest being in individuals of Northern European heritage, with an incidence of 1 in every 2,500-3,000 newborns[3,4].

CF was first described as a digestive disorder in 1938[5], but it was only in 1989 that the gene responsible for CF was identified and named Cystic Fibrosis Transmembrane Conductance Regulator (CFTR)[6]. This gene encodes a cAMP-regulated chloride (Cl^-) and bicarbonate (HCO_3^-) channel expressed at the apical membrane of a variety of epithelial cells[7], and it harbours mutations in all people with CF[8]. Most people with CF develop lung disease, but other organs, such as the sweat glands, pancreas, liver, intestine, and reproductive tract, are also affected[9,10].

Heretofore, more than 2,100 CFTR genetic variants have been reported. The most frequent mutation is F508del, a single phenylalanine deletion in the first nucleotide binding domain (NBD1) of CFTR, that occurs in approximately 70% of CF alleles worldwide[11].

1.2 Pathophysiology

Although CF is a multi-organ disorder, obstructive lung disease is the primary cause of morbidity and mortality among individuals with CF[9,12]. CFTR primarily functions as an anion channel[8], but it was also shown to regulate other channels, namely to have an inhibitory effect on sodium (Na^+) absorption through the epithelial Na^+ channel (ENaC), although there is some controversy regarding the role of CFTR on ENaC hyperabsorption[13,14]. Consequently, CFTR dysfunction destabilizes the epithelial ionic and water homeostasis, leading to the dehydration of the airway surface liquid layer (ASL)[15]. As a result, mucus viscosity increases, which in turn compromises mucociliary clearance (MCC) and causes recurring bacterial infections[16] and chronic neutrophil-dominated inflammation[12,17]. A vicious cycle of mucus accumulation and clogging, bacterial infections and chronic inflammation ultimately causes epithelial destruction, tissue remodeling and fibrosis, culminating in respiratory failure[18] (Fig. 1).

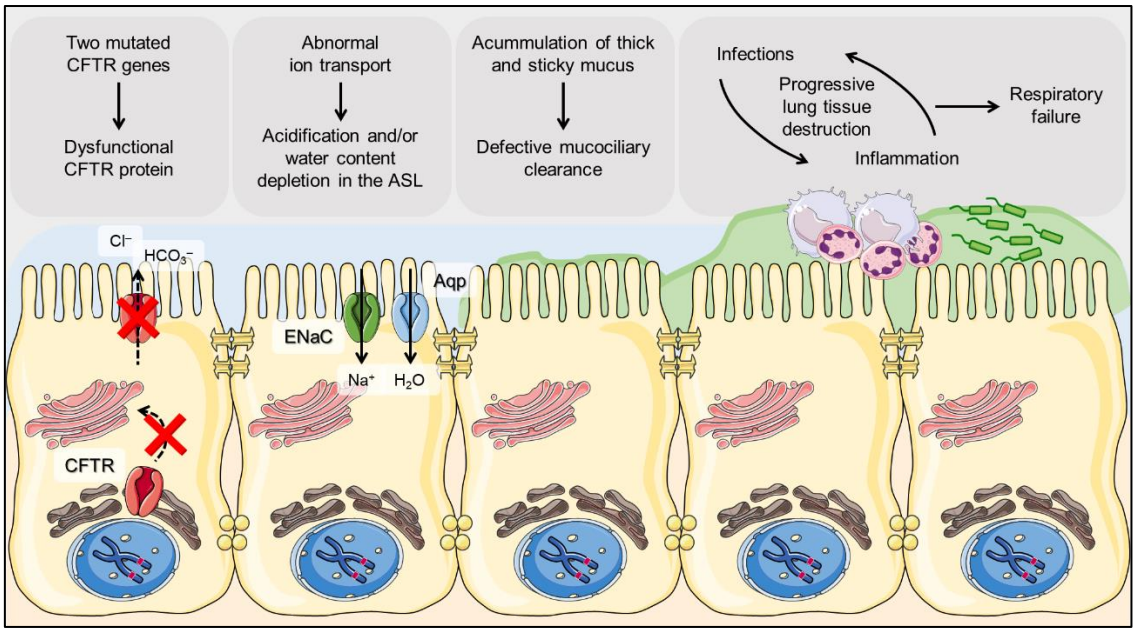

Figure 1 – Pathophysiological cascade of respiratory disease in CF. Adapted from [2,19].

Besides the above-mentioned airway complications, CFTR dysfunction also affects several other organs, including the sweat glands, thus leading to elevated Cl^- concentrations in the sweat[10]. Measurement of the sweat Cl^- levels is the most common test used for CF diagnosis, although it should also be confirmed by genetic tests[20]. Most patients with severe CF phenotypes also suffer from pancreatic insufficiency (PI) as a result of the obstruction of the pancreatic ducts and subsequent loss of exocrine function[21]. Pancreatic disease is caused by decreased/absent HCO_3^- secretion, which acts as an alkaline buffer for pancreatic fluid, providing an optimal pH for the function of digestive enzymes. The more acidic pH in the pancreatic ducts prematurely activates digestive enzymes which gradually destroy pancreas leading to its fibrosis[7,21]. In addition, CF disease may include other complications such as meconium ileus, liver disease[22], diabetes[23], and male infertility, as a consequence of congenital bilateral absence of the vas deferens (CBAVD)[10].

1.3 CFTR – Gene and mutations

The CFTR gene is located on the long arm of chromosome 7 (q31-q32 region) and consists of a highly complex TATA-less promoter and 27 exons spanning about 190 kb of genomic sequence, being one of the largest in the human genome[24].

Among the more than 2,100 CFTR genetic variants reported, only a minority (466) have been characterized for their disease liability and of these, 382 were confirmed to

be CF-causing[25]. These CFTR mutations have been grouped into 7 different functional classes, according to the molecular/cellular defect they confer. **Class I** mutations (e.g., G542X) cause a disruption in the synthesis of the CFTR protein, being nonsense mutations, i.e., introducing premature stop codons (PTCs). **Class II** mutations (e.g., G85E, N1303K) result in defective protein trafficking and processing, due to protein misfolding. The F508del mutation belongs to this class, and it is associated with a severe phenotype[26]. F508del-CFTR adopts an abnormal protein conformation which is recognized and retained by the endoplasmic reticulum (ER) quality control (ERQC) and prematurely targeted for proteasomal degradation. Consequently, only a small amount or no F508del-CFTR, depending on the cell type, reaches the plasma membrane (PM)[27]. However, when it does reach the cell surface, its function is also defective[28]. **Class III** mutations (e.g., G551D and also PM-rescued F508del-CFTR) allow for the formation and traffic of the CFTR protein to the cell surface but with no function due to impaired channel gating. **Class IV** mutations (e.g., R117H) also provide a PM-localized protein, but with a diminished conductance, leading to decreased ion transport. **Class V** mutations (e.g., A455E) result in decreased protein synthesis, most commonly due to splicing defects. Class IV and V are known as residual function mutations. **Class VI** mutations (e.g. 120del23 and also PM-recued F508del-CFTR) destabilize CFTR at the cell surface, either by increasing CFTR endocytosis or by decreasing its recycling back to the PM[10,29]. Finally, in **class VII** (e.g. dele2,3(21kb)) are those which result from large deletions or insertions and hence are considered to be “unrescuable” by pharmacological agents[12].

1.4 CFTR – Protein structure, folding and trafficking to the plasma membrane

CFTR is a transmembrane protein with 1,480 amino acid residues[6] expressed at the apical PM of epithelial cells[30]. It is a member of the ATP-binding cassette (ABC) transporter superfamily – ABCC7 – and is composed of five domains[31] (Fig. 2): two membrane-spanning domains (MSD1/TMD1 and MSD2/TMD2), with six transmembrane helices each, that anchor the protein to the PM and contribute to the formation of the selective pore; two nucleotide-binding domains (NBD1 and NBD2) that bind ATP and hydrolyse it (at least NBD2) thus regulating channel gating; and a regulatory domain (RD) that contains multiple phosphorylation sites, also relevant for regulation of channel activity[32,33]. Both the amino (N) and carboxyl (C) terminal tails of CFTR are cytosolic and mediate the interaction of CFTR with a variety of proteins[30]. The C-terminus of CFTR

contains a PDZ domain-binding motif, to which several PDZ-domain proteins have been shown to bind[34], namely Na^+/H^+ exchanger regulatory factor 1 (NHERF1)[35], responsible for its anchoring to the apical actin cytoskeleton. These interactions are involved in CFTR regulation, namely through the modulation of its trafficking, processing, stabilization at the PM and channel gating[36].

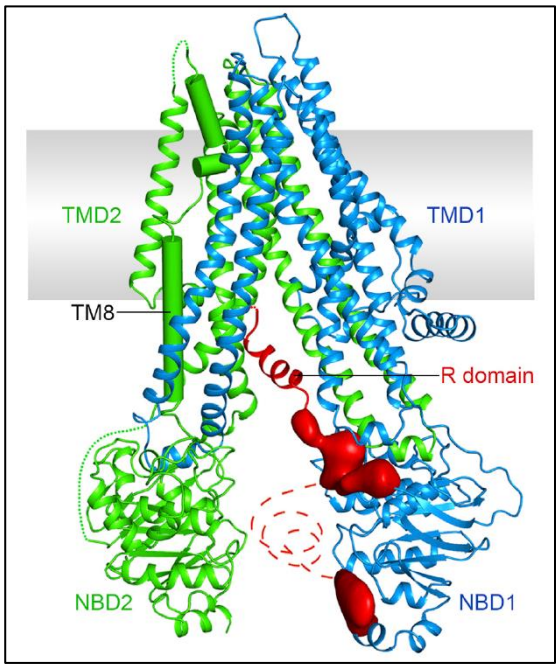

Figure 2 – Molecular structure of human CFTR in the dephosphorylated, ATP-free form[31].

CFTR assembly starts with synthesis and co-translational folding in the ER, where it is core glycosylated. Once checked for correct folding by the ERQC – a process occurring at several checkpoints and involving multiple chaperones and co-chaperones[37] – this immature form of CFTR is packed into COPII vesicles at ER exit sites (ERES) and traffics to the Golgi apparatus, where it undergoes glycoside maturation, evolving into its fully-glycosylated form[38]. Mature CFTR is then transported in vesicles from the trans-Golgi network to the apical PM[39], where its levels result from a balance between membrane delivery (anterograde trafficking), endocytosis (retrograde trafficking), and recycling[40]. Besides this so-called conventional trafficking, some membrane proteins, including CFTR[41], have been described to deviate from the classical secretion route[42], either by exiting the ER in non-COPII-vesicles or bypassing the Golgi, but this has been shown to occur mostly under non-physiological conditions[40].

1.5 CFTR function

CFTR functions mainly as a cAMP-regulated anion channel transporting Cl^- and HCO_3^- at the apical PM of epithelial cells, where it provides a pathway for anion movement across epithelia and regulates their flow[9].

Activation of the CFTR channel occurs upon its phosphorylation by protein kinase A (PKA) followed by ATP binding and hydrolysis. CFTR phosphorylation by PKA requires an increase in intracellular cyclic AMP (cAMP) by the activation of adenylate cyclase[43,44]. The CFTR channel displays a time and voltage-independent gating behavior, and an

anion over cation selectivity. Its permeability sequence is thiocyanate (SCN^-) > nitrate (NO_3^-) > bromide (Br^-) > Cl^- > iodide (I^-) > acetate ($C_2H_3O^-$), with a corresponding conductance, i.e. the rate of ion flow through the pore per unit driving force, sequence of $Cl^- > NO_3^- > Br^- > C_2H_3O^- > I^- > SCN^-$[45,46].

Besides its role as a channel, CFTR has been implicated in many other processes that include regulation of other ion channels/transporters[47], regulation of intracellular vesicle transport, acidification of intracellular organelles[48], fetal development, epithelial differentiation, regeneration, and epithelial–mesenchymal transition (EMT)[49].

1.6 Therapeutic Approaches

The classical clinical management of CF focuses mainly on alleviating the symptoms to help ameliorating a person's quality of life and slowing disease progression. Such symptomatic treatments include chest physiotherapy and mucolytic drugs to improve MCC of the thick mucus that accumulates in the airways, administration of antibiotics and anti-inflammatory drugs to treat bacterial lung infections and handle the chronic airway inflammation, respectively, and pancreatic enzyme replacement and hypercaloric diet to maintain a good nutritional status[4,50]. As the disease progresses, lung transplantation remains the last therapeutic option for people with end-stage lung disease[51].

Over the last decade, the implementation of early diagnosis and optimization of these classical therapeutic regimens has substantially enhanced life expectancy of individuals with CF. Indeed, the median predicted age of survival in the US has increased to 44 years in 2018[26]. However, as more individuals with CF reach adulthood, many late-onset health complications have become increasingly common such as CF-related diabetes (CFRD), liver disease, distal intestinal obstruction syndrome, osteoporosis, and cancer[49,52]. Additionally, both the physical and psychological burdens as well as the financial costs of CF therapeutics are still very high[53], and quality of life and life expectancy of most people with CF are still limited. There is, therefore, a strong need to develop novel and more effective treatments to correct the basic defect of the disease[54].

Recently, treatment strategies targeting CFTR itself and rescuing specific CFTR mutations and/or classes of mutations have emerged. For class I mutations, read-through agents (such as aminoglycoside antibiotics[55], like G418 and gentamycin[56], or Ataluren, also known as PTC-124) that can overturn premature termination codons (PTC), and/or inhibit nonsense-mediated mRNA decay (NMD) have been used to restore

mRNA levels. These, however, are not in current clinical use as they have not demonstrated significant efficiency.

Additional CFTR-modulator therapies include potentiators, correctors, amplifiers, and stabilizers. Potentiators (e.g., Ivacaftor/VX-770) improve channel gating by increasing its open probability, and are used to correct class III/IV mutations[57,58]. CFTR correctors improve the trafficking to the PM (and processing) of mutant CFTR (class II mutations). Clinically approved correctors include Lumacaftor/VX-809, Tezacaftor/VX-661 and Elexacaftor/VX-445[59]. The first two correctors are used in combination with the potentiator VX-770 (Orkambi® – VX-809 + VX-770; Symkevi® – VX-661 + VX-770) in individuals who have two copies of the F508del mutation[59,60]. The latter is also approved for individuals with only a copy of the F508del mutation and a residual function mutation in the second allele. Recently, VX-445 was approved in a triple combination with VX-661 and VX-770 (Kaftrio®) for people over 12 years old carrying at least one copy of the F508del mutation, which represents around 80% of all people with CF worldwide[61,62]. There are several other potentiators and correctors under experimental and early-stage clinical investigation. Amplifiers (e.g., PTI-428) enhance CFTR protein expression and are useful to treat mutations that lead to decreased CFTR synthesis (class V). Actually, these compounds can help rescuing all CFTR mutations, as they increase the amount of CFTR protein synthesis and may be used in combination with correctors and/or potentiators[63]. Additionally, antisense oligonucleotides that correct splicing defects have been successfully used in vitro to rescue class V mutants[64]. Lastly, stabilizers (e.g., cavosonstat[65]) increase the residence time of CFTR at the PM and/or decrease protein degradation and are used for class VI and corrected class II mutants[66].

Nevertheless, not all mutants belonging to the same functional class are equally responsive to the same therapeutic molecule. Additionally, the above-mentioned CF therapies cannot be applied to pharmacologically rescue all CFTR mutations. Indeed, there are mutations, e.g., large deletions such as dele2,3(21kb), or frameshift mutations, which are pharmacologically ‘unrescuable’ (class VII)[12]. For individuals with these mutations, the potential alternative therapeutic strategies include gene therapy, such as DNA or RNA delivery, CFTR gene/mRNA editing[66,67], or the activation of alternative (non-CFTR) anion channels[27].

2. Alternative (non-CFTR) Channels as Targets for CF Therapy

2.1 TMEM16 proteins

a. Protein Family Overview

TMEM16 proteins, also known as anoctamins, belong to a family of 10 different proteins (TMEM16A-H, J and K or ANO1-10), with some of its members reported to be Cl^- channels. For this reason, proteins in this family, particularly TMEM16A and TMEM16F given their expression in the lungs, have raised interest as possible alternative channels that can restore epithelial anion secretion in CF.

The TMEM16 protein family is only expressed in eukaryotic organisms, and its members show high sequence conservation, particularly around the putative pore forming region[68,69]. Despite their close sequence and topological homology, the proteins of this family play a variety of physiological functions including ion transport, phospholipid scrambling, cell volume regulation, proliferation, smooth muscle contraction, olfaction, phototransduction, nociception, and control of neuronal excitability[70–72]. TMEM16A and TMEM16B have been reported to be calcium (Ca^{2+})-activated Cl^- channels (CaCC)[73–76], but only TMEM16A is expressed in the respiratory tract[68]. Surprisingly, TMEM16F was found to be essential for Ca^{2+}-dependent phospholipid scrambling[77], facilitating the movement of phospholipids between the two leaflets of the membrane bilayer. TMEM16F was also suggested to be an anion channel[78], and a non-selective cation channel[79]. Subsequently, most TMEM16 paralogs (TMEM16C-G and J) were described as Ca^{2+}-dependent phospholipid scramblases[72], which suggests that the few family members working as ion channels may have evolved from an ancestral scramblase[80].

b. TMEM16A/F structure and function

The X-ray structure of a TMEM16 homologue from the fungus *Nectria haematococca* (nhTMEM16) was the first high-resolution structure of a TMEM16 family member[69]. The structure of nhTMEM16 reveals that it is a dimeric protein with ten transmembrane helices per subunit that functions primarily as a phospholipid scramblase. Both N- and C-termini are located on the cytoplasmic side of the PM. The structure contains two regions that are predicted to be in contact with the membrane: the dimer cavity, at the dimer interface, which is mostly composed of hydrophobic and aromatic residues conserved within the protein family; and the subunit cavity, a hydrophilic membrane-spanning crevice contained within each subunit, which is linked

to Ca^{2+} binding and activation. The hydrophilic environment, the size and the membrane accessibility of the subunit cavity suggest that this might be the place for phospholipid movement across the bilayer[69].

Recent studies have presented several cryo-electron microscopy (cryo-EM) structures of murine TMEM16 (mTMEM16A), revealing a strong similarity between its general architecture and the one reported for nhTMEM16[69,81]. Murine (m)TMEM16A also shows a homodimeric structure, with each subunit containing ten membrane-spanning helices and cytosolic N- and C- terminal domains (Fig. 3A). Moreover, two Ca^{2+} ions were identified at equivalent locations to those in nhTMEM16 (helices α6–α8)[81]. The most striking differences appear on the pore region of TMEM16A, that is formed by helices α3–α8 within each subunit[82]. These transmembrane helices are noticeably displaced from the positions of the equivalent ones in nhTMEM16A[83]. These differences illustrate how TMEM16 proteins use a similar architecture to play distinct functions: in mTMEM16A, the conformation rearrangements of helices result in occlusion of the hydrophilic subunit cavity, while opening an aqueous membrane-shielded ion conduction pore that might be partly accessible to lipids on its intracellular side[82]. The most pronounced conformational changes occur in helix α6[84] (Fig. 3B,C), which is in a relaxed state when the channel is closed. The binding of Ca^{2+} ions to four acidic residues on α7 and α8 helices creates a positive charge density that attracts residues on α6, changing its conformation and leading to the opening of the channel[81]. Additionally, TMEM16A appears to have a PDZ-interacting motif present at the C-terminus, which mediates interactions with other proteins, possibly including CFTR[85].

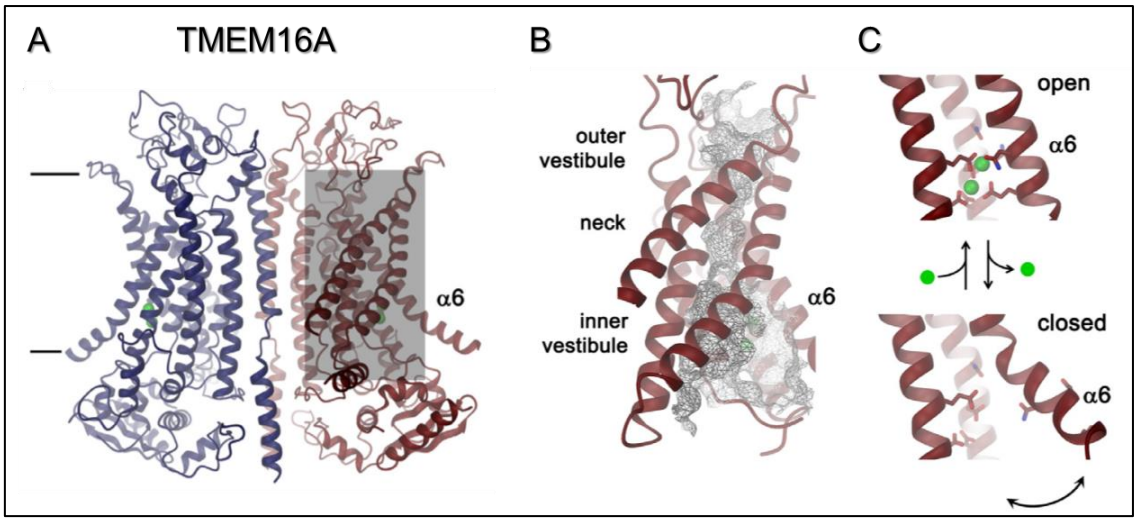

Figure 3 – Ribbon representation of TMEM16A. (A) The dimeric structure of TMEM16A. Region containing the ion conduction pore in one of the subunits is highlighted as a grey box. **(B)** Close up of the anion permeation pore. The molecular surface of the pore is shown as grey mesh. **(C)** Conformational

changes upon Ca^{2+}-binding (Ca^{2+} ions shown as green spheres) to a site within the transmembrane domain. Top, Ca^{2+}-bound open conformation; bottom, Ca^{2+}-free closed conformation, with movements of α6 indicated by the arrow. Adapted from[86].

The structure of TMEM16F, with respect to phylogenetic relationships, appears to be an intermediate between the structure of nhTMEM16 and mTMEM16A, being closer related to the latter[87] (Fig. 4). However, only one Ca^{2+} ion was identified in the structure of Ca^{2+}-bound TMEM16F. Binding of the Ca^{2+} ion not only induces conformational changes in helix α6 (Fig. 4B), but also facilitates the binding of lipids to the transmembrane loops TM9-TM10 (Fig. 4C,D). The funnel-shaped channel pore of TMEM16F opens towards the cytoplasmic side and is surrounded by helices α3-α7. In the presence of Ca^{2+} and phosphatidylinositol (4,5)-bisphosphate (PIP_2), TMEM16F adopts conformational changes that widen the funnel opening and cause membrane distortion, therefore facilitating lipid scrambling, while maintaining an intact ion permeation pore[88].

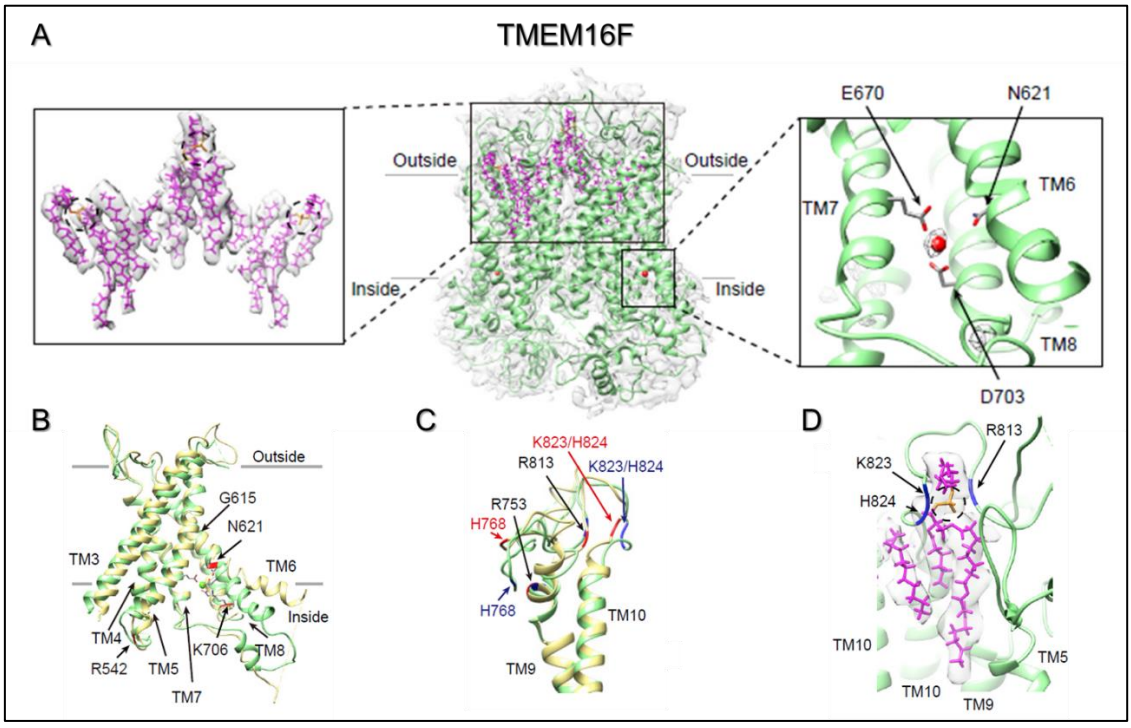

Figure 4 – Ribbon representation of TMEM16F. (A) Ca^{2+}-bound TMEM16F in digitonin (model in green, overlaid on the electron density map in light grey), showing associated lipids (magenta) and one Ca^{2+} ion (red sphere) in each monomer. **(B)** Superimposition of ribbon diagrams of Ca^{2+}-bound (green) and Ca^{2+}-free (yellow) TMEM16F in digitonin, showing a bend of TM6 in the Ca^{2+}-bound form. **(C)** Superimposition of ribbon diagrams of Ca^{2+}-bound and Ca^{2+}-free TMEM16F in digitonin, showing different conformations of TM9-TM10 loop. **(D)** A lipid with its headgroup bound to TM9-TM10 loop of Ca^{2+}-bound TMEM16F. Adapted from[88].

The Ca^{2+}-activated Cl^- channel TMEM16A is expressed in various epithelia, namely in the airways, large intestine, salivary gland, pancreatic gland, and hepatocytes[70]. Additionally, it is expressed in the nervous system[89,90], smooth muscles[91], and tumour cells[92]. Such a broad tissue expression justifies its multiple physiological roles, that include airway and exocrine gland secretion, smooth muscle contraction, neuronal signalling control and regulation of movements of the gastrointestinal system[93].

TMEM16A is activated by extracellular ATP or UTP through stimulation of purinergic (P2Y) receptors and generation of inositol 1,4,5-trisphosphate (IP_3) by phospholipase C (PLC), which leads to Ca^{2+} release from ER stores (Fig. 5)[73]. The TMEM16A channel shows a Ca^{2+} and voltage-dependent activation, with an anion selectivity sequence of $SCN^- > I^- > NO_3^- > Br^- > Cl^- > HCO_3^-$ [94]. TMEM16A channels are also characterized by a time-dependent current decay, also called “rundown” or “desensitization”, after prolonged Ca^{2+}-dependent activation. Although not completely understood, this process is believed to be regulated by PIP_2 [95]. Indeed, PIP_2 binds to a putative binding site located close to the cytosolic interface of helices α3-5, and stabilizes the open pore conformation of TMEM16A[95,96].

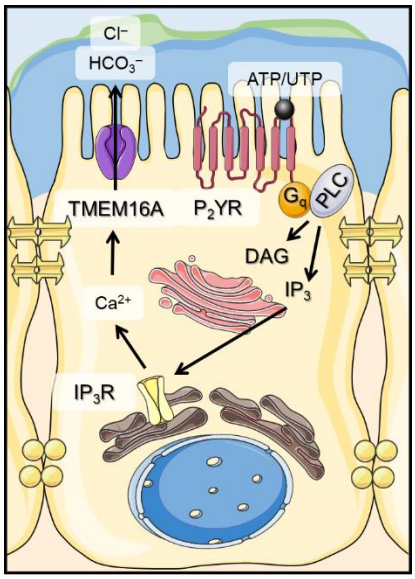

Figure 5 – P2Y receptor-mediated activation of TMEM16A[73].

TMEM16F is expressed ubiquitously and functions mostly as a Ca^{2+}-dependent phospholipid scramblase. It has an essential role on the exposure of phosphatidylserine (PS) on the cell surface, a process required for blood coagulation[77]. Additionally, TMEM16F has been characterized as a small-conductance Ca^{2+}-activated nonselective cation channel[79] and as a component of outwardly rectifying Cl^- channels (ORCCs)[97] being activated by Ca^{2+} [78]. Interestingly, TMEM16F is the only lipid scramblase for which rapidly activated Ca^{2+}-dependent currents were recorded in excised patches[79,87]. The Ca^{2+}-influx mediated by TMEM16F may constitute positive feedback to facilitate phospholipid scrambling[72], with potential deleterious effects, including Ca^{2+}-overloading and cytotoxicity, if not regulated. To prevent this negative outcome, TMEM16F gating is regulated by PIP_2. As observed for TMEM16A, at low Ca^{2+}, membrane voltage and PIP_2 stabilize Ca^{2+} binding and channel activation. Depletion of PIP_2 caused by elevated cytoplasmic Ca^{2+} or PIP_2 hydrolysis triggers TMEM16F channel rundown and desensitization[98].

c. TMEM16A/F in Cystic Fibrosis

Both TMEM16A and TMEM16F are expressed at the cell surface of airway epithelial cells[71,99], which makes them interesting targets for CF therapies, given their putative role in Cl^- secretion.

Not much is known about the possible role of TMEM16F in the lungs and its interaction with CFTR. However, due to its main role as a phospholipid scramblase, it is unlikely that it can be used as a therapeutic target in CF. In what concerns TMEM16A however, there is an ongoing debate on whether it should be activated or inhibited in the context of CF.

Excessive airway mucus is a problem in CF, chronic obstructive pulmonary disease (COPD), and asthma. TMEM16A has been associated with goblet cell metaplasia, as its expression is strongly upregulated concomitantly with mucus hypersecretion[100,101]. Additionally, during inflammation, TMEM16A expression is increased namely by Th2 interleukins (IL-4 and IL-13), particularly in mucus producing cells, with only little expression in ciliated cells[102]. A number of studies have shown that inhibition of TMEM16A occurs concomitantly with decreased mucus secretion in primary human airway surface epithelial cells[91] and also in intestinal cells[101], thus proposing a causal relationship between the two events. It has thus been argued that TMEM16A inhibition, rather than activation, may have a beneficial effect by blocking mucus release from goblet cells[91], thereby preventing mucus hypersecretion in asthma and CF. In parallel, activation of TMEM16A in airway smooth muscles results in membrane depolarization causing muscular contraction and potentially bronchoconstriction[91]. Thus, blocking TMEM16A may induce bronchodilation, which should be beneficial in airway inflammatory diseases[103]. Notwithstanding, the use of bronchodilators has not shown any benefits in individuals with CF[104].

In contrast, other reports showed that TMEM16A knockout (KO) mice present symptoms resembling those of CF, like low Cl^- secretion, accumulation of mucus in the airways and abnormal MCC[105–107]. Genetic inactivation of TMEM16A in mice also compromises airway barrier function, results in early signs of inflammation, and alters the airway cellular landscape by depleting epithelial cell progenitors[107]. Additionally, tissue specific KO of TMEM16A in mouse intestine and airways not only eliminates Ca^{2+}-activated Cl^- currents, but also abrogates CFTR-mediated Cl^- secretion[85]. Likewise, in human cells, the absence of TMEM16A dramatically reduces wt-CFTR PM expression and function[85]. Interestingly, recent studies show that inhibition of TMEM16A decreases ASL height in vitro, therefore causing airway dehydration by reducing fluid secretion[108].

A TMEM16A potentiator (ETX001, Enterprise Therapeutics), was shown to increase anion secretion and ASL height in primary human bronchial epithelial cells from individuals with CF, and promoted MCC in in vivo sheep models[109].

In summary, activators of TMEM16A could potentially be useful to treat CF lung disease by compensating for the absence of functional CFTR through improvement of fluid secretion and MCC. Such an approach could be beneficial for all individuals with CF regardless of their CFTR genotype. Without a pharmacological stimulus however, TMEM16A may not be able to compensate for the defective CFTR in CF due to the small contribution of CaCCs to airway Cl^- secretion, and their Ca^{2+}-mediated transient activation, in contrast to the permanent CFTR-dependent Cl^- secretion[110]. Additionally, this strategy would need to be carefully designed to avoid possible undesired effects such as bronchoconstriction. Further studies are needed to clarify the consequences of TMEM16A modulation[111].

d. TMEM16A/F and other disorders

Mutations in the TMEM16F gene lead to Scott syndrome, a rare congenital bleeding disorder characterized by a defective platelet procoagulant activity[77,112]. In the absence of functional TMEM16F-mediated phospholipid scrambling activity, platelets and other blood cells fail to expose PS in response to Ca^{2+}-mobilizing agonists or Ca^{2+} ionophores, and coagulation factors are no longer activated[113].

Regarding TMEM16A, besides its involvement in respiratory disorders, such as asthma and CF, it has also been linked to other diseases. For instance, TMEM16A dysfunction causes multiple defects in epithelial organs. TMEM16A KO mice die early and exhibit severe tracheal cartilage malformations[114], curiously as also described in human babies, mice, rats and pigs with CF[115–118]. Patients with a loss-of-function TMEM16A gene variant present impaired intestinal motility, distended abdomen, dysmorphic features, failure to thrive and potentially fatal course in early infancy[119].

Conversely, aberrant upregulation of TMEM16A has been found in various types of cancers, including gastro-intestinal squamous cancer[120], head and neck squamous cell carcinoma[121], breast cancer[122], and lung cancer[123], and it is generally linked with a poor prognosis[124]. Inhibition of TMEM16A can thus block proliferation, migration, and invasion of cancer cells, and also increase the sensitivity to chemotherapy[92]. TMEM16A overexpression may be explained by the localization of TMEM16A gene within the 11q13 amplicon[125], a chromosomal locus that is frequently amplified in cancer[126]. Furthermore,

TMEM16A levels in cancer cells could be modulated via transcriptional and epigenetic regulation, and microRNAs. Another possible explanation is that TMEM16A upregulation simply occurs under conditions that also stimulate cell proliferation[108,127].

In fact, TMEM16A upregulation in many cancers has led others to postulate that it plays a role in cancer cells, although the mechanism for its contribution to tumorigenesis is still unclear. Multiple studies suggest that both the protein expression, namely through protein-protein interactions and TMEM16A involvement in various signalling pathways, and the ion conduction of TMEM16A may contribute to its pro-oncogenic functions[92]. Recent findings propose that TMEM16A plays distinct roles in different cancer cells via a cell-type specific mechanism[127].

Owing to its importance in physiology and pathology, as well as to its therapeutic potential, there is an urgent need to improve our understanding of how TMEM16A contributes to human disease, and to better define drugs and conditions for using TMEM16A as a therapeutic target.

2.2 SLC26 transporters

a. Protein Family Overview

The SLC26 family of multifunctional anion transporters is composed of 11 members in humans (SLC26A1-A11, A10 likely being a pseudogene), capable of transporting, with different affinities, Cl^-, I^-, sulfate (SO_4^{2-}), HCO_3^-, hydroxyl (OH^-), oxalate ($C_2O_4^{2-}$) and formate (CHO_2^-) anions[128,129]. SLC26 exchangers are a part of the large sulfate permease (SulP) family, with homologs in bacteria, plants, fungi, and other animals[128].

The core structure of these proteins appears to be conserved among family members as well as different species[130]. The crystal structure of SLC26Dg, a prokaryotic ortholog from *Deinococcus geothermalis*, suggests that SLC26 proteins have 14 transmembrane segments, with cytoplasmic N- and C- termini[131]. Additionally, these proteins are composed of a membrane-inserted transport domain and a C-terminal cytoplasmic STAS (sulfate transporter and anti-sigma factor antagonist) domain, relevant for intracellular trafficking and protein–protein interactions[131,132].

Mutations and/or changes in expression levels of SLC26 family members have been associated with several disorders, such as diastrophic dysplasia (SLC26A2)[133],

congenital chloride diarrhea and human colon adenomas and adenocarcinomas (SLC26A3)[134], Pendred's syndrome, an autosomal recessive disorder characterized by hearing loss and goiter (SLC26A4)[135], and male infertility (SLC26A8)[130]. Additionally, SLC26A9 polymorphisms are associated with asthma, as well as with enhanced incidence of meconium ileus and diabetes in individuals with CF[136–138]. Finally, dysfunctional SLC26A11 has been associated with cytotoxic brain edema[139].

Among the SLC26 family members, SLC26A9 stands out as an interesting candidate for the CFTR "bypass" therapeutic approach. SLC26A9 is predominantly expressed in epithelial cells of the respiratory tract, stomach, duodenum, ileum, and the pancreas[133,140], thus holding the promise of compensating for the absence of functional CFTR through non-CFTR pharmacological therapies.

b. SLC26A9 structure and function

High-resolution structure of murine SLC26A9, highly similar to the human homolog, has shown that it forms homodimers with cytoplasmic N- and C-termini, and 7+7 membrane-inserted α-helices in an inverted repeat architecture[141,142] (Fig. 6A). Each transmembrane domain is arranged into two subdomains: a core module that holds the anion-binding site, and a gate module that shields one side of the core domain (Fig. 6B). This shielded side is mostly hydrophobic and contains very few charged residues that surround the anion-binding site[132,142] (Fig. 6C,D). SLC26A9 operates via ascending and descending rigid-body movements of the core module with respect to the immobilized gate module[141]. The C-terminal cytoplasmic region includes a STAS domain[130] important for interactions between the two subunits of the homodimeric SLC26A9, and for protein-protein interactions[141]. Additionally, some reports suggest that SLC26A9 has a type-I PDZ-binding domain at its C-terminus, which is thought to mediate the interaction between SLC26A9 and other proteins, facilitating trafficking and promoting stabilization at the PM[143].

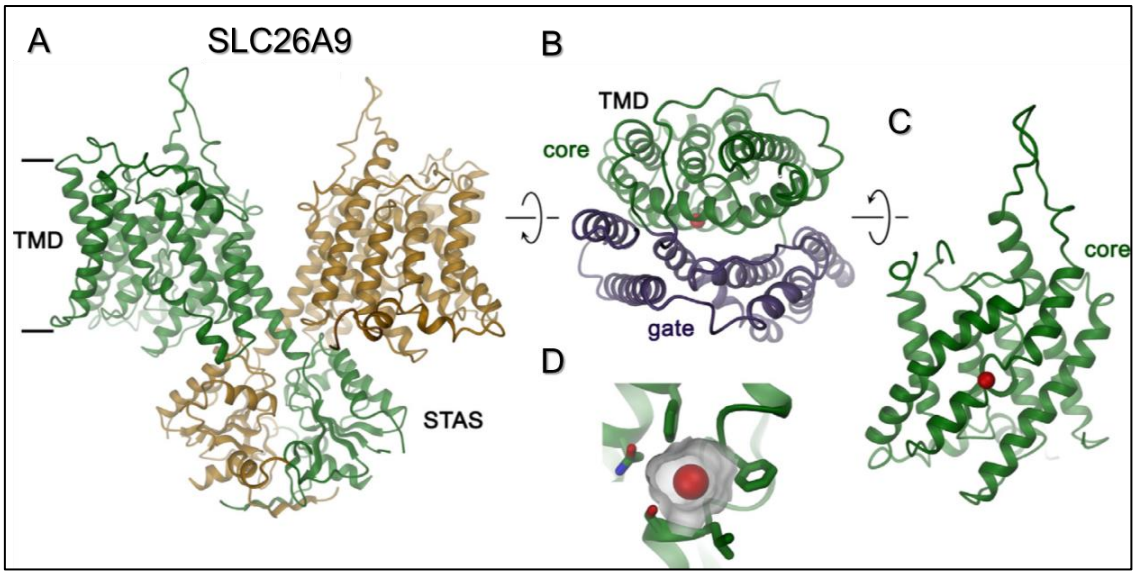

Figure 6 – Ribbon representation of SLC26A9. (A) The dimeric structure of SLC26A9 (each dimer represented in a different colour – green or yellow). **(B)** Single transmembrane domain (TMD) viewed from the extracellular side with core (shown in green) and gate (shown in purple) modules labelled. **(C)** Core module viewed from within the membrane. **(D)** Close-up of the anion binding pocket (Cl^- ion shown as red sphere) with sidechains of surrounding residues displayed as sticks. Molecular surface of the binding pocket is shown in grey. Adapted from[86].

SLC26A9 has been proposed to function as a constitutively active Cl^- transporter[86,141], a Cl^-/HCO_3^- exchanger[138], and a Na^+ transporter[143,144], and it shows a selectivity order of $SCN^- > I^- > Br^- > NO_3^- > Cl^-$ [145]. Studies in mice indicate that SLC26A9 presents a diverse range of biological functions, including acid secretion in the stomach[146] and bicarbonate transport in the intestine[147]. In human airways, it contributes to constitutive Cl^- secretion and MCC[136], and, in contrast to CFTR and TMEM16A, it is spontaneously active once inserted into the apical PM of airway epithelial cells[148].

SLC26A9 cellular localization was found to be mostly cytoplasmic or at the tight junctions (TJs)[149]. However, it was proposed to functionally interact with CFTR, which regulates its transport, function and targeting to the PM[140]. The interaction between these two proteins is mostly mediated by the STAS domain of SLC26A9 and the RD of CFTR[150], and possibly also via their PDZ-binding domains[148]. F508del-CFTR reduces SLC26A9 expression through SLC26A9 retention in the ER and premature degradation by the proteasome[149].

c. SLC26A9 in Cystic Fibrosis

Recently, the importance of studying SLC26A9 in the context of CF has been highlighted due to its striking effects in the pathophysiology of organs affected in CF as well as other disorders.

SLC26A9 has been described as a modifier of lung function and of response to CFTR modulator therapies[151,152], and SLC26A9 polymorphisms have been associated with the risk of developing meconium ileus and early exocrine pancreatic disease in individuals with CF[137,153,154]. Moreover, recent studies show that increased SLC26A9 expression in ductal cells of the pancreas delays the age at onset of CF-related diabetes[138].

Interestingly, SLC26A9 polymorphisms have also been linked to asthma in children, namely due to reduced SLC26A9 protein expression[136]. SLC26A9 contributes to epithelial Cl^- transport and prevents mucus obstruction under inflammatory conditions[136], possibly playing a role in the regulation of the ASL.

Taken together, these data support a role of SLC26A9 as a clinically relevant disease modifier and promising therapeutic target to circumvent deficient Cl^- secretion in CF. However, SLC26A9 trafficking is strongly dependent on CFTR. Namely, when co-expressed with wt-CFTR, SLC26A9 and CFTR traffic together from the ER to the PM. Yet, if co-expressed with F508del-CFTR, SLC26A9 is retained intracellularly[155].

Existing evidence enforces the necessity to further investigate the relationship between SLC26A9 and CFTR, namely, to determine whether SLC26A9 traffic/function can be modulated independently of CFTR. Moreover, due to SLC26A9 spontaneous activation once inserted into the membrane[148], an interesting therapeutic option for CF would include the identification of genes/small molecules that increase SLC26A9 expression at the PM, thus contributing to increase epithelial Cl^- secretion.

3. Objectives of the present work

The main goal of this doctoral work was to gain further insight into the regulation of alternative Cl^- channels/transporters and their relationship with CFTR so as to determine their potential as targets for the development of novel (“mutation-agnostic”) therapies for CF by compensating for the absence of functional CFTR (Fig. 7).

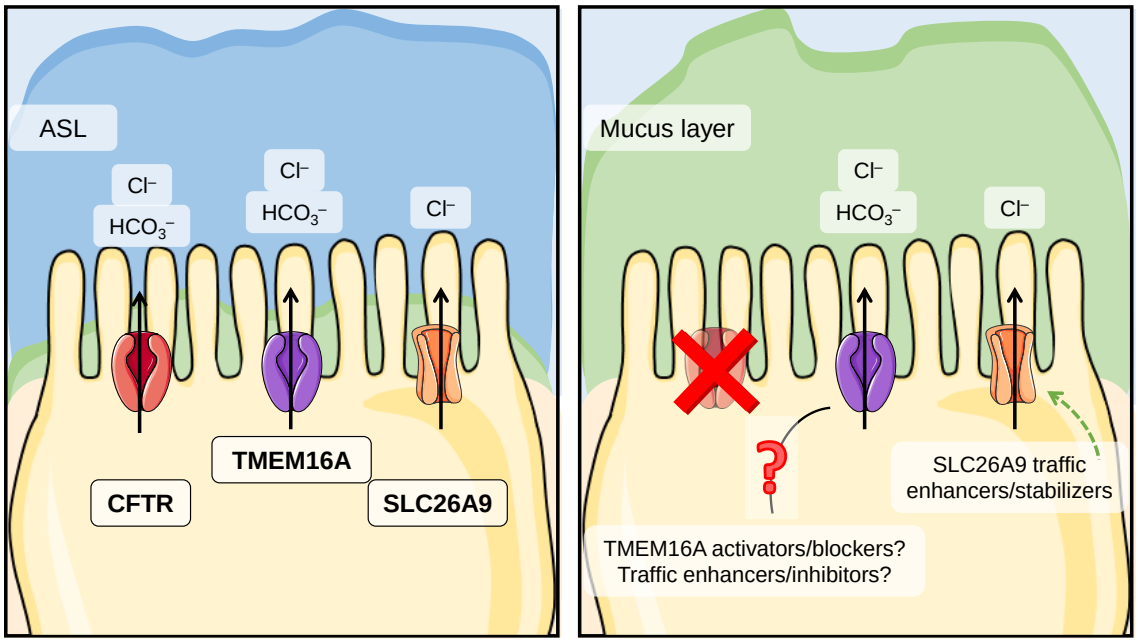

Figure 7 – Modulation of ion channels/transporters as alternative therapies for CF. In healthy airways, CFTR, TMEM16A and SLC26A9 are expressed at the plasma membrane (PM) of epithelial cells where they contribute to ion and water homeostasis. In CF airways, due to the absence of functional CFTR, Cl^- secretion is compromised and Na^+ absorption is upregulated, leading to a dehydrated air surface liquid (ASL) and impaired mucociliary clearance (MCC). Expression of TMEM16A and SLC26A9 at the PM are also diminished in CF ciliated cells, although the effect of TMEM16A overexpression in secretory cells and its role in mucus secretion are still controversial. Alternative therapies for CF thus include enhancing SLC26A9 expression at the PM and modulating TMEM16A. Even though for the latter it is still not clear whether activators or inhibitors are beneficial, a TMEM16A potentiator in currently under clinical investigation[156].

To achieve this goal, this project was divided into the following specific objectives:

1) To unveil the functional relationship between alternative Cl^- channels/ transporters (TMEM16A, TMEM16F, SLC26A9) and CFTR.
2) To determine the role of TMEM16A and SLC26A9 in the context of CF, so as to understand whether these channels can compensate for the absence of functional CFTR in CF (or assist in cases where there is CFTR residual function).
3) To identify traffic regulators of TMEM16A and SLC26A9 through high-throughput (HT) siRNA microscopy screens and to functionally validate the role of top hits.

The studies performed to accomplish these objectives are described in the following three chapters.

II. Materials and Methods

1. Cell culture

1.1 Cells and cell culture conditions

Human B-lymphocytes (wt or derived from a patient with Scott syndrome) were grown in suspension in RPMI 1640 medium with L-Glutamine (Gibco, 21875), supplemented with 10% Foetal Bovine Serum (FBS [Gibco, 10270-106]) and 5 mM HEPES [Thermofisher Scientific, 15630106]).

BHY and Cal33 cells, derived from head and neck squamous cell carcinoma, were grown in DMEM (Dulbecco's Modified Eagle Medium, Gibco #11965-092) with 10% FBS.

Calu3 cells (human lung cancer cells) were cultured in DMEM F12 (Gibco, 11320-033), supplemented with 2 mM L-glutamine (Gibco, 25030081), 10 mM HEPES and 10% FBS.

Cystic Fibrosis Bronchial Epithelial cells (CFBE 41o- cells)[157], further referred to as CFBE, were cultured in MEM (Minimum Essential Media [Gibco, 11090-081]) supplemented with 10% FBS. These immortalized cells were developed from bronchial epithelial cells derived from a CF patient (F508del-CFTR homozygous) and allowed the development of other types of cells used in this work.

CFBE cells stably overexpressing 3HA-TMEM16A-eGFP or eGFP-3HA-SLC26A9 were cultured in MEM with 10% FBS supplemented with 400 µg/mL G418 (Sigma-Aldrich, A1720) and 2.5 µg/mL puromycin (Sigma-Aldrich, P8833).

CFBE cells stably expressing wt-CFTR (CFBE wt-CFTR) or F508del-CFTR (CFBE F508del-CFTR) were cultured in MEM with 10% FBS supplemented with 2.5 µg/mL puromycin.

CFBE cells stably expressing wt-CFTR or F508del-CFTR with a FLAG tag and a N-terminus mCherry (CFBE mCherry FLAG wt-/F508del-CFTR) were cultured in DMEM with 10% FBS supplemented with 2.5 µg/mL puromycin and 10 µg/mL blasticidin (Sigma-Aldrich, 15205).

Immortalized Human Bronchial Epithelial cells (16HBE41o-), further referred to as 16HBE, endogenously expressing wt-CFTR (16HBE wt-CFTR) or F508del-CFTR (16HBE F508del-CFTR) were cultured in MEM with 10% FBS.

Human Embryonic Kidney (HEK) 293T cells and HeLa cells (cervical adenocarcinoma) were cultured in DMEM supplemented with 10% FBS.

HEK cells stably co-expressing TMEM16A and halide-sensitive YFP (YFP-H148Q/I152L/V163S) – HEK-TMEM16A-hsYFP – were cultured in DMEM supplemented with 10% FBS, 2 mM L-Glutamine, 10 mM HEPES, 0.5 µg/mL puromycin and 150 µg/mL hygromycin B (Sigma-Aldrich, H3274).

Primary human nasal epithelial (pHNE) cells were obtained from nasal brushing of healthy individuals or people with CF with the F508del/F508del genotype. Nasal brushings were obtained from Hospital Santa Maria and Hospital Dona Estefânia (Lisbon, Portugal) after receiving patient's written consent and approval by the hospital Ethics Committee. After isolation, cells were expanded and differentiated according to protocols established by Jeffrey Beekman's lab (Utrecht, The Netherlands)[158]. Briefly, after expansion, cells were seeded in a porous membrane and cultured under Air-Liquid Interface (ALI) conditions for 14-21 days.

shRNA stably transfected cells were cultured with their respective medium, supplemented with either 2.5 µg/mL puromycin or 400 µg/mL G418, according to the resistance gene in the respective shRNA-containing plasmid.

All cells were cultured at 37ºC in a humidified atmosphere of 5% (v/v) CO_2.

1.2 Generation of novel cell lines as research tools

a. Mutagenesis and cloning

Novel cell lines derived from CFBE or 16HBE cells were generated to stably express double tagged TMEM16A or SLC26A9, with an enhanced green fluorescent protein (eGFP) and a hemagglutinin tag inserted in triplicate (3HA) in an extracellular loop of each protein.

Hemagglutinin (HA) tags (HA: 5' – TAC CCA TAC GAT GTT CCA GAT TAC GCT – 3') were inserted in triplicate into TMEM16A/SLC26A9 cDNAs. The mutagenesis reactions were performed using the KOD Hot Start Kit (Novagene, 71086) with complementary pairs of the custom designed HPLC-purified mutagenic primers described in Table S6 – Appendix 4 (ordered from StabVida). The result of these mutagenesis reactions is a mixture of the template plasmid and a new plasmid containing the desired insertion. Therefore, PCR products were incubated for 1 h at 37ºC with DpnI (Invitrogen, ER1702), a restriction enzyme that specifically hydrolyses methylated DNA. This results in complete degradation of the template DNA, heavily methylated because of its bacterial origin, leaving the mutated DNA, synthesized in vitro, intact.

For TMEM16A, eGFP was fused to its C-tail (via a small linker: LEFLNCCPGCCMEPSTT) and the 3HA tag was inserted between His^{396} and Asn^{397}, i.e., in the first extracellular loop of TMEM16A (Appendix 1 and 4). The numbering corresponds to TMEM16A isoform X5 (NCBI Reference Sequence: XP_011543427.1).

A similar protocol was used for SLC26A9, where an eGFP was inserted in the N-terminus (with the linker: GGSLGGPD), and the 3HA tag was inserted in the second putative extracellular loop, between Glu^{157} and Ser^{158} (mutagenesis and cloning performed by Rainer Schreiber). The numbering corresponds to SLC26A9 isoform a (NCBI Reference Sequence: NP_443166.1)

The 3HA-TMEM16A-eGFP construct was cloned into the pLVX-TRE3G inducible lentiviral vector (Clontech, Enzifarma S.A., Portugal), using the In Fusion® HD Cloning Kit (Clontech). The cDNA of the construct was amplified through PCR reactions (Table S6 – Appendix 4) creating 16 bp extensions in both C- and N- terminals. The lentiviral plasmid pLVX-TRE3G was linearized using BamHI (Promega, R6021) and MluI (Fermentas, ER0561) for 2 h at 37ºC. The linearized vector as well as the cDNA with extensions were spin-column purified using the NZYGelpure kit (NZYTech, MB011). The In-Fusion cloning reaction was then performed according to the manufacturer's conditions, and competent cells were transformed with the cloning reaction product.

The correct insertion of mutations and cloning were confirmed through Sanger sequencing (StabVida). The pLVX-TRE3G-3HA-TMEM16A-eGFP or pLVX-TRE3G-eGFP-3HA-SLC26A9 constructs were then transfected into HEK 293T cells to produce lentiviral particles which were used to transduce CFBE or 16HBE cells. The Tet-On 3G transactivator protein was co-transduced to have a doxycycline-inducible expression of the double-tagged constructs.

b. Lentivirus preparation and transduction

HEK 293T cells were used to produce lentiviral particles containing the cDNA of genes of interest (GOI) or shRNAs (MISSION® shRNAs from Sigma-Aldrich).

HEK cells were seeded at a density of 5×10^5 cells per well of a poly-lysine coated 6-well plate and incubated for 24 h at 37ºC, 5% CO_2. Then, cells were transfected with 5 µg of DNA per well – 2.38 µg of packaging plasmid pCMV-dR8.74psPAX2, 0.24 µg of envelop plasmid VSV-G/pMD2.G, and 2.38 µg of the plasmid with the GOI or shRNA. Cells were then incubated for 18 h at 37ºC, 5% CO_2. The medium was replaced to remove the transfection reagent and cells were incubated for 30 h at 37ºC, 5% CO_2.

Media containing the lentiviral particles were harvested and the packaging cells were discarded. The harvested viral particles were immediately used to transduce the cells seeded the day before on 6-well plates. Cells were infected with 2 mL of lentivirus-containing medium, plus 4 µg/mL Polybrene (Hexadimethrine bromide) infection enhancer. The plates were centrifuged at 200 g for 1 h at 25ºC and then incubated for 24 h at 37ºC, 5% CO_2. The medium was then changed to the respective cell medium supplemented with selection antibiotics to eliminate the non-transduced cells. Gene expression/knockdown was assessed by Western Blot or semi-quantitative PCR. After antibiotic selection, CFBE 3HA-TMEM16-eGFP and CFBE eGFP-3HA-SLC26A9 cells were sorted to obtain a more homogeneous pool of cells, with higher eGFP fluorescence.

2. Biochemical and Molecular Biology Techniques

2.1 DNA and RNA Transfections

Cells were transfected with different cDNAs/siRNAs for 48h or 72h using Lipofectamine 2000 (Invitrogen #11668019) or Lipofectamine 3000 transfection reagents (Invitrogen #L3000075), according to manufacturer's conditions. Briefly, cells were seeded the day before transfection, in order to be ~70% confluent at the time of transfection. On the day of transfection, DNA/RNA-Lipofectamine complexes were prepared in OptiMEM reduced-serum medium (Gibco, 31985-047) and were added to the cells in normal culture medium without antibiotics. The amount of Lipofectamine and DNA/RNA used varied depending on the cell type.

Cells in suspension (B-lymphocytes), or cells in which the transfection with lipofectamine showed very low efficiencies, were transfected using electroporation, where cells were exposed to a pulsed electrical field of sufficient strength to cause a reversible permeabilization of the cell membrane in localized areas. Cells were transfected with the Neon transfection system (ThermoFisher), according to the manufacturer's conditions. Briefly, cells were harvested, washed with sterile PBS, and resuspended in 100 µL of R buffer at a density of 2 x 10^7 cells/mL. The cells and molecules to be delivered (DNA/RNA) were loaded into the 100 µL Neon Pipette tip, the pipette was plugged into position in the Neon transfection device, and cells were transfected with an optimized protocol (3 pulses of 10 ms at 1650 V). Cells were immediately transferred into the prepared culture plate containing prewarm medium with serum and supplements but without antibiotics.

All siRNAs used (Silencer™ Select, Table S7 – Appendix 4) were purchased from ThermoFisher.

2.2 PCR

Semi-quantitative reverse-transcriptase(RT)-PCR was performed to detect the expression of genes or to quantify gene knockdown. Total RNA was isolated using the NZY Total RNA Isolation kit (Nzytech, Portugal). Total RNA (1 µg/20 µL reaction) was reverse-transcribed using random primers and NZY M-MuLV Reverse Transcriptase (Nzytech, Portugal). Each RT-PCR reaction contained sense and antisense primers for the genes of interest (0.5 µM, Table S4 – Appendix 4) or for GAPDH (0.5 µM), 0.5 µL cDNA and NZYTaq II DNA polymerase (Nzytech, Portugal). After 2 min at 95°C cDNA was amplified during 35 cycles for 30 s at 95°C, 30 s at 56°C and 1 min at 72°C. PCR products were visualized by loading on RedSafe Nucleic Acid Staining Solution (Intron Biotechnology) containing agarose gels and analysed using Image Lab (BioRad).

2.3 Western Blot

Protein was isolated from cells using a sample buffer containing 50 mM Tris-HCl, 150 mM NaCl, 50 mM Tris, 100 mM dithiothreitol, 1% Nonidet P-40 (NP40), 0.5% deoxycholate sodium, and 1% protease inhibitor mixture (Sigma-Aldrich, P2714).

Protein extracts were separated on 7, 8.5, or 10% (w/v) polyacrylamide gels and transferred into polyvinylidene difluoride (PVDF) membranes. Membranes were blocked with 1 or 5% (w/v) non-fat milk powder (NFM) in Tris buffer saline with Tween 20 (TBS-T) or in PBS-T for 1 h at room temperature (RT) and incubated overnight at 4°C with primary antibodies (Table S1 – Appendix 4). Membranes were then incubated with HRP-conjugated secondary antibodies (Table S1 – Appendix 4) for 2 h at RT. Chemiluminescent detection was performed using the Clarity™ Western ECL substrate (BioRad, 170-5061) and the Chemidoc™ XRS system (BioRad). The quantification of band intensity was performed using the Image Lab software (BioRad) and normalized to the loading control as appropriate.

2.4 Co-Immunoprecipitation

Cells were collected and lysed in PD buffer (50 mM Tris, 100 mM NaCl, 1% Glycerol, 1% NP40) containing 1X protease inhibitor cocktail, followed by mechanical

homogenization and centrifugation to eliminate nuclei and cellular debris. Lysate was precleared by incubation of the input for 2 h at 4 °C with Protein-A conjugated beads.

Protein was incubated with 6 µL of antibody (anti-TMEM16A, Table S1 – Appendix 4) on a rotator at 4 °C overnight. Afterwards, beads were centrifuged and washed three times with wash buffer (100 mM Tris, 300 mM NaCl, 1% TritonX-100). The immunocomplexes were eluted with sample buffer 1 h rotating at RT. Samples were centrifuged, and the supernatants were analysed by Western Blot.

2.5 Cell surface biotinylation

Cells were grown in p60 plates and incubated at 4ºC with NHS LC Biotin buffer (1 mg biotin (EZ-Link Hydrazide-LC-Biotin, Thermo Scientific, 21339)/1 mL PBS with 1 mM $MgCl_2$, 0.1 mM $CaCl_2$, pH 8.2) for 1 h protected from the light. Cells were lysed with 1 mL of BL buffer (25 mM HEPES, 1% (v/v) Triton X-100, 10% (v/v) glycerol, pH 8.2), supplemented with a 1x Complete protease inhibitor cocktail (PIC, Roche, 11697498001) and collected with a cell scraper. Cell membranes and debris were pelleted by centrifugation at 14,000 g for 10 min at 4ºC. 100 µL of the supernatants were collected (whole cell lysate). The remaining samples were incubated overnight at 4ºC with streptavidin beads (Thermo Scientific, 20353). The beads were pelleted, washed 2x with PBS and 1x with BL buffer and the samples were then analysed by Western Blot.

2.6 Immunostainings

a. Immunofluorescence – Cells

Cells were grown on glass coverslips and fixed with methanol and acetone (4:1) for 10 min at -20 ºC or with 4% (v/v) paraformaldehyde (PFA) for 10 min at RT. In case of PFA fixation, cells were permeabilized with 0.2% (v/v) Triton X-100 in PBS for 5 min at RT. After washing 3 times with PBS supplemented with $CaCl_2$ (0.7 mM) and $MgCl_2$ (1.1 mM), cells were blocked with 3% (w/v) bovine serum albumin (BSA, Sigma-Aldrich, A9056) in PBS for 30 min at RT and incubated with the primary antibody (Table S2 – Appendix 4) in 1% BSA overnight at 4ºC. Binding of the primary antibody was visualized by incubation with a fluorescent secondary antibody (Table S2 – Appendix 4) in 1% BSA for 1 h at RT. Nuclei were stained with Hoechst 33342 (0.1 µg/mL in PBS, Aplichem, Darmstadt, Germany). Cells were mounted on glass slides with mounting medium (DAKO Cytomation, Hamburg, Germany) and examined with an Axiovert 200M microscope equipped with ApoTome and AxioVision (Zeiss, Germany), with a Leica TCS

SP8 confocal microscope, or with a widefield epifluorescence microscope Leica DMI 6000B with a metal halide light source (EL6000) and a DFC365 FX CCD camera (Leica).

b. Immunofluorescence – Human lung tissue

Explanted CF lungs (F508del/F508del) and control tissues were collected in the Paediatrics Department of Motol University Hospital (Prague, Czech Republic) under approval of applied regulations and the hospital's Ethics Committee and shipped over 24 h to Lisboa. Informed consent was obtained from all subjects. After tissue cleaning, secondary and tertiary bronchi were fixed overnight with electron microscopy grade PFA (0.2% v/v, Electron Microscopy Sciences, 15710) and then dehydrated and slowly frozen. After lung cleaning and fixation, the pieces of secondary/tertiary bronchi were kept for 12 h at a time in phosphate buffers with increasing sucrose (Fluka, 84100) content (4% to 15%) and then incubated in a final solution with 15% sucrose and 7.5% gelatine (Sigma-Aldrich, G9391) for 1 h at 37°C. Dry ice-chilled isopentane (VWR, 24872) was then used to slowly freeze the tissues, which were kept at -80°C until sectioning. Tissue sections were cryocut using a Leica CM1850 UV cryostat. Cryosections 15-30 µm thick were generated on Superfrost® Plus slides (Thermo Scientific, 10149870), and used right away for immunohistochemistry, or stored at -20°C until further use.

Lung tissue sections on Superfrost® Plus slides were permeabilized with triton X-100 (Amersham Biosciences, 17-1315-01) 0.2% (v/v), after which tissue autofluorescence was quenched with $NaBH_4$ (1 mg/mL, Sigma-Aldrich, 213462). A blocking step with 1% BSA (w/v) was performed before incubating overnight at 4°C with primary antibodies (except for the negative controls which were incubated with 1% BSA). The following primary antibodies were used: rabbit monoclonal anti-DOG1 (Cell Marque, 244R-14), rabbit polyclonal anti-SLC26A9 (BioTechne, NBP2-30425), mouse monoclonal anti-CFTR (CFF, 570), and mouse monoclonal anti-ZO-1 (Invitrogen, 33-9100).The following day a mix of the secondary antibodies (anti-mouse or anti-rabbit Alexa 488 and anti-rabbit Alexa 568, Life Technologies, A21202*,* A21206 and A10042) and nuclear dye (4 µg/mL, Methyl Green, Sigma-Aldrich, 67060) was applied for 2 h at RT. Tissue sections were mounted in a mix of N-propylgallate (Sigma-Aldrich, P3130) and Glycerol for microscopy (Merck, 104095). The tissues stained were secondary/tertiary bronchi and were as similar as possible for comparison. Areas of extensive shedding/remodelling in CF tissue were avoided in the analysis, and areas of intact epithelia preferred. Imaging was performed with a Leica TCS SP8 confocal

microscope coupled to a Hamamatsu Flash4 sCMOS camera, using a HC Plan Apo 20x/0.75 objective. Software used for acquisition was Leica's LAS x, and image processing was performed on ImageJ FIJI[159]. FIJI was used to generate maximum image projections (MIPs). Experiments performed in collaboration with Margarida Quaresma.

2.7 Chemiluminescence

For TMEM16A chemiluminescence, CFBE 3HA-TMEM16A-eGFP cells were seeded on coated black 96-well plates (Corning, 3631) at a density of 8 x 10^3 cells/well. On the following day, cells were induced with 1 µg/mL doxycycline and were transfected with the siRNAs targeting the genes of interest. 48 h after transfection, cells were washed once with ice cold PBS supplemented with 0.7 mM $CaCl_2$ and 1.1 mM $MgCl_2$. Then, cells were incubated for 1 h at 4ºC with monoclonal anti-HA antibody (1:500). Afterwards, cells were washed 3 times with ice cold PBS, incubated 10 min with 4% PFA at 4ºC and transferred to room temperature for the remaining staining procedure. Cells were then washed 3 times with PBS and incubated for 1 h at RT with a goat anti-mouse HRP-conjugated secondary antibody (1:500). For wt-/F508del-CFTR chemiluminescence, a similar protocol was followed. In this case, CFBE mCherry-FLAG-wt/F508del-CFTR cells were used and incubated with mouse anti-FLAG-HRP conjugated antibody (Sigma-Aldrich, A8592, 1:1000) for 1 h at 4ºC before fixation with 4% PFA.

Signals were detected with SuperSignal West Pico chemiluminescence substrate (Thermo Fisher Scientific) using a NOVOstar Microplate Reader (BMG LABTECH GmbH, Ortenberg, Germany). All solutions were prepared in Dulbecco's PBS freshly supplemented with 0.7 mM $CaCl_2$ and 1.1 mM $MgCl_2$. Antibody solutions contained 1% (w/v) BSA.

2.8 Proliferation and cell viability assays

a. Proliferation assay – MTT

3-(4,5-dimethylthiazol-2-yl)-2,5-diphenyl-2H-tetrazolium bromide – MTT (Sigma-Aldrich, M2128) – was dissolved in PBS to a final concentration of 5 mg/mL. The solution was filtered and stored at -20ºC protected from the light. To determine proliferation, Cal33 or BHY cells (1.5 x 10^3 cells) were seeded on 96-well plates and allowed to adhere overnight. The next day, cells were transfected with siRNAs and/or treated with compounds. Every 2 days cells were again transfected and/or the medium with drugs was replaced, and experiments were performed. The medium was removed and 10 µL

of MTT were added per well together with 90 µL of new medium. MTT produces a yellowish solution that is converted to dark blue, water insoluble MTT formazan by mitochondrial dehydrogenases of living cells, therefore allowing the quantification of living cells per well. After 2 h of incubation at 37ºC, the blue crystals were solubilized with DMSO, and the intensity was measured colorimetrically at 570 nm using the plate reader NOVOstar (BMG Labtach, Offenburg, Germany).

b. Cell viability assay

Cal33 cells were seeded at a density of 1.5 x 10^3 cells/well on 96-well plates. Same as in the proliferation assay, cells were transfected with siRNAs and/or treated with compounds. Every 2 days cells were again transfected and/or the medium with drugs was replaced, and experiments were performed. Cells were washed twice with PBS with 0.7 mM $CaCl_2$ and 1.1 mM $MgCl_2$ and incubated for 30 min with PBS containing Hoechst 33342 (0.1 µg/mL) and Propidium Iodide – PI (1 µg/mL). Living cells have intact membranes that exclude PI which easily penetrates the damaged, permeable membranes of non-viable cells. Cells were then washed twice with PBS and imaged using an automated widefield epifluorescence microscope Leica DMI 6000B with a metal halide light source (EL6000) and a DFC365 FX CCD camera (Leica). Automatic image analysis was performed with open-source software tools (CellProfiler[160] and R) and the percentage of dead cells was calculated by dividing the number of dead cells (PI-positive cells) by the total cell number (Hoechst-stained cells).

2.9 cAMP measurements

cAMP direct immunoassay Kit (Abcam, ab138880) was used following the manufacturer's protocol. This assay is based on the competition between HRP-labelled cAMP and free cAMP present in the sample for cAMP antibody binding sites. Briefly, CFBE F508del-CFTR cells were treated either with IBMX (3-isobutyl-1-methylxanthine, 100 µM)/Forskolin (2 µM) or ATP (100 µM) and then collected and centrifuged in order to obtain the cAMP containing supernatant. The supernatant was incubated in the cAMP antibody coated 96-well plate for 10 min and, after incubation, cAMP-HRP conjugated was added. The amount of cAMP-HRP bound to the plate was determined by reading HRP activity at OD450nm using a NOVOstar Microplate Reader (BMG LABTECH GmbH, Ortenberg, Germany). The intensity of OD450 nm is inversely proportional to the concentration of cAMP in samples and cAMP concentration was obtained using a

standard curve with known cAMP-HRP concentrations. Experiments performed by Roberta Benedetto.

Alternatively, HEK cells were transfected with a fluorescence resonance energy transfer (FRET)-based Epac cAMP sensor (YFP-Epac-CFP)[161,162] to analyse changes in intracellular cAMP levels. When expressed in cells, YFP-Epac-CFP displays significant FRET, due to close proximity of CFP (donor) and YFP (acceptor). Rises in cAMP levels induce a conformational change that rapidly lowers FRET, which can then be recovered by adding cAMP-lowering agents[163]. Therefore, increases in the ratio CFP/YFP (measured using a fluorescence microscope) indicate higher concentrations of cAMP and, consequently, unfolding of Epac.

3. High-throughput Screens

3.1 Coating of multi-well plates with siRNA/lipofectamine mix

To identify genes that affect TMEM16A/SLC26A9 trafficking to the plasma membrane (PM), screens were performed using microscopy plates coated with different siRNAs pre-mixed with lipofectamine. Multi-well plates (BD Falcon, 353962) were coated with customized siRNAs (Silencer® Select, Ambion) for solid-phase reverse transfection adapted from a reported protocol[164] with adjustments also described before[165].

Briefly, siRNA stock solutions were prepared by dissolving lyophilized siRNAs with milliQ water to a concentration of 30 µM (mother plate). These siRNAs were then diluted to a final concentration of 3 µM. A 0.2% (w/v) gelatine solution was prepared and filtered with a 0.45 µm pore size filter and a 0.4 M sucrose solution was prepared in OptiMEM. Then, a transfection mix was prepared by mixing 1.662 mL of the sucrose/OptiMEM solution, 969 µL of Lipofectamine 2000 and 969 µL double distilled water. This transfection mix was distributed into a 96-conic well plate (35 µL/well ‘‘Plate A’’). In parallel, fibronectin was diluted in the 0.2% gelatine solution to a concentration of 1%. This solution was distributed into another 96-conic well plate (96 µL/well, ‘‘Plate B’’). Then, 5 µL of the 3 µM siRNA solution and 7 µL of the transfection mix (‘‘Plate A’’) were incubated in each well of a low volume 384 well plate (‘‘Plate C’’) for 20 min at RT. Afterwards, 7 µL of the gelatine solution (‘‘Plate B’’) were added. 3 µL of the contents of each well in ‘‘Plate C’’ were diluted fifty-fold in a 384 deep well plate using double distilled water, and 15 µL of each well were transferred to 384-well imaging plates. Multi-well plates were immediately placed on a multi-well Speed Vac vacuum concentrator (miVac,

Genevac™) for drying and afterwards placed in a box containing drying pearls (anhydrous atmosphere).

3.2 TMEM16A/SLC26A9 trafficking assays

3HA-TMEM16A-eGFP or eGFP-3HA-SLC26A9 expressing CFBE cells were grown to confluence and split (50%). Twenty-four hours later, cells were trypsinized to antibiotic-free medium and seeded on siRNA coated 384-well plates (50 µL/well, 3 x 10^3 cells/well) using a Multidrop™ Combi peristaltic dispenser (Thermo Scientific, 5840300). TMEM16A or SLC26A9 expression was induced 24 h after seeding with antibiotic-free medium supplemented with 1 µg/mL doxycycline (Sigma-Aldrich, 9891), and immunofluorescence experiments were performed 48 h after induction (72 h post-siRNA transfection).

The extracellular HA-tag of CFBE 3HA-TMEM16A-eGFP or CFBE eGFP-3HA-SLC26A9 cells was immunostained in non-permeabilized cells. Cells were washed in cold PBS and incubated 1 h at 4ºC with an anti-HA antibody (5 µg/mL). Cells were washed 3 times with PBS, incubated 20 min with 3% PFA at 4°C and transferred to room temperature. Cells were washed 3 times with PBS and incubated 1 h with an Alexa Fluor® 647 conjugated secondary antibody (2 µg/mL). Cells were washed 3 times with PBS, incubated with Hoechst 33342 solution (200 ng/mL) for 1 h, and finally washed and incubated with PBS overnight before imaging. All solutions were prepared in PBS freshly supplemented with 0.7 mM $CaCl_2$ and 1.1 mM $MgCl_2$. Antibody solutions additionally contained 1% (w/v) BSA. All liquid handling was performed with a manual 96 channel pipette liquidator (Liquidator™ 96, Mettler Toledo #17010335). Solution volumes were (µL/well): 15 antibodies, 25 PFA, 50 Hoechst.

3.3 Analysis of time-lapse microscopy images

Time-lapse microscopy images were processed and quantified in Image J/Fiji. Briefly, a cell-free region was used for baseline correction. Then, representative cells were selected – i.e., cells which remain viable and within the field of view during the whole time-lapse – and their average fluorescence intensity was determined and plotted as a function of time. Finally, the grayscale lookup table was adjusted for optimal contrast. Analysis performed by Hugo Botelho.

3.4 Image acquisition, processing, and analysis

Cell imaging was performed with a (automated) widefield epifluorescence microscope with a Scan^R software (Olympus Biosystems) equipped with a motorized stage and a metal halide light source (MT20), a 12-bit 1344 x 1024 pixel resolution C8484 CCD camera (Hamamatsu OrcaFlash4) and a 10x UPlanApo objectives (Olympus) and 0.4 numerical aperture. Exposure times at maximum light brightness were for Hoechst, eGFP and Alexa Fluor 647 of (ms) 10-20, 500 and 2000, respectively. The Hoechst channel was used for contrast-based autofocus (fixed samples) and hardware autofocus for time-lapse imaging. Fixed samples were imaged at RT and filter settings (Excitation wavelengths/excitation band (nm) – Ex, Emission wavelengths/emission band (nm) – Em): Hoechst – Ex 347/50, Em 460/50; eGFP – Ex 470/40, Em 525/50; Alexa 647 – Ex 640/30, Em 690/50. For the SLC26A9 traffic screen, imaging was performed using a Leica TCS SP8 confocal microscope with a 20x (0.75 NA) dry objective, using similar filter settings.

Automatic image analysis was performed with opensource software tools (CellProfiler[160], R), using pipelines tailored to the specific application as described before for CFTR[165]. Initially, overall transfection efficiency was assessed by observing if cells transfected with siRNAs compromising chromosome segregation exhibited mitotic phenotypes[166]. Failure to observe these phenotypes in more than 75% of images implied the rejection of the corresponding plate from the analysis. The algorithm for background subtraction was also described before[165]. Briefly, it comprised: 1) the computation of illumination correction functions for each fluorescence channel, which defines the pixel-by-pixel fluorescence baseline for each channel as produced by image illumination and background fluorescence; 2) subtraction of the corresponding illumination correction function from each image. The pipeline includes quality control (QC) steps excluding cells which do not significantly express the protein of interest (TMEM16A or SLC26A9), have abnormal morphology (e.g., apoptotic cells) or contain a significant number of saturated pixels. This fluorescence quantification data allowed for the determination of TMEM16A traffic (chapter 1.1) in each cell according to the following formula:

$$Traffic\ Efficiency = \frac{PM\ TMEM16A}{Total\ TMEM16A} = \frac{Alexa\ 647\ Integrated\ Fluorescence}{GFP\ Integrated\ Fluorescence}$$

For chapters 1.3 (TMEM16A) and 3.2 (SLC26A9), we considered only the increase of PM expression as the screen readout, as we were interested in enhancing PM-localized TMEM16A and SLC26A9 even if the PM/Total ratio was not altered.

For each image, the TMEM16A/SLC26A9 Traffic Efficiency or PM expression was considered to be the median for all cells in the image, as previously described[165]. After averaging the traffic efficiency/PM expression for all images from the same siRNA treatment, the effect of different siRNAs on TMEM16A/SLC26A9 trafficking was compared with the results obtained with the one measured under the effect of “siScrbld” (chapter 1.1) or "siNEG1" non-targeting siRNA treatment, using one of the following formulas:

$$Deviation\ score = \frac{Traffic\ efficiency - Traffic\ efficiency_{siScrbld}}{SD_{siScrbld}}$$ (Chapter 1.1)

$$Z - score\ (x_{plate_i}) = \frac{x_{plate_i} - Average_{siNEG1,plate_i}}{SD_{siNEG1,plate_i}}$$ (Chapters 1.3 and 3.2)

Where $SD_{siScrbld}$ or SD_{siNEG1} is the standard deviation for the Traffic Efficiency/PM expression with the treatment with the non-targeting siRNA. Significant effects were considered when the magnitude was larger than the SD of the control siRNA (siScrbld/siNEG1). Therefore, genes in which the score was above +1, were considered traffic enhancers. Accordingly, genes having a score below -1 were considered traffic inhibitors. Additionally, two-tailed Student’s t-tests were performed to quantify statistical significance versus the corresponding negative control. Analysis performed in collaboration with Hugo Botelho.

4. Functional Assays

4.1 YFP-Quenching assay

HEK-TMEM16A-hsYFP were seeded at a density of 3 x 10^4 cells/well on siRNA-coated 96-well plates. 48 h after seeding, cells were washed once with 20 mM Na-Gluconate solution (in mM: NaCl 120, Na-Gluconate 20, KCl 5, $MgCl_2$ 1, $CaCl_2$ 2, Glucose 10, HEPES 10), and placed in the plate reader for measurements (NOVOstar, BMG Labtech). After measuring the baseline fluorescence, cells were incubated with 10 mM NaI solution (final concentrations - in mM: NaCl 120, NaI 10, KCl 5, $MgCl_2$ 1, $CaCl_2$ 2, Glucose 10, HEPES 10) for 20 s, and then were stimulated with 5 µM ATP (final concentration) for 30 s, to induce I^- uptake and consequently the quenching of the YFP fluorescence. The experiments were performed at 37ºC, and the excitation and emission wavelengths were, respectively, 485 and 520 nm.

The maximum slope of the curves obtained with the different siRNA treatments was calculated using the BMG LABTECH's MARS Data Analysis Software. After averaging the maximum slope after ATP stimulation of the same siRNA treatment, the effect of different siRNAs on TMEM16A function was compared with the results obtained with the non-targeting "NEG1" siRNA treatments, using the following formula:

$$Score = \frac{Max\ slope_{siRNA} - Max\ slope_{siNEG1}}{SD_{siNEG1}}$$

Alternatively, HEK-TMEM16A-hsYFP were seeded at a density of 10.000 cells/well on collagen-coated 96-well plates. Cells were then transfected using the Lipofectamine 3000 protocol and/or treated with different compounds. I^- uptake and YFP quenching (maximum slope) was calculated as described above.

4.2 Ussing Chamber measurements

Cells were seeded at approximately 3.5 x 10^5 cells/mL onto Costar Transwell® permeable supports of pore size 0.4 µm (Snapwell, Corning-Costar®, Tewksbury, MA, USA) and 1.13 cm^2 area, or at ~5 x 10^4 cells/ml onto Corning 6.5 mm Transwell permeable supports and kept in liquid-liquid interface (LLI). Transepithelial electrical resistance (TEER) of the cell monolayers was measured with a chopstick electrode (STX2 from WPI®, Berlin, Germany) and electrophysiological analyses were carried out in monolayers with resistance values above 600 Ω/ cm^2. Transepithelial resistance R_{te} was determined by applying 1 s current pulses of 0.5 µA (5 s-period). For Ussing chamber measurements, filters were mounted in the chamber device and continuously perfused with Ringer containing (mM): NaCl 145, K_2HPO_4 1.6, $MgCl_2$ 1, KH_2PO_4 0.4, Ca-Gluconate 1.3, Glucose 5, pH 7.4. Low Cl^- ringer (NaCl 30 mM) was added to the luminal side to create an electrochemical driving force when using CFBE or 16HBE cells. Values for the transepithelial voltage (V_{te}) were referenced to the luminal epithelial surface. Equivalent short-circuit current ($I_{eq\text{-}sc}$) were calculated according to Ohm's law from V_{te} and R_{te} ($I_{eq\text{-}sc}=V_{te}/R_{te}$), with appropriate correction for fluid resistance.

Experiments were performed in the presence of Amiloride (20 µM), an inhibitor of the Epithelial Sodium Channel (ENaC), and TRAM34 (100 nM), a potent and highly selective blocker of intermediate conductance Ca^{2+}-activated K^+ channels.

TMEM16A was activated by ATP or UTP (100 µM) added to the luminal as well as to the basolateral side and inhibited by the CaCCinh-A01 (30 µM) or Ani9 (10 µM).

CFTR was activated by forskolin (2 µM) and genistein (25 µM) or IBMX (100 µM) added to the luminal side and inhibited by the specific inhibitor CFTR inhibitor 172 (30 µM).

4.3 Whole-cell Patch-Clamp analysis

Cells grown on glass-coated cover slips were mounted on the stage of an inverted microscope (Zeiss, Munich, Germany) and kept at 37 °C. Patch pipettes were filled with a cytosolic-like solution containing KCl 30, K-gluconate 95, NaH_2PO_4 1.2, Na_2HPO_4 4.8, EGTA 1, Ca-gluconate 0.758, $MgCl_2$ 1.03, D-glucose 5, ATP 3, pH 7.2. The intracellular (pipette) Ca^{2+} activity was 0.1 µM. Patch-clamp experiments were performed in the fast whole-cell configuration.

The bath was perfused continuously with Ringer solution (mM): NaCl 145, KH_2PO_4 0.4, K_2HPO_4 1.6, D-glucose 5, $MgCl_2$ 1, Ca-gluconate 1.3, pH 7.4, containing 50 nM TRAM34 (Abcam, ab141885) at a rate of 8 mL/min. Ca^{2+}-activated currents were obtained after stimulation with ATP (100 µM), ionomycin (Iono, 0.1/1 µM), carbachol (CCH, 100 µM) or histamine (50 µM). cAMP-induced currents were obtained with forskolin (Fsk, 2 µM) together with genistein (Gen, 25 µM) or IBMX (100 µM) in the presence or absence of CFTR potentiator VX-770 (3 µM). Patch pipettes had an input resistance of 2–4 MΩ and whole cell currents were corrected for serial resistance. Currents were recorded using a patch-clamp amplifier (EPC 7, List Medical Electronics, Darmstadt, Germany), the LIH1600 interface and PULSE software (HEKA, Lambrecht, Germany) as well as Chart software (AD Instruments, Spechbach, Germany). In regular intervals, membrane voltage (V_c) was clamped in steps of 20 mV from -100 to +100 mV from a holding voltage of -60 mV. Current density was calculated by dividing whole-cell currents by cell capacitance.

4.4 Ca^{2+} measurements

CFBE cells were seeded on coated glass coverslips and transfected with plasmids or siRNAs for 48/72 h. Cells were then loaded with 5 µM Fura-2/AM and 0.02% Pluronic F-127 (Life Technologies, Germany) in ringer solution (in mM: NaCl 145; KH_2PO_4 0.4; K_2HPO_4 1.6; Glucose 5; $MgCl_2$ 1; Ca-Gluconate 1.3) for 1 h at RT. Fluorescence was detected in cells perfused with Ringer solution at 37ºC using an inverted microscope (Axiovert S100, Zeiss, Germany) and a highspeed polychromator system (VisiChrome, Germany). Fura-2 was excited at 340/380 nm, and emission was recorded between 470 and 550 nm using a CoolSnap camera (CoolSnap HQ, Visitron).

The control of the experiment, imaging acquisition and data analysis were done with the software package MetaFluor (Universal imaging, USA).

$[Ca^{2+}]_i$ was calculated from the 340/380 nm fluorescence ratio after background subtraction. The formula used to calculate $[Ca^{2+}]_i$ was the following:

$$[Ca^{2+}]_i = K_d \times (R - R_{min})/(R_{max} - R) \times (S_{f2}/S_{b2})$$

Where R is the observed fluorescence ratio. The values R_{max} and R_{min} (maximum and minimum ratios) and the constant S_{f2}/S_{b2} (fluorescence of free and Ca^{2+}-bound Fura-2 at 380 nm) were calculated using 1 µM ionomycin (Calbiochem), 5 µM nigericin, 10 µM monensin (Sigma-Aldrich), and 5 mM EGTA to equilibrate intracellular and extracellular Ca^{2+} in intact Fura-2-loaded cells.

5. Materials and statistical analysis

All compounds used were of highest available grade of purity.

Data are represented as means ± SEM. The number of replicates is described in the legend of each figure (“n”) and represents independent experiments performed with cells with different passage numbers. Student’s t test (for paired or unpaired samples as appropriate) or ANOVA were used for statistical analysis. A value of $p < 0.05$ was accepted as a significant difference.

III. Results and Discussion

Chapter 1

Identification of TMEM16A regulators through high-throughput screening

Data included in this chapter were published in:

1. Lérias JR*, **Pinto MC***, Botelho HM, Awatade NT, Quaresma MC, Silva IAL, Wanitchakool P, Schreiber R, Pepperkok R, Kunzelmann K, Amaral MD. A novel microscopy-based assay identifies extended synaptotagmin-1 (ESYT1) as a positive regulator of anoctamin 1 traffic. *Biochim. Biophys. Acta - Mol. Cell Res.* **2018**, *1865*, 421–431, doi:10.1016/j.bbamcr.2017.11.009 [*Shared first authorship]

2. **Pinto MC**, Schreiber R, Lérias JR, Ousingsawat J, Duarte A, Amaral MD, Kunzelmann K. Regulation of TMEM16A by CK2 and Its Role in Cellular Proliferation. *Cells* **2020**, *9*, doi:10.3390/cells9051138.

3. **Pinto MC**, Botelho HM, Silva IAL, Railean V, Neumann B, Pepperkok R, Schreiber R, Kunzelmann K, Amaral MD. Systems Approaches to Unravel Molecular Function: High-content siRNA Screen Identifies TMEM16A Traffic Regulators as Potential Drug Targets for Cystic Fibrosis. *Journal of Molecular Biology* **2022**, *434*, 167436, doi:10.1016/j.jmb.2021.167436.

1. A novel microscopy-based assay identifies extended synaptotagmin-1 (ESYT1) as a positive regulator of TMEM16A traffic

Introduction

Cystic Fibrosis (CF) is rare genetic disease caused by mutations in the gene encoding the CF transmembrane conductance regulator (CFTR), an epithelial chloride (Cl^-) and bicarbonate (HCO_3^-) anion channel. Despite symptomatic therapies, quality of life and life expectancy are still limited. Thus, correction of the CF basic defect, i.e., restoration of epithelial Cl^-/HCO_3^- secretion through CFTR modulators, is the much-ambitioned alternative[29]. Despite some success in getting to the clinic, CFTR modulators nevertheless cannot be used to pharmacologically rescue all CFTR mutations, e.g., large deletions such as the dele2,3(21 kb) mutation, quite frequent in Slavic countries. For CF patients with these 'unrescuable' mutations, recently grouped into class (theratype) VII[12], the alternative is to develop 'mutation-agnostic' therapies. One such possibility is through the activation of alternative (non-CFTR) anion channels[27].

Anoctamins/TMEM16 proteins consist in a family of 10 different proteins, TMEM16A-H, J and K (also known as ANO1-10, respectively), with some of its members reported to be (or to regulate) Cl^- channels. Indeed, TMEM16A was identified as a calcium (Ca^{2+})-activated Cl^- channel (CaCC)[73–75]. Also TMEM16B was reported to be the CaCC mediating olfactory signal transduction[76] and TMEM16F was identified as the main component of outwardly rectifying chloride channel (ORCC)[97]. However, TMEM16E, G, H, J and K do not appear to mediate ion transport[70,71]. Besides transepithelial ion transport, some TMEM16 proteins were reported to also play a variety of physiological functions ranging from being Ca^{2+}-dependent lipid scramblases[72,167], regulating other ion channels, to mediating smooth muscle contraction, olfaction, phototransduction, nociception, and control of neuronal excitability[70,71,168].

TMEM16A has a fundamental importance for Ca^{2+}-dependent Cl^- secretion in various epithelia, namely in the airways, salivary gland, pancreatic gland, and hepatocytes[105,106,169]. Indeed, in vivo knockdown of TMEM16A resulted in reduced fluid secretion in salivary glands[169]. Importantly, native epithelia of mice with genetic ablation of TMEM16A fail to generate Ca^{2+}-activated Cl^- transport, namely in the airways, and also evidence compromised mucociliary clearance with accumulation of mucus in the airways, in striking similarity to CF respiratory disease[105,106,170]. In addition to Cl^-,

TMEM16A was also shown to transport HCO_3^- after physiological stimulation[171,172], suggesting that this channel could also replace CFTR-mediated HCO_3^- transport. Altogether, these data demonstrate the important role of TMEM16A in fluid secretion and make it an attractive candidate for novel treatments for CF to compensate for defective CFTR-mediated anion transport.

Notwithstanding, we still miss essential knowledge on how to stimulate TMEM16A independently of Ca^{2+}, an essential requirement for its potential pharmacological applications. Although TMEM16A was reported to localize in the apical membrane of airway epithelial cells[99,170], it is present at the cell surface at low levels[170]. Moreover, little is known about regulation of TMEM16A traffic, namely which factors promote its plasma membrane (PM) localization. Intriguingly, recent studies show that TMEM16A can also play a tethering role of receptors, e.g., the inositol trisphosphate (IP_3) receptor - and endoplasmic reticulum (ER) Ca^{2+} stores to the PM[173]. According to this hypothesis, intracellular TMEM16A (and possibly other TMEM16 proteins) may not be the channels themselves, but instead mediate activation through coupling of Ca^{2+} signals of other membrane-localized channels[174]. Understanding how this regulation takes place is very relevant for human disease, since TMEM16A was also reported to play a role in other disorders, namely various forms of cancer[175].

In any case, substantial knowledge is missing regarding the molecular basis of Ca^{2+}-dependent Cl^- transport by TMEM16 proteins, as we still lack key pieces of information on most basic aspects, like how (and whether) they traffic to the PM. Yet, this is a crucial aspect for a detailed molecular mechanism of TMEM16A regulation or of its regulation of other channels. An outstanding question is thus under which conditions is TMEM16A located intracellularly and what factors promote its PM localization.

Early studies on TMEM16A proposed the alternative name of anoctamin 1 since it exhibited selectivity for anions and was believed to have eight (oct-) transmembrane domains[73]. In fact, high-resolution structural analysis of the fungal homologue from the fungus *Nectria haematococca* nhTMEM16, revealed 10 instead of eight transmembrane domains[69] which was subsequently confirmed by a topological model proposed for TMEM16A. TMEM16A operates as a dimer according to initial biochemical analyses and to the structural studies[176].

Within this background, we report here the establishment of a microscopy-based traffic assay on the physiologically relevant CFBE (CF Bronchial Epithelial) cell line stably transduced to express a reporter of TMEM16A traffic under an inducible promoter. This TMEM16A traffic reporter contains enhanced green fluorescent protein (eGFP) fused to

the C-tail of TMEM16A and a triple hemagglutinin (3HA) tag at its first extracellular loop so as to detect PM localized TMEM16A by use of anti-HA antibody without cell permeabilization. Similarly to previously described for CFTR[165], this double-tagged reporter allows for ratiometric readouts of traffic efficiency on a single cell basis, thus constituting a reliable cellular model to study TMEM16A traffic. Results shown here for this cellular model demonstrate the robustness and sensitivity of the assay. Applying this assay in systematic loss-of-function (siRNA knockdown) gene screens[164] will allow identification of TMEM16A traffic regulators and potential drug targets for CF.

Results

Although TMEM16A was previously reported to localize in the apical membrane of airway epithelial cells[99,170], we also first aimed to confirm this observation. Interestingly, specific staining of TMEM16A in cryosections of human airways (CF and non-CF) evidenced that some TMEM16A localizes to the apical surface, but there is a significant fraction which remains intracellularly located, particularly in CF airways (Fig. S4 – Appendix 1). These data thus emphasize the need to identify traffic regulators that promote TMEM16A PM expression, so as to use this Cl^- channel as a robust alternative to compensate for the absence of CFTR-mediated Cl^- transport in CF.

TMEM16A traffic reporter

The inducibility of the expression of 3HA-TMEM16A-eGFP traffic reporter (Figs. 8A, S1 – Appendix 1) by 1 µg/mL doxycycline (Dox) was confirmed by WB with the TMEM16A-specific antibody (anti-DOG1) showing a very significant increase in the levels of TMEM16A in induced vs non-induced cells (Fig. 8B). We then determined the time course of the induction which starts to be noticeable after 6 h of Dox induction (Fig. S5 – Appendix 1). PM localization of 3HA-TMEM16A-eGFP is observed after 13 h of Dox, becoming quite distinct from 20 h onwards. Next, we assessed the stability of TMEM16A expression after shutdown of transcription and our data indicate no reduction of TMEM16A steady-state levels at least up to 13 h after Dox removal.

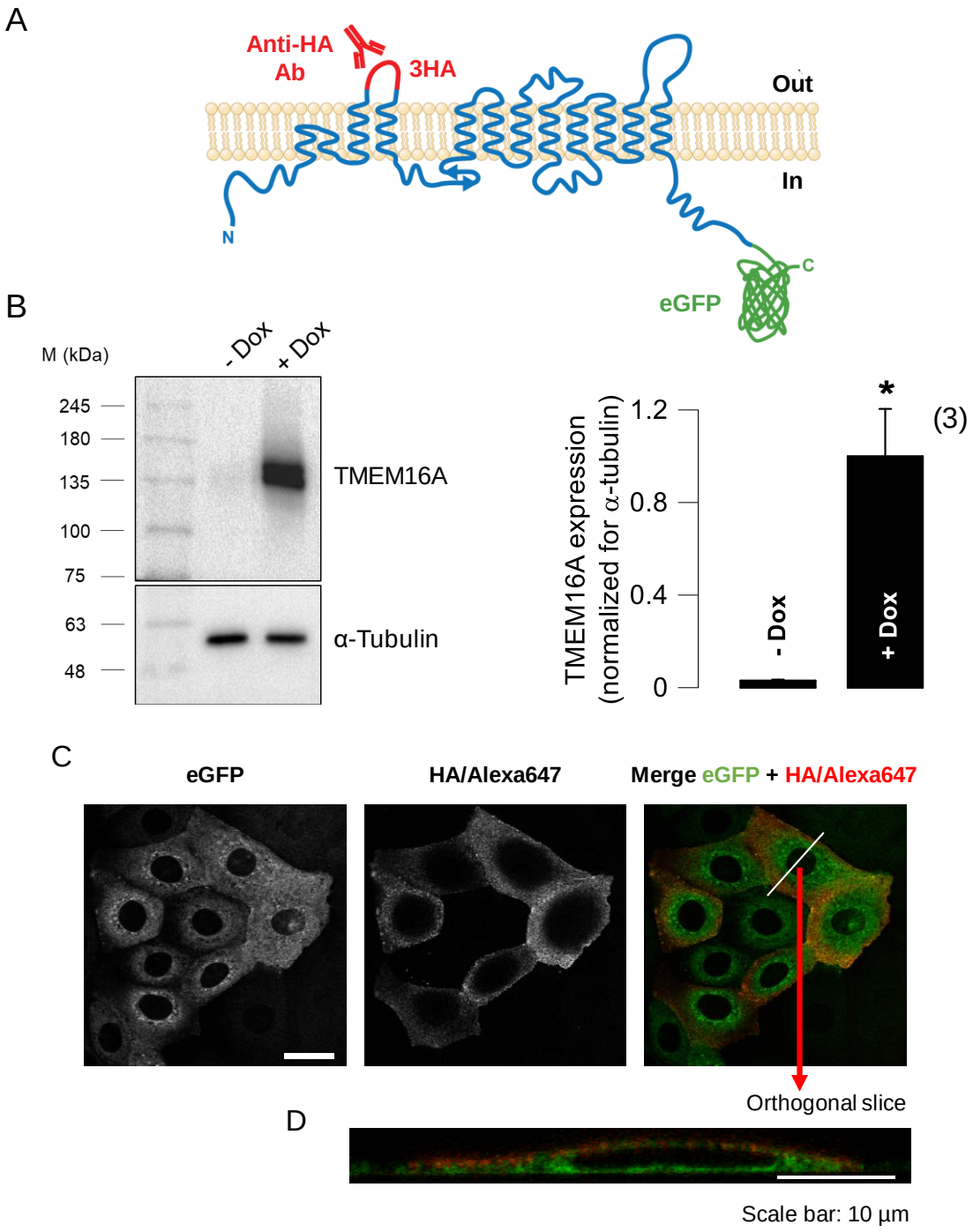

Figure 8 – Schematic representation of the 3HA-TMEM16A-eGFP traffic reporter construct and TMEM16A expression levels and intracellular localization after induction. (A) Topology of the TMEM16A protein showing the ten transmembrane domains. eGFP was fused to the C-terminus of TMEM16A via a 17-amino acid linker sequence (Fig. S1 – Appendix 1). The triple hemagglutinin (3HA) tag was introduced in the first extracellular loop and becomes accessible to the extracellular space when the construct is inserted in the PM. Cells were grown in the presence of 1 µg/mL Dox for 48 h so as to induce double-tagged TMEM16A expression. **(B)** WB of CFBE 3HA-TMEM16A-eGFP cells non-induced (−Dox) or induced (+Dox) where TMEM16A was detected by the primary antibody DOG1 (1:500) demonstrating the higher levels of TMEM16A in induced vs non-induced cells and thus confirming TMEM16A-inducibility in this cell line. Endogenous protein is not detected since it is expressed at much lower levels. α-Tubulin was used as a loading control and molecular mass markers are shown on the left (number of experiments). **(C)** Images showing TMEM16A expression and PM fraction in unpermeabilized CFBE cells. Left panel: total amount of

expressed TMEM16A, represented by eGFP fluorescence. Middle panel: Alexa Fluor® 647 (immuno) fluorescence of anti-HA antibody detecting 3HA tags exposed extracellularly, i.e., TMEM16A molecules present at the PM. Right panel: merged image of the two fluorescence channels: Green – eGFP, red – HA/Alexa 647. Images were acquired in Leica TCS SP8 confocal microscope (objective: 60x water, NA 1.4). Scale bar = 30 μm. **(D)** Orthogonal slice (z plane) of a representative cell displayed where it is possible to confirm that the anti-HA antibody (HA/Alexa647) – represented in red – is staining only the PM subcellular localization of the CFBE 3HA-TMEM16A-eGFP cells. Scale bar = 10 μm.

Given its localization at an extracellular loop (Fig. 8A), the 3HA-tag only becomes exposed to the extracellular environment when the construct is inserted in the PM. Thus, its detection via immunofluorescence with anti-HA Ab-Alexa Fluor® 647 without cell permeabilization confirms the presence of 3HA-TMEM16A-eGFP at the cell surface (Fig. 8C). PM subcellular localization of the 3HA-TMEM16A-eGFP construct in CFBE cells is further supported by the orthogonal projection (z-plane) of a representative cell (Fig. 8D) showing that the anti-HA antibody staining is only observed at the PM. The CFBE 3HA-TMEM16A-eGFP cells were subject to cell sorting to optimize the homogeneous expression of the construct (Figs. S2, S3 – Appendix 1). The efficiency of TMEM16A traffic can then be determined in individual cells using a ratiometric (Alexa Fluor® 647/ eGFP) fluorescence microscopy-based measurement.

Electrophysiological characterization

To functionally characterize the 3HA-TMEM16A-eGFP construct, Ussing chamber experiments in polarized cell monolayers of CFBE cells demonstrated that cells treated with Dox to induce 3HA-TMEM16A-eGFP expression exhibit equivalent short-circuit currents ($I_{eq\text{-}SC\text{-}ATP}$) upon stimulation with ATP (Fig. 9A, upper panels) which were significantly larger than those measured in non-induced cells (Fig. 9B). In order to determine that the observed differences were due to CaCC currents (and not to e.g., Ca^{2+}-activated potassium (K^+) channels), similar experiments were also performed in the presence of CaCC inhibitor A01 (Fig. 9A, lower panels), which showed a large decrease in ATP-induced currents, being the remaining observed currents no different between induced and non-induced CFBE cells (Fig. 9B).

To further validate the physiological relevance of this cell line as a bona fide model for a screening platform, we next characterized the activity of the double-tagged TMEM16A construct for their ability to conduct Cl^- using the patch-clamp technique (Fig. 9C). Analysis of the whole-cell currents detected in Dox-treated cells upon ATP stimulation showed, similarly to Ussing chamber data, significantly larger currents than

those measured in non-induced cells (Fig. 9D,E). Moreover, patch-clamp experiments were also performed in HEK 293 – as TMEM16A-null cells – by transient transfection with the 3HA-TMEM16A-eGFP construct either with or without induction (Fig. S6 – Appendix 1). Doxycycline induced cells showed significantly increased current densities when compared with non-induced cells. PM expression of the double-tagged TMEM16A construct was also confirmed in these cells (Fig. S7 – Appendix 1). Altogether, these data fully demonstrate that the double-tagged construct preserves the TMEM16A functional integrity and thus likely its regulation by multiple protein interactions is maintained in the physiologically relevant CFBE cells.

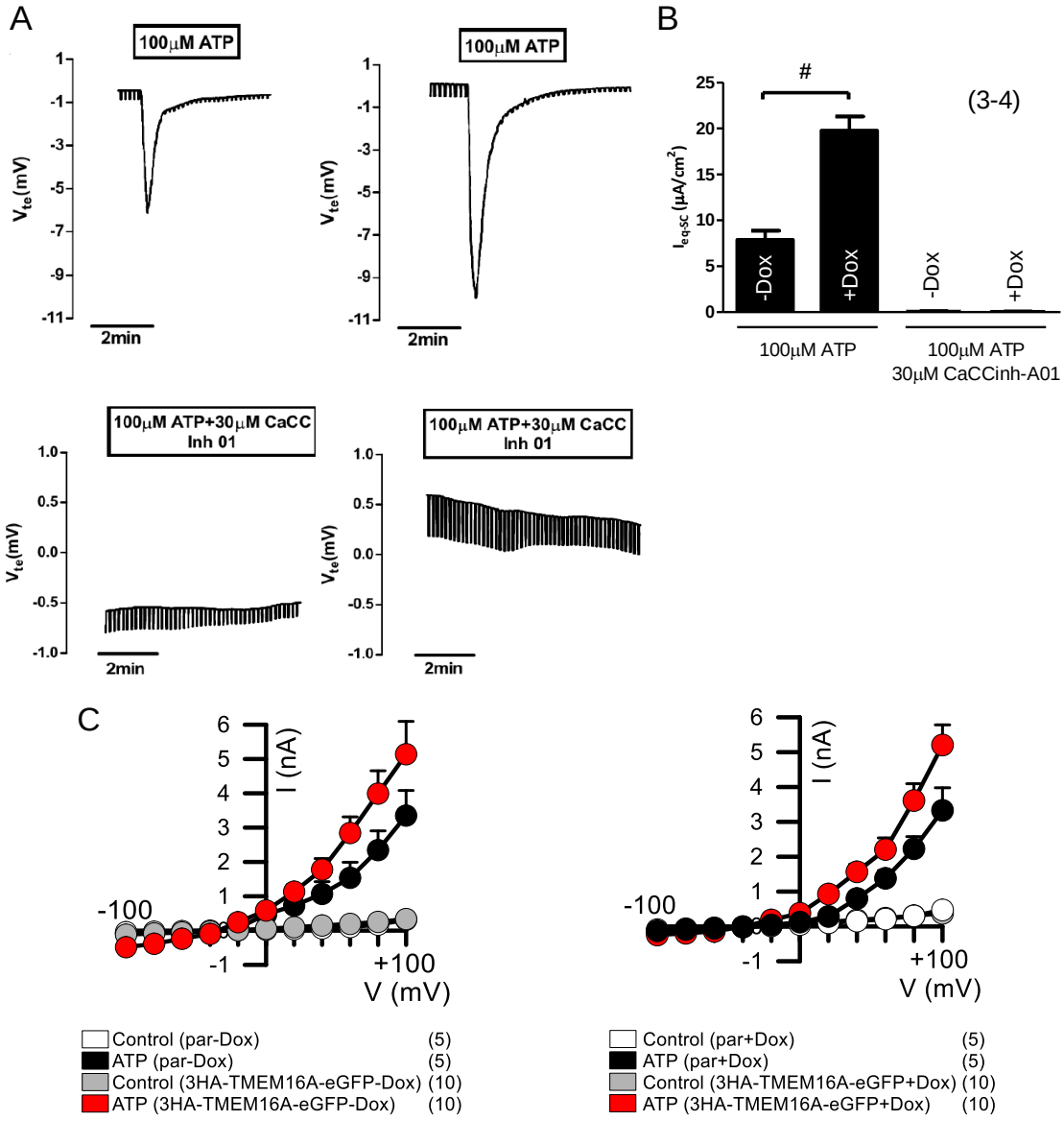

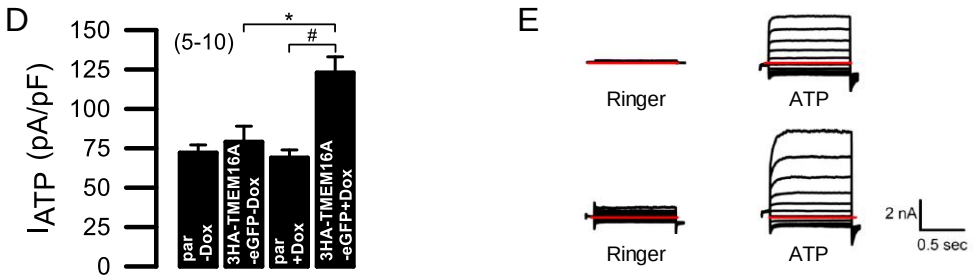

Figure 9 – Functional assessment of 3HA-TMEM16A-eGFP construct in CFBE cells by transepithelial Cl^- transport measurements in Ussing chamber and whole-cell patch-clamp. (A) Original Ussing chamber tracings obtained for ATP-induced Cl^- currents in the absence (top tracings) or in the presence (lower tracings) of CaCC inhibitor AO1 for CFBE 3HA-TMEM16A-eGFP cells non-induced (left) or after Dox induction (right); **(B)** Summary of $I_{sc\text{-}eq}$ currents of CFBE 3HA-TMEM16A-eGFP cells non-induced (−Dox) or after Dox induction (+Dox). Data are represented by mean ± SEM (number of experiments) and statistical analyses were performed by GraphPad Prism 6.0 using unpaired t-test where "#" indicates statistically significant differences ($p < 0.05$). Functional assessment of 3HA-TMEM16A-eGFP construct in CFBE cells vs parental CFBE cells by whole-cell patch-clamp; **(C)** Current/voltage (I/V) curves -100 mV to +100 mV for 3HA-TMEM16A-eGFP (grey, red) and parental (white, black) CFBE cells. Cells in Ringer (white, grey) or after stimulation with 100 µM ATP (black, red) non-induced (left) or after Dox induction (right). All solutions contained 50 nM TRAM34, a potassium (K^+) channel inhibitor to discard Ca^{2+}-activated K^+ currents and the number (n) of experiments is indicated in front of each label. **(D)** Delta of the average of ATP-induced current densities. **(E)** Overlay currents induced by ATP (100 µM) in CFBE 3HA-TMEM16A-eGFP cells. Data show a pronounced increase in whole-cell currents after Dox induction (bottom) vs non-induced cells (top) upon ATP stimulation. '*' indicates statistical significance of induced (+Dox) vs non-induced (−Dox) CFBE 3HA-TMEM16A-eGFP cells ($p < 0.05$ in unpaired t-test) and '#' indicates statistical significance of 3HA-TMEM16A-eGFP vs parental CFBE cells ($p < 0.05$ in unpaired t-test). Data in collaboration with Joana Lérias, Nikhil Awatade and Iris Silva.

siRNA microscopy-based traffic assay

To assess the suitability of the microscopy-based traffic assay as a platform to identify putative novel regulators of TMEM16A traffic, we next performed reverse transfection in siRNA pre-coated microscopy plates. As previously optimized[165,177], a treatment time of 72 h for siRNAs was selected. Expression of the 3HA-TMEM16A-eGFP construct was induced during the last 48 h of siRNA treatment. Image quantification was performed with CellProfiler[160] using the previously described analysis pipelines for CFTR: one to calculate the illumination correction (for background subtraction) and another to perform background subtraction, cell segmentation, fluorescence integration and basic quality control[165].

Screening a pilot siRNA library with the 3HA-TMEM16A-eGFP cell line revealed several siRNAs significantly affecting its traffic, as shown in representative immunofluorescence images (Fig. 10A). After expression induction of 3HA-TMEM16A-eGFP, a significant amount of TMEM16A is detected at the PM in the negative control assay, i.e., "Scrambled" siRNA (siScrbld) treated cells. The high sensitivity and large dynamic range of this assay are shown by the significant changes in the fluorescence

ratio of PM versus total TMEM16A (Fig. 10B), for which the screen avgScores ranged between −5.8 and +5.4 (data not shown). In our pilot screen, we identified COPB1 siRNA (Fig. 10A, 2nd row from top) as a significant TMEM16A traffic enhancer (avgScore = +3.81), without increasing total TMEM16A protein expression levels (Fig. S8 – Appendix 1) and the siRNA targeting ESYT1 – extended synaptotagmin-1 (Fig. 10A, 3rd row from top) gene as a reproducible traffic inhibitor (avgScore = −1.67). Treatment with TMEM16A-siRNA (siTMEM16A) significantly decreased the fluorescence signal in almost all cells (Fig. 10A, bottom row), indicating a high transfection efficiency as well as correct association of the Alexa Fluor® 647-fluorescence signal to TMEM16A-eGFP expression. Although the expression level is not totally homogenous across all cells, traffic efficiency is robust to such variations due to the ratiometric measurements.

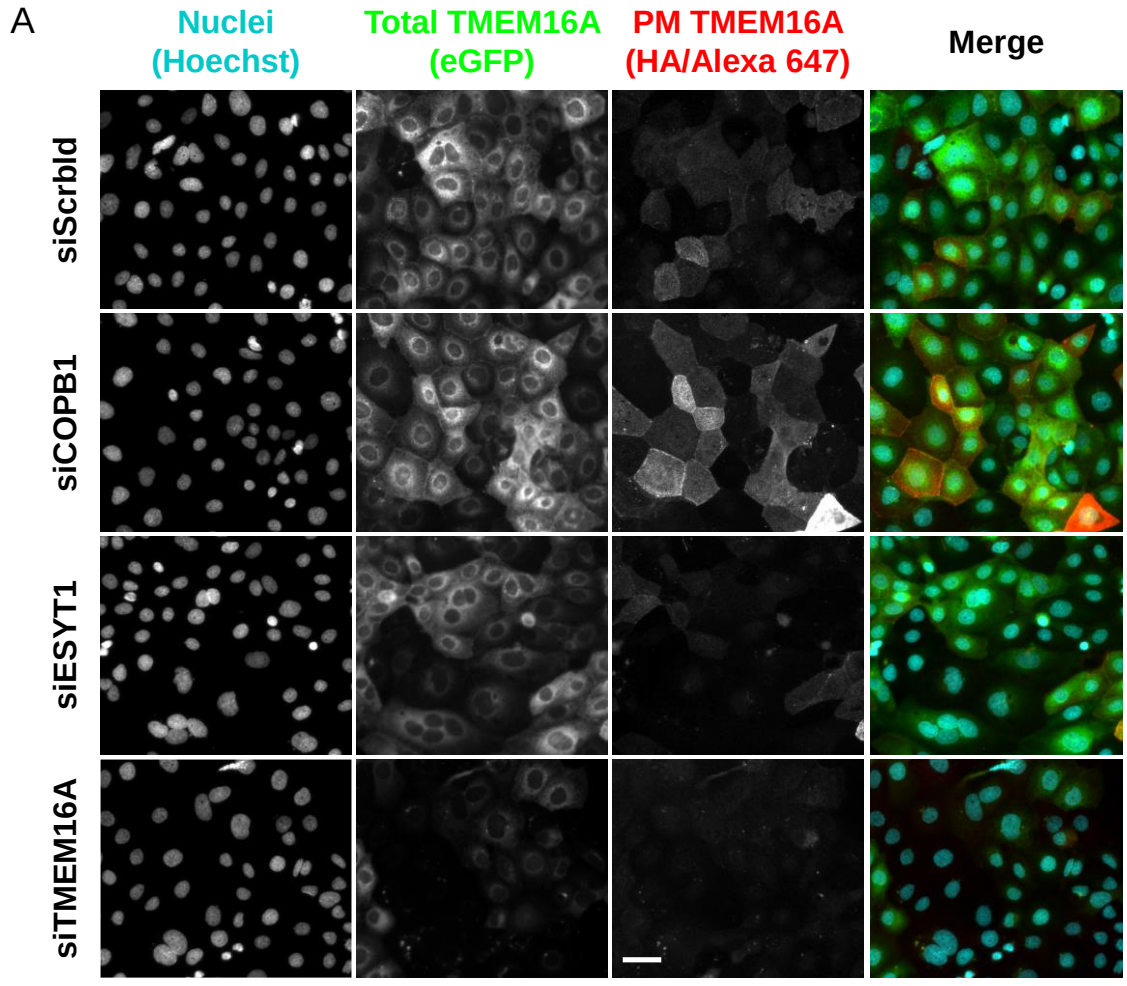

B

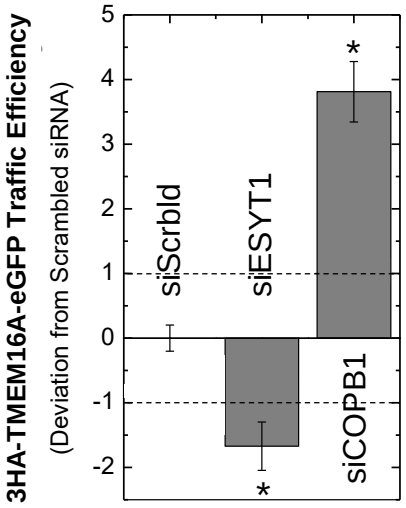

Figure 10 – Representative widefield epifluorescence microscopy images obtained for the TMEM16A traffic screen. (A) CFBE cells expressing the 3HA-TMEM16A-eGFP construct were treated with distinct siRNAs and stained with the anti-HA antibody without cell permeabilization (see Methods). Treatment with a siRNA targeting TMEM16A itself (siTMEM16A) shows a specific detection of TMEM16A and a high transfection efficiency (Bottom row). Knocking down COPB1 (siCOPB1) significantly enhanced traffic of 3HA-TMEM16A-eGFP (2nd row from top) and knocking down ESYT1 (siESYT1) significantly decreased it (2nd row from bottom). Images were acquired in an Olympus Scan^R microscope. Exposure times at maximum light brightness for Hoechst, eGFP and Alexa Fluor® 647 were 10–20 ms, 500 ms and 2000 ms, respectively. Scale bar = 50 μm. Images were quantified to determine traffic efficiency (see Methods). **(B)** Data are presented as the mean deviation to negative controls ± SD for all siRNAs with the mentioned targets and '*' represents statistical significance of COPB1 or ESYT1 vs Scrambled siRNA ($p < 0.05$) in a WelchTwo-Sample t-test (n = 3).

Biological relevance of a hit: the role of extended synaptotagmin (ESYT1) on TMEM16A

In order to demonstrate the biological relevance and significance of this novel microscopy-based traffic assay, we showed the impact of extended synaptotagmin-1 (ESYT1) on TMEM16A traffic and function. The reason why we chose ESYT1 (FAM62A) is because, besides having an interesting biological function (being an ER-PM tethering protein), this protein was also described as a TMEM16A interactor in a previous proteomics study by Hartzell and colleagues[178]. Although ESYT2 and ESYT3 were not hits in such study, we decided to also assess their effect on TMEM16A, given their proximity to ESYT1. To this end, we performed additional experiments to determine both PM localization (immunostaining) after liquid transfection (see Methods) and function (patch-clamp) in CFBE 3HA-TMEM16A-eGFP cells transfected for 72 h with siRNAs targeting COPB1 as well as ESYT1, ESYT2 and ESYT3. Our immunostaining data (Fig. 11) demonstrate that the knockdown of COPB1 significantly increased TMEM16A PM expression. Also by immunostaining, we observed that the knockdown of ESYT1 and ESYT2 significantly decreased TMEM16A PM expression (Fig. 11); ESYT3 knockdown

did not cause a significant change in TMEM16A PM levels, but this is likely due to its very low levels in CFBE cells (Fig. S9 – Appendix 1).

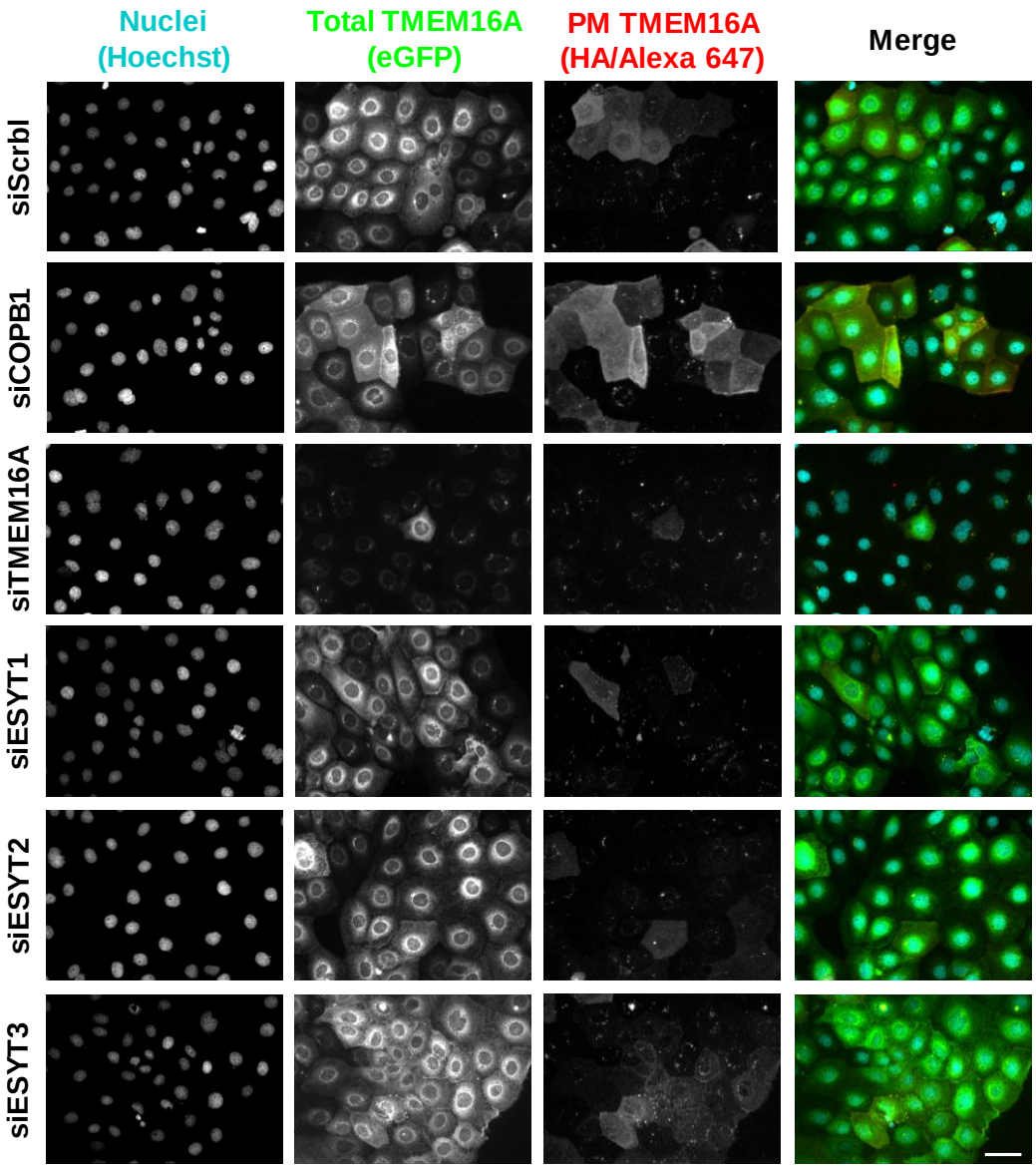

Figure 11 – Confirmation of effects of screen hits on TMEM16A PM localization. Representative widefield epifluorescence microscopy images were obtained after liquid siRNA transfection of CFBE 3HA-TMEM16A-eGFP cells with distinct siRNAs (Table S7 – Appendix 4) and stained with the anti-HA antibody without cell permeabilization. Treatment with an siRNA targeting TMEM16A (siTMEM16A) shows once more a specific detection of TMEM16A and a high transfection efficiency. Traffic of 3HA-TMEM16A-eGFP was greatly enhanced by knocking-down COPB1 (siCOPB1) and significantly decreased by knocking-down ESYT1 (siESYT1) and ESYT2 (siESYT2). The knockdown of ESYT3 (siESYT3) did not seem to cause any effect on TMEM16A PM levels, what must be due to its very low expression levels in CFBE cells (see Fig. S9 – Appendix 1). Images were acquired with an Axiovert 200M fluorescence microscope (Zeiss, Jena, Germany), using a 20x dry objective (n = 3). Scale bar = 50 µm.

Patch-clamp data (Fig. 12) demonstrate that COPB1 knockdown (KD) significantly increases TMEM16A current density, compared to scrambled siRNA

transfected cells, used as negative control (Fig. 12B) and that knockdown of ESYT1, ESYT2 and ESYT3 significantly decreases TMEM16A current density, also in comparison to scrambled siRNA transfected cells (Fig. 12B).

Our approach to address the specificity of the siRNA ESYT1 experiments was 2-fold: 1) by targeting ESYT1 with three different siRNAs, namely: s23605 and s23606 (both used in the screen with negative scores of −1.4 and −1.9, respectively) and s23607 which was used in immunofluorescence validation as well as in all functional experiments; 2) by showing the correspondent decrease on ESYT1 mRNA levels (Fig. S9 – Appendix 1).

Further, to determine the specificity of COPB1 and ESYT1 on TMEM16A, we tested their effects on another PM protein – the epidermal growth factor receptor (EGFR) by cell-surface biotinylation. Our data (Fig. S10 – Appendix 1) show that the knockdown of either siCOPB1 or siESYT1 does not alter PM levels of EGFR.

Moreover, we performed additional experiments to determine whether the regulatory mechanisms determined here for 3HA-TMEM16A-eGFP also apply to endogenously expressed TMEM16A in parental CFBE cells (Fig. S11 – Appendix 1). These data indeed demonstrate that the impact of screen hits COPB1 and ESYT1 on endogenous TMEM16A function is similar to that observed for 3HA-TMEM16A-eGFP (compare with data in Fig. 12) being thus physiologically relevant.

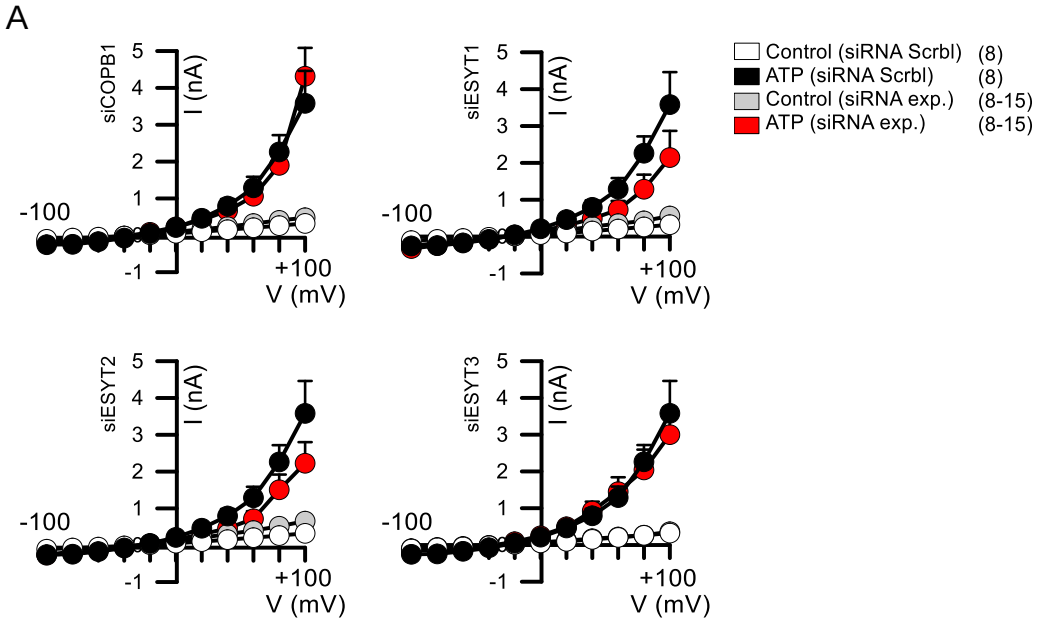

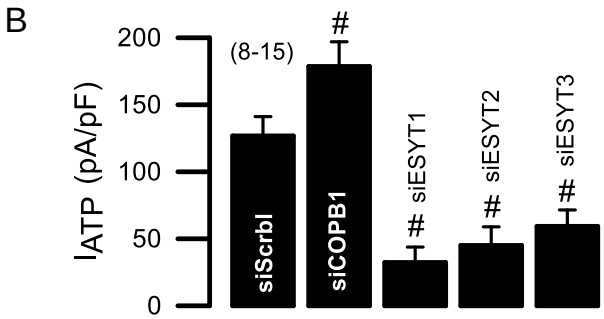

Figure 12 – Impact of screen hits on TMEM16A function. (A) Whole-cell patch-clamp data obtained for CFBE 3HA-TMEM16A-eGFP cells induced with doxycycline and transfected with siRNAs targeting COPB1 (upper left), ESYT1 (upper right), ESYT2 (lower left), ESYT3 (lower right) or Scrambled (control). Current/voltage (I/V) curves -100 mV to +100 mV for each siRNA under test (grey, red) or Scrambled (white, black) in Ringer (white, grey) or after stimulation by 100 µM ATP (black, red). All solutions contained 50 nM TRAM34, and the number (n) of experiments is indicated in front of each label. **(B)** Delta of the average of ATP-induced current densities. '#' indicates statistical significance of ATP-stimulated currents of the respective siRNA vs Scrambled ($p < 0.05$ in unpaired t-test). Experiments performed by Joana Lérias.

Discussion

Overall features of the cell-based TMEM16A traffic assay

Herein we report the development of a new cell-based assay for the identification of regulators of TMEM16A. Indeed, scaling-up of the current assay to high-throughput screening (HTS) microscopy allows to identify, on a global scale, genes regulating TMEM16A traffic and also drug discovery. So far, no traffic studies have been conducted for this clinically relevant protein mostly because no good cellular model was available. Yet, this is a crucial aspect to our mechanistic understanding of TMEM16A physiological and pathological role.

The new tool described here includes a novel cell line expressing an inducible TMEM16A traffic reporter, a traffic assay adequate to be scaled-up for microscopy-based HTS and an automated quantification method.

We have validated this traffic assay by applying it to a small number of siRNAs. These siRNA experiments showed that the TMEM16A traffic assay is specific (as evidenced by control siRNAs) and robust (good dynamic range), thus demonstrating that it can be used to identify gene regulators of TMEM16A traffic as potential drug targets.

As already previously described for a similar screening platform[165], the current tool has various major advantages vs other alternative assays, such as the one measuring TMEM16A activity in FRT cells[179–181]. These advantages include: i) the

conditional (Tet-inducible) expression of TMEM16A which allows assessing the effects of genes/compounds before the target protein (TMEM16A) is expressed, so as to detect their impact on the early stages of secretory traffic; ii) the double-tagged construct allows for a ratiometric readout (the protein fraction at the PM vs total protein expressed); and iii) the microscopy approach employed for the current assay enables the application of a quality control based on several cell parameters (e.g., total number of cells, cell shape, cell size, etc) and statistical analyses based on individual cells, which is not possible in the plate reader. Such characteristics make the current assay to be of higher potential for screening than the previously reported methods.

A tool to study physiological regulation of TMEM16A

The current novel cellular model clearly demonstrates that TMEM16A localizes to the PM, recapitulating the initially reported findings[99,170]. This constitutes a crucial requirement for the physiological relevance of this assay in CF biomedical research. In some neuron subtypes the TMEM16A PM localization was described to be restricted to just specific membrane domains[173] and the fungal homologue nhTMEM16 was not found to be present at all at the PM when heterologously expressed in HEK cells[175]. Although TMEM16A was reported to localize in the apical membrane of airway epithelial cells [99,170], our data show that TMEM16A occurs mostly at the apical surface of non-CF bronchial epithelia, but it is remains largely intracellularly localized in CF epithelia.

Admittedly, our assay employed a double-tagged construct and the cellular sorting of CFBE cells for high expression levels, which are far from physiological context. Nevertheless, our data demonstrate that the impact of screen hits COPB1 and ESYT1 on endogenous TMEM16A function is similar to that observed for 3HA-TMEM16A-eGFP. Therefore, and as demonstrated for our siRNA data shown here, the use of this cellular model can help identify physiologically relevant genes and/or compounds that regulate TMEM16A PM traffic, having thus potential to be used in functional genomic screens.

Indeed, in the siRNA experiments performed here, we identified that siCOPB1, a component of the COPI trafficking machinery enhances the PM localization of TMEM16A. Although COPI has been implicated in secretory traffic between the Golgi and the ER both in the anterograde and retrograde direction, inhibition of one COPI component with enhanced TMEM16A at PM is in line with the observed increase in the anterograde traffic of some PM proteins, such as CFTR[165]. Moreover, and confirming the

present data, a recent study[182] also described that TMEM16A cell surface expression is suppressed by protein-protein interactions with ß-COP, of which COPB1 is a component.

We also found that siESYT1 inhibits TMEM16A PM traffic, thus indicating that the extended synaptotagmin-1 protein should promote the PM insertion of TMEM16A.

Physiological relevance of ESYT1 in promoting PM traffic of TMEM16A

Interestingly, ESYT1 is a member of the extended synaptotagmins (ESYTs) family of proteins with a new role in tethering the ER to the PM in a Phosphatidylinositol 4,5-bisphosphate (PIP_2) – and Ca^{2+}-dependent way[183]. This is consistent with the localization of TMEM16A yeast analogue Ist2 at these ER-PM junctions[184] and the recently proposed role of TMEM16 proteins in generating compartmentalized Ca^{2+} signals[175].

ESYTs participate in lipid transfer between the ER and PM[185], a role somewhat related to the scramblase function of some TMEM16 proteins. Thus, we have chosen ESYT1 and the two other members of this protein family – ESYT2 and ESYT3 – to be examined in more detail using immunostaining and patch-clamp analysis. The three ESYTs are ER proteins that participate in such tethering function via C2 domain dependent interactions with the PM that require PIP_2 in the case of ESYT2 and ESYT3 and also elevation of cytosolic Ca^{2+} in the case of ESYT1[183]. Although ESYT-dependent contacts are not required for store-operated Ca^{2+} entry, we found a clear inhibitory effect on receptor-mediated activation of TMEM16A which was confirmed by decreased PM levels of TMEM16A. This is somewhat surprising as the ESYTs were shown not to participate in the targeting of $InsP_3Rs$ to the apical region of hepatocytes[186]. Thus, although it was shown that the simultaneous loss of all three ESYTs has no effect on overall development and survival of mice, genes encoding Orp5/8, Orai1, STIM1 and TMEM110, other ER-PM membrane junction proteins are upregulated, which could potentially compensate for ESYT loss[187,188]. Our observation that GPCR-mediated activation of TMEM16A is compromised in cells with knockdown of ESYTs suggests that the Ca^{2+} dependent lipid transfer between ER membrane and PM is compromised, which also fits to the earlier observation of an enhanced and sustained accumulation of PM diacylglycerol (DAG) following PIP_2 hydrolysis by PLC activation[189].

Potential of the TMEM16A traffic assay for disease-related studies

In the context of CF, the TMEM16A traffic assay described here allows for: (i) identification of regulators of TMEM16A traffic (potential drug targets); (ii) development of compounds modulating high-potential drug targets from (i); (iii) direct discovery of compounds modulating TMEM16A traffic; (iv) gaining insight into mechanisms of TMEM16A secretory traffic. Moreover, insertion of the current construct into the previously described CFBE models of normal and mutant double-tagged CFTR[165] will also provide mechanistic insight into one currently TMEM16A key question, i.e., whether and how are the traffic of TMEM16A and CFTR coregulated.

Besides its relevance for CF, TMEM16A has also been reported to be a major player in tumorigenesis, having high TMEM16A expression levels been reported in multiple forms of cancer (reviewed in[175]). Although it is still unclear whether such high levels are cause or consequence of carcinogenesis, the current platform also allows for the identification of negative regulators of TMEM16A traffic as exemplified here for ESYT1. This demonstrates that the current assay enables similar workflows to identify traffic enhancers and inhibitors alike. Also, the 3HA-TMEM16A-eGFP construct could also be used to transform cellular models which could be more relevant to these pathologies.

TMEM16A was likewise proposed to modulate mucin secretion and airway muscle contraction[91] contributing to airway hyperresponsiveness[190,191]. These studies suggest that it may constitute a therapeutic target for limiting airway constriction in asthma, in which case it would be important to look for TMEM16A inhibitors. Although more recently TMEM16A was also described to have a protective role in the hyperresponsiveness of airway cells to lipopolysaccharide (LPS)[192], the current traffic assay can be of equal value to identify inhibitors/enhancers as well as to help clarifying a mechanistic role for TMEM16A also in these processes.

TMEM16 proteins have been described to operate as dimers, as also confirmed by high-resolution structural analysis of the fungal homologue nhTMEM16[69]. Nonetheless very little is known regarding the formation of heterodimers as well as on the properties of different TMEM16 dimers combinations. Insertion of similarly tagged constructs of other TMEM16 family members into the current CFBE cell model will certainly be useful to gain functional and mechanistic insight into such heterodimer combinations of TMEM16A.

Altogether, many studies on TMEM16A report a broad range of yet poorly understood properties many of high relevance to multiple diseases. The cellular model and traffic assay reported here can help shed light into these biological processes by the global identification of the intervenients in the molecular and cellular pathways underlying these conditions.

In conclusion, the TMEM16A traffic assay reported here is an improvement over current strategies for TMEM16A-based drug development for several human diseases, namely for CF. Moreover, it can also be used in functional genomic (siRNA/cDNA) screens to identify genes which regulate TMEM16A traffic which may be used as pharmacological targets to bypass the lack of functional CFTR in CF patients. This work model will also set the stage for a better knowledge of TMEM16A traffic, regulation, and its relationship with CFTR.

2. Regulation of TMEM16A by CK2 and its role in cellular proliferation

Introduction

Casein kinase 2 (CK2) is a highly ubiquitous and conserved serine/threonine kinase that forms a tetramer consisting of a catalytic subunit (CK2α) and regulatory subunit (CK2β)[193]. CK2 phosphorylates hundreds of substrates. It contributes to a large number of cellular processes, but its main functions are related to cell growth, proliferation, and cell survival[194]. It supports cell proliferation and survival by antagonizing caspase activity and by potentiating survival signals. A multitude of mechanisms may contribute to these antiapoptotic functions[195]. A common inhibitor of CK2 that has been frequently used in previous studies is 4,5,6,7-tetrabromobenzotriazole (TBB)[196]. The orally bioavailable selective inhibitor of CK2, CK4945 (silmitasertib), has been shown to be antiproliferative and anti-angiogenic. It has the potential to be the first oral CK2 inhibitor that may advance from clinical trials to treatment of cancer patients[197,198].

TMEM16A belongs to a family of Ca^{2+}-activated phospholipid scramblases and ion channels[70,71]. The 10 TMEM16 paralogs (ANO1-10; TMEM16A-K) are broadly expressed in epithelial and non-epithelial tissues[99]. TMEM16A is a Cl^- selective anion channel[82], with well described functions in a number of tissues. TMEM16A is upregulated during cellular dedifferentiation and in cultured cells. It increases proliferation in many different tissues[124,199–207], and is expressed at high levels, particularly in head and neck cancers[121,124,203]. Niclosamide has recently been identified as a potent inhibitor of TMEM16A[103]. Niclosamide is an anthelminthic drug approved by the U.S. Food and Drug Administration that was also shown to inhibit Notch signalling[208], a pathway that is well known to participate in tumorigenesis[209]. A number of antineoplastic mechanisms of niclosamide have been described. Thus, niclosamide was shown to inhibit nuclear factor kappa B (NF-κB), Wnt/ßcatenin signalling, the IL-6-JAK1-STAT3-pathway, GSK-3 and more[210–218]. A recent paper suggests cell cycle arrest by niclosamide through activation of the Let-7d/CDC34 axis[219].

Niclosamide has been used in a number of preclinical studies and even in clinical trials in patients suffering from prostate and colorectal cancer[213,215,220–224]. Apart from various anti-cancer effects, niclosamide also inhibits the Ca^{2+}-activated Cl^- channel TMEM16A. Blockade of TMEM16A is likely to take part in the inhibition of cell proliferation and cancer by niclosamide[124,203,225]. The present paper identifies a link between CK2 and TMEM16A, as CK2 supports membrane expression of TMEM16A.

Both silmitasertib and niclosamide inhibited proliferation of head and neck cancer cells. Importantly, simultaneous application of both drugs strongly augmented their antiproliferative effects. The data suggest a combined treatment by silmitasertib and niclosamide to strongly augment anti-cancer potency of the individual drugs[225].

Results

High-throughput assay identifies CK2 as a regulator of TMEM16A

A microscopy-based assay has been performed to identify novel regulators of the Ca^{2+}-activated Cl^- channel TMEM16A[226] (chapter 1.1). siRNA screening for interactors of TMEM16A was performed in CFBE airway epithelia cells overexpressing double-tagged TMEM16A. CFBE cells were chosen because we intended to identify proteins that could be targeted in order to improve TMEM16A function, and thus Ca^{2+}-dependent Cl^- secretion in cystic fibrosis airway epithelial cells[227]. We identified CK2 as a positive regulator of TMEM16A. Because TMEM16A is particularly known to be upregulated in head and neck squamous cell carcinomas (HNSCC), where CK2 also has a pro-cancerous role[227], we examined the hypothesis that CK2 promotes proliferation of the HNSCC cell lines Cal33 and BHY through activation of TMEM16A, which would have consequences for the treatment of HNSCC. siRNA-knockdown of the broadly expressed casein kinase 2 subunit α' (CK2α') was found to downregulate membrane expression of overexpressed TMEM16A containing a C-terminal green fluorescence protein (GFP) and an extracellular (human influenza hemagglutinin) HA tag (Fig. 13A–C). Membrane expression was detected using an extracellular HA tag and binding of a fluorescent antibody to the extracellular HA tag. We examined whether endogenously expressed TMEM16A is equally regulated by CK2 and used CFBE cells that express only endogenous TMEM16A. Indeed, plasma membrane (PM) expression of endogenous TMEM16A was significantly inhibited upon knockdown of CK2α' (Fig. 13D,E). This effect of knockdown of CK2α' appears to be specific as membrane expression of the common housekeeper ATPase Na^+/K^+-ATPase was not affected by the knockdown (Fig. S12 – Appendix 1).

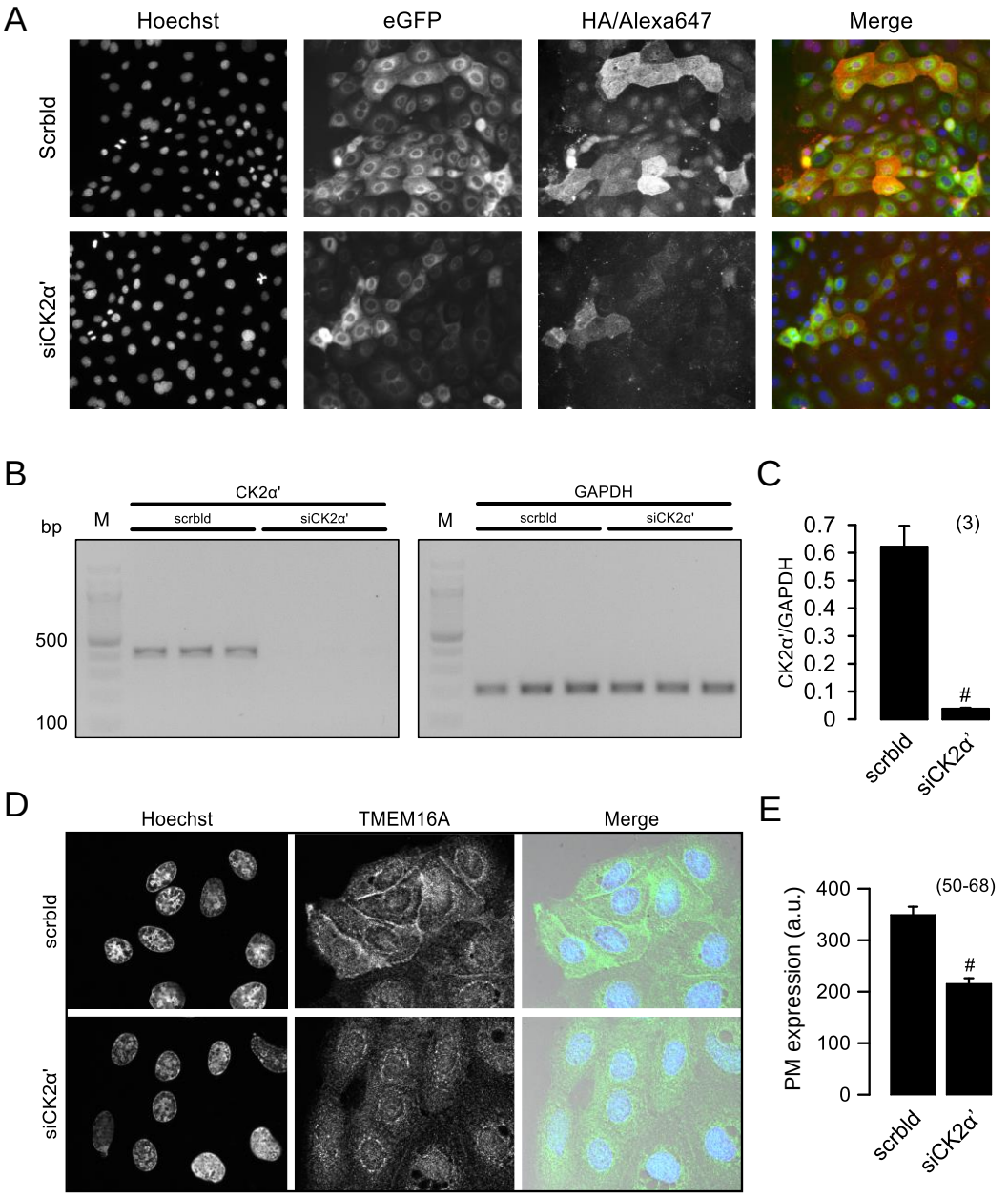

Figure 13 – CK2 controls membrane expression of TMEM16A in CFBE airway epithelial cells. (A) Expression of double tagged (eGFP and extracellular HA-tag) TMEM16A in CFBE airway epithelial cells. Membrane localized TMEM16A (Alexa647 positivity) was detected by an extracellular anti-HA antibody. **(B,C)** RT-PCR and densitometric analysis indicating successful knockdown of CK2α'. **(D,E)** Immunocytochemistry of TMEM16A expressed endogenously in CFBE cells. Membrane expression was reduced by knockdown of CK2α'. Mean ± SEM (number of experiments, or total number of cells measured in different experiments [>3]). #Significant inhibition ($p < 0.05$; unpaired t-test).

Knockdown or inhibition of CK2 inhibits activation of TMEM16A

TMEM16A is a Ca^{2+}-activated Cl^- channel that is activated through stimulation of G-protein coupled receptors (GPRCs) that couple to phospholipase C, such as ATP-activated purinergic receptors. Stimulation of CFBE cells with extracellular ATP

increases intracellular Ca^{2+}, which in turn will activate TMEM16A[226,228]. As shown in Fig. 14, ATP activated TMEM16A whole cell currents in CFBE cells. Activation was strongly suppressed by preincubation of the cells for 30 min with the CK2 inhibitor TBB (Fig. 14A). The summary of these experiments is shown in Fig. 14B as current/voltage relationships of ion currents activated in control cells (left) and in TBB-treated cells (right). We also found that the CK2 inhibitor CX4945 suppressed ATP-induced whole cell currents even more potently than TBB (Fig. 14C,D). In contrast, acute application of CX4945 to pre-activated TMEM16A did not clearly inhibit whole cell currents. Finally, knockdown of CK2α' (siCK2α') strongly attenuated TMEM16A currents stimulated by ATP (Fig. 14E,F). Similar to knockdown of CK2α' (Fig. 13D), CX4945 also inhibited membrane expression of TMEM16A (Fig. 14G, H).

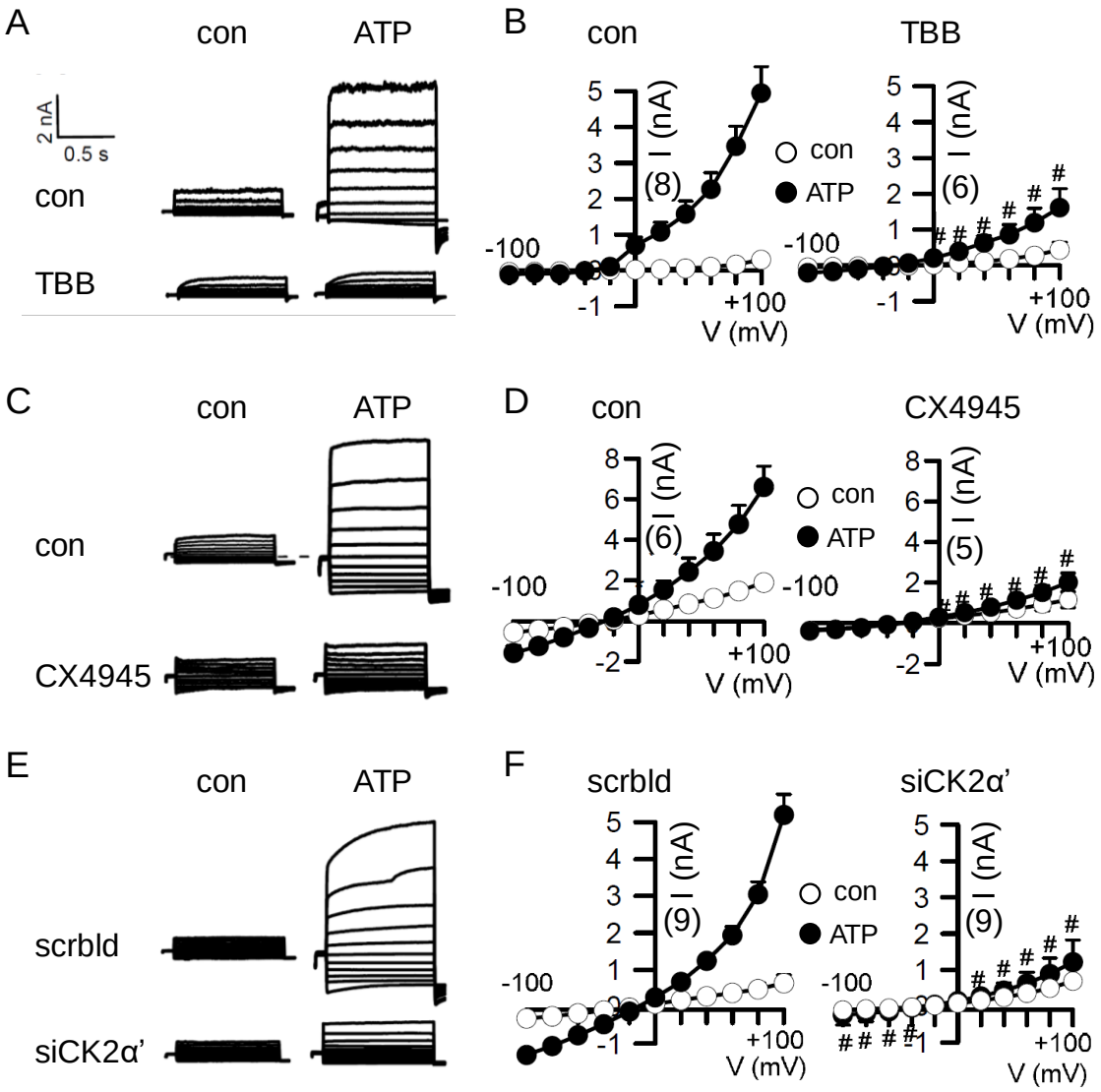

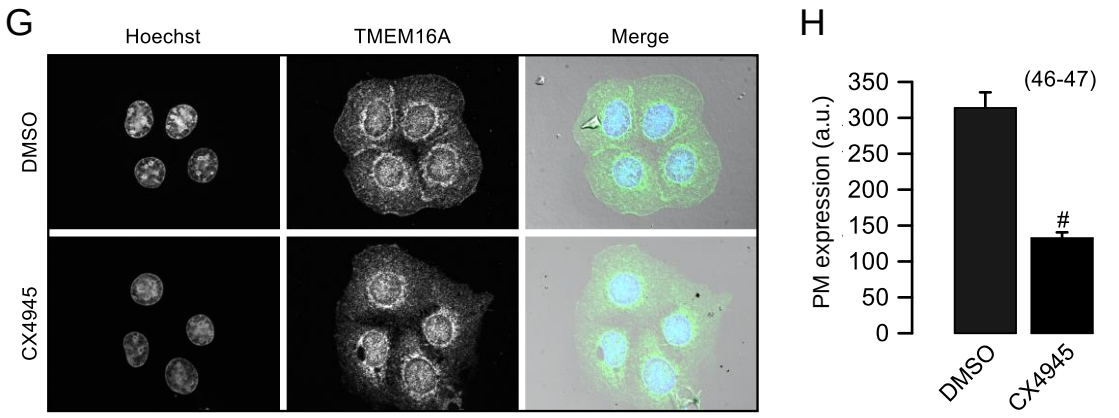

Figure 14 – Inhibitors of CK2 inhibit TMEM16A in CFBE airway epithelial cells. (A-F) Whole cell current overlay recorded in patch-clamp experiments and current/voltage relationships. ATP (100 µM) activated TMEM16A whole cell Cl^- currents that were strongly inhibited by the CK2 inhibitors TBB (10 µM; A,B) and CX4945 (20 µM; C,D), and siRNA-knockdown of CK2α' (E,F). **(G,H)** Plasma membrane (PM) expression of endogenous TMEM16A in CFBE cells and inhibition of PM expression by the CK2-inhibitor CX4945. Mean ± SEM (number of cells measured). #Significant inhibition ($p < 0.05$; unpaired t-test). Data in collaboration with Jiraporn Ousingsawat and Joana Lérias.

CK2 regulates membrane expression of TMEM16A in Cal33 head and neck cancer cells

TMEM16A is strongly expressed in head and neck cancer cells. The coding sequence of TMEM16A is located in the tumour-associated amplicon 11q13. High expression levels for TMEM16A correlate with poor survival of patients with head and neck cancers[203]. Our previous studies demonstrated the proliferative effect of TMEM16A in different head and neck cancer cell lines such as Cal27, Cal33 and BHY, as well as growth of soft tissue cancer in nude mice[124,203,225].

We therefore analysed CK2-dependent regulation of TMEM16A expression in Cal33 cells using siRNA for CK2α', which potently suppressed CK2α' mRNA as well as protein (Fig. 15A-C). However, siRNA-knockdown of CK2α' did not affect total expression of TMEM16A, as shown by Western blotting (Fig. 15D). In contrast and similar to CFBE cells, knockdown of CK2α' clearly reduced PM expression of TMEM16A in Cal33 cells (Fig. 15E,F). Accordingly, TMEM16A currents activated by ATP were also inhibited by knockdown of CK2α' (Fig. 15G). However, attenuation of TMEM16A currents was less pronounced than in CFBE cells, which is due to excessive levels of TMEM16A expression in Cal33 cells[203].

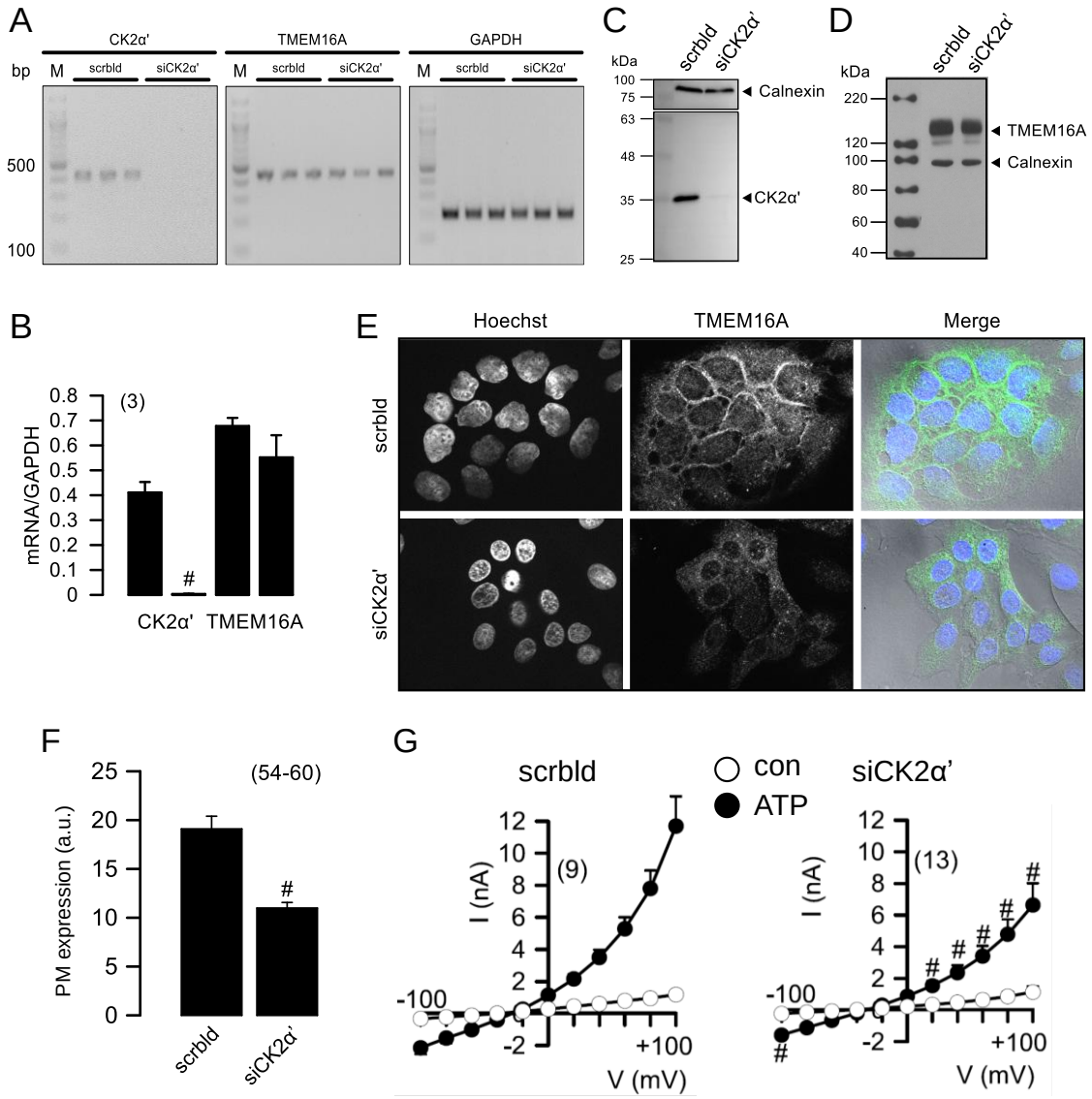

Figure 15 – Role of CK2 for PM expression of TMEM16A in Cal33 head and neck cancer cells. (A,B) RT-PCR and densitometric analysis indicating successful knockdown of CK2α' by siRNA for CK2α' in Cal33 head and neck cancer cells. Knockdown of CK2α' did not inhibit transcription of TMEM16A. **(C,D)** Western blot analysis indicating successful knockdown of CK2α' but unaffected expression of TMEM16A. **(E,F)** PM expression of TMEM16A expressed endogenously in Cal33 cells and inhibition of PM expression by knockdown of CK2α'. **(G)** Current/voltage relationships of ATP-activated TMEM16A whole cells currents, indicating inhibition of TMEM16A by knockdown of CK2α'. Mean ± SEM (number of experiments or total number of cells measured in different experiments [>3]). #Significant inhibition ($p < 0.05$; unpaired t-test).

Inhibition of CK2 and TMEM16A inhibits cell proliferation

Knockdown of TMEM16A attenuates cell proliferation[203], and this was also observed in the present study with Cal33 cells (Fig. 16A). siRNA-knockdown of CK2α' inhibited cell proliferation equally well. Notably, combined knockdown of both TMEM16A and CK2α' had a more pronounced inhibitory effect on cell proliferation (Fig. 16A). It

suggests that CK2 and TMEM16A control cell proliferation in part by independent mechanisms. This was also found when CK2 was inhibited by CX4945 instead of siRNA-knockdown. CX4945 alone inhibited proliferation similar to siRNA-CK2α', but CX4945 + siRNA-TMEM16A abolished proliferation completely (Fig. 16B).

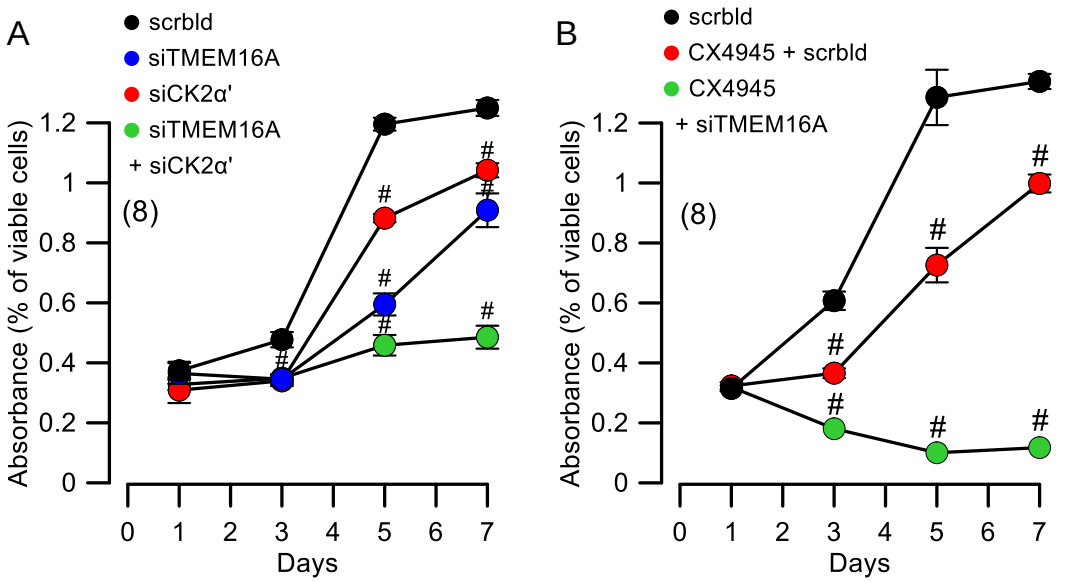

Figure 16 – Inhibition of proliferation by knockdown of CK2α' and TMEM16A. (A) Cell proliferation assessed in MTT assays and shown as absorbance. Both siRNA-knockdown of CK2α' and TMEM16A inhibited cell proliferation. Simultaneous knockdown of CK2α' and TMEM16A had a more pronounced inhibitory effect on cell proliferation. **(B)** Inhibition of cell proliferation by the CK2-inhibitor CX4945 (20 µM) and additional inhibitory effect of TMEM16A knockdown. Cells were transfected/treated with drugs 24h after seeding. Every 2 days, cells were again transfected and/or the medium with drugs was replaced, and experiments were performed. Mean ± SEM (number of experiments). #Significant inhibition ($p < 0.05$; unpaired t-test).

As outlined above niclosamide is a potent inhibitor of TMEM16A and an anticancer drug. It also inhibited proliferation of Cal33 cells in the present study (Fig. 17A). Again, the combination of niclosamide together with CX4945 completely inhibited cell proliferation (Fig.17A). We performed similar studies in BHY cells, another head and neck cancer cell line[203], in order to validate the results obtained in Cal33 cells. Application of only CX4945 or niclosamide inhibited cell proliferation by about 50%. In contrast, simultaneous application of CX4945 and niclosamide essentially abolished proliferation (Fig. 17B). Interestingly, the activator of TMEM16A, Eact[180], further augmented proliferation of BHY cells (Fig. 17B).

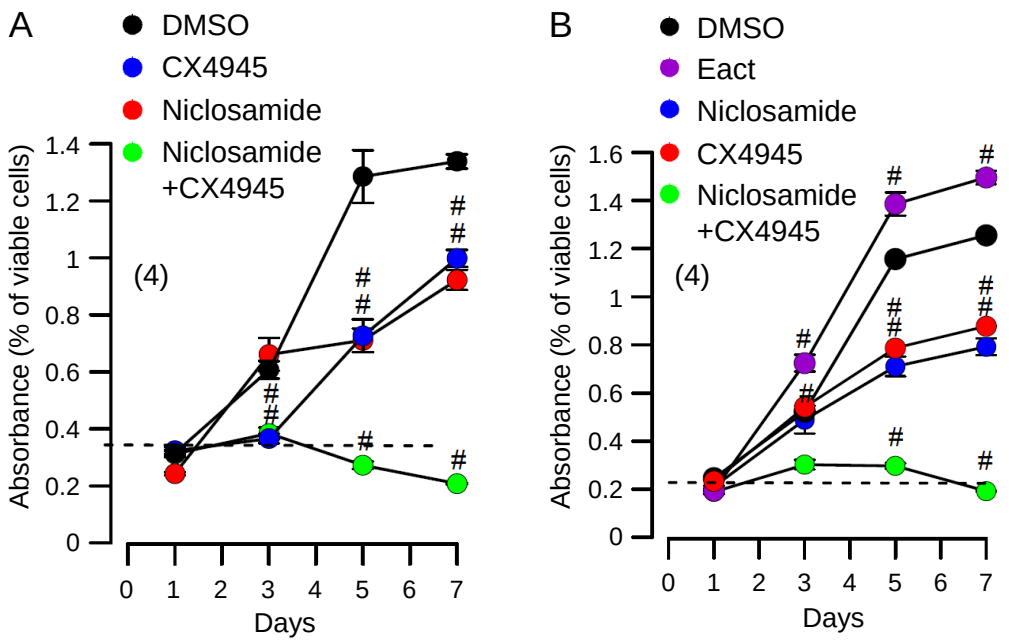

Figure 17 – Blockers of CK2 and TMEM16A inhibit proliferation of Cal33 and BHY head and neck cancer cells. (A) Blocking CK2 by CX4945 (20 µM) and blocking TMEM16A by niclosamide (0.5 µM) inhibited proliferation of Cal33 cells. Simultaneous application of both blockers had an additive effect. **(B)** Enhanced cell proliferation of BHY cells induced by the TMEM16A-activator, Eact. Blocking CK2 by CX4945 (20 µM) and blocking TMEM16A by niclosamide (0.5 µM) inhibited proliferation of BHY cells. Simultaneous application of both blockers had an additive effect. Cells were treated with drugs 24h after seeding. Every 2 days, the medium with drugs was replaced, and experiments were performed. Mean ± SEM (number of experiments). #Significant inhibition ($p < 0.05$; unpaired t-test). Data in collaboration with Jiraporn Ousingsawat.

Inhibition of TMEM16A and inhibition of CK2 attenuates receptor-mediated increase in the intracellular Ca^{2+} concentration

TMEM16A has a pronounced impact on intracellular Ca^{2+} ($[Ca^{2+}]_i$) signalling as reported earlier, which is explained by its interaction with the endoplasmic reticulum (ER) inositolphosphate receptor IP_3R and possibly by the impact of TMEM16A-mediated Cl^- transport on Ca^{2+} signalling[173,225,229]. Because intracellular Ca^{2+} is a major regulator of cell proliferation, we examined if inhibition of TMEM16A by niclosamide exerts similar effects on intracellular Ca^{2+} signalling in Cal33 cells. Niclosamide did not change basal intracellular Ca^{2+} concentrations but strongly attenuated Ca^{2+} rise, induced by 10 and 100 µM ATP, respectively (Fig. 18). It is notable that the CK2-inhibitor CX4945 also strongly reduced intracellular Ca^{2+} levels. This previously unrecognized effect of CX4945 on intracellular Ca^{2+} is likely to contribute to its antiproliferative/anticancer effects. Simultaneous inhibition of TMEM16A and CK2 did not further increase the inhibitory effect on $[Ca^{2+}]_i$.

Taken together, blocking CK2 and TMEM16A inhibits cell proliferation, partially by overlapping mechanisms. Because inhibition of both pathways significantly augments inhibition of cell proliferation, it may be considered to use CX4945 and niclosamide simultaneously in patients with cancer.

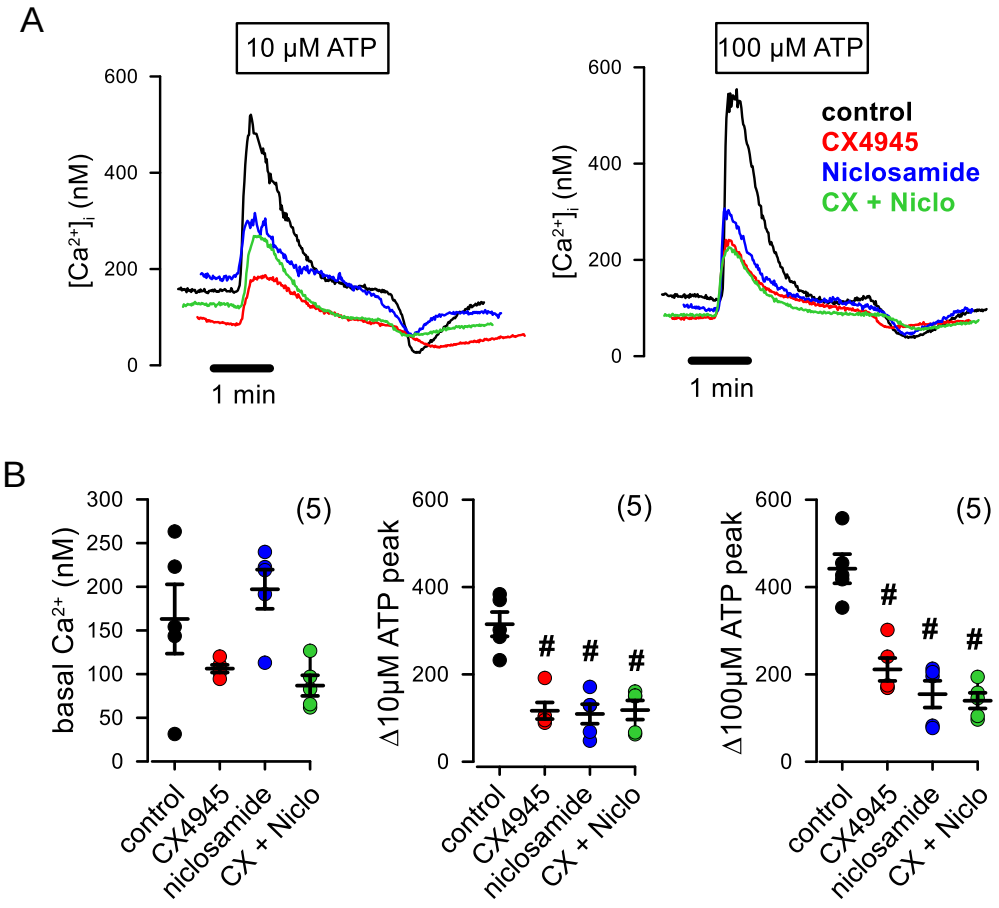

Figure 18 – Blockers of CK2 and TMEM16A inhibit receptor mediated Ca^{2+} signalling. (A,B) Original recordings and summaries for basal and ATP-induced intracellular Ca^{2+} concentrations in Cal33 cells. Increase of intracellular Ca^{2+} by 10 and 100 µM ATP, respectively. Both CX4945 (20 µM) and niclosamide (1 µM) largely reduce ATP-induced Ca^{2+} increase. Cells were treated with drugs 24h after seeding, and experiments were performed after 24h of incubation. Mean ± SEM (number of experiments). #Significant inhibition ($p < 0.05$; ANOVA). Experiments performed by Rainer Schreiber.

Discussion

In the present study, we have shown that the ubiquitous and constitutively active kinase CK2 controls membrane expression of the Ca^{2+}-activated Cl^- channel, TMEM16A, in vitro. High-throughput screening was performed by stably expressing a

TMEM16A construct (3HA-TMEM16A-eGFP) in CFBE cells, that contains a hemagglutinin tag (YPYDVPDYA) inserted in triplicate (3HA) between His^{396} and Asn^{397}, i.e., in the first extracellular loop of TMEM16A. This extracellular HA-tag, if present, can be immuno-detected in non-permeabilized cells, as the antibody binds only to the PM-localized TMEM16A. The results identify TMEM16A as another ion channel that is regulated by CK2.

Earlier studies demonstrated that the cystic fibrosis transmembrane conductance regulator (CFTR) requires CK2 to be fully active[230–233]. We and others also demonstrated that CK2 positively regulates the epithelial Na^+ channel, ENaC, which is important to control renal Na^+ excretion[234,235]. For both CFTR and ENaC, consensus sites for CK2-dependent phosphorylation have been found. We searched for putative CK2 phosphorylation sites in human TMEM16A (abcd isoform) using PROSCAN/ PROSITE databases and identified 10 putative CK2 phosphorylation sites. Two stronger consensus CK2 sites were located at the N-terminus and one was located at the C-terminus of TMEM16A. The N-terminus is relevant for membrane trafficking. Its elimination abolished expression. Truncation of the C-terminus reduced ATP-activated whole cell currents in our previous report[236,237]. This could suggest a role of CK2 phosphorylation for activation of TMEM16A. However, it is currently unclear whether these sites are truly phosphorylated by CK2. For example, a serine is located at position 42 within the N-terminus and may possibly affect membrane targeting when phosphorylated. S42 phosphorylation could also change the interaction of TMEM16A with accessory proteins, such as the ezrin–radixin–moesin network[178].

A role of CK2 has been found for several other ion channels and transporters[233,238,239]. As for TMEM16A, also for CFTR and ENaC, CK2 was shown to support their intracellular processing and trafficking to the PM[234,240]. In this context, it is noteworthy that CK2 phosphorylates Sec31 and regulates ER-To-Golgi trafficking[241]. Also, peripheral steps of membrane fusion, exocytosis and insertion of proteins into the PM via the synaptosomal-associated protein receptor (SNARE) machinery are controlled by CK2[242]. Transcription of TMEM16A is under the control of the transcription factor signal transducer and activator of transcription 6 (STAT6), while CK2 is known to affect STAT6 activity[243,244]. However, we did not find evidence for reduced expression of TMEM16A by inhibition of CK2. Taken together, inhibition of CK2 is likely to inhibit TMEM16A activity, in part by inhibition of PM expression and probably by inhibition of intracellular Ca^{2+} signalling[236].

An essential result of the present study is that co-application of niclosamide enhanced the antiproliferative effect of CX4945 remarkably (Fig. 17), but at the same time, lowered the cytotoxic (cell death) effect exerted by CX4945 (Fig. S13 – Appendix 1). The inhibitory effect of niclosamide on cell proliferation was validated by Ani9, another more specific inhibitor of TMEM16A (Fig. S14 – Appendix 1). Therefore, combined inhibition of CK2 and TMEM16A by CX4945 and niclosamide respectively, would maybe reduce the concentration of CX4945 required in a cancer patient. While our present data only demonstrate inhibitory effects of CX4945 in vitro, previous experiments also demonstrated the role of TMEM16A for cancer growth in vivo[124,203]. Although CX4945 was used at µM concentrations in the present in vitro study, additional experiments show that it also inhibits proliferation at nanomolar concentrations (Fig. S15 – Appendix 1). Taken together, we may speculate that co-application of niclosamide together with CX4945 could allow for further reduction of the CX4945 dosage in vivo, to maybe reach effective picomolar concentrations that would come close to the concentrations used in monoclonal antibody therapy. This could reduce unwanted side effects of an anti-cancer therapy by inhibitors of CK2[245].

However, it is important to point out the controversial role of TMEM16A in cell proliferation. Namely, a recent report suggests that TMEM16A is upregulated by cell proliferation and not the opposite[108]. Indeed, the data showed that, during wound, expression levels of TMEM16A rise concomitantly with the proliferation marker Ki-67, indicating that it is proliferation that triggers TMEM16A upregulation. Therefore, the effects on TMEM16 expression and function observed here with silencing/inhibition of CK2 might be a consequence of changes in proliferation. Moreover, despite the existence of various TMEM16A inhibitors, the potency and selectivity of these compounds, such as niclosamide, are a considerable limitation. Also, the effects of TMEM16A blockers on proliferation may be due to binding to the channel and inducing internalisation as opposed to a pore blocking mechanism[246]. Nonetheless, with this study we were able to show that: i) the TMEM16A screening platform allows for the identification of both traffic enhancers and blockers, with therapeutic potential for several disorders; ii) CK2 inhibitors together with niclosamide might provide an alternative, more efficacious, therapy for head and neck cancers.

3. Systems approaches to unravel molecular function: High-content siRNA screen identifies TMEM16A traffic regulators as possible drug targets for Cystic Fibrosis

Introduction

Cystic Fibrosis (CF) is a life-threatening autosomal recessive disease caused by mutations in the CFTR (CF Transmembrane Conductance Regulator) gene[4,6], which encodes a cAMP-regulated chloride (Cl^-) and bicarbonate (HCO_3^-) channel expressed at the apical membrane of epithelial cells[7]. CFTR dysfunction destabilizes the epithelial ion and water homeostasis, and possibly also pH, resulting in dehydrated lung secretions, enhanced mucus viscosity and impaired mucociliary clearance (MCC), culminating in progressive obstruction of the airways[15,18].

More than 2,100 CFTR genetic variants have been reported, of which ~360 are confirmed as CF-causing mutations. Various CFTR modulators have been approved for clinical use for individuals with specific CF genotypes. Recently, a new highly effective CFTR modulator therapy, consisting of a combination of two correctors and one potentiator (Trikafta/Kaftrio®) was approved for people over 12 years old carrying at least one copy of the most common CFTR mutation, F508del, which represents around 80% of all people with CF worldwide[61,62]. Although these drugs are significantly improving the quality of life of individuals carrying this mutation, they cannot be used to pharmacologically rescue all CFTR mutations, e.g., large gene deletions or frameshift mutations. Hence, people with CF bearing these non-rescuable mutations[12] (also grouped as Class VII), and other mutations which are not eligible for Kaftrio, still lack an effective therapy and constitute ~20%[247]. Although gene therapy/editing constitutes an appealing approach[66], efficacious and safe protocols are still not foreseen in the short/medium term.

An interesting alternative is to develop "mutation-agnostic" therapies, namely through the activation of other (non-CFTR) anion channels that could compensate for the absence of CFTR-mediated Cl^-/HCO_3^- secretion. Anoctamin 1 (ANO1)/TMEM16A, a calcium (Ca^{2+})-activated Cl^- channel (CaCC)[73–75] expressed in lung epithelia[68], is one of the most promising alternative channels that can compensate for the absence of epithelial CFTR-mediated anion secretion in CF[111,248,249].

TMEM16A has a fundamental importance for Ca^{2+}-dependent Cl^- secretion in numerous tissues, namely in the airways, salivary gland, pancreatic gland, and hepatocytes[105,106,169]. There is, however, some controversy in the field since some authors question whether activation of TMEM16A will have a positive impact in the lives of people with CF, mostly because TMEM16A has been claimed to play a positive role in mucus secretion, this implying that its activation may possibly cause further harm for people with respiratory obstructive diseases. TMEM16A has been associated with goblet cell metaplasia, as its expression is strongly upregulated concomitantly with mucus hypersecretion[100,101]. Additionally, during inflammation, TMEM16A expression is increased namely by Th2 interleukins (IL-4 and IL-13), particularly in mucus producing cells, with only little expression in ciliated cells[102]. A number of studies has shown that inhibition of TMEM16A occurs alongside with decreased mucus secretion in primary human airway surface epithelial cells[91] and also in intestinal cells[101], thus proposing a causal relationship between the two events. Notwithstanding, other studies indicate that there is no causal link between TMEM16A and production of MUC5AC, the main constituent of human respiratory mucus and that cell proliferation is the main driver of TMEM16A upregulation[108]. Indeed, it was demonstrated that in the absence of proliferation (goblet cell metaplasia) MUC5AC is still upregulated, but not TMEM16A. Moreover, the same studies indicate that TMEM16A inhibition has a negative impact in airways homeostasis by decreasing the height of airway surface liquid, thus causing airway dehydration[108]. Additionally, it has been recently shown that a TMEM16A potentiator (ETX001, Enterprise Therapeutics) increases anion secretion and ASL height in primary human bronchial epithelial cells from individuals with CF, and promotes MCC in in vivo sheep models[109], without any stimulation of airway mucus secretion[250]. Another important aspect to consider is the relationship between TMEM16A and CFTR, since tissue-specific TMEM16A-KO in mouse intestine and airways not only eliminates Ca^{2+}-activated Cl^- currents, but also abrogates CFTR-mediated Cl^- secretion, similarly to human cells[85]. Thus, we propose that potentiating TMEM16A trafficking and, consequently, its function as a Cl^- channel, is a potentially good approach to take advantage of this channel in CF, compensating for the absence of functional CFTR.

Although there are several arguments supporting both sides, many studies relied on rather unspecific (possibly affecting other TMEM16A-related effects, e.g., cell proliferation) and low-potency TMEM16A modulators to draw conclusions on the effect of this channel in CF. The identification of novel regulators of TMEM16A can provide meaningful information on the possible applications of this protein as a therapeutic target.

While TMEM16A was described to localize to the apical PM of airway epithelial cells, it is present at the cell surface at low levels, particularly in CF airways[226]. Our hypothesis is that TMEM16A PM levels can be pharmacologically stimulated by modulating its (yet unknown) traffic regulators, ideally also potentiating the channel activity independently of Ca^{2+}. The goal of the present study was thus to identify TMEM16A regulators as potential drug targets for novel ("mutation-agnostic") therapies for CF. Using high-throughput microscopy screens (HTS), we have identified 262 candidate TMEM16A modulators (179 siRNAs enhanced and 83 decreased TMEM16A traffic), being G-protein coupled receptors (GPCRs) enriched on the primary hit list. Among hits in the latter group, we have functionally validated ADRA2C and CXCR3, two G-protein coupled receptors (GPCRs), as potent modulators of TMEM16A trafficking and function. Antagonists of these GPCRs can thus be used to improve Cl^- secretion in people with CF, regardless of their CFTR mutations.

Results

Identification of TMEM16A traffic regulators by high-content siRNA screening

Using a highly specific TMEM16A antibody to stain cryosections of human airways (CF and non-CF), we have previously shown that there is TMEM16A at the apical surface of epithelial cells of CF airways, albeit at low levels[226] (chapter 1.1). The same was observed in cellular models, namely in CFBE cells expressing F508del-CFTR, which display significantly reduced PM expression of TMEM16A when compared to wt-CFTR expressing cells[251]. These data emphasize the need to identify TMEM16A traffic regulators that promote its traffic to the cell surface in the absence of CFTR expression, in order to use this Cl^- channel as an alternative drug target to compensate for the loss of CFTR-mediated Cl^- transport in CF.

We have previously generated a cell model expressing double tagged TMEM16A (CFBE 3HA-TMEM16A-eGFP cells) and used it to develop, optimize and validate a screening platform to identify TMEM16A traffic regulators[165,226] (chapter 1.1). Using this tool, we performed here a high-content siRNA screen to assess the effect of knocking down 691 genes on TMEM16A traffic to the PM (Fig. 19A,B). This siRNA library comprised siRNAs that: 1) enhance F508del-CFTR PM expression; 2) interact with CFTR; 3) or are involved in general protein trafficking (Amaral lab, unpublished data).

The rationale for testing such set of siRNAs was two-fold, firstly to increase TMEM16A PM expression and consequently increase the potential for Cl^- secretion; and secondly, by targeting these genes in F508del-CFTR expressing cells, besides TMEM16A, CFTR-mediated Cl^- secretion would also be enhanced. Nonetheless, the screen was performed in CFTR-null cells (CFBE 41o-), to enable the identification of TMEM16A traffic enhancers independently of CFTR. As a negative control, a non-targeting siRNA ("siNEG1") was used. This primary traffic screen identified 262 regulators of TMEM16A traffic: 179 inhibitor genes, i.e., targeted by siRNAs enhancing TMEM16A traffic, and 83 enhancer genes, i.e., targeted by siRNAs inhibiting TMEM16A traffic (Fig. 19A,B, Tables S8 and S9 – Appendix 5).

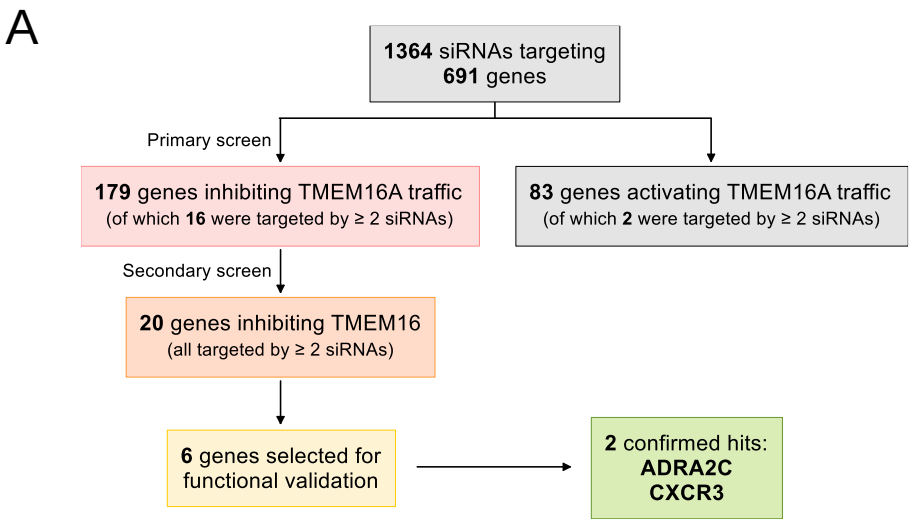

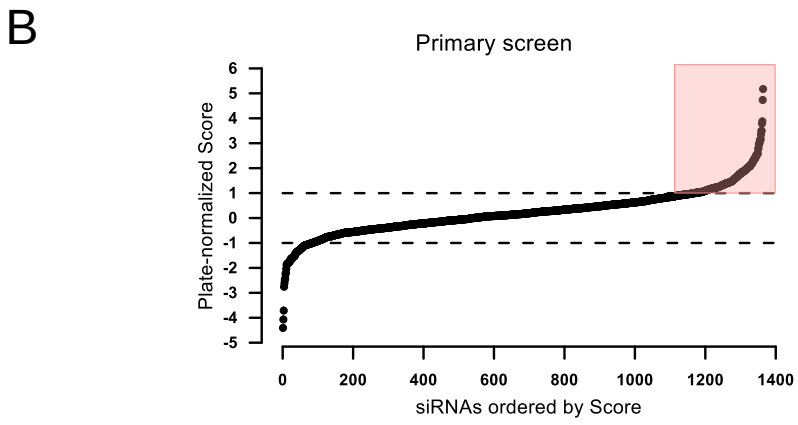

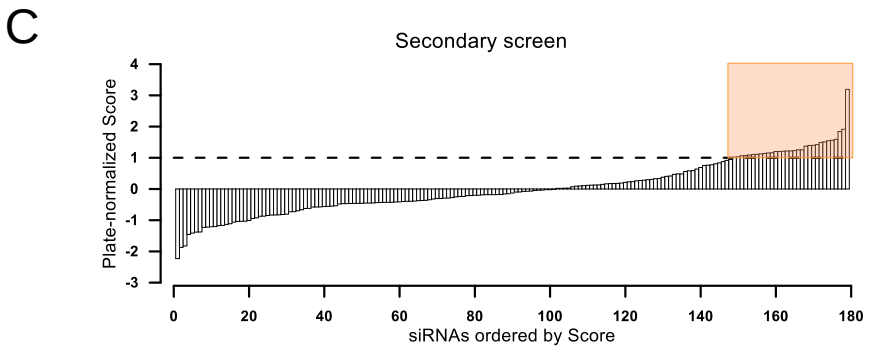

Figure 19 – Overview of the screen data. (A) Workflow showing the different steps in the primary and secondary screens and the number of hit genes found in each step. **(B)** Distribution of averaged scores obtained for every siRNA in the primary TMEM16A traffic screen. siRNAs with scores above +1 (red shade) were considered as TMEM16A traffic enhancers (inhibitory genes) and with score below -1 were considered TMEM16A traffic inhibitors (enhancer genes). **(C)** Distribution of averaged scores obtained for every siRNA in the secondary screen. siRNAs with scores above +1 (orange shade) were considered as enhancers of TMEM16A function.

Since the main goal in CF therapies is to increase anion secretion, we focused on the 179 siRNAs augmenting TMEM16A PM expression for further validation. Representative images obtained for TMEM16A traffic enhancers are shown in Fig. 20A.

Analysis of these 179 genes using the Gene Ontology Bioinformatics Resource[252,253], employing a high classification stringency, identified as most important biological processes: *i)* regulation of transcription; *ii)* G-protein coupled receptor (GPCR) signalling; *iii)* protein phosphorylation; *iv)* inflammatory response; and *v)* negative regulation of cell proliferation.

Secondary screen: functional validation of TMEM16A traffic hits

Next, we aimed to assess how the knockdown of the 179 genes affected TMEM16A function using the halide-sensitive (HS)-YFP assay upon ATP-stimulation, as previously described[99] (Fig. 19C). We used HEK cells stably expressing TMEM16A and a HS-mutant (YFP-H148Q/I152L) form of YFP (HEK-TMEM16A-YFP) and analysed the rate of iodide (I^-) uptake after siRNA knockdown of target genes by calculating the slope of the curves after ATP stimulation (see Methods).

The knockdown of 20 out of the 179 genes significantly increased the rate of ATP stimulated I^- transport into the cells, as determined by the steeper slopes observed in the YFP fluorescence decay curves (Fig. 20B,C, Table S10 – Appendix 5). The ATP-mediated YFP-quenching is essentially accomplished by TMEM16A alone since, in the

presence of an siRNA targeting TMEM16A (Fig. 20B), there is a substantially reduced effect. Accordingly, we can confirm that these siRNAs increase TMEM16A function (Fig. 20B,C).

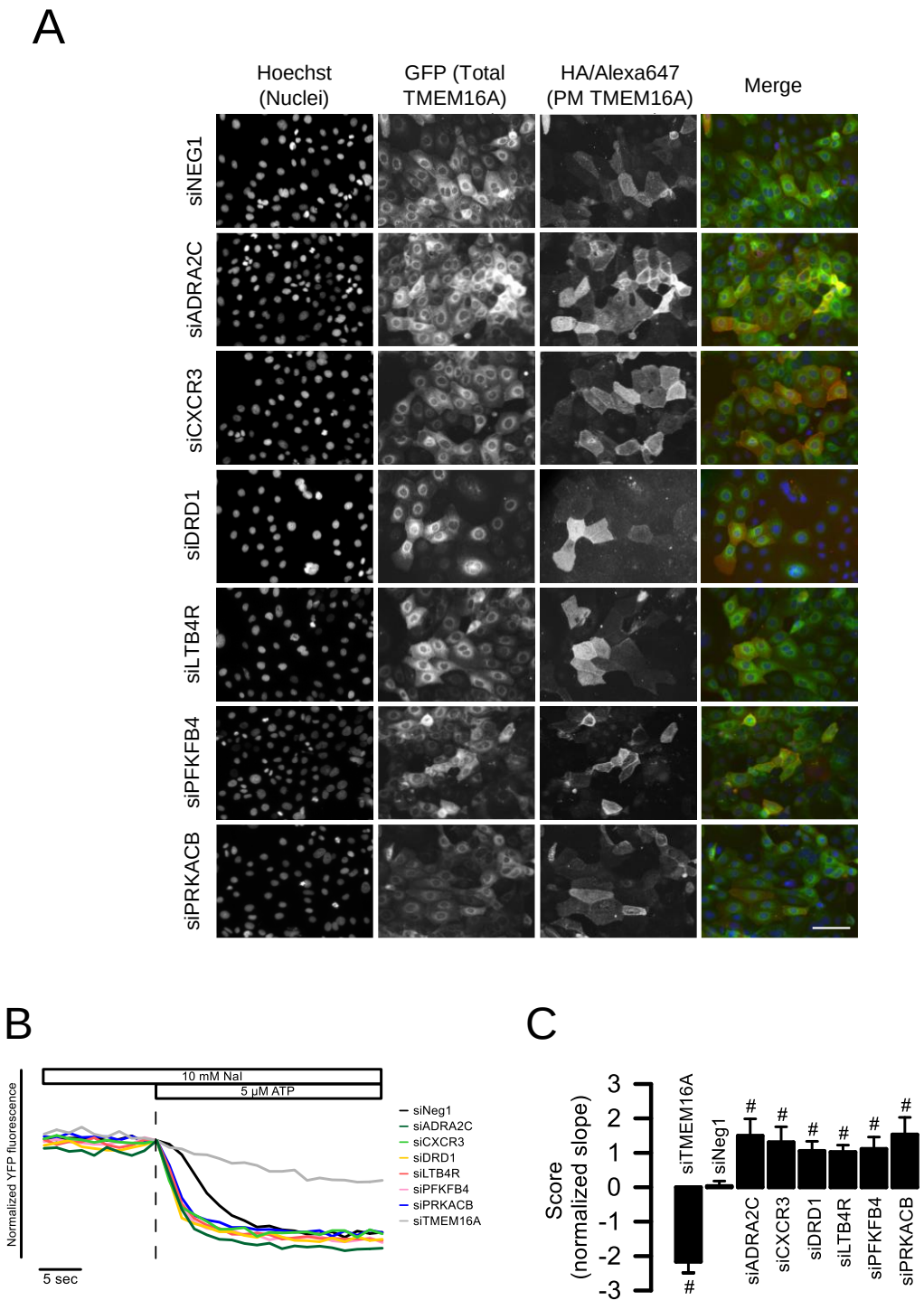

Figure 20 – Summary of the TMEM16A trafficking and functional screens. (A) Representative widefield epifluorescence microscopy images obtained for the TMEM16A traffic screen using siRNAs targeting the selected genes (n = 4). Cell imaging was performed with (automated) widefield epifluorescence microscope with a Scan^R software (Olympus Biosystems) with a 10x UPlanApo objective (Olympus). Scale bar: 50 µm. **(B)** Representative ATP-induced (5 µM) YFP-quenching curves obtained by knocking-down the selected genes in HEK-TMEM16A-YFP cells. **(C)** Average of the normalized scores obtained for the selected hits in

the YFP-quenching validation screen. Data are represented by mean ± SEM (n = 4). #Significant difference when compared with the negative control siNEG1 ($p < 0.05$; unpaired t-test).

Out of the 20 TMEM16A regulators, we selected the top 6 hits for mechanistic validation (Table 1) based on several factors, namely: *i)* their scores are positive and consistent in both screens; *ii)* they are druggable by specific inhibitors (e.g., receptors and kinases); *iii)* they are biologically relevant, as their knockdown does not appear to have deleterious/pleiotropic effects on cells; and *iv)* GPCRs have a strong relationship with TMEM16A[251]. We confirmed the expression of the 6 selected genes in both CFBE and HEK cells by PCR (Fig. S16 – Appendix 1).

Table 1 – Primary and secondary screen hits selected for mechanistic validation.

Hits selected for validation	Gene name
ADRA2C	Adrenoceptor alpha 2C
CXCR3	C-X-C motif chemokine receptor 3
DRD1	Dopamine receptor D1
LTB4R	Leukotriene B4 receptor
PFKFB4	6-phosphofructo-2-kinase/fructose-2,6-biphosphatase 4
PRKACB	Protein kinase cAMP-activated catalytic subunit beta

To further functionally validate these 6 hits, the effects of the respective siRNAs on TMEM16A function were first evaluated by whole-cell patch-clamp, where TMEM16A was activated using the Ca^{2+} ionophore ionomycin (Fig. 21). We considered that the use of ATP for TMEM16A activation could be disadvantageous in this case due to its possible interactions with the GPCRs identified as hits (namely through purinergic receptors), therefore masking the real regulatory effects on TMEM16A. Therefore, we stimulated the cells with ionomycin. Experiments were performed in CFBE cells stably expressing F508del-CFTR (CFBE F508del-CFTR), which endogenously express TMEM16A, transfected with siRNAs targeting each of the 6 selected hits. Two siRNAs, targeting ADRA2C and CXCR3 (α2C-adrenergic receptor [α2C-R], and C-X-C chemokine receptor type 3, respectively), significantly increased Ca^{2+}-activated currents at larger depolarizing currents, when compared to the non-targeting control (siNEG1) (Fig. 21).

Notably, no siRNA affected the cAMP-activated currents (IBMX + Forskolin), therefore showing no direct effects on F508del-CFTR function (Fig. S17 – Appendix 1).

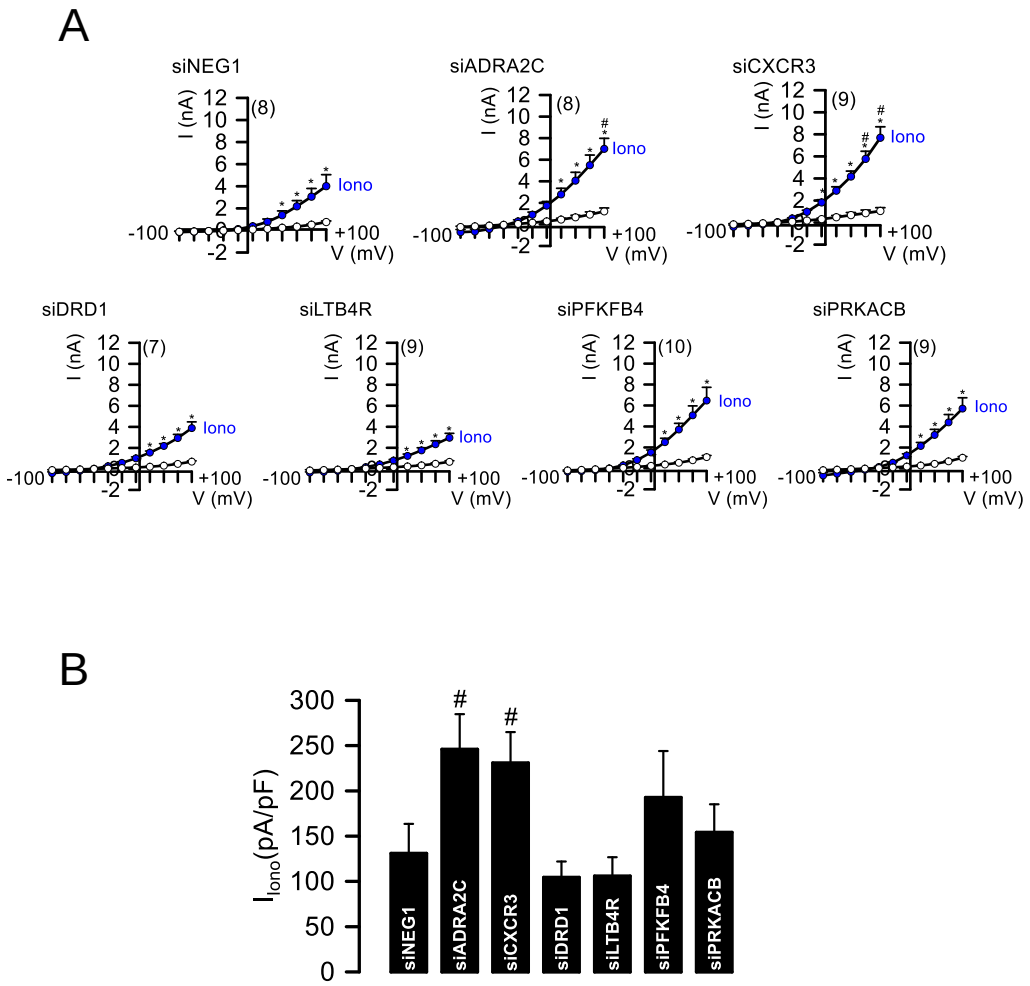

Figure 21 – Validation of hits in CFBE F508del-CFTR cells that endogenously express TMEM16A by whole-cell patch clamp. (A) Whole cell currents obtained in siRNA-transfected cells (current/voltage (I/V) curves) activated by ionomycin (Iono; 1 μM). The number of cells (n) measured in each condition is shown in each graph. **(B)** Summary of Iono-induced currents with different siRNA treatments. Data represented as mean ± SEM. *Significant current activation ($p < 0.05$; paired t test). #Significant difference when compared with the negative control siNEG1 ($p < 0.05$; unpaired t-test).

To confirm that the increase in TMEM16A function observed by knocking down ADRA2C and CXCR3 is not unspecific, such as due to an increase in the concentration of intracellular Ca^{2+} ($[Ca^{2+}]_i$), total $[Ca^{2+}]_i$ was measured using a FURA2-AM probe (Fig. S18 – Appendix 1). The knockdown of these GPCRs did not alter $[Ca^{2+}]_i$, neither basal nor after ionomycin stimulation. Interestingly, their knockdown seems to decrease the $[Ca^{2+}]_i$ peak (and plateau) observed after ATP stimulation. These data suggest that the increase in TMEM16A function observed by knocking down ADRA2C or CXCR3 is not caused by an increase in $[Ca^{2+}]_i$, but instead by increased TMEM16A PM expression,

pointing these genes as suitable drug target candidates to enhance Cl^- secretion in CF. These data, however, do not exclude an undetectable increase in localized $[Ca^{2+}]_i$, namely in microdomains located close to the PM.

Regulation of TMEM16A by G_i-Protein Coupled Receptors ADRA2C and CXCR3

Since knocking down ADRA2C or CXCR3 significantly enhances endogenous TMEM16A function (Fig. 21), next we aimed to confirm whether this effect on endogenously expressed TMEM16A also resulted from increased trafficking. Indeed, TMEM16A immunostaining in CFBE F508del-CFTR cells showed a significant increase in its PM expression after transfection with siRNAs targeting ADRA2C or CXCR3 (Fig. 22A,B).

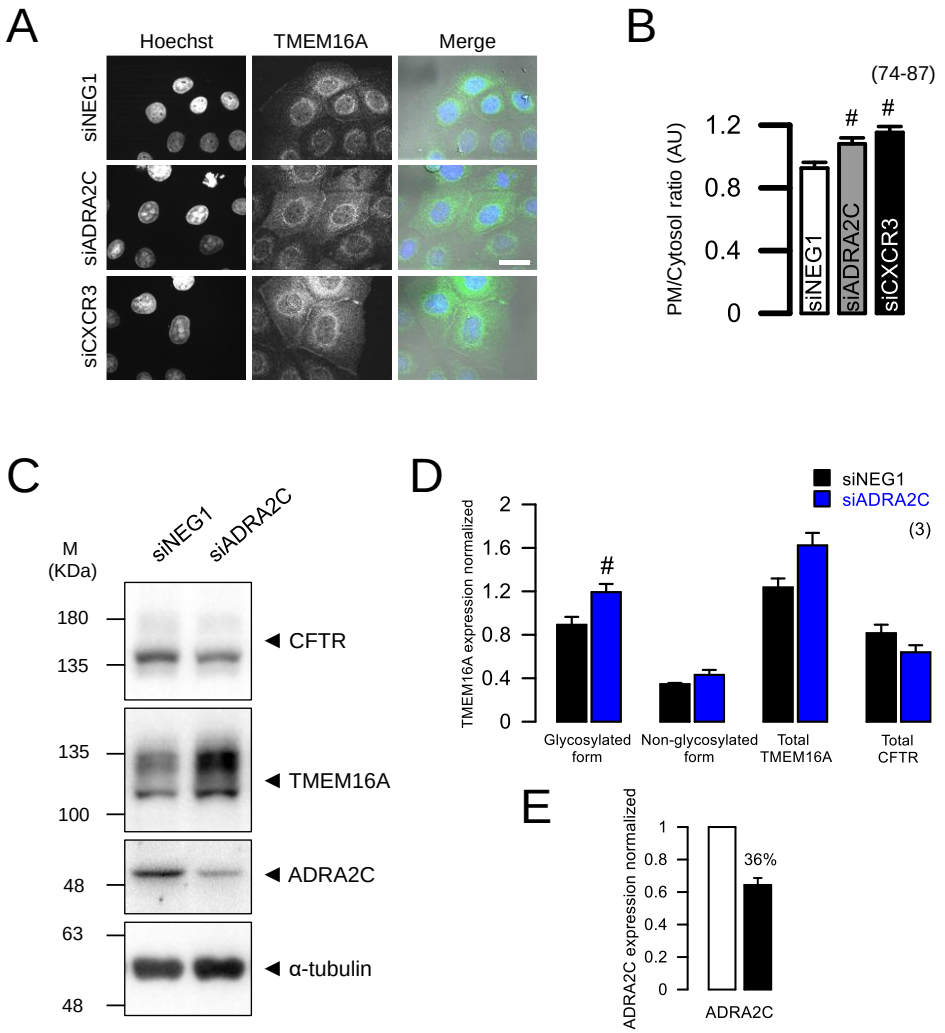

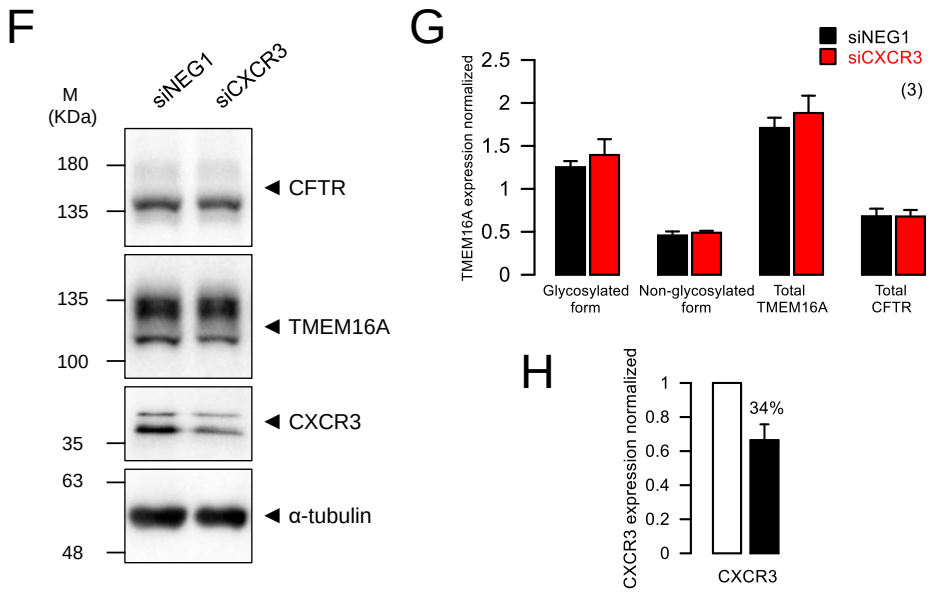

Figure 22 – Effects of ADRA2C or CXCR3 knockdown on endogenous TMEM16A expression and function. (A) Representative fluorescence microscopy images of endogenous TMEM16A in CFBE F508del-CFTR cells transfected with siNEG1 or siRNAs targeting ADRA2C or CXCR3 and respective quantification in **(B)**. **(C)** Western Blot of CFBE F508del-CFTR cells transfected with a siRNA targeting ADRA2C. siNEG1 non-targeting siRNA was used as control. **(D)** Quantification of TMEM16A and CFTR expression detected in (C), showing only a significant difference in glycosylated TMEM16A expression after transfection with siADRA2C when compared to the control. **(E)** Quantification of ADRA2C knockdown. **(F)** Western Blot of CFBE F508del-CFTR cells transfected with a siRNA targeting CXCR3 or siNEG1 non-targeting siRNA as control. **(G)** Quantification of TMEM16A and CFTR expression detected in (F). **(H)** Quantification of CXCR3 knockdown. Mean ± SEM (number of cells measured). #Significant difference when compared with the negative control ($p < 0.05$; unpaired t-test).

To understand how ADRA2C and CXCR3 regulate TMEM16A, we evaluated TMEM16A protein expression by Western Blot (WB) after knocking down these genes in CFBE F508del-CFTR cells. TMEM16A expression appears to be increased with the knockdown of ADRA2C, while no changes were observed with siCXCR3, when compared to siNEG1 (Fig. 22C-H). Importantly, only the expression of the glycosylated form [251] of TMEM16A (i.e., putatively the PM form) was significantly increased when ADRA2C was knocked down. These results reinforce the evidence that the knockdown of ADRA2C is increasing TMEM16A PM expression, either by promoting its anterograde traffic or by stabilizing it at the cell surface. Additionally, the knockdown of ADRA2C or CXCR3 did not affect F508del-CFTR expression (Fig. 22C,D,F,G).

To analyse the opposite effects on TMEM16A trafficking and function, we overexpressed the ADRA2C or CXCR3 receptors with either no tags, or with an mCherry tag at the C-terminus of each protein. Even without ligand stimulation, the overexpression of ADRA2C and CXCR3 in CFBE F508del-CFTR cells decreased the trafficking of endogenously expressed TMEM16A (Fig. 23A,B). Likewise, TMEM16A

function, measured by whole-cell patch clamp, was strongly reduced after overexpression of either ADRA2C or CXCR3 (Fig. 23C-E). As we confirmed that these GPCRs do not affect purinergic receptor signalling (Fig. S18), and because it is known that receptor-dependent activation of TMEM16A is more efficient than stimulation by elevating $[Ca^{2+}]_i$ [73,251], we used ATP to activate TMEM16A in further experiments. Agonist stimulation of overexpressed ADRA2C and CXCR3 (with 10 µM clonidine or 100 ng/mL CXCL11, respectively) did not further decrease TMEM16A function (Fig. S19).

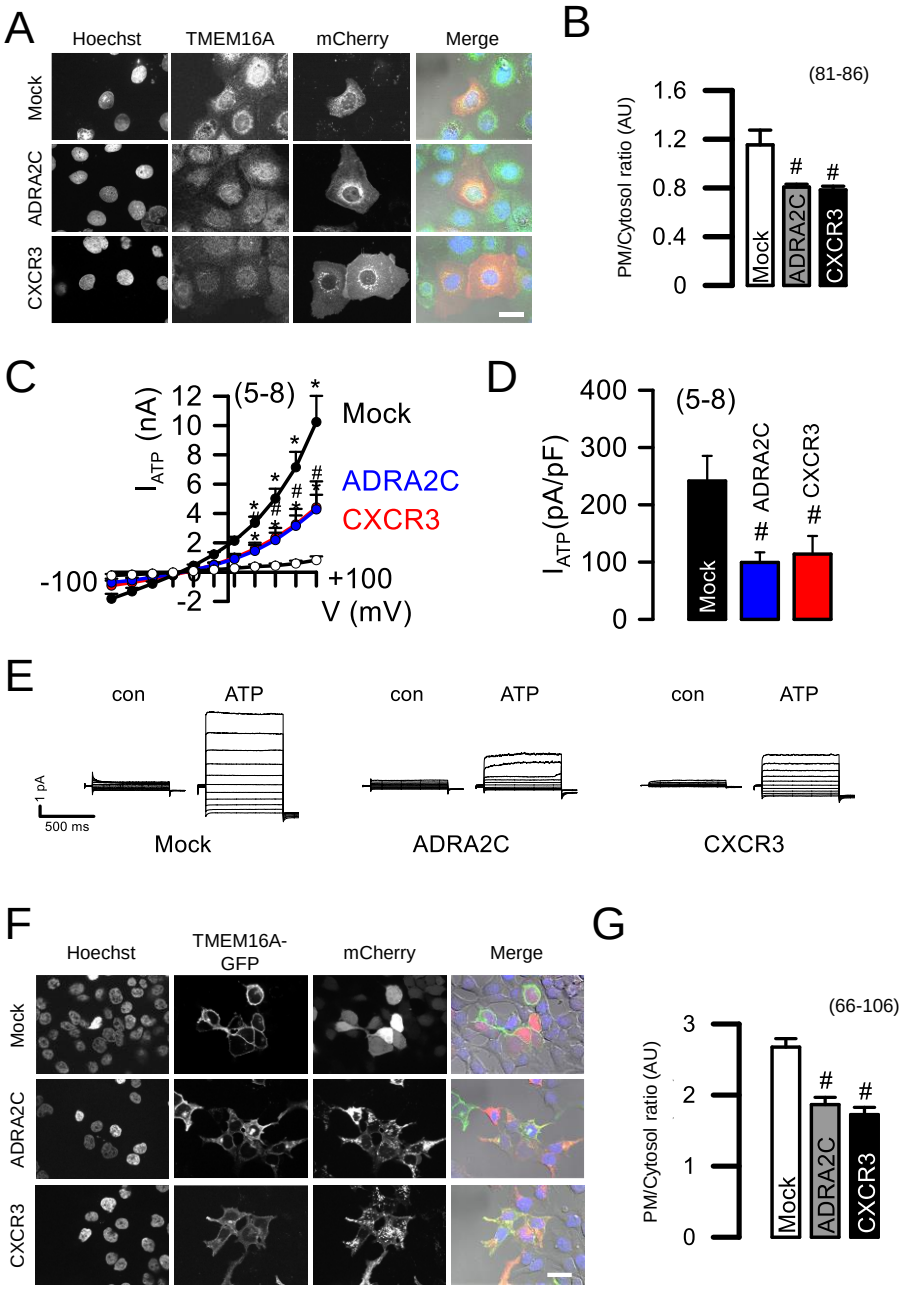

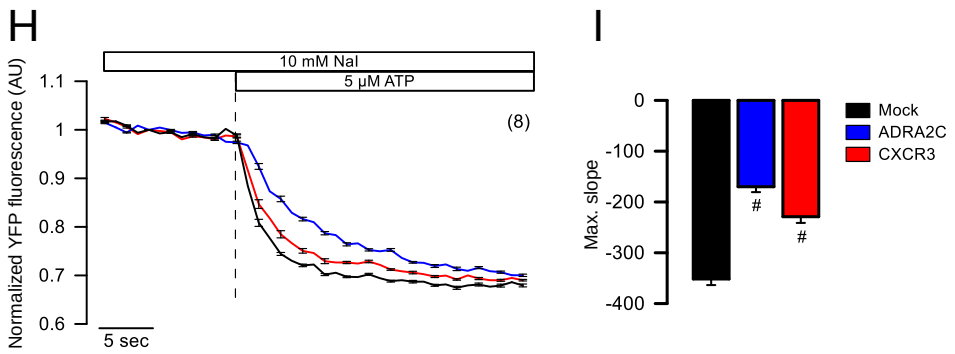

Figure 23 – Effects of ADRA2C or CXCR3 overexpression on TMEM16A expression and function. (A) Representative images of endogenous TMEM16A staining in CFBE F508del-CFTR cells overexpressing mCherry-tagged ADRA2C or CXCR3 and respective quantification in **(B)**. Images were acquired with an Axiovert 200 microscope equipped with ApoTome and AxioVision (Zeiss, Germany), with a 63x objective. Scale bars = 30 µm (number of cells measured). **(C, D)** Current/voltage curves and corresponding summary of ATP-induced currents in CFBE F508del-CFTR cells transfected with ADRA2C, CXCR3 or an empty vector, calculated at +100 mV. **(E)** Whole cell overlay currents (Vc = ± 100 mV, steps 20 mV) activated by ATP (100 µM). **(F)** Representative fluorescence microscopy images of TMEM16A in HEK cells co-transfected with a mCherry vector or with ADRA2C/CXCR3 tagged with mCherry and respective quantification in **(G)**. Scale bar = 30 µm. The number of cells (n) measured is shown in the graph. **(H)** ATP-induced YFP quenching curves of HEK-TMEM16A-YFP cells transfected with ADRA2C or CXCR3 and respective slope quantification in **(I)**. Mean ± SEM (number of experiments or total number of cells measured in different experiments [>3]). *Significant current activation ($p < 0.05$; paired t-test). #Significant difference when compared with mock-transfected cells ($p < 0.05$; unpaired t-test).

These results were also validated in a system expressing heterologous TMEM16A, namely HEK cells co-transfected with TMEM16A and ADRA2C or CXCR3. In these cells, TMEM16A traffic to the PM was significantly reduced vs mock-transfected cells (Fig. 23F,G). TMEM16A function was also compromised upon overexpression of ADRA2C or CXCR3, as YFP-quenching data in HEK-TMEM16A-YFP showed a strongly diminished I^- uptake in cells overexpressing ADRA2C or CXCR3 when compared to mock-transfected cells (Fig. 23H,I).

TMEM16A function and cAMP levels

Both the ADRA2C and the CXCR3 genes encode G_i protein-coupled receptors, being adrenoceptor alpha 2c (α2C-R) activated by catecholamines (e.g., epinephrine or norepinephrine[254]), and c-x-c motif chemokine receptor 3 (CXCR3) by chemokines CXCL9, CXCL10 or CXCL11[255]. Since receptor stimulation leads to the inhibition of adenylyl cyclase (AC) and consequently blocks the synthesis of the second messenger cAMP from ATP[256], we can infer that knocking down these genes (and consequently inhibiting G_i) can increase intracellular cAMP levels. On the other hand, receptor overexpression could lead to AC inhibition, thus lowering intracellular cAMP levels

([cAMP]$_i$). Moreover, due to crosstalk between Ca^{2+} and cAMP signalling reported before[251], it is expected that higher concentrations of cAMP also lead to an increase in Ca^{2+}-activated Cl^- currents. We thus postulated that the observed effects of these G_i protein-coupled receptors on TMEM16A function could be related to changes in cAMP levels.

To test this hypothesis, we started by measuring [cAMP]$_i$ in HEK cells transfected with either ADRA2C or CXCR3, using a fluorescence resonance energy transfer (FRET)-based Epac cAMP sensor (YFP-Epac-CFP)[161,162]. The exchange protein directly activated by cAMP (Epac) sensor allows for a quantitative analysis of changes in [cAMP]$_i$, where increases in the ratio CFP/YFP indicate higher concentrations of cAMP (see Methods). No differences were observed in basal cAMP levels in cells transfected with either ADRA2C or CXCR3 (Fig. S20A – Appendix 1). Inhibition of G_i protein-coupled signalling pathways by pertussis toxin (PTX)[257] strongly increased intracellular cAMP, thus augmenting the FRET signal. Cells overexpressing either ADRA2C or CXCR3 showed significantly higher cAMP levels when compared to control (mock-transfected) cells after PTX incubation. AC stimulation by forskolin led to the same levels of intracellular cAMP in all conditions. Finally, incubation with phosphodiesterase inhibitor IBMX did not further increase cAMP levels, reflecting a near-complete saturation of cAMP binding to Epac (Fig. S20A – Appendix 1). These data suggest that, even though basal [cAMP]$_i$ is unaltered in cells transfected with ADRA2C or CXCR3, G_i protein-coupled signalling is more active than in control cells, even without ligand stimulation.

Thus, to determine if this increase in G_i protein-coupled signalling activation is reflecting on TMEM16A function, we incubated HEK-TMEM16A-YFP cells with compounds that increase [cAMP]$_i$. If the overexpression of the GPCRs ADRA2C and CXCR3 were inhibiting TMEM16A function due to the inhibition of cAMP synthesis, then adding exogenous cAMP would likely restore TMEM16A function in ADRA2C/CXCR3-transfected cells. After incubating cells for 2h with compounds that increase [cAMP]$_i$, namely PTX, the membrane permeable cAMP analogue 8-bromo-cAMP, or forskolin (with or without co-stimulation with IBMX), we observed an increase in the ATP-induced YFP quenching in HEK-TMEM16A-YFP cells (Fig. S20B,C – Appendix 1). Yet, the increase in ATP-induced YFP quenching was proportional in all conditions – either in cells transfected with an empty vector or with ADRA2C or CXCR3 – being the YFP quenching always higher in the control cells (mock), as observed before (Fig. 23).

Altogether, these data suggest that although the overexpression of ADRA2C or CXCR3 increase G_i protein-coupled signalling, and the rise in cAMP levels leads to

higher TMEM16A activity, possibly by a crosstalk in cAMP and Ca^{2+} signalling pathways, the regulation of TMEM16A by these GPCRs is most likely not directly due to changes in cAMP concentration.

ADRA2C and CXCR3 regulate TMEM16A expression by influencing its PM stability

To further investigate the mechanism of action (MoA) of the identified hits, we assessed the effects of combining siADRA2C and siCXCR3 with siRNAs targeting known components of the COPI trafficking machinery (COPB1 and COPZ1) – which were hits in the present study, and had already been described as modulators of TMEM16A PM expression[182,226] – or AP2M1 (Adaptor Related Protein Complex 2 Subunit μ), a subunit of AP-2 clathrin adaptor, an essential component of the endocytic clathrin coat[258], on the PM localization of TMEM16A. The combination of siADRA2C or siCXCR3 with siCOPB1 and siCOPZ1 were additive to the effect of the knockdown of the receptors alone by further increasing TMEM16A PM expression (Fig. 24A,B). Interestingly, the simultaneous knockdown of ADRA2C and CXCR3 is not additive, and even decreased the effect of the separate knockdown of these GPCRs (although the difference is not statistically significant), suggesting that their MoA is similar. Finally, although the knockdown of AP2M1 did not significantly increase TMEM16A PM expression (score = 0.843), when combining the siRNAs targeting AP2M1 and one of the GPCRs (ADRA2C or CXCR3), the potentiation of TMEM16A PM expression observed with the individual knockdown of the receptors is abolished (Fig. 24A,B). Thus, these data suggest that ADRA2C and CXCR3 are influencing TMEM16A PM expression in a post-Golgi process, probably by destabilizing it at the PM and/or enhancing its endocytosis (Fig. 25).

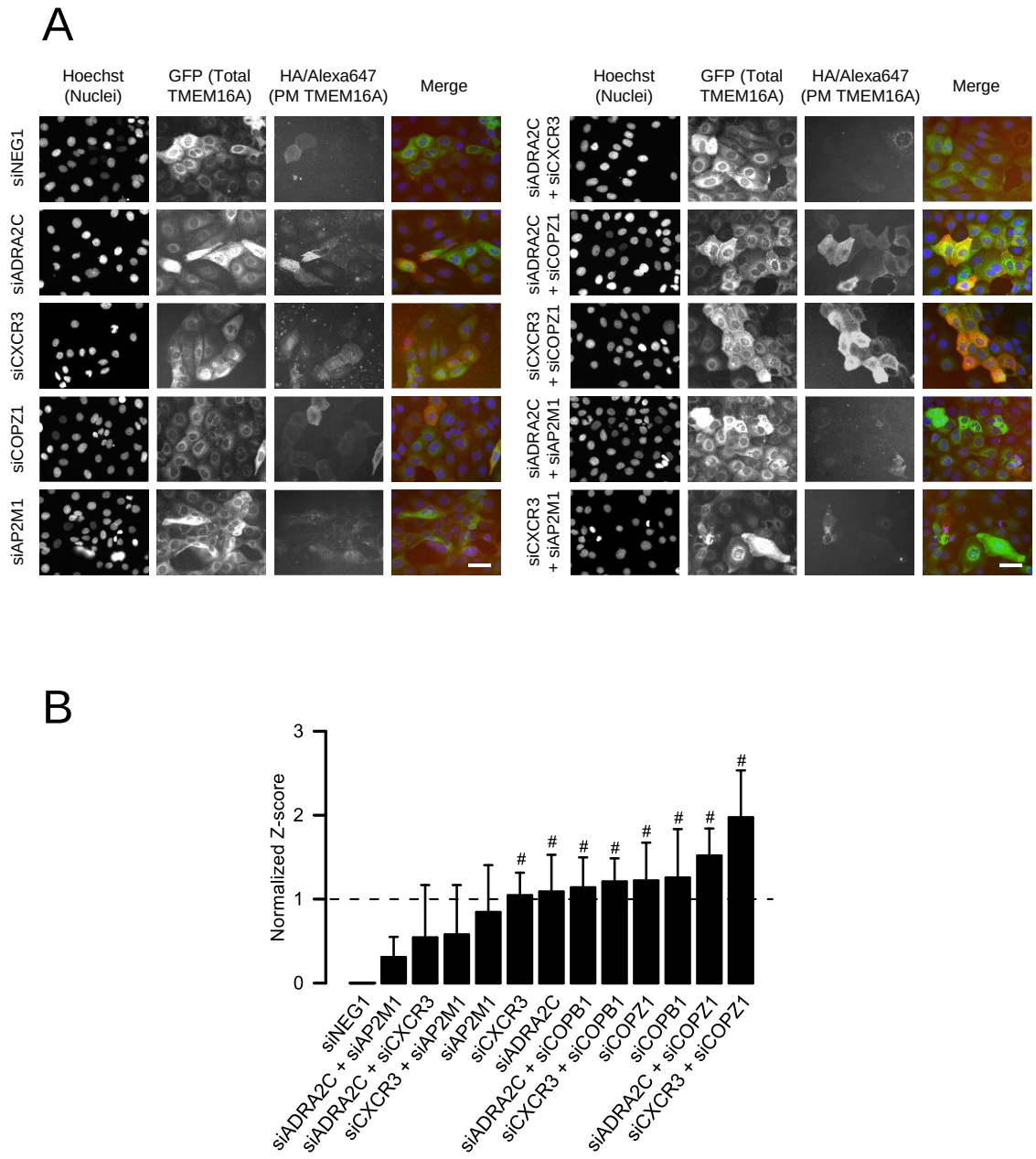

Figure 24 – The effect of knocking down ADRA2C and CXCR3 on TMEM16A PM expression is additive with siCOPB1 and siCOPZ1 but not with siAP2M1. (A) Representative widefield epifluorescence microscopy images obtained for TMEM16A PM expression using siRNAs targeting the two selected hits (ADRA2C and CXCR3) in combination with other siRNAs involved in endocytosis/trafficking. Cell imaging was performed with a Leica DMI 6000B widefield microscope (objective: 20x water, 0.75 NA; exposure times: Hoechst: 50 ms, GFP: 3 s, Alexa647: 3 s). Scale bar: 30 µm (n = 4). **(B)** Average of the normalized scores obtained for TMEM16A PM expression obtained in (A). #Significant difference when compared with siNEG1-transfected cells ($p < 0.05$; unpaired t-test).

Discussion

Searching for new therapies for all: TMEM16A as an alternative Cl^- channel in CF

Recent advances in drug development have made it possible to deliver an effective therapy for the majority of CF patients (~80-85%). Yet, the remaining ~20% with mutations that are not effectively corrected by the available modulators justify the need to search for new therapies suitable for all individuals with CF, regardless of their CFTR genotype. Targeting alternative Cl^- channels might just be an effective way of doing so.

While there is still some controversy on whether TMEM16A should be activated or inhibited in the context of CF, it is nevertheless essential to understand the multiple cellular roles of TMEM16A and how this channel is regulated before using it as a therapeutic target. Thus, the TMEM16A traffic screening data generated here constitute a highly valuable tool, as they shed light on the global regulatory network of TMEM16A. Indeed, in a recent study using cancer cell lines (chapter 1.2), we showed how the traffic screen can also be useful for the identification of TMEM16A inhibitors, namely in the context of head and neck cancers[259]. Aberrant upregulation of TMEM16A has been reported in various types of cancers, including gastro-intestinal squamous cancer[120], head and neck squamous cell carcinoma[121], breast cancer[122], and lung cancer[123], being generally linked with a poor prognosis[124]. Interestingly, in some cancer cell lines, although TMEM16A expression is highly upregulated, the Ca^{2+}-activated currents are not increased. This may be explained by the fact that TMEM16A is mostly localized intracellularly and not at the cell surface[203]. Also, TMEM16A upregulation has been shown to occur under conditions that also stimulate cell proliferation[108], being therefore not clear if TMEM16A aberrant expression in cancer is a cause or a consequence of increased proliferation.

Concerns about the effects of activating TMEM16A on bronchoconstriction have also been raised[91]. However, a new TMEM16A potentiator, ETX001, increased Cl^- secretion and ASL height and promoted MCC in primary CF bronchial epithelial cells in in vivo sheep models, while showing no effects on airway smooth muscle contraction[109]. This compound is currently in phase I clinical trials, and the results will be fundamental to understand the potential of using TMEM16A as an alternative Cl^- channel in CF.

Furthermore, it is important to note that TMEM16A and CFTR are intimately connected. The knockout of TMEM16A in mouse airways and intestine, and also in human cells, eliminates both Ca^{2+} and cAMP-activated Cl^- currents[85]. The expression of CFTR at the PM is also compromised in the absence of TMEM16A. Moreover, we have

previously reported that there is a significant overlap between cAMP-dependent and Ca^{2+}-activated Cl^- currents due to the crosstalk of compartmentalized signalling molecules[251] (chapter 2.1). We found that in the absence of PM-localized CFTR, a significant portion of the cAMP-activated Cl^- current is due to TMEM16A[251] (chapter 2.1). Additionally, we have recently observed in several cell models that TMEM16A and TMEM16F, another PM-localized TMEM16 paralogue, are essential for CFTR function and insertion at the PM, as well as for F508del-CFTR correction by its modulator drugs VX-809 + VX-770[260] (chapter 2.2).

ADRA2C and CXCR3 as regulators of TMEM16A PM expression and function

In the present study, because we focused on increasing the PM expression of TMEM16A to potentiate Cl^- secretion in CF cells, we searched for modulators that improved its traffic and not its total expression levels, while also not increasing Ca^{2+} levels inside the cell. In our HTS, among the 691 genes screens, we identified 262 hits putative regulators (179 siRNAs enhancing and 83 decreasing) of TMEM16A PM traffic (38% hit rate). This number is quite high, but in order to avoid having false negatives in the primary screen, we considered all genes with at least one siRNA with a score above +1. However, only 20 hits out of 179 putative inhibitor genes were confirmed during the secondary screen, validating their role on TMEM16A function (11% validation rate). This validation rate is actually lower that the one reported in data from multiple high-content screens, which have estimated that ~30% of siRNAs effects can be confirmed[166,177,261]. The reason for this may be two-fold: 1) our parameters to consider genes as hits were more stringent in the validation screen; 2) different cell lines express different genes, and consequently some of the hits obtained in CFBE cells (traffic screen) may not be expressed in HEK cells (functional assay).

ADRA2C and CXCR3 are negative regulators of TMEM16A PM expression and function in a CF relevant cellular model (CFBE cells). While these data highlight again the importance of this screening platform for unravelling the TMEM16A interactome and for drug discovery, they demonstrate that the two GPCRs identified, when blocked, might enhance TMEM16A-mediated Cl^- secretion in all individuals with CF, thus being potential novel targets for CF therapies.

ADRA2C and CXCR3 encode G_i protein-coupled receptors (α_{2C}-adrenergic receptor [α_{2C}-R], and C-X-C chemokine receptor type 3, respectively). Upon receptor stimulation, the α_i subunit of the heterotrimeric G protein is activated and dissociated

from the βγ dimer, leading to the inhibition of AC, and consequently blocking the synthesis of the second messenger cAMP from ATP[256]. Hence, our first hypothesis was that inhibition (or in this case silencing) of GPCRs would lead to an increase in cAMP levels, which could be the cause of TMEM16A increased activity, due to the crosstalk between Ca^{2+} and cAMP signalling pathways. Accordingly, receptor overexpression would decrease $[cAMP]_i$, also diminishing TMEM16A activity. Our data with ADRA2C or CXCR3 overexpression, however, showed no differences in basal cAMP levels when compared to control cells, while demonstrating a strong increase in $[cAMP]_i$ when G_i was inhibited by PTX, indicating that G_i is more active in cells overexpressing ADRA2C or CXCR3. These data suggest that these GPCRs, when overexpressed, are either active without ligand stimulation or they can be activated due to the presence of receptor agonists in the culture medium, which is true at least for ADRA2C, as epinephrine and/or norepinephrine are present in foetal bovine serum (FBS) used in cell culture[262].

In fact, our microscopy experiments with mCherry-tagged ADRA2C and CXCR3 show a great number of internalized receptors, which then co-localize with TMEM16A intracellularly, suggesting ligand-induced desensitization/internalization of these GPCRs. Also, our data show that agonist stimulation of ADRA2C (with clonidine) or CXCR3 (with CXCL11) does not further inhibit TMEM16A activity. Functional studies of TMEM16A under the presence of cAMP-increasing agents confirmed that the effects of ADRA2C and CXCR3 on TMEM16A traffic and function are not caused by changes in global cAMP levels. Small, localized changes, however, cannot be excluded.

Although inhibition of AC is the main coupling pathway for the α_2-adrenergic receptors, studies showed that α_{2A}-R (another α_2 receptor subtype) agonist stimulation leads to an increase in $[Ca^{2+}]_i$ that involves activation of phospholipase C (PLC) by $G_{\beta\gamma}$ subunits[263]. Likewise, agonist stimulation of CXCR3 leads to $[Ca^{2+}]_i$ increase in T cells in a PLC-dependent process[264]. Additionally, studies in rat aorta suggested that increased cAMP (which is expected with ADRA2C/CXCR3 knockdown) depletes intracellular Ca^{2+} stores through activation of Protein Kinase A (PKA) and EPAC, thus reducing the amount of Ca^{2+} released by IP_3-generating agonists, such as ATP[265]. This is a possible explanation for the lower $[Ca^{2+}]_i$ upon ATP stimulation observed in siRNA-transfected cells, and for the small (not significant) increase in basal $[Ca^{2+}]_i$ in these cells.

Altogether, these data suggest that the increase in TMEM16A PM expression and function observed with the knockdown of ADRA2C and CXCR3 are not caused by intracellular Ca^{2+} nor cAMP increase. Instead, the two GPCRs seem to interact with TMEM16A in a similar way, likely by destabilizing it in a post-Golgi event, either by

promoting endocytosis or preventing its recycling to the PM (Fig. 25). This was confirmed by simultaneously knocking down the GPCR hits and genes involved in the retrograde transport or in clathrin-mediated endocytosis.

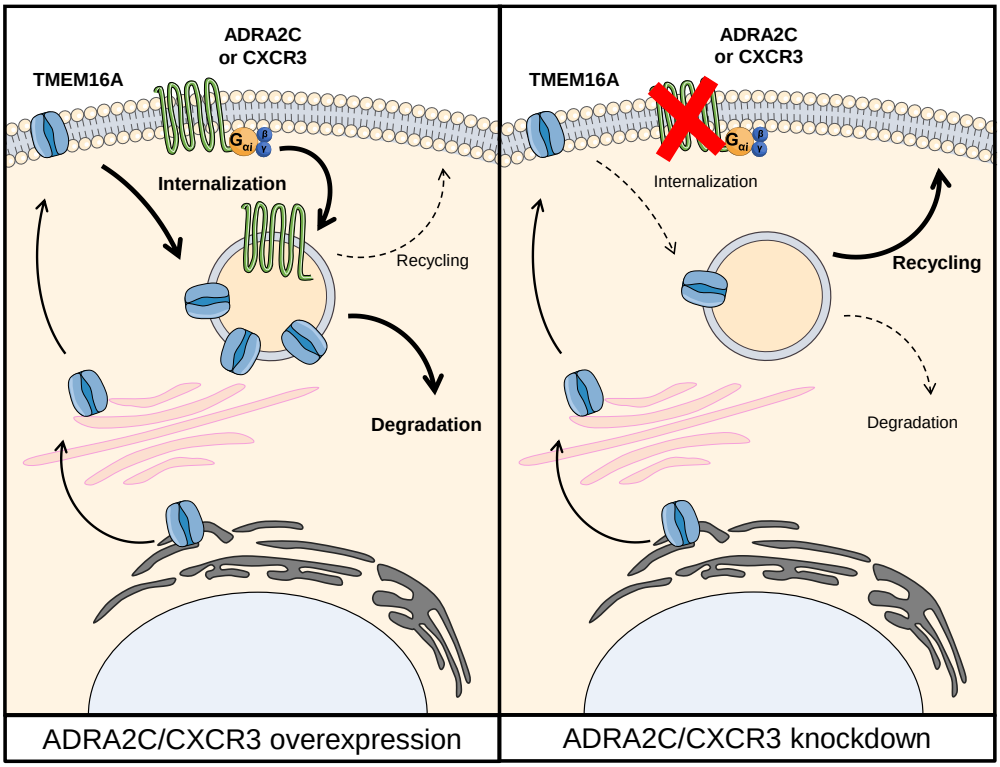

Figure 25 – Model for the regulation of TMEM16A traffic by ADRA2C/CXCR3.

The increase in TMEM16A PM expression caused by knocking down ADRA2C or CXCR3 was further augmented by the knockdown of COPB1 and COPZ1, which mediate traffic within the Golgi and from the cis-Golgi back to the ER (retrograde). Silencing of components of the COPI trafficking machinery had already been shown to promote TMEM16A PM expression[226] (chapter 1.1). These results suggest that the interaction between the hits and TMEM16A occurs after the latter exits the Golgi (Fig. 25).

GPCR signalling is commonly regulated by receptor phosphorylation and internalization, processes which depend on agonist binding. Agonist-bound GPCRs are phosphorylated by GPCR kinases (GRKs), which then bind to arrestin proteins and are internalized[266]. Internalization seems to be important for dephosphorylation and resensitization of GPCRs[267]. α_2 receptors, such as the α_{2C}-adrenergic receptor, seem to follow the same mechanism[268]. In contrast, although CXCR3 is also endocytosed after

ligand binding, it is not recycled to the PM, being instead degraded after internalization[269]. Therefore, since overexpressed ADRA2C and CXCR3 were partially internalized and co-localized with TMEM16A intracellularly, our interpretation of this data is that TMEM16A is endocytosed together with ADRA2C and/or CXCR3 when they are internalized. Consequently, siRNA knockdown of these GPCRs leads to increased stabilization of TMEM16A at the PM, which is further potentiated when there is more TMEM16A exiting the Golgi (namely after COPB1 and COPZ1 knockdown).

Although not much is known regarding TMEM16A endocytosis and recycling, CFTR is endocytosed in clathrin-coated vesicles, and approximately 50% is recycled back to the PM[270]. Also, we have previously seen that treatment of CFBE cells with brefeldin A (which collapses the Golgi and thus blocks secretory traffic) does not decrease Ca^{2+}-activated Cl^- currents nor TMEM16A PM levels up to 24 hours[251] (chapter 2.1), which indicates that TMEM16A is either following an alternative trafficking route, or, most likely, that it is rapidly recycled to the PM after internalization.

AP-2 is an endocytic adaptor important for cargo uptake in clathrin-mediated endocytosis[258,271]. The knockdown of the subunit μ of AP-2 (siAP2M1), did not significantly alter TMEM16A expression at the PM, although its score is close to the hit threshold (score = 0.843). This result might be explained by previous data showing a small but detectable expression of AP-2 in the clathrin coated pits that still form (although in lower amounts) in the siRNA treated cells[258]. Alternatively, TMEM16A might have additional endocytosis routes. However, co-transfection of cells with siAP2M1 and siRNAs targeting either ADRA2C or CXCR3 strongly reduced the effects observed when the siRNAs are employed individually. Other findings suggest that depletion of AP-2 affects endocytic trafficking through the non-clathrin, ADP-ribosylation factor (Arf) 6 regulated pathway, promoting lysosomal targeting and degradation of Arf6-pathway cargo over recycling[272]. Therefore, siAP2M1 might not completely inhibit endocytosis, but instead block TMEM16A recycling to the PM. Consequently, although siADRA2C or siCXCR3 prevent some endocytosis of TMEM16A, simultaneous knockdown of AP2M1 inhibits TMEM16A recycling, eliminating the positive effects of silencing the GPCRs.

Conclusions

Here we present two GPCRs (ADRA2C and CXCR3) as novel modulators of TMEM16A, which appear to work as destabilizers of TMEM16A at the PM. Uncoupling of TMEM16A membrane sorting from these GPCRs or silencing/blocking them may be

a way of increasing Cl^- secretion in CF. However, owing to TMEM16A importance in physiology and pathology, as well as to its therapeutic potential, there is an urgent need to improve our understanding of how TMEM16A contributes to human disease, and to better define drugs and conditions for using this channel as a therapeutic target in CF and other respiratory disorders. We believe that, similarly to what happens with CFTR modulator drugs, CF patients would benefit from a combination of therapies. Namely, the knockdown (and possibly the inhibition) of these GPCRs would increase the PM expression of TMEM16A, and its activation could be further potentiated by compounds such as EXT001 that has been proven to enhance fluid secretion and ASL height in CF-HBE cells, and also mucociliary clearance in ovine models[109].

Chapter 2

Digging into the relationship between TMEM16 proteins and CFTR

Data included in this chapter were published in:

1. Lérias JR*, **Pinto MC***, Benedetto R, Schreiber R, Amaral MD, Aureli M, Kunzelmann K. Compartmentalized crosstalk of CFTR and TMEM16A (ANO1) through EPAC1 and ADCY1. *Cell. Signal.* **2018**, *44*, 10–19, doi:10.1016/j.cellsig.2018.01.008. [*Shared first authorship]

2. Benedetto R, Ousingsawat J, Cabrita I, **Pinto MC**, Lérias JR, Wanitchakool P, Schreiber R, Kunzelmann K. Plasma membrane–localized TMEM16 proteins are indispensable for expression of CFTR. *J. Mol. Med.* **2019**, 97(5):711-722, doi:10.1007/s00109-019-01770-4.

1. Compartmentalized crosstalk of CFTR and TMEM16A (ANO1) through EPAC1 and ADCY1

Introduction

TMEM16A (anoctamin 1, ANO1) is a Ca^{2+} activated chloride (Cl^-) channel[73–75]. In their ground-breaking publication Yang et al. reported receptor-activated and Ca^{2+}-dependent Cl^- currents conferred by TMEM16A[73]. Larger ATP-activated TMEM16A currents have been regularly observed in the presence of additional purinergic $P2Y_2$ receptors, although ATP-induced increase in intracellular Ca^{2+} was not changed by additional receptors[273]. This suggests i) that ATP-induced Ca^{2+} signals take place within a well shielded plasma membrane (PM) domain/compartment and ii) that additional mechanisms for receptor-channel coupling may exist in such a compartment.

In Xenopus oocytes the Cl^- ion channel cystic fibrosis transmembrane conductance regulator (CFTR) is activated through stimulation of purinergic $P2Y_2$ receptors[274]. Recent work also demonstrated activation of CFTR by purinergic stimulation of airway epithelial cells[85,275]. Thus, CFTR may serve as Cl^- secretory pathway for Ca^{2+} enhancing agonists, probably via Ca^{2+}-sensitive adenylate cyclase[85,275]. Also other G-protein coupled receptors (GPCRs) such as muscarinic receptors can activate CFTR via increase in intracellular cAMP, by the help of tyrosine kinases[276]. An intimate relationship between TMEM16A and CFTR has been suggested earlier[110], and was demonstrated recently in TMEM16A-knockout mice, which exhibit both compromised Ca^{2+}-dependent and cAMP-activated Cl^- transport[85]. Here we provide for the first time evidence for a colocalization of GPCRs, CFTR and TMEM16A in functional membrane compartments/microdomains together with Ca^{2+}-sensitive adenylate cyclase type 1 (ADCY1) and exchange protein directly activated by cAMP (EPAC1). Compartmentalization of these signalling molecules will provide intense crosstalk between Ca^{2+} and cAMP signals and explains parallel activation of the Cl^- channels CFTR and TMEM16A.

Results

G-protein coupled receptors control activation of the Ca^{2+} dependent Cl^- channel TMEM16A

In human airway epithelial cells expressing wild type CFTR (CFBE wt-CFTR) stimulation of $P2Y_2$ receptors ($P2Y_2R$) with ATP (100 µM) activates whole cell currents (Fig. 26A,B). Expectedly, siRNA-knockdown of $P2Y_2R$ ($siP2Y_2$; Fig. S21A – Appendix 2) inhibited activation of currents by ATP, but surprisingly also attenuated direct activation by the Ca^{2+} ionophore ionomycin (IONO) (Fig. 26C). However, increase in intracellular Ca^{2+} ($[Ca^{2+}]_i$) by IONO was not affected by $siP2Y_2R$, in contrast to ATP-induced $[Ca^{2+}]_i$ (Fig. 26D,E). Overexpression of $P2Y_2R$ in CFBE cells expressing wt-CFTR or F508del-CFTR, dramatically enhanced Cl^- currents activated by ATP as well as by IONO (Fig. 26F,G), while global cytosolic $[Ca^{2+}]_i$ increase by ATP and IONO were not affected (Fig. 26H,I). The effect of additional $P2Y_2R$ on current increase was remarkably bigger in cells expressing wt-CFTR than F508del-CFTR (Fig. 26F,G).

Very similar results were obtained by overexpressing muscarinic M3 receptors (M3R), which are not expressed endogenously in CFBE cells. Expression of M3R not only induced carbachol (CCH)-activated whole cell currents, but unexpectedly also enhanced ATP-activated currents (Fig. S21B,C – Appendix 2). Finally, stimulation of histamine H1 receptors, another type of phospholipase C (PLC)-coupled GPCR, activated larger whole cell currents in cells overexpressing $P2Y_2R$ (Fig. S21D – Appendix 2). These experiments suggest that i) expression of $G_{q/11}$ and PLC-coupled GPCRs translocate additional signalling proteins to the PM to activate Cl^- currents, and that ii) Ca^{2+}-dependent whole cell currents are strongly CFTR-dependent[85]. Additional proteins are probably required to assemble the signalosome, such as scaffold proteins. In further preliminary experiments we found that siRNA-knockdown of Na^+/H^+ Exchanger Regulatory Factor 1 (NHERF1) attenuated both CFTR and TMEM16A-related Cl^- currents[277].

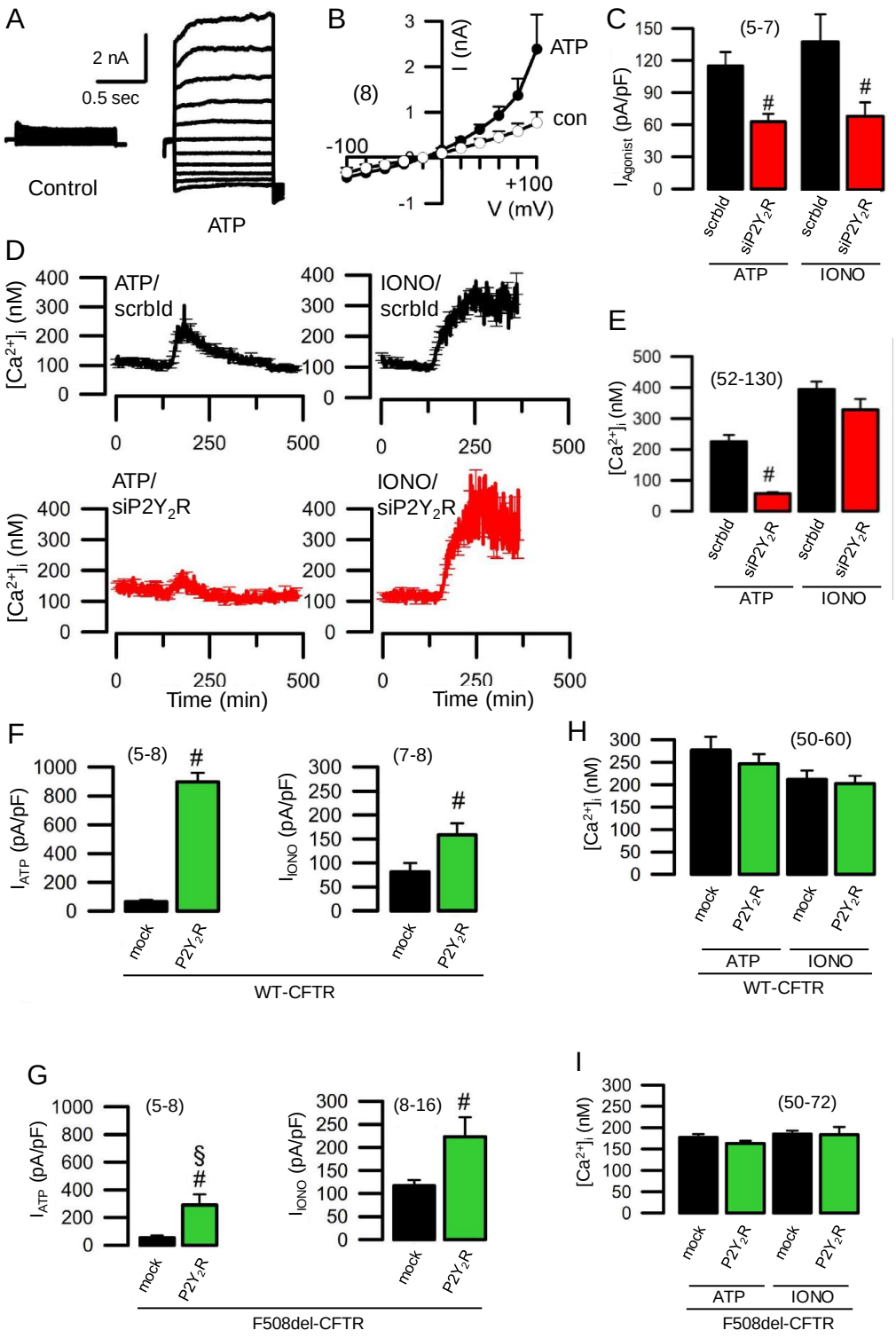

Figure 26 – $P2Y_2$ G-protein coupled receptors control activation of the Ca^{2+} dependent Cl^- channel TMEM16A. (A) Whole cell currents activated by ATP (100 µM) in CFBE airway epithelial cells. **(B)** Corresponding current/voltage relationships. **(C)** Activation of TMEM16A by ATP (100 µM) or ionomycin (IONO; 0.1 µM). Summary of current densities in cells treated with scrambled RNA (Scrbld) or siRNA for $P2Y_2$ receptors (siP2Y_2R). ATP- and IONO-dependent activation of TMEM16A were inhibited by knockdown of P2Y_2R. **(D)** Increase in intracellular Ca^{2+} ($[Ca^{2+}]_i$) by stimulation with ATP or IONO, as measured by Fura2 (mean curves ± SEM). **(E)** Summary of $[Ca^{2+}]_i$ indicates no inhibition of IONO-induced increase in $[Ca^{2+}]_i$ by knockdown of P2Y_2R. In contrast, ATP-induced $[Ca^{2+}]_i$ increase was reduced. **(F)** Overexpression of P2Y_2R largely augmented ATP (100 µM)-induced TMEM16A currents and doubled IONO-activated TMEM16A

currents in CFBE wt-CFTR cells. **(G)** Overexpression of $P2Y_2R$ in CFBE F508del-CFTR cells caused a smaller increase in ATP/IONO-activated whole cell currents. **(H,I)** Expression of additional $P2Y_2R$ did not change intracellular Ca^{2+} signals in CFBE wt-CFTR or CFBE F508del-CFTR cells. Mean ± SEM (number of cells measured). # Significant difference when compared with Scrbld or Mock ($p < 0.05$, unpaired t-test). § Significantly smaller than in wt-CFTR ($p < 0.05$, unpaired t-test). Data in collaboration with Joana Lérias.

CFTR but not GPCRs affect membrane expression of TMEM16A

CFTR and/or $P2Y_2R$ may affect activation of whole cell currents by changing expression levels or PM localization of TMEM16A. However, similar levels of TMEM16A were found with knockdown or overexpression of $P2Y_2R$ in CFBE wt-/F508del-CFTR cells or in HEK293 cells (Fig. 27A,B, Fig. S21E – Appendix 2). Moreover, membrane expression of TMEM16A was not affected by knockdown or overexpression of $P2Y_2R$, when analysed by immunofluorescence or chemiluminescence (Fig. 27C–H, Fig. S21F – Appendix 2). Membrane expression of TMEM16A was also not changed by overexpression of M3R but was generally lower in CFBE F508del-CFTR cells (Fig. 27C–H, Fig. S21G – Appendix 2).

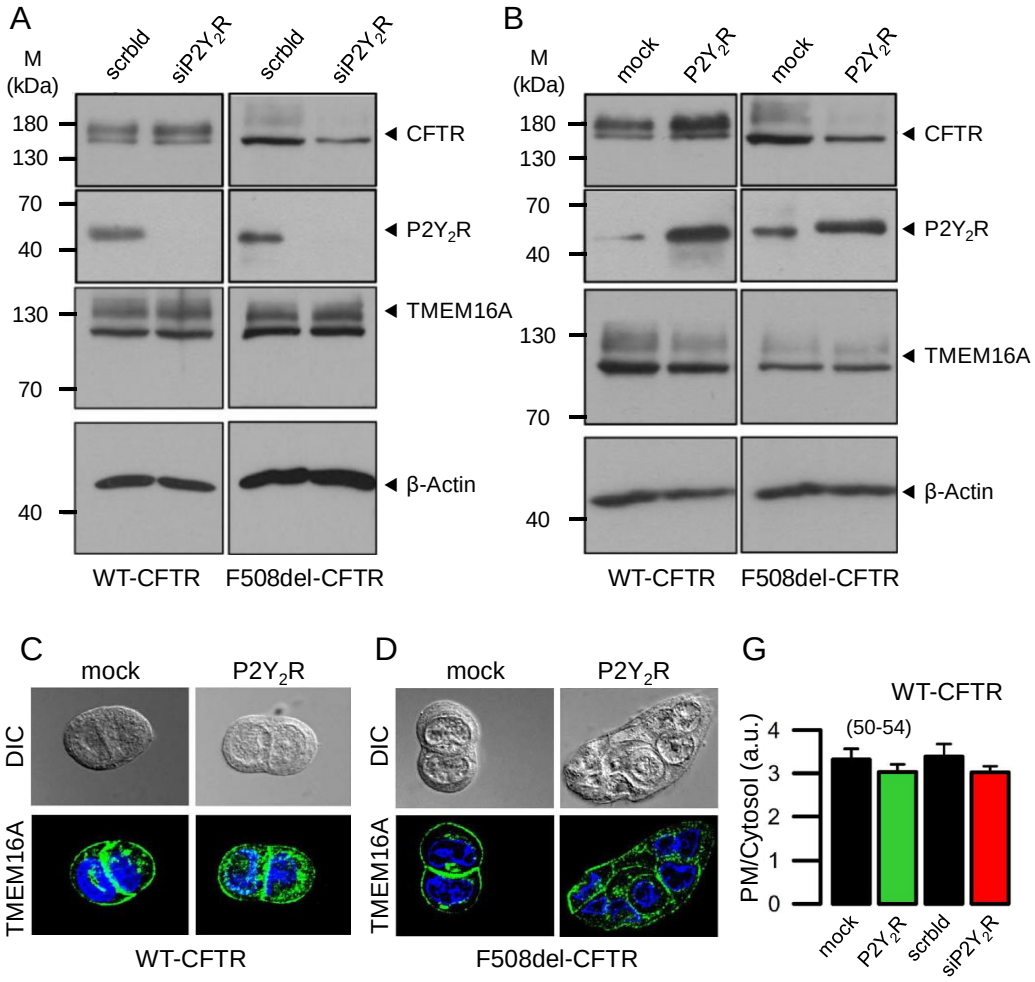

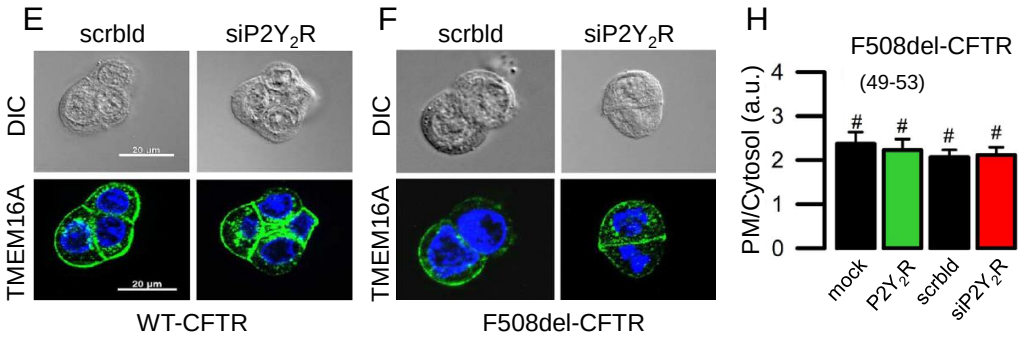

Figure 27 – $P2Y_2R$ do not change expression and localization of TMEM16A. (A,B) Western blots showing expression of CFTR, $P2Y_2R$ and TMEM16A. ß-actin is shown as gel loading control. Similar expression levels were detected for TMEM16A in CFBE wt-/F508del-CFTR cells. siRNA-knockdown of $P2Y_2R$ or overexpression of $P2Y_2R$ had no clear effects on TMEM16A expression. **(C-F)** Immunofluorescence of TMEM16A in CFBE wt-/F508del-CFTR cells. siRNA-knockdown of $P2Y_2R$ or overexpression of $P2Y_2R$ had no obvious effect on cellular localization of TMEM16A. **(G,H)** Analysis of cellular distribution of TMEM16A in CFBE wt-/F508del-CFTR cells by quantitative assessment of fluorescence in PM/cytoplasm (au; arbitrary units). Bars indicate 10 µm. Mean ± SEM (number of experiments or total number of cells measured in different experiments [>3]). # Significant difference when compared with wt-CFTR ($p < 0.05$, unpaired t-test). Data in collaboration with Joana Lérias.

Purinergic receptors augment CFTR whole cell currents

We found that the presence of $P2Y_2R$ not only enhances ATP- and IONO-activated Cl^- currents (Fig. 26), but also CFTR Cl^- currents stimulated with IBMX and forskolin (I/F) (Fig. 28A–D). Notably, significant I/F activated Cl^- currents could even be detected in CFBE cells expressing F508del-CFTR, upon additional expression of $P2Y_2R$ (Fig. 28C,D). Expression of wt-CFTR and F508del-CFTR were not affected by knockdown or overexpression of $P2Y_2R$, when analysed by immunofluorescence and chemiluminescence (Fig. 28E–L). wt-CFTR is well expressed in the PM, but not F508del-CFTR, and thus I/F should be unable to activate F508del-CFTR. However, I/F activated a whole cell current in F508del-CFTR expressing cells (Fig. 28C,D). We found that wt-CFTR currents activated by membrane permeable 8-Br-cAMP were largely independent of $P2Y_2R$, in contrast to activation by I/F (Fig. 29A). This result suggests that Ca^{2+}-dependent adenylate cyclases are translocated to the PM by $P2Y_2R$. We also noticed that 8-Br-cAMP activated a small, albeit significant Cl^- current in CFBE cells expressing F508del-CFTR. This current demonstrated a TMEM16A-typical time dependent activation and outward rectification (inset in Fig. 29A) and is therefore not a CFTR-current. Activation of this current by 8-Br-cAMP was abolished by knockdown of $P2Y_2R$ (Fig. 29A). These results strongly suggest that the 8-Br-cAMP signal has been converted most likely by EPAC1, into a Ca^{2+} signal, which activated TMEM16A. EPAC1 (also known as RAPGEF3) functions as a guanine nucleotide exchange factor (GEF) for both

Rap1 and Rap2. EPAC1 may have been translocated to a PM compartment by $P2Y_2R$. In fact, 8-substituted cAMP derivatives such as 8-Br-cAMP or 8-pCPT-2-O-MecAMP (007-AM) are known to be potent activators of EPAC1[278]. The current activated by 8-Br-cAMP or 8-pCPT-2-O-Me-cAMP (007-AM) was inhibited by the TMEM16A-inhibitor A01 (Fig. 29C). As an earlier study was unable to demonstrate a direct relation of TMEM16A by cAMP/TMEM16A, it is unlikely that 8-Br-cAMP directly activated TMEM16A[236].

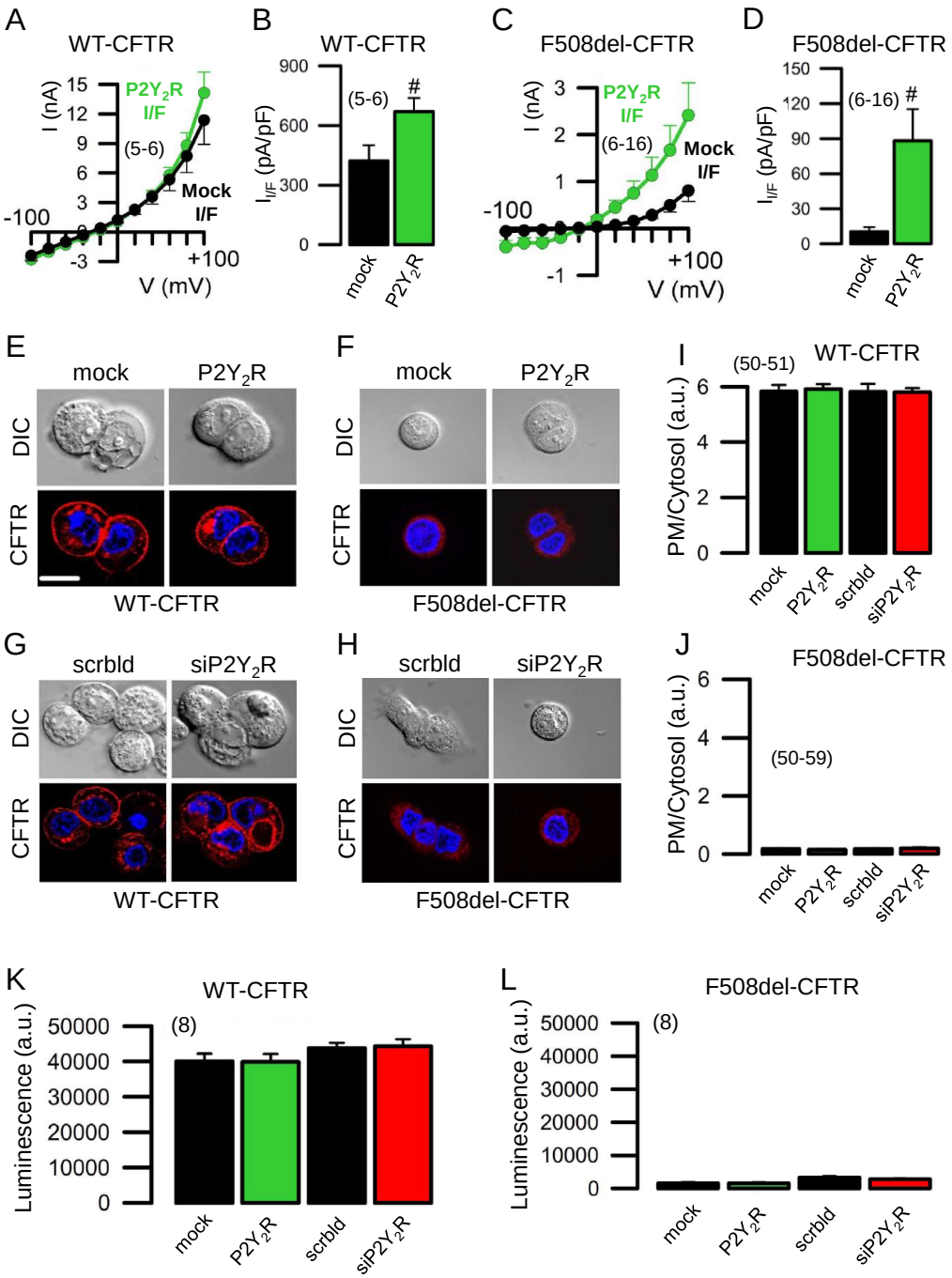

Figure 28 – $P2Y_2R$ control activation of CFTR but not CFTR membrane expression. (A-D) Current/voltage relationships and current densities from patch-clamp experiments in mock transfected and $P2Y_2R$ overexpressing CFBE wt-/F508del-CFTR cells. Cells were stimulated with 100 µM IBMX and 2 µM

forskolin (I/F). **(E,H)** Expression of wt-CFTR and F508del-CFTR as detected by mCherry-fluorescence (live-cell imaging). $P2Y_2R$ was overexpressed or endogenous $P2Y_2R$ was knocked down by $siP2Y_2R$. **(I,J)** Ratios for expression of wt-CFTR or F508del-CFTR in PM versus cytoplasm (au; arbitrary units). **(K,L)** Membrane expression of wt-CFTR and F508del-CFTR as detected by chemiluminescence, using an extracellular FLAG tag inserted into the first extracellular loop of CFTR and an anti-FLAG antibody. Mean ± SEM (number of experiments or total number of cells measured in different experiments [>3]). # Significant difference when compared with mock ($p < 0.05$, unpaired t-test). Scale bar, 10 µm. Data in collaboration with Joana Lérias.

Role of EPAC1 for activation of Cl^- currents

Expression of EPAC1 was well detected in CFBE cells (Fig. 29B). Using the EPAC1 activator 007-AM, whole cell Cl^- currents were activated in CFBE wt-CFTR cells that were strongly inhibited by removal of extracellular Cl^- (5 Cl^-). Both TMEM16-inhibitor CaCCinh-A01 (A01) and CFTR inhibitor CFTRinh172 partially inhibited 007-AM-activated Cl^- currents, suggesting that both (CFTR and TMEM16A) Cl^- secretory pathways are activated by 007-AM (Fig. 29C). The role of EPAC1 for activation of TMEM16A and CFTR was further examined using the EPAC1-inhibitor ESI09. While ESI09 did not block stimulation of Cl^- currents by ATP or IONO in mock transfected CFBE wt- and F508del-CFTR cells, it inhibited ATP/IONO-activated Cl^- currents in cells overexpressing $P2Y_2R$. Inhibition by ESI09 was more pronounced in CFBE F508del-CFTR cells (Fig. 29D). Moreover, I/F-induced currents in wt-CFTR and F508del-CFTR expressing cells were inhibited by ESI09 by about 50%. Additional currents in the presence of $P2Y_2R$ were completely inhibited by ESI09 (Fig. 29E). Immunocytochemistry detected localization of EPAC1 (in red) closer to the PM in cells expressing additional $P2Y_2R$ (in green) (Fig. 29F,G). Taken together, a significant portion of the I/F-activated Cl^- current is EPAC1-dependent and this portion is further enhanced by additional expression of GPCRs.

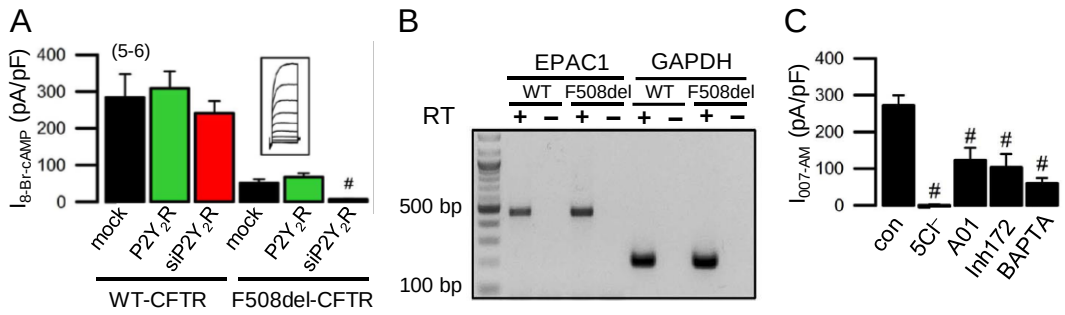

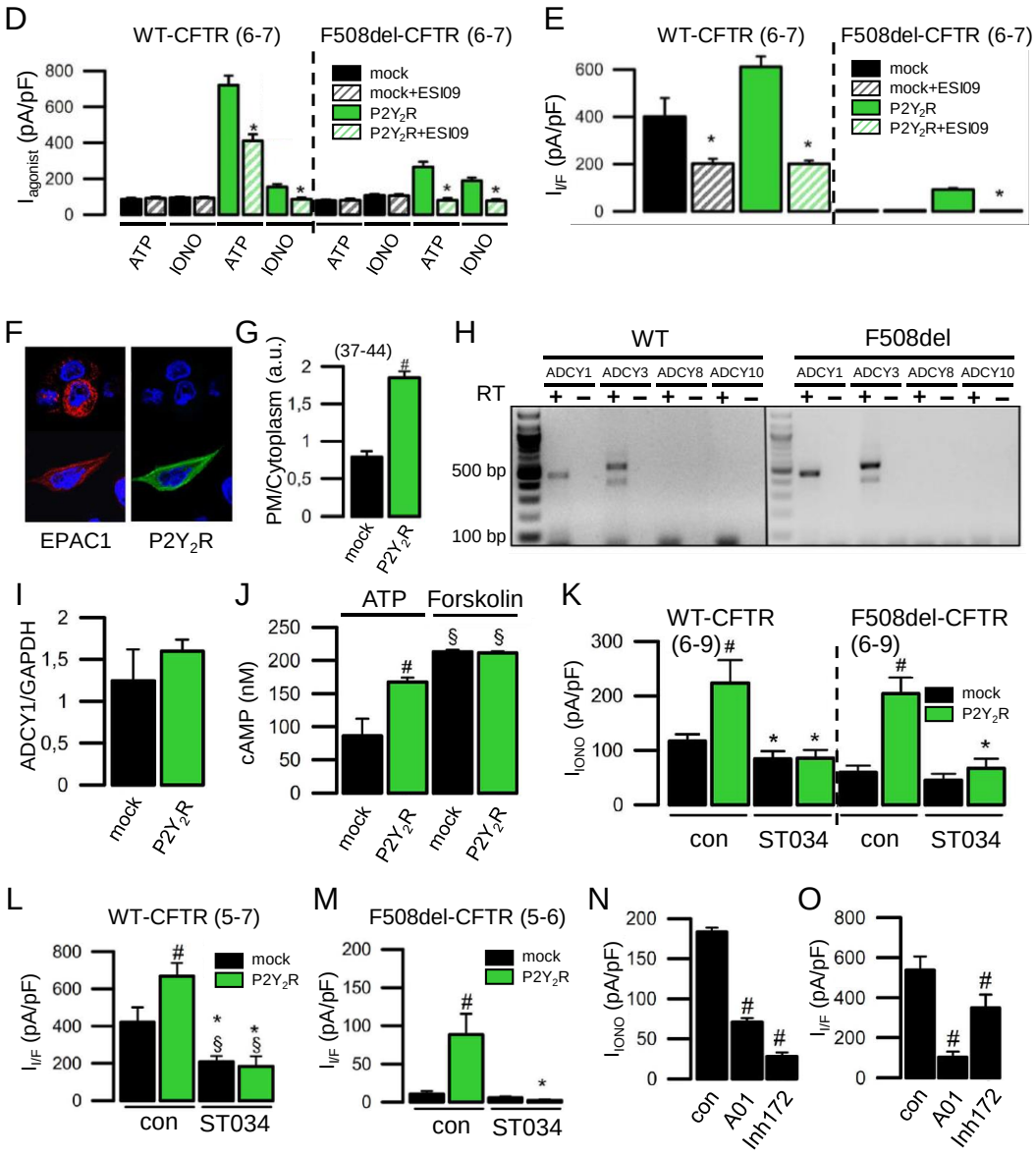

Figure 29 – EPAC1 and ADCY1 mediate cAMP/Ca^{2+} crosstalk and cross-activation of TMEM16A and CFTR. (A) Summary of current densities obtained by stimulation of CFBE wt- and F508del-CFTR cells with 8-Bromo cAMP (25 µM). Cells overexpressed $P2Y_2R$ or endogenous $P2Y_2R$ was knocked-down by si$P2Y_2R$. **(B)** RT-PCR demonstrating expression of EPAC1 in CFBE wt-/F508del-CFTR cells. **(C)** Summary of current densities measured in cells stimulated with the EPAC1 activator 007-AM (30 µM). Replacement of extracellular Cl^- by impermeable gluconate ($5Cl^-$), or application of the TMEM16A inhibitor CaCCinh-A01 (A01; 30 µM), or application of the CFTR-inhibitor CFTRinh172 (Inh172; 30 µM) inhibited current densities. Ca^{2+} chelating by BAPTA-AM (50 µM) also inhibited activation by 007-AM. **(D)** Currents densities activated by ATP (100 µM) and ionomycin (IONO; 0.1 µM), respectively, and inhibition by the EPAC1 inhibitor ESI09 (10 µM) in CFBE wt-/F508del-CFTR cells. **(E)** Current densities activated by 100 µM IBMX and 2 µM forskolin (I/F) in CFBE wt-/F508del-CFTR cells. Cells were mock transfected or overexpressed $P2Y_2R$. Effects of the EPAC1-inhibitor ESI09. **(F)** Immunocytochemistry of EPAC1 and $P2Y_2R$ in CFBE wt-CFTR cells. **(G)** Ratio of EPAC1 expression in PM versus cytoplasm in mock transfected cells and cells overexpressing $P2Y_2R$ (arbitrary units; au). **(H)** RT-PCR indicating expression of the Ca^{2+}-sensitive adenylate cyclases (ADCY) 1 and 3 but not 8 and 10. **(I)** Relative expression of ADCY1-mRNA in mock transfected and $P2Y_2R$-overexpressing cells. **(J)** Increase in intracellular cAMP levels induced by stimulation with ATP (100 µM) and 100 µM IBMX/2 µM forskolin (I/F). **(K)** Current densities activated by IONO (0.1 µM) in mock transfected and $P2Y_2R$-expressing CFBE wt- and F508del-CFTR cells, and inhibition by the ADCY1-inhibitor ST034307 (ST034; 30 µM). **(L,M)** Current densities activated by I/F in mock and $P2Y_2R$-expressing CFBE wt-CFTR **(L)** and F508del-CFTR **(M)** cells, and inhibition by the ADCY1-inhibitor ST034. **(N,O)** Inhibition of Cl^- currents

(current densities) by CaCCinh-A01 (A01; 30 µM) and CFTR inhibitor CFTRinh172 (30 µM). Mean ± SEM (number of cells measured). # Significant difference when compared with con or mock ($p < 0.05$, unpaired t-test). § Significant difference when compared with wt-CFTR expressing cells ($p < 0.05$, unpaired t-test). * Significant inhibition by ST034 ($p < 0.05$, paired t-test). Experiments performed by Joana Lérias and Rainer Schreiber.

Role of ADCY1 for activation of Cl^- currents

Because CFTR can be activated by ATP, we examined expression of the Ca^{2+}-sensitive adenylate cyclases (ADCYs). ADCY1 and ADCY3 (but not ADCY8 or ADCY10) are expressed in both CFBE wt-CFTR and F508del-CFTR cells at approximately similar levels (Fig. 29H). We found that activation of purinergic receptors with ATP increased intracellular cAMP, and cAMP increase was further enhanced by additional expression of $P2Y_2R$. Remarkably, in the presence of $P2Y_2R$, ATP-induced rise in intracellular cAMP was almost as high as with stimulation by I/F (Fig. 29J). Yet, expression levels for ADCY1 were not affected by additional $P2Y_2R$ (Fig. 29I). Namkung et al. demonstrated the role of ADCY1 for ATP-activated and CFTR-dependent Cl^- secretion in airway epithelial cells[275]. We therefore used the ADCY1-specific inhibitor ST034307 (ST034) to further examine the role of ADCY1 for IONO activated Cl^- secretion. In the presence of additional $P2Y_2R$, Ca^{2+} activated Cl^- secretion by IONO was strongly inhibited by ST034 (Fig. 29K). Remarkably, ST034 potently blocked I/F-activated currents in CFBE wt-CFTR cells and inhibited I/F-induced currents in $P2Y_2R$-expressing CFBE F508del-CFTR cells, indicating the dominating role of ADCY1 for generation of cAMP (Fig. 29L,M). Taken together, an intensive crosstalk between cAMP- and Ca^{2+}-dependent signalling exists in airway epithelial cells due to EPAC1 and ADCY1, converting cAMP into Ca^{2+} signals and vice versa (Fig. S22 – Appendix 2). Intensive crosstalk prevents clear discrimination between adrenergic/CFTR and purinergic/TMEM16A dependent Cl^- secretion. This is further indicated by the fact that specific inhibitors for CFTR (CFTRinh172) and TMEM16 (CACCinh-A01) inhibit both, Ca^{2+} and I/F-activated currents (Fig. 29N,O). Crosstalk and interaction between CFTR and TMEM16A amplify electrolyte secretion. This new insight is applicable to cystic fibrosis and the search for novel pathways to improve defective Cl^- secretion[85].

Discussion

The present data demonstrate the role of EPAC1 and ADCY1 for cross activation of CFTR and TMEM16A by cAMP and Ca^{2+}. Previous studies indicated an intimate functional relationship between CFTR and TMEM16A and demonstrated cAMP-activated transport being almost absent in epithelia from TMEM16A knockout mice[85]. TMEM16A was shown to be essential for proper activation as well as membrane expression of CFTR. We showed that TMEM16A causes ER Ca^{2+} store release, thereby engaging Store Operated cAMP Signalling (SOcAMPS) and activation of Ca^{2+} regulated adenylyl cyclases (ADCYs)[229]. Here we show that cAMP-dependent and Ca^{2+} activated Cl^- currents in airway epithelial cells strongly overlap due to the crosstalk of intracellular signalling molecules. The present results are in line with an earlier study that reported activation of CFTR via $P2Y_2R$[274]. Notably, evidence was provided that TMEM16A can also be activated by a Ca^{2+} independent but G-protein-dependent mechanism[199]. Apart from the described crosstalk between TMEM16A and CFTR via Ca^{2+} dependent ADCY1 and cAMP regulated EPAC1, additional crosstalk via Ca^{2+} dependent cAMP phosphodiesterase (PDE1), and possibly via PDE4 may take place. Such an additional regulatory circuit would further modulate the cooperativity between these channels. As our studies were performed in the presence of the PDE-inhibitor IBMX and non-hydrolysable analogues of cAMP, subsequent studies will have to clarify the contributions of PDEs.

Crosstalk of TMEM16A and CFTR is relevant in ciliated airway epithelial cells and intestinal epithelial cells, which are both Cl^- and fluid secreting. However, TMEM16A is expressed at higher levels in mucus producing club cells and goblet cells. Upregulation of TMEM16A during inflammation might therefore increase its impact on fluid and mucus secretion. This may be even more relevant in the case of cystic fibrosis (CF), where functional CFTR is absent and thus the direct impact of TMEM16A on fluid secretion (which requires functional CFTR) might be negligible. Nevertheless, a direct small molecule opener of TMEM16A could be beneficial in CF.

This signalling/functional overlap is likely to take place in a shielded membrane compartment. Membrane bound ADCYs are known to colocalize with PLC-coupled GPCRs possibly in lipid raft-like membrane compartments[279]. TMEM16A and CFTR have been both located in lipid rafts[173,280], while EPAC1 was shown to colocalize with CFTR[278]. EPAC1 is a known hub for cAMP/Ca^{2+} crosstalk[278,281,282]. We found enrichment of $P2Y_2R$ in an immunoprecipitate against TMEM16A, further supporting the existence of such functional membrane platforms (Fig. 30). Signalling occurring in such functional

compartments is well shielded. The EPAC1 activator 007-AM induced a whole cell Cl^- current. Activation of this current was suppressed by the Ca^{2+} chelator BAPTA-AM, demonstrating the role of intracellular Ca^{2+} (Fig. 29C). Moreover, 50–60% of the whole cell current activated by I/F were inhibited by the EPAC1-inhibior ESI09, indicating a central role of EPAC1 in regulating Cl^- secretion (Fig. 29E). However, I/F did not increase global intracellular Ca^{2+} levels measured by Fura2 (Fig. 30B). In contrast, local compartmentalized Ca^{2+} was increased by I/F and 007-AM in close proximity of CFTR, which was detected by the Ca^{2+} sensor G-CAMP6 fused to the C-terminus of CFTR (Fig. 30C–E).

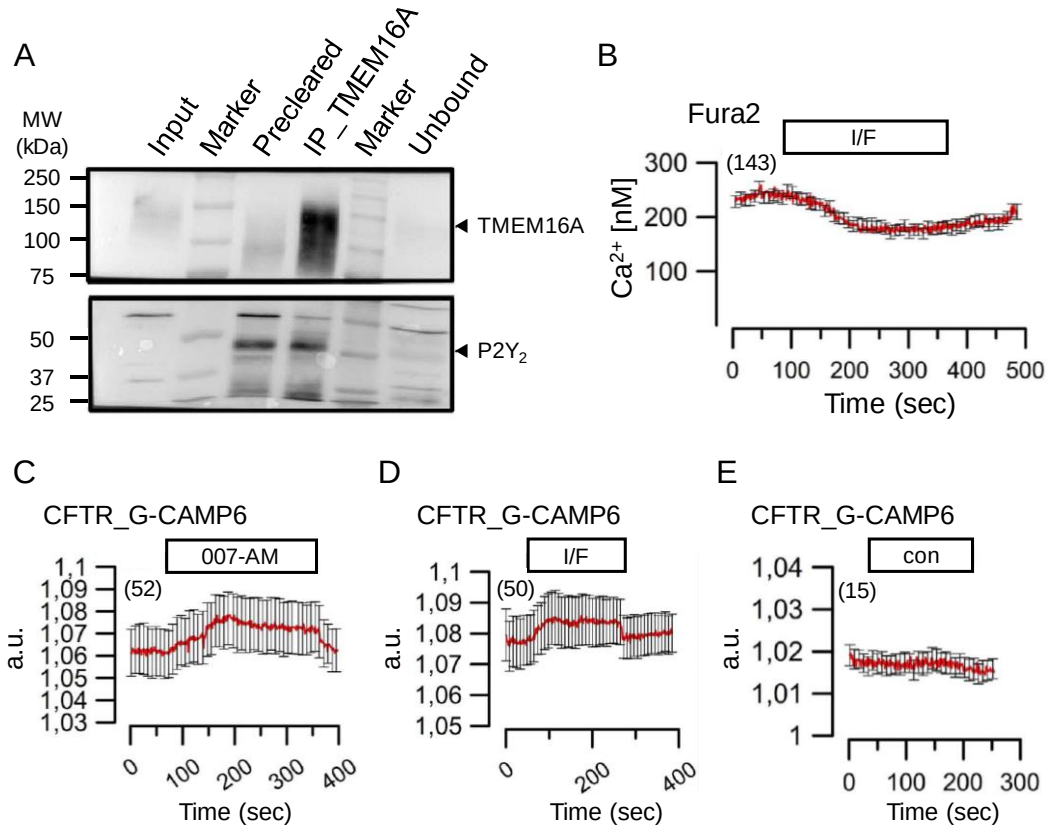

Figure 30 – Compartmentalized Ca^{2+} signalling. (A) Immunoprecipitation of TMEM16A pulled down $P2Y_2R$. Input; cell lysate. Precleared; negative control obtained by incubation of Input for 2 h with Protein-A and Protein-G conjugated beads. IP_TMEM16A; Immunoprecipitation of TMEM16A. Unbound; Supernatant remaining after IP. **(B)** Global intracellular Ca^{2+} (mean ± SEM; n=143), measured by Fura2 in CFBE wt-CFTR cells. I/F rather decreased than increased global intracellular Ca^{2+} levels. **(C,D)** Intracellular compartmentalized Ca^{2+} levels close to the PM, as detected by the Ca^{2+} sensor G-CAMP6, which was fused to the C-terminal end of CFTR. Both I/F and the EPAC1-activator 007-AM slightly enhanced compartmentalized intracellular Ca^{2+} in close proximity to CFTR. **(E)** Control (con); absence of any stimulus. Mean ± SEM (number of cells measured). Experiments performed by Joana Lérias and Roberta Benedetto.

We found earlier (chapter 1.1) that extended synaptotagmins (ESYT1-3) strongly affect activation of TMEM16A through stimulation of $P2Y_2R$. ESYT1-3 tether the

endoplasmic reticulum (ER) close to PM thereby facilitating local Ca^{2+} signalling[283]. Thus ESYT1 stabilizes PM/ER microdomains to allow proper coupling of the Ca^{2+} sensor STIM1 to store operated Orai1 Ca^{2+} influx channels[284]. It seems noteworthy that I/F-activated currents were also found to be ESYT1-dependent: About 50% of the I/F-activated whole cell current was inhibited by siRNA knockdown of ESYT1 (388.1 ± 63.4; n=5, scrambled RNA vs. 195.5 ± 49.3; n=5, siESYT1). This corroborates the intimate relationship between TMEM16A and CFTR and supports colocalization of signalling machines allowing Ca^{2+}/cAMP-crosstalk.

CFTR and TMEM16A are both glycosylated[40,73,285]. Indeed, collapsing the Golgi and thus blocking secretory traffic using BFA eliminated the glycosylated forms of CFTR and TMEM16A (Fig. 31A). Interestingly, membrane trafficking of CFTR was completely inhibited by BFA, while membrane trafficking of TMEM16A remained largely unchanged by BFA (Fig. 31B–E). Astonishingly, although CFTR was completely absent from the cell membrane in BFA-treated cells, whole cell currents activated by I/F were still considerable (about 50%). In fact, I/F-induced currents remained almost unaffected by BFA in cells overexpressing $P2Y_2R$ (Fig. 31F,G). Ca^{2+} (IONO) activated currents were not reduced by BFA (Fig. 31H,I). These rather surprising results confirm that a significant portion of the cAMP-activated Cl^- current is due to TMEM16A and that it appears well justified to screen for more potent activators of TMEM16A to activate Cl^- secretion in cystic fibrosis.

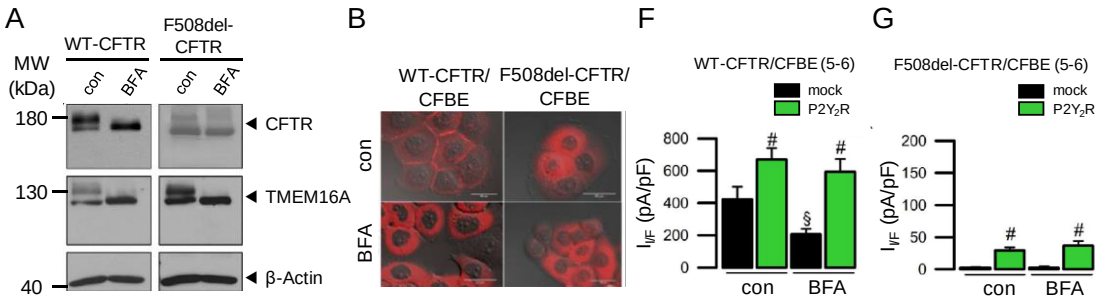

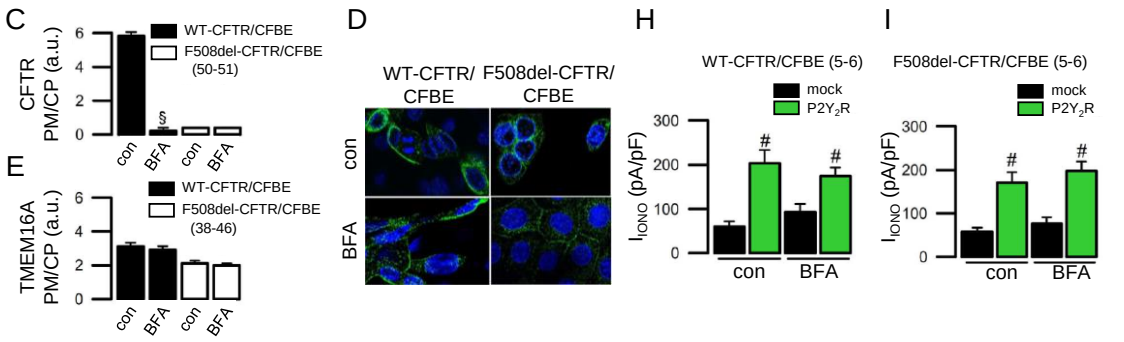

Figure 31 – TMEM16A can compensate for the lack of CFTR in BFA treated cells. (A) Western blots of CFTR and TMEM16A in CFBE wt- and F508del-CFTR cells exposed to control solution (con) or the protein transport inhibitor brefeldin A (BFA; 10 µM/24 h). BFA eliminated the glycosylated forms of CFTR (Band C) and TMEM16A (upper band at 130 kDa). **(B)** Expression of CFTR (mCherry fluorescence in living cells) indicating membrane localization of wt-CFTR (left upper panel), which was completely suppressed by BFA (left lower panel). F508del-CFTR (right panels) was located intracellularly, independent of BFA. **(C)** Ratio of PM vs. cytoplasmic (CP) localization of CFTR, as analysed by fluorescence intensities in regions of interest (ROI). **(D)** Expression of TMEM16A (primary anti-TMEM16A (DOG1)-antibody; secondary fluorescent labelled antibody) indicating variable membrane localization that was not changed by BFA in either CFBE wt-CFTR (left panels) or CFBE F508del-CFTR (right panels) cells. **(E)** Ratio of PM vs. CP localization of TMEM16A indicating no significant changes by BFA. In F508del-CFTR expressing cells, less TMEM16A was membrane localized. **(F)** Whole cell currents activated by IBMX/forskolin (I/F; 100 µM/2 µM) in CFBE wt- and F508del-CFTR cells. In wt-CFTR expressing cells, BFA inhibited only 50% of the I/F-activated current in mock transfected cells. BFA did not inhibit currents in cells overexpressing the purinergic receptors $P2Y_2R$. **(G)** In F508del-CFTR expressing cells, additional currents produced by expression of $P2Y_2R$ were not affected by BFA. **(H,I)** Whole cell currents activated by Ionomycin (IONO; 100 nM) in CFBE wt- and F508del-CFTR cells were not affected by BFA. Mean ± SEM (number of experiments or total number of cells measured in different experiments [>3]). # Significant difference when compared with mock ($p < 0.05$; unpaired Student's t-test). § Significant difference when compared with con ($p < 0.05$; unpaired Student's t-test).

In summary, we demonstrate an intimate relationship between TMEM16A and CFTR, which is enabled by cAMP/Ca^{2+} crosstalk due to EPAC1 and ADCY1. Future studies may supply further details regarding the origin of the compartmentalized submembranous Ca^{2+} signals, and the possible contribution of Ca^{2+}-regulated phosphodiesterases.

2. Plasma membrane–localized TMEM16 proteins are indispensable for expression of CFTR

Introduction

Cystic Fibrosis (CF) is an autosomal recessive disease caused by mutations in the gene encoding cystic fibrosis transmembrane conductance regulator (CFTR). CF affects epithelial tissues such as lungs, the gastrointestinal tract, and reproductive organs. It is characterized by chronic bacterial airway infections with neutrophilic inflammation, airway mucus plugging, and progressive bronchiectasis. The pancreas undergoes cystic and fibrotic degeneration, the intestinal lumen may be occluded by a meconium ileus, and males often demonstrate a bilateral absence of the ductus deferens[286].

Apart from these and other symptoms, the lung disease causes most morbidity and death in people with CF. TMEM16A (anoctamin 1) is a Ca^{2+}-activated Cl^- channel. It belongs to a family of 10 proteins (TMEM16A-K)[71]. TMEM16A is localized in the apical plasma membrane (PM) of epithelial cells, but it can be also found in basolateral and in intracellular compartments[287].

CFTR and TMEM16A are chloride (Cl^-) channels activated by PKA phosphorylation and increase in intracellular Ca^{2+}, respectively. An enigmatic functional relationship between CFTR and TMEM16A has been suggested earlier[110], and recent data show that TMEM16A controls PM expression of CFTR[85]. Intestinal epithelial knockout of TMEM16A in mice surprisingly eliminated both Ca^{2+}-dependent and cAMP-activated Cl^- currents, when measured in isolated colonic epithelial crypt cells. Unlike CFTR-knockout mice lacking intestinal cAMP-dependent Cl^- currents, animals with intestinal epithelial knockout of TMEM16A did not develop small intestinal obstruction[85,287]. Small intestinal epithelium (duodenum, jejunum, and ileum) does not express TMEM16A, and no Ca^{2+}-activated Cl^- channels are found in this tissue. However, the epithelium of the small intestine does present cAMP-activated (CFTR) Cl^- currents[85]. We speculated that CFTR currents might be detectable in the absence of TMEM16A, when other TMEM16 paralogues are present. Moreover, recombinant CFTR is functional when overexpressed in cells without endogenous expression of TMEM16A.

TMEM16F (anoctamin 6) is another TMEM16 paralogue, expressed at low levels in the PM of many mammalian cell types[99,237]. Using a broad range of different cell types,

we demonstrate that either TMEM16A or TMEM16F must be co-expressed in the same cell, to detect PM expression of CFTR and to record cAMP-activated CFTR Cl^- currents.

Results

No CFTR currents without TMEM16A or TMEM16F

We compared CFTR whole cell currents expressed in Scott B lymphocytes[288], with those detected in wt lymphocytes. In contrast to wt lymphocytes, Scott lymphocytes lack expression of functional TMEM16F, which leads to Scott syndrome, a rare bleeding disorder (Fig. 32A). Neither wt nor Scott B lymphocytes express endogenous TMEM16A or CFTR and therefore do not produce whole cell currents after stimulation by ATP (Ca^{2+} increase) or IBMX and forskolin (cAMP increase) (I/F; Fig. 32B,C)[288]. After overexpression of CFTR, whole cell currents were activated by I/F in wt lymphocytes but were absent in Scott lymphocytes (Fig. 32B,C). However, when either TMEM16F or TMEM16A was co-expressed in Scott cells in addition to CFTR, currents were readily activated by I/F. CFTR whole cell currents measured in Scott cells expressing TMEM16F/CFTR or TMEM16A/CFTR were inhibited by CFTRinh172, but interestingly showed a variable response when extracellular Cl^- was replaced by I^- (Fig. 32C,D). These results clearly demonstrate a requirement of TMEM16 proteins for CFTR to operate.

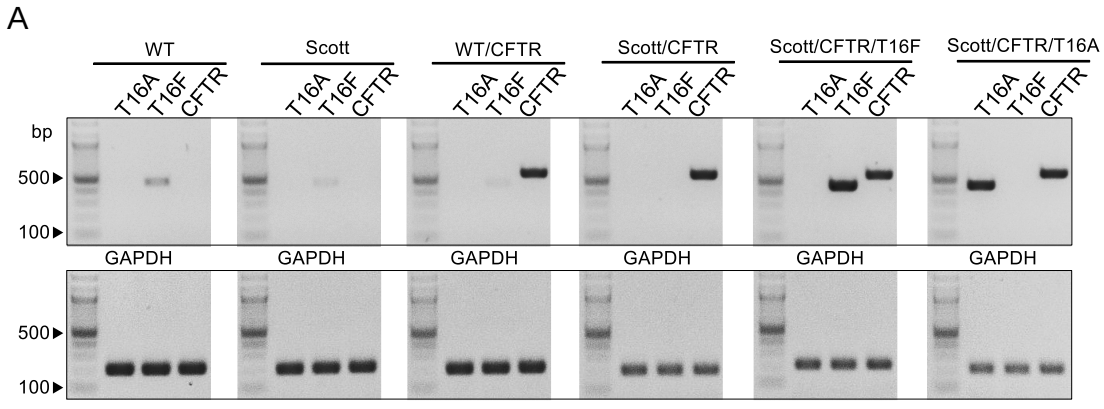

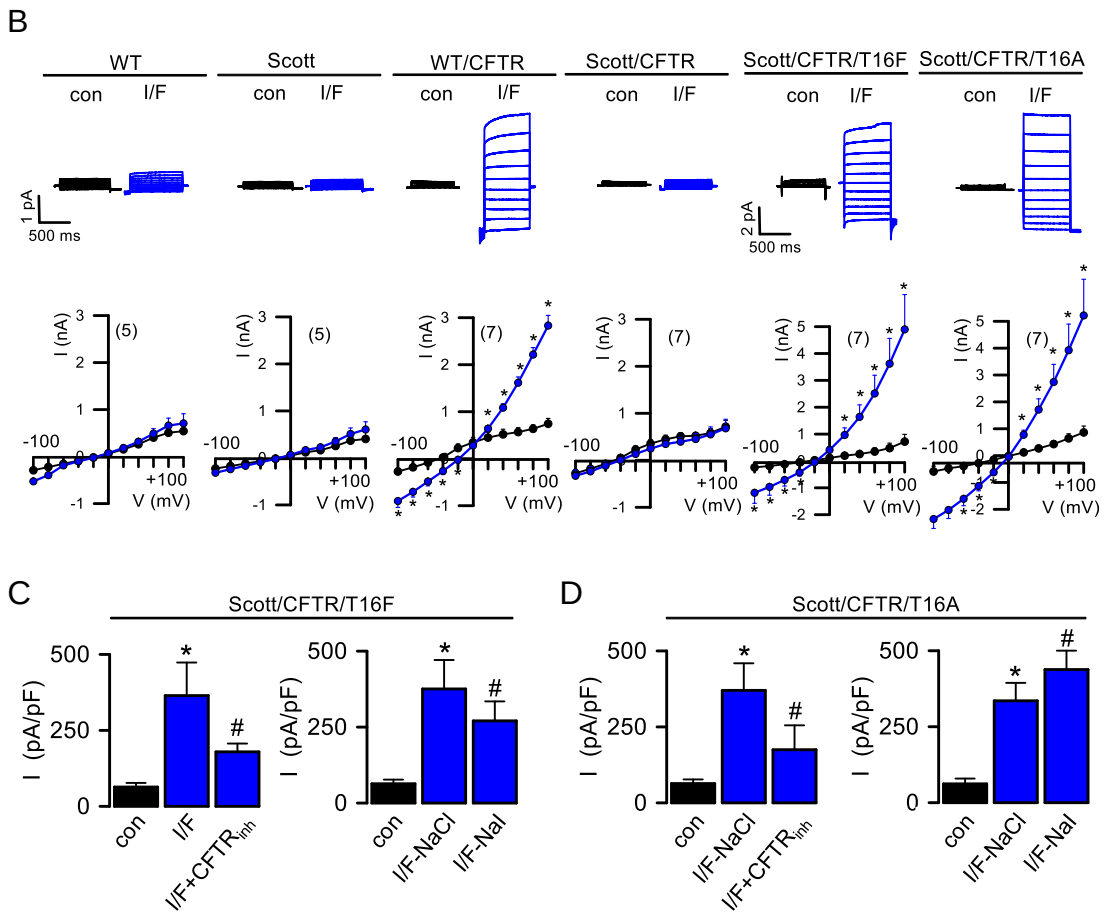

Figure 32 – No CFTR currents without TMEM16A or TMEM16F. (A) Semi-quantitative PCR analysis of TMEM16A (T16A), TMEM16F (T16F), and CFTR in wt and Scott B lymphocytes. Expression determined in non-transfected, CFTR-transfected, and CFTR/T16F or CFTR/T16A co-transfected cells. **(B)** Whole cell current overlays (Vc = ± 100 mV, steps 20 mV) activated by IBMX and forskolin (I/F; 100/2 μM) in non-transfected and overexpressing cells. Lower panels: corresponding current/voltage relationships. **(C, D)** Effect of CFTRinh172 (30 μM) and replacement of extracellular Cl^- by I^- on current densities (Vc = + 100 mV) in CFTR/T16F- and CFTR/T16A-transfected Scott cells. Mean ± SEM (number of cells measured). *Significant current activation ($p < 0.05$; paired t test). #Significant inhibition by CFTRinh172 and Cl^- replacement by I^- ($p < 0.05$; paired t test). Data in collaboration with Roberta Benedetto and Rainer Schreiber.

Membrane expression of CFTR requires TMEM16A or TMEM16F

The results obtained with B lymphocytes were further corroborated by experiments performed in Calu3 cells, which express TMEM16A, TMEM16F, and CFTR endogenously, and which produce large CFTR whole cell currents when activated by I/F (Fig. 33A–C). In Calu3 cells, siRNA knockdown of TMEM16A showed little inhibition of CFTR currents. This is explained by the fact that although these cells express high levels of TMEM16A, it does not move to the cell membrane. Thus, purinergic stimulation by ATP does not activate whole cell Cl^- currents (data not shown[289]). In contrast, knockdown

of TMEM16F inhibited CFTR currents markedly. In contrast to TMEM16A, TMEM16F is very well expressed in the PM of Calu3 cells. This also explains the lack of CaCC in these cells. Double knockdown of TMEM16A/F showed only little additional inhibition of CFTR currents (Fig. 33C,D). Thus, in Calu3 cells, TMEM16F is crucial for the function of CFTR. Using the Ca^{2+} ionophore ionomycin, we found that increase of intracellular Ca^{2+} in cells lacking expression of TMEM16F (siTMEM16F-treated cells) does not enhance I/F activation of CFTR currents (Fig. 33E,F).

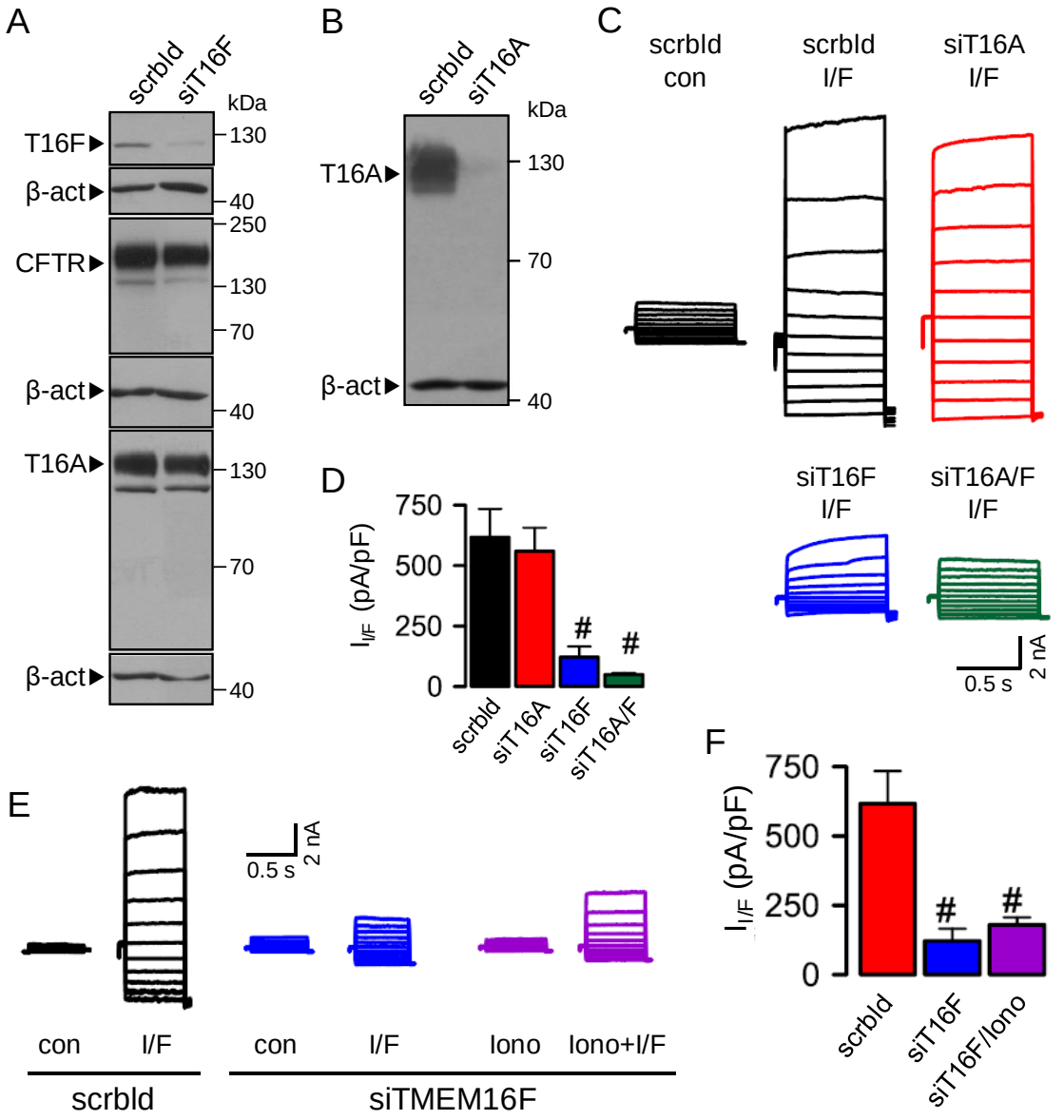

Figure 33 – TMEM16F but not TMEM16A is essential for CFTR function in Calu3 cells. (A, B) Western blots for TMEM16F, CFTR, and TMEM16A. Knockdown of TMEM16F and TMEM16A, respectively, by siRNA. Densitometry analysis and ratios of bands for TMEM16F/β-actin and TMEM16A/β-actin indicates a knockdown of 90.5 ± 7.1% for TMEM16F and 96.3 ± 6.9% for TMEM16A. CFTR expression was not changed significantly by siTMEM16F. **(C)** Whole cell current overlays (Vc = ± 100 mV, steps 20 mV) activated by IBMX and forskolin (I/F; 100/2 µM) in cells treated with siRNA for TMEM16A/F or scrambled RNA. **(D)** Corresponding current densities obtained at Vc = + 100 mV. **(E)** Suppression of I/F-activated whole cell

currents in the absence and presence of ionomycin (1 µM). **(F)** Summary of corresponding current densities. Mean ± SEM (number of cells measured). #Significant difference when compared with scrambled ($p < 0.05$, ANOVA). Data in collaboration with Roberta Benedetto and Joana Lérias.

Immunofluorescence showed that TMEM16F is well expressed in the PM, while TMEM16A showed little membrane expression (Fig. 34A). We found that siRNA knockdown of TMEM16F largely reduced membrane expression of CFTR, while knockdown of TMEM16A attenuated membrane expression of CFTR only marginally (Fig. 34B,C). The poor PM expression of TMEM16A is probably the reason why knockdown of TMEM16A had little effects on CFTR currents. In contrast, TMEM16F is well expressed in the PM of Calu3 cells, and strongly regulated CFTR. Using membrane surface biotinylation, we examined if knockdown of TMEM16A/F affects membrane expression of CFTR. After treatment of the cells with scrambled RNA (siScrbld) or combined knockdown of TMEM16A/F, biotinylated proteins were separated by SDS page. The results show indeed poor PM expression of TMEM16A and demonstrate a strong PM expression for TMEM16F. A large portion of CFTR is expressed in the PM of cells treated with scrambled RNA (Fig. 34D). siRNA knockdown of TMEM16A together with siTMEM16F strongly suppressed expression of TMEM16 proteins and basically abolished PM expression of CFTR (Fig. 34D). Additionally, we found that knockdown of TMEM16F also inhibited membrane expression of CFTR in CFBE cells similar to the effects observed for TMEM16A[85] (Fig. S23 – Appendix 2).These results clearly indicate the requirement of TMEM16A/F for PM expression of CFTR.

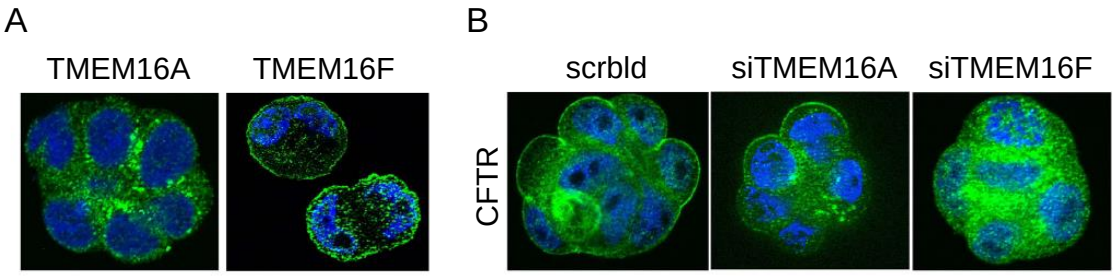

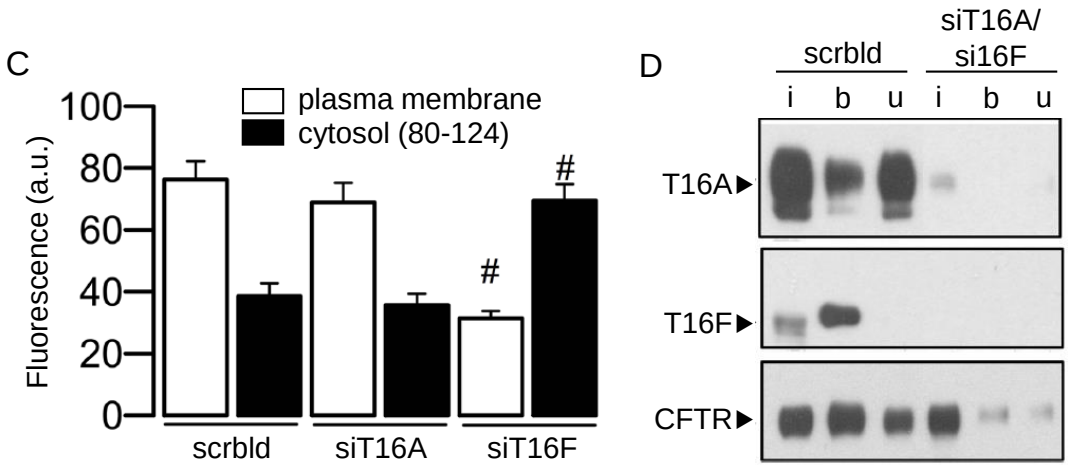

Figure 34 – TMEM16F controls membrane expression of CFTR in Calu3 cells. (A) Immunocytochemistry of TMEM16A and TMEM16F. **(B)** Effect of knockdown of TMEM16A/F on PM expression of CFTR. **(C)** Analysis of fluorescence intensity for CFTR staining in PM and cytosol. **(D)** Membrane biotinylation of TMEM16A, TMEM16F, and CFTR, and effect of double knockout of TMEM16A/F on membrane expression of CFTR. I, input; b, biotinylated; u, unbound. Densitometry analysis revealed a knockdown of 94.2% for TMEM16A and 98.7% for TMEM16F. CFTR expression was not changed significantly by siTMEM16F. Mean ± SEM (number of cells measured). #Significant difference when compared with scrambled ($p < 0.05$, ANOVA). Data in collaboration with Podchanart Wanitchakool.

In an additional set of experiments with HeLa cells, we confirmed these findings and examined if TMEM16A and TMEM16F have comparable effects on membrane expression of CFTR. HeLa cells express endogenousTMEM16F (T16F), but not TMEM16A (T16A) or CFTR (Fig. 35A). Upon overexpression of CFTR, whole cell Cl^- currents were activated by stimulation with I/F. However, CFTR currents were completely absent after knockdown of TMEM16F (Fig. 35A, B). Additional expression of TMEM16A (in cells with TMEM16F knockdown) fully restored CFTR currents. CFTR currents measured in the presence of either TMEM16A or TMEM16F had a selectivity of $Cl^- > I^-$ (Fig. 35C). Currents activated by I/F were almost completely inhibited by the CFTR blocker CFTRinh172 (30 µM; data not shown). CFTR was well biotinylated when expressed in HeLa cells expressing endogenousTMEM16F, indicating PM expression (Fig. 35E; siScrbld). However, knockdown of endogenous TMEM16F almost eliminated PM expression of CFTR, while additional overexpression of TMEM16A restored PM expression of CFTR. The results clearly show that TMEM16A and TMEM16F have a comparable positive impact on expression of CFTR in the PM.

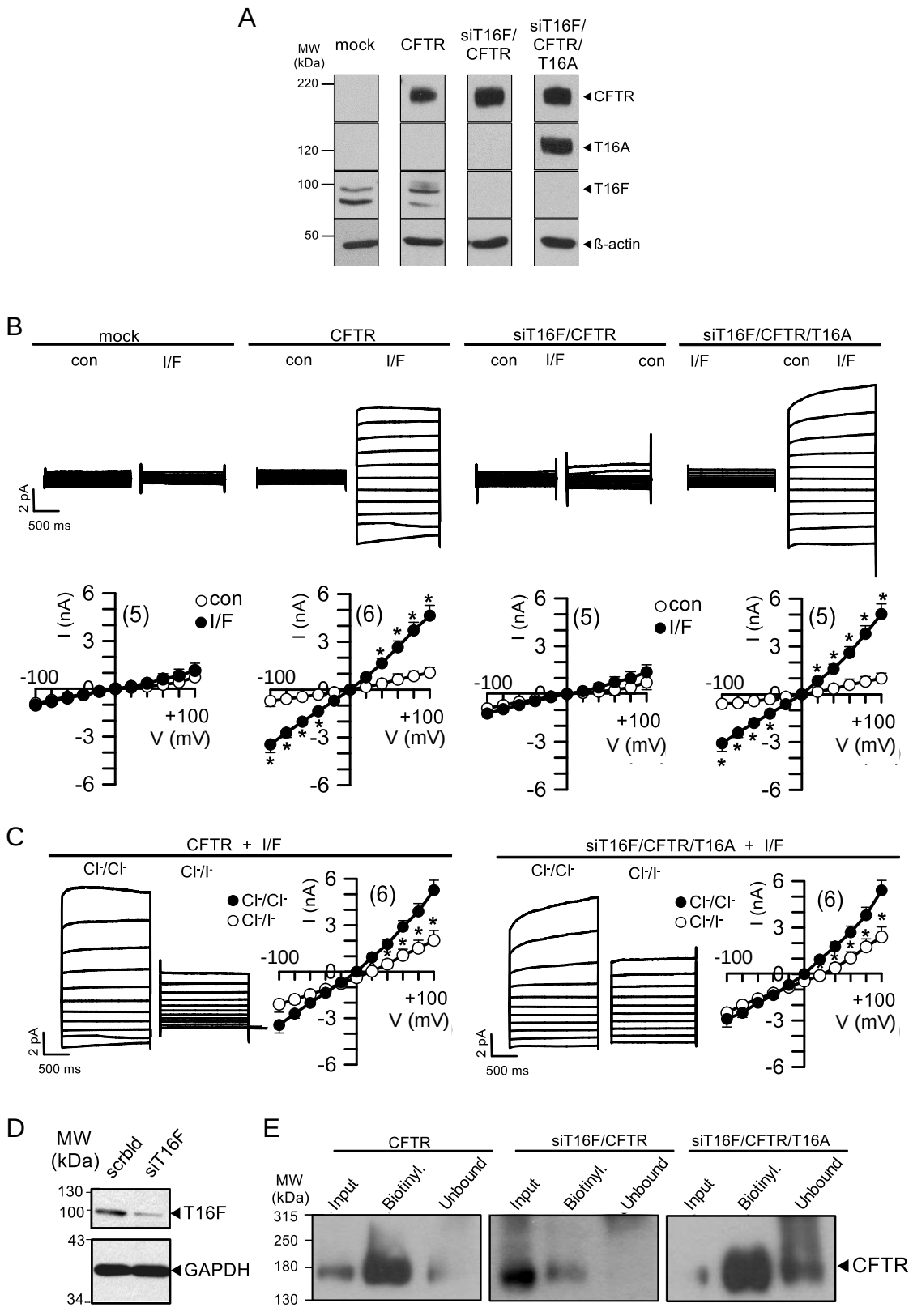

Figure 35 – TMEM16A can replace TMEM16F to control membrane expression of CFTR. (A) Western blots for TMEM16A, TMEM16F, and CFTR. siRNA knockdown of endogenous TMEM16F and overexpression of CFTR and TMEM16A. **(B)** Whole cell currents overlays (Vc = ± 100 mV, steps 20 mV) before and after stimulation with I/F in mock-transfected and in overexpressing cells. Lower panels:

corresponding current/voltage relationships. **(C)** Inhibition of CFTR whole cell currents by replacement of extracellular Cl^- by I^- in the presence of endogenous TMEM16F or overexpressed TMEM16A. **(D)** Western blot indicating siRNA knockdown of TMEM16F. **(E)** Membrane biotinylation of CFTR in the presence and absence of endogenous TMEM16F. Regain of CFTR biotinylation after TMEM16F knockdown by expression of TMEM16A. Densitometry analysis revealed a knockdown of 98% for TMEM16F. Mean ± SEM (number of cells). *Significant activation by I/F, and current inhibition by replacement of extracellular Cl^-, respectively ($p < 0.05$; paired t test). Data in collaboration with Roberta Benedetto and Podchanart Wanitchakool.

Effect of TMEM16A/F knockdown on F508del-CFTR correction by Orkambi

Given the clear relationship between TMEM16A/F expression and the efficient trafficking and function of wt-CFTR, we assessed the rescue of F508del-CFTR (the most common CFTR mutant, with a trafficking defect) by CFTR-modulator drugs in the presence or absence of TMEM16A/F.

Incubation of CFBE cells expressing F508del-CFTR for 24h with the corrector VX-809 (lumacaftor) together with the acute addition of the potentiator VX-770 (ivacaftor) – combination sold under the brand name Orkambi – led to a significant activation of whole cell currents by I/F (Fig. 36). However, double knockdown of TMEM16A and TMEM16F strongly diminished the F508del-CFTR whole cell currents rescued by Orkambi, almost to the levels of non-treated cells (Fig. 36). As expected, Ca^{2+}-activated Cl^- currents were also reduced with the siRNA knockdown of TMEM16A/F (Fig. 36C). These results confirm, once more, the role of TMEM16A/F on membrane insertion of CFTR.

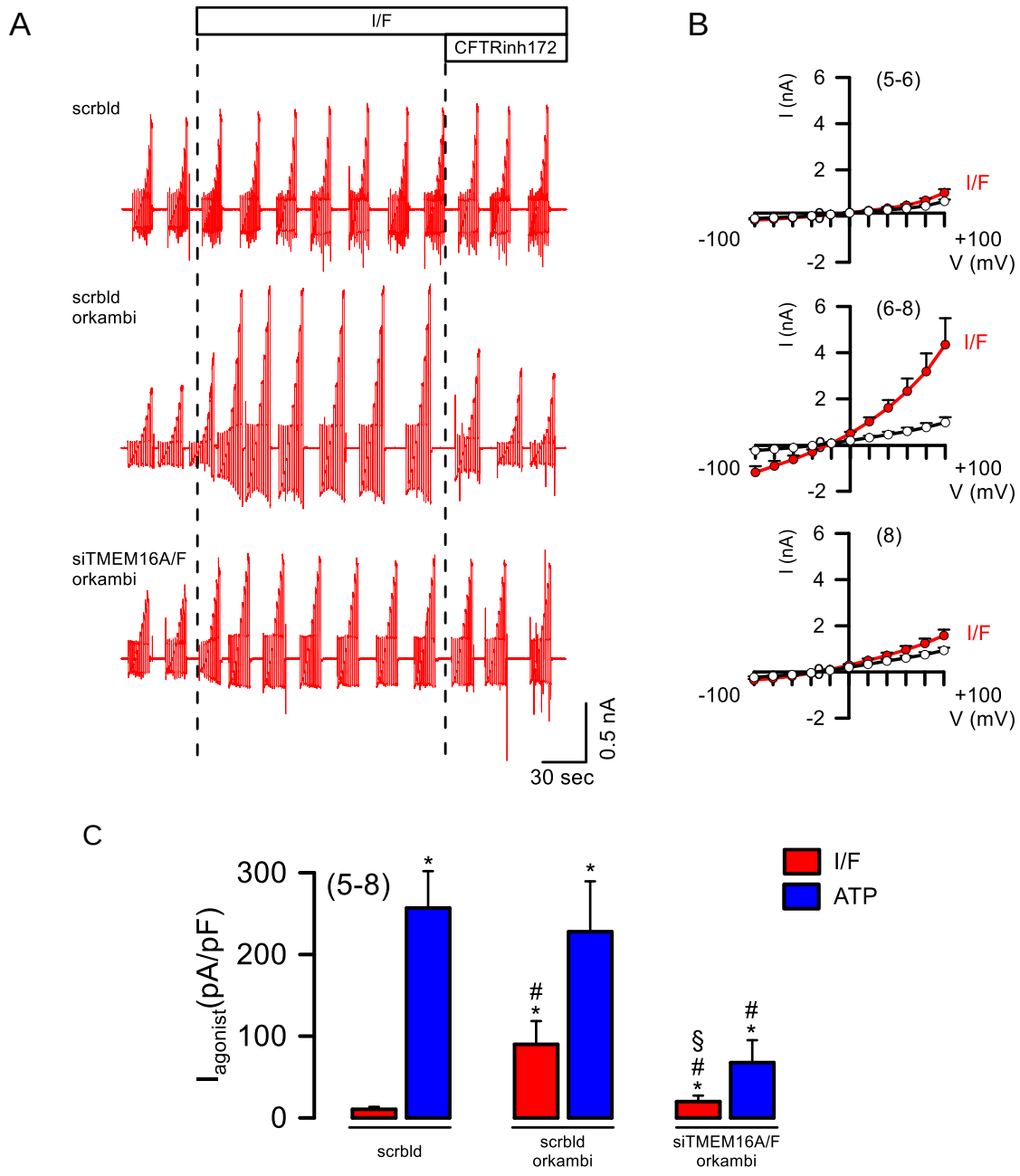

Figure 36 – Correction of F508del-CFTR by Orkambi is inhibited by knockdown of TMEM16A/F. (A) Continuous whole cell patch-clamp recordings showing no activation of F508del-CFTR overexpressed in CFBE cells by forskolin (2 μM) and IBMX (100 μM) (I/F) (upper panel). 24 hrs exposure of CFBE F508del-CFTR cells with VX809 + short exposure to VX-770 (both 3 μM; Orkambi) rescued F508del-CFTR currents, i.e., CFTR currents could be activated by I/F (middle panel). Knockdown of TMEM16A/F by siRNA (48 hrs) inhibited the effect of Orkambi (lower panel). **(B)** Corresponding current / voltage relationship. **(C)** Summary of the whole cell currents activated by I/F and ATP (100 μM) in the different cells. Mean ± SEM (number of cells measured). *Significant activation by I/F and ATP, respectively ($p < 0.05$; paired t-test). #Significant difference when compared to scrambled siRNA ($p < 0.05$; unpaired t-test). §Significant difference when compared to scrambled siRNA + Orkambi treatment ($p < 0.05$; unpaired t-test).

Discussion

TMEM16 proteins control membrane expression

Using different cell types, we show that regulation of CFTR by TMEM16A/F is not a tissue-specific event, but rather a general phenomenon. Most cells express variable levels of endogenous TMEM16A/F. Typically, TMEM16F is expressed at low levels in most cell types, except of osteoblasts, macrophages, lymphocytes, and other immune cells, which show higher levels of PM expression[167].

The human submucosal airway cells Calu3 express TMEM16A, TMEM16F, and CFTR. Although TMEM16A is expressed at high levels, CaCC is very small in these cells (100 µM ATP actives only 25 ± 1.8 pA/pS; n = 5), because most TMEM16A does not reach the PM but is located intracellularly[289] (Fig. 34A). This may also explain its marginal impact on CFTR: obviously, only PM-localized TMEM16 proteins control exocytosis and PM expression of CFTR.

Although the cell types examined here express a number of additional TMEM16 paralogues[99,237,287], they are not able to rescue PM expression of CFTR after knockdown of TMEM16A/F, as they are expressed in intracellular compartments[99].

Cl^- channel, Ca^{2+} levels, and phospholipid scramblase

TMEM16A regulates membrane expression of CFTR by controlling intracellular Ca^{2+} [85]. PM–localized TMEM16A tethers ER Ca^{2+} stores to raft compartments, thereby augmenting compartmentalized Ca^{2+} signals. Described initially in nociceptive neurons[173], regulation of intracellular Ca^{2+} signals by TMEM16A was also found in the airways, kidney, intestine, and numerous cell lines[85,229,287]. Also for TMEM16F, a role for intracellular Ca^{2+} signalling was reported in naïve macrophages, osteoblasts, and a number of different cell lines[229,290–292]. It is therefore likely that TMEM16F controls exocytosis and membrane expression of CFTR by regulation of Ca^{2+} levels near the PM, corresponding to the function of TMEM16A[85].

However, TMEM16A is a Cl^- channel, while TMEM16F is a phospholipid scramblase that effectively moves phosphatidylserine (PS) from the inner to the outer membrane leaflet. It is also permeable for anions and cations[70,71]. Phospholipid scrambling by TMEM16F may offer another potential explanation for its impact on exocytosis and membrane insertion of CFTR: PS is normally located in the inner PM

leaflet, where it causes a negative charge[293]. PS scrambling at exocytic sites and removal of negative charges from the inner leaflet may affect fusion of intracellular vesicles with the PM, and thus insertion of transmembrane proteins. It could therefore be hypothesized that (i) PS scrambling may modify protein/lipid interactions as proposed for neuroendocrine cells[294]; (ii) lowering PS content in the inner leaflet at the site of membrane insertion may reduce repulsive forces between PS in the PM and PS present in the cytoplasmic leaflet of the exocytic vesicle[295]; and (iii) PS forms an inverted cone shaped lipid that prevents fusion when present in the inner leaflet, but promotes a negative membrane curvature and vesicle fusion when present in the outer leaflet[296].

TMEM16A controls cytoplasmic Cl^- which organizes the phosphoinositide PtdIns(4,5)P_2 within PM microdomains, thereby promoting PM remodelling[297]. TMEM16A, when activated through purinergic stimulation, may even support activation of TMEM16F by enhancing intracellular Ca^{2+} levels. Notably, a cooperativity of TMEM16A and TMEM16F on Ca^{2+}-activated Cl^- currents has been detected in olfactory sensory neurons[298], and was also observed in the present study in co-expressing HEK293 cells (Fig. S24 – Appendix 2). Identification of the precise mechanisms for TMEM16A/F-induced exocytosis and PM insertion of transmembrane proteins such as CFTR will require subsequent studies.

Implications for Cystic Fibrosis

The present findings may have significant implications for Cystic Fibrosis because activation of TMEM16A or TMEM16F may help to insert additional CFTR Cl^- channels into the PM. In fact, the most common mutation F508del present in about 85% of all CF patients leads to misfolded protein that cannot escape the ER quality control. It is therefore degraded and does not traffic to the apical membrane of airway and intestinal epithelial cells[27]. However, the present data and previous reports suggest that the pro-exocytic effects of TMEM16A/F and membrane insertion of CFTR are very distal events during biosynthesis, possibly involving fusion of exocytic vesicles with the PM[85,101,299]. Thus, activation of TMEM16A/F will probably not help to transport more F508del-CFTR into the membrane.

The effect of TMEM16A/F on membrane insertion of CFTR is distal to the biosynthetic pathway, i.e., distal to the endoplasmic reticulum and Golgi. Thus, mutant F508del-CFTR rescued by CFTR correctors such as Orkambi[102] are likely not to reach the PM and to produce whole cell Cl^- currents upon stimulation with cAMP, in the

absence of TMEM16A/F. In fact, siRNA knockdown of TMEM16A/F strongly reduced F508del-CFTR whole cell currents rescued by Orkambi (Fig. 36). Moreover, as shown previously, additional expression of TMEM16A did not rescue F508del-CFTR in CFBE cells[85].

Chapter 3

Role of SLC26A9 on CFTR expression and function

Data included in this chapter were published in:

1. **Pinto MC**, Quaresma MC, Silva IAL, Railean V, Ramalho SS, Amaral MD. Synergy in Cystic Fibrosis Therapies: Targeting SLC26A9. *Int. J. Mol. Sci.* **2021**, *22*(23), 13064, doi:10.3390/ijms222313064.

2. **Pinto MC**, Botelho HM, Silva IAL, Railean V, Amaral MD. Identification of SLC26A9 traffic regulators as novel targets for Cystic Fibrosis therapies. In preparation. **2022**

1. Synergy in Cystic Fibrosis therapies: Targeting SLC26A9

Introduction

Cystic Fibrosis (CF), a life-shortening genetic disorder affecting ~90,000 individuals worldwide[2], is caused by mutations in the CFTR (Cystic Fibrosis Transmembrane Conductance Regulator) gene[6], which encodes a cAMP-regulated chloride (Cl^-) and bicarbonate (HCO_3^-) channel expressed at the apical plasma membrane (PM) of epithelial cells[7]. Defective CFTR leads to an imbalance in salt and fluid transport that results in dehydrated and viscous secretions. CF is a multi-organ disease, affecting the intestine, pancreas, and reproductive tract, but the lungs are the most critically affected organ. In fact, lung failure is the main cause of mortality and morbidity in individuals with CF[9,10,19].

More than 2,100 CFTR genetic variants have been described so far, with only less than 20% (~360 variants) having been confirmed as disease-causing mutations[11,25]. These different mutations originate distinct cellular defects, including protein misfolding and aberrant PM trafficking (class II, which includes the most common mutation, F508del), reduced or absent channel function, lower PM stability, and diminished or even absent CFTR expression[12,29]. Recently, a new highly effective modulator therapy (HEMT) named Kaftrio[61,62] has made a significant change in the lives of people with CF with at least one copy of F508del-CFTR, altogether representing ~80-85% of all individuals with CF[61,62]. This drug combines two CFTR correctors – VX-661 and VX-445 – improving CFTR trafficking to the PM, and one potentiator – VX-770 – increasing CFTR open channel probability. Nevertheless, the remaining 15-20% do not respond to this HEMT nor to other currently available modulators (e.g., VX-809)[12], making the search for alternative therapies a priority in CF research.

A popular alternative therapeutic strategy has been the activation of other (non-CFTR) channels/transporters, as it would apply to any individual with CF, irrespective of the CFTR mutations, i.e., a "mutation-agnostic" approach. An example of one such potential therapeutic target is Solute carrier family 26 member 9 (SLC26A9), a member of the SLC26 family of multifunctional anion transporters[128]. SLC26A9 functions as a constitutively active Cl^- transporter[148] and is predominantly expressed in epithelia lining the airways, stomach, duodenum, ileum, and pancreas[133,140], thus holding the potential to compensate for the absence of functional CFTR. Moreover, besides this potential role,

SLC26A9 has been reported to act as a CF gene modifier, with some of its polymorphisms and expression levels influencing disease severity and response to CFTR-modulator drugs[151,152,300]. SLC26A9 polymorphisms have been linked to an increased risk of developing meconium ileus and pancreatic disease in people with CF[137,153,154], and higher expression of SLC26A9 correlates to a delayed manifestation of CF-related diabetes[138]. Furthermore, reduced expression of SLC26A9 is linked to asthma in children[136]. Moreover, previous studies showed that siRNAs targeting SLC26A9 cause a decrease in wt-CFTR function[301], and proposed that SLC26A9 expression favours the biogenesis and/or stabilization of CFTR, resulting in turn, in enhanced cAMP-activated currents[302].

The exact direct role that SLC26A9 plays in CF and in other respiratory disorders is, however, yet to be elucidated. Although it is described as a Cl^- transporter, its localization was found to be mainly cytoplasmic or at the tight junctions (TJ) level[149]. It was also proposed to interact with both wild-type (wt) and F508del-CFTR, being its PM expression strongly dependent on CFTR[155,301]. Namely, SLC26A9 appears to be retained in the endoplasmic reticulum (ER) when co-expressed with F508del-CFTR, which leads to the degradation of both proteins by the proteasome[149].

Altogether, these data not only highlight the impact of SLC26A9 expression in lung disease and response to CFTR modulator drugs, but also motivated our research on the interaction between SLC26A9 and CFTR. Thus, our main goal here was to better understand the interplay between these two proteins, and how SLC26A9 might be used to develop novel CF therapies to be applied on their own or in combination with those currently available to further enhance their effects. Our data first confirmed that SLC26A9 and CFTR co-localize in human native lung tissue, including in CF epithelia where SLC26A9 expression is reduced. We then demonstrated that in native non-CF lung epithelia SLC26A9 localizes at the TJ level as well as in the sub-apical compartment. In human bronchial (CFBE) cells, we showed that SLC26A9 expression levels strongly affect CFTR expression and function. Particularly, F508del-CFTR rescue by HEMT is influenced by SLC26A9 expression. Interestingly, SLC26A9 overexpression did not significantly alter the PM expression of other CFTR traffic mutants, namely those that are not rescued by HEMT. This suggests a role for SLC26A9 in stabilizing CFTR at the ER, thus increasing the pool available to traffic along the secretory pathway and reach the PM. Taken together, these data support a role for SLC26A9 as a clinically relevant disease modifier and promising therapeutic target not only to circumvent deficient Cl^- secretion in CF but also to increase the effect of the already available CFTR modulator therapies.

Results

SLC26A9 and CFTR show distinct expression patterns in control vs CF airway tissues and primary cells

To address the interaction of SLC26A9 with CFTR in human airways, we first investigated their subcellular localization in native human airway tissue. To this end, we stained healthy control and F508del/F508del bronchi sections for SLC26A9, CFTR and tight junctions (TJ) marker zonula occludens-1 (ZO-1). In control tissue SLC26A9 appears to co-localize with CFTR (Fig. 37, arrows), although CFTR shows a more discrete staining whereas some SLC26A9 localizes diffusely in the sub-apical compartment of the epithelium. Similarly, SLC26A9 also seems to co-localize with ZO-1 (Fig. 37, arrows), concentrating at the TJ, but also being present sub-apically. Interestingly, in CF tissue (F508del/F508del), SLC26A9 also appears to co-localize with F508del-CFTR and ZO-1 (Fig. 37, arrowheads). However, as expected, F508del-CFTR shows faint and diffuse cytoplasmic staining (albeit sub-apical), as a consequence of dysfunctional CFTR and so does ZO-1 as a consequence of aberrant TJ[303,304]. Importantly, in CF tissue, SLC26A9 localization is also intracellular, and its expression levels appear to be decreased.

Thus, these data support the co-localization of SLC26A9 with CFTR and ZO-1 in human native airway tissue: either apically in non-CF tissue, or as a diffuse sub-apical localization in CF (F508del/F508del) tissue.

Based on this co-localization of CFTR and SLC26A9 with TJ protein ZO-1, we assessed how CFTR and SLC26A9 expression levels vary over the course of differentiation by Western Blot (WB) in primary human nasal epithelial (pHNE) cells derived from an individual with CF homozygous for the F508del mutation and from a non-CF control. In non-CF pHNE cells we observed that CFTR expression increased during differentiation, while SLC26A9 expression is constant over the course of differentiation, it still showed a trend towards higher expression levels after 7 and 14 days in ALI conditions (Fig. S25A,B – Appendix 3). However, in F508del/F508del pHNE cells, although F508del-CFTR expression is strongly augmented on day 7 (same as wt-CFTR), SLC26A9 shows a trend towards reduced expression when compared to control pHNE cells ($p = 0.01$ for day 7 wt vs F508del, Fig. S25C,D – Appendix 3). Interestingly, there is a delay in SLC26A9 expression in F508del/F508del pHNE cells, being only increased on day 14 (Fig. S25C,D – Appendix 3).

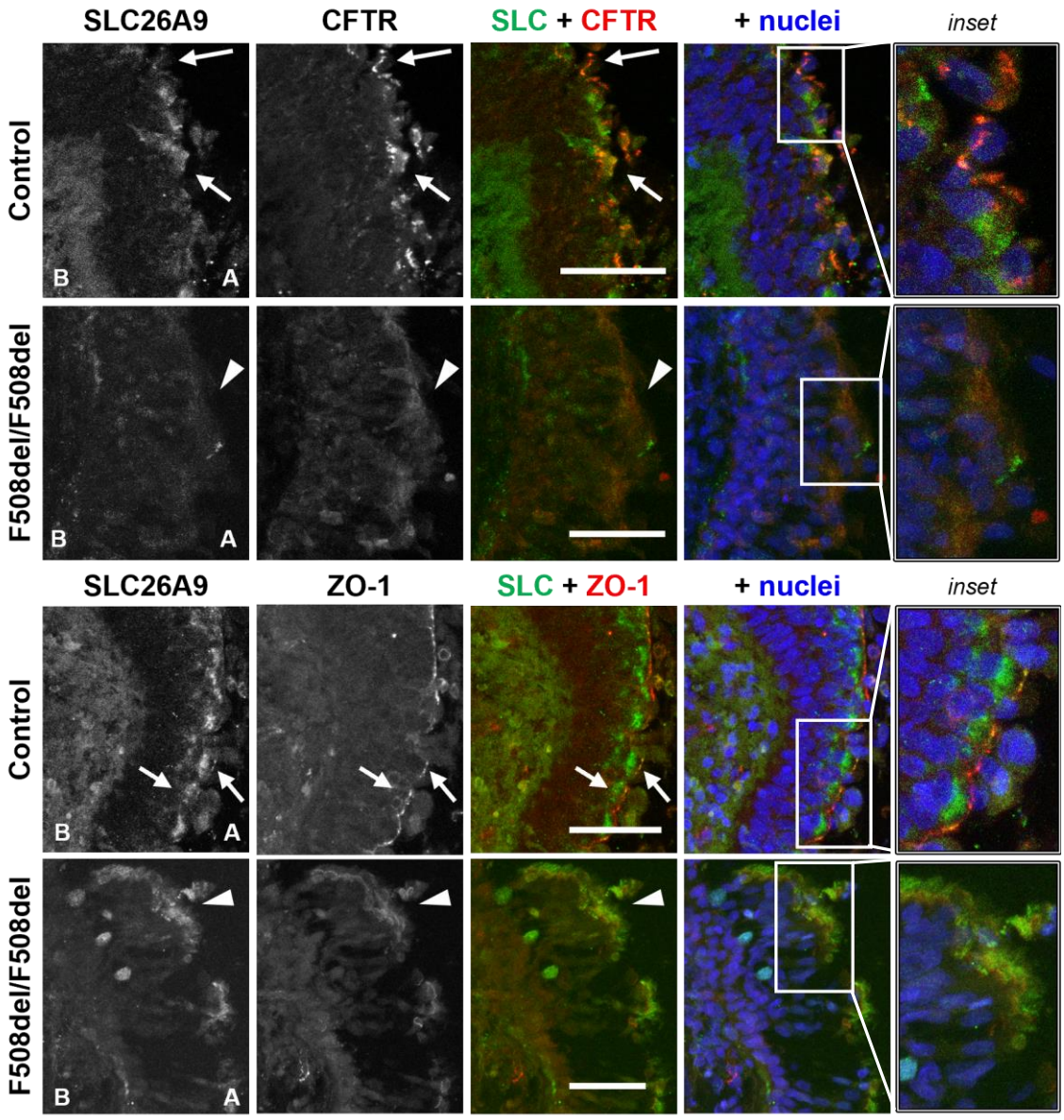

Figure 37 – SLC26A9 has a sharp apical TJ-like localization in control lung but a faint (apical) cytoplasmic localization in F508del/F508del lung. Representative images of native human bronchial tissue (Control and F508del/F508del) immunostained for SLC26A9, CFTR and ZO-1. Nuclei are depicted in blue, SLC26A9 in green and CFTR/ZO1 in red. Scale bars represent 50 µm. Images are displayed as maximum image projections (MIPs). Apical and basal (A and B respectively) sides of the epithelia are identified. SLC26A9 co-localizes with CFTR and ZO-1, weather they show proper apical localization (arrows, control) or diffuse cytoplasmic expression (arrowheads). Close-ups of the areas identified with arrows/ arrowheads (insets) are shown on the right-hand side. The stained tissues display secondary/tertiary bronchi and were as similar as possible for comparison. Areas of extensive shedding/remodelling in CF tissue were avoided, and areas of intact epithelia preferred (n=3 sections). Data in collaboration with Margarida Quaresma.

SLC26A9 knockdown decreases CFTR expression and function

Next, we aimed to confirm how reducing SLC26A9 expression influences CFTR expression, trafficking, function, and the response to HEMT, i.e., the combination of

correctors tezacaftor (VX-661) with elexacaftor (VX-445). We stably transduced CFBE cells expressing wt- or F508del-CFTR (see Methods) with a specific shRNA targeting SLC26A9 (or shLuciferase [shLuc] as a negative control). After confirming SLC26A9 knockdown (KD) by both WB and semi-quantitative PCR (Fig. 38A,C, Fig. S26A – Appendix 3, respectively), we assessed CFTR protein levels by WB, and observed a significant decrease in wt-CFTR expression upon SLC26A9 KD (Fig. 38A,B). Regarding F508del-CFTR, SLC26A9 KD led to a significant decrease in its rescue by VX-661 + VX-445 in comparison to shLuc-treated cells (Fig. 38A,B), as observed by the lower amount of fully glycosylated CFTR (Band C), indicating a reduced expression at the PM. Moreover, when comparing the fold increase of band C between conditions exposed or not to VX-661 + VX-445 for shLuc and shSLC26A9, the former (under shLuc) is substantially higher (~9 and ~6, respectively).

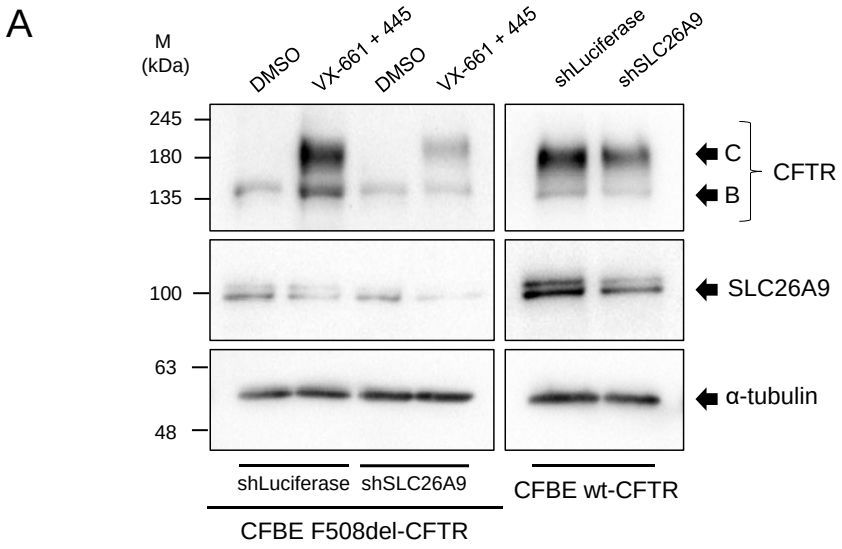

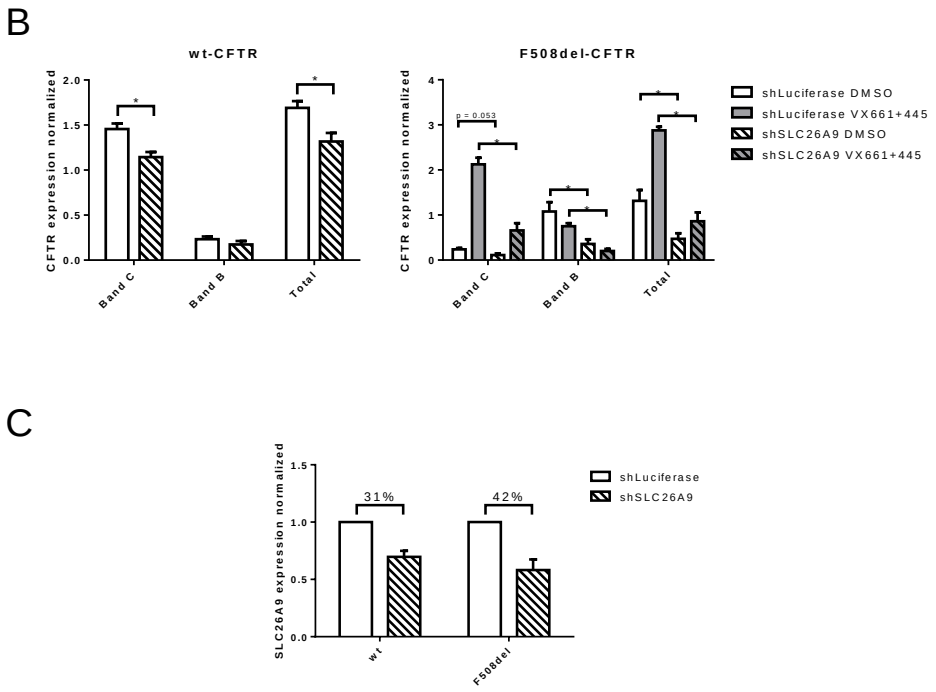

Figure 38 – SLC26A9 knockdown decreases both wt- and F508del-CFTR expression and F508del-CFTR correction by VX-661 + VX-445. (A) Western Blot showing CFTR and SLC26A9 expression in shLuciferase vs shSLC26A9 transduced cells. α-tubulin was used as a loading control. **(B)** Quantification by densitometry of CFTR protein expression detected by WB in (A). From left to right: Band C, which corresponds to fully glycosylated (PM-localized) CFTR; Band B, the core-glycosylated form of CFTR; and total protein expression. **(C)** Quantification of SLC26A9 knockdown, showing a decrease of ~31% and ~42% of SLC26A9 expression in wt-CFTR and F508del-CFTR CFBE cells, respectively, when compared to shLuciferase-transduced cells. Data are normalized to loading control and showed as arbitrary units, mean ± SEM (number of experiments (n) = 3). Statistical analyses were performed by GraphPad Prism 6.0 using unpaired t-test where "*" indicates statistically significant differences ($p < 0.05$, unpaired t-test) between cells transduced with shLuciferase and shSLC26A9.

We then evaluated the effect of SLC26A9 KD on CFTR function by Ussing chamber. Despite that SLC26A9 KD was modest in CFBE wt-CFTR cells (~31%, Fig. 38C), cAMP-activated currents (i.e., CFTR-mediated currents) were significantly inhibited (~65%) when compared to shLuc-treated cells (Fig. 39A,C). Likewise, in CFBE F508del-CFTR cells, although the negligible currents of DMSO-treated cells were not significantly changed by SLC26A9 KD, its rescue by VX-661 + VX-445 was reduced by ~35% (Fig. 39B,C).

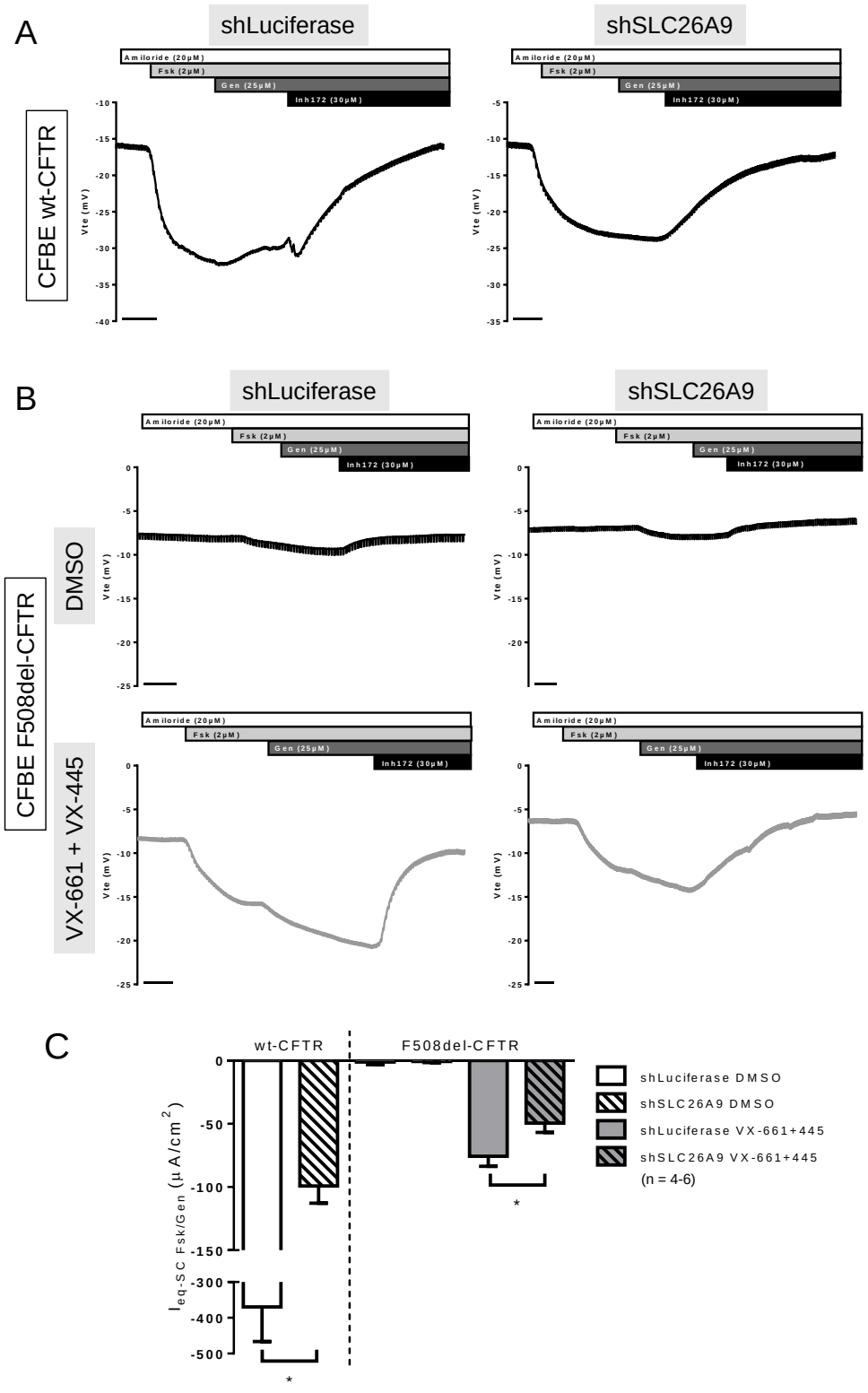

Figure 39 – SLC26A9 knockdown inhibits wt-CFTR function and the correction of F508del-CFTR by VX-661 + VX-445. (A) Original Ussing chamber tracings obtained for CFBE wt-CFTR cells transduced with the control shRNA shLuciferase (left) or shSLC26A9 (right). CFTR was activated by 2 µM Forskolin (Fsk) and 25 µM Genistein (Gen) in the presence of the epithelial sodium channel (ENaC) inhibitor (Amiloride, 20 µM) and was inhibited by CFTR-inhibitor 172 (Inh172, 30 µM). All compounds were added to the luminal side. **(B)** Original Ussing chamber tracings obtained for cAMP-induced Cl^- currents activated and inhibited as in (A) in the absence (top tracings, black) or in the presence (lower tracings, grey) of 5 µM VX-661 + 3 µM VX-445 for CFBE F508del-CFTR cells transfected with shLuciferase (left) or shSLC26A9 (right); **(C)** Summary of $I_{sc\text{-}eq}$ currents of CFBE wt-/F508del-CFTR stably transduced with shLuciferase vs shSLC26A9

and treated with DMSO vs VX661+VX-445. Data are represented by mean ± SEM and "*" indicates statistically significant differences (unpaired t-test, $p < 0.05$). The number of filters (n) used in the statistical analyses is indicated in the graph. Scale bars in (A) and (B) represent 1 min. Data in collaboration with Iris Silva.

To confirm the effects of SLC26A9 KD on CFTR expression and function in a system expressing endogenous CFTR, we then stably transduced the 16HBE cell lines expressing either wt- or F508del-CFTR with the same shRNAs targeting either SLC26A9 or Luciferase (control) and assessed the effect of all the clinically available CFTR correctors VX-809, VX-661 and VX-445. As expected, total wt- and F508del-CFTR protein expression were significantly reduced, and the rescue of F508del-CFTR PM expression (band C) by VX-445 alone, or in combination with VX-661, was also diminished (Fig. S27 – Appendix 3). SLC26A9 KD in 16HBE cells expressing wt-CFTR also originated lower cAMP-activated currents (Fig. S28A,C – Appendix 3), and both the untreated and VX-809-treated F508del-CFTR expressing cells showed lower CFTR activity (Fig. S28B,C – Appendix 3).

These data suggest that SLC26A9 KD decreases CFTR PM expression and function in both endogenous and overexpression settings.

SLC26A9 overexpression potentiates CFTR expression and function

Given the negative impact of SLC26A9 KD on wt-CFTR expression and function, and importantly, on F508del-CFTR rescue by the clinically available modulators, our next step was to examine the effect of increasing SLC26A9 levels on F508del-CFTR mediated Cl^- currents and protein expression. To this end, we stably transfected CFBE F508del-CFTR cells with a GFP-tagged SLC26A9 construct, under the control of an inducible (Tet-On) promoter system.

After adding doxycycline (Dox) to induce the SLC26A9 construct expression in F508del-CFTR CFBE cells, we could detect SLC26A9 (Fig. 40A,C) by WB. Notably, since in this WB exposure times were very short (due to high expression levels of the inducible labelled construct) endogenous SLC26A9 was not detected here (in contrast to Fig.38A) due to its significantly lower expression levels. SLC26A9 overexpression, and still without VX-661 + VX-445, still led to the appearance of the fully glycosylated form of F508del-CFTR (Band C), albeit in very small amounts (Fig. 40A,B). Remarkably, in SLC26A9 overexpressing cells, rescue of F508del-CFTR by VX-661 + VX-445 was much stronger when compared to control cells (- Dox) (Fig. 40A,B). This greater rescue

of F508del-CFTR by VX-661 + VX-445 in the presence of higher levels of SLC26A9 was further corroborated by the significantly increased cAMP-activated currents obtained in Ussing chamber experiments (Fig. 41A,B).

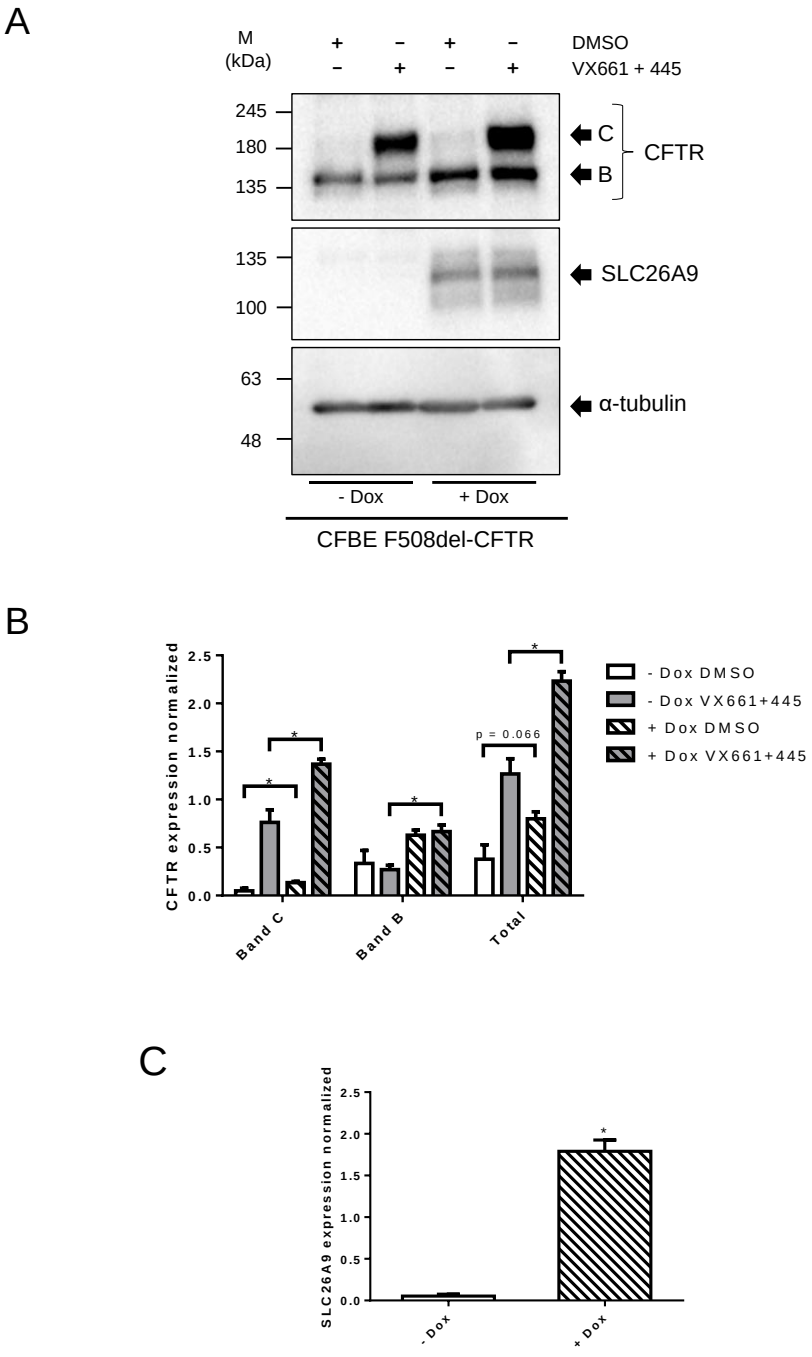

Figure 40 – SLC26A9 overexpression increases F508del-CFTR expression and correction by VX-661 + VX-445. (A) Western Blot showing CFTR and SLC26A9 expression in CFBE F508del-CFTR cells stably transduced with SLC26A9 in a Tet-On system, where SLC26A9 is only expressed after Doxycycline induction (+ Dox). α-tubulin was used as a loading control. **(B)** Quantification by densitometry of CFTR protein expression detected by WB in (A). **(C)** Quantification of SLC26A9 expression after Dox induction, as shown in (A). Data are normalized to loading control and showed as mean ± SEM (n = 3). (*) indicates significant differences between cells in the absence (- Dox) or presence (+ Dox) of doxycycline, the latter meaning overexpression of SLC26A9 (unpaired t-test, $p < 0.05$).

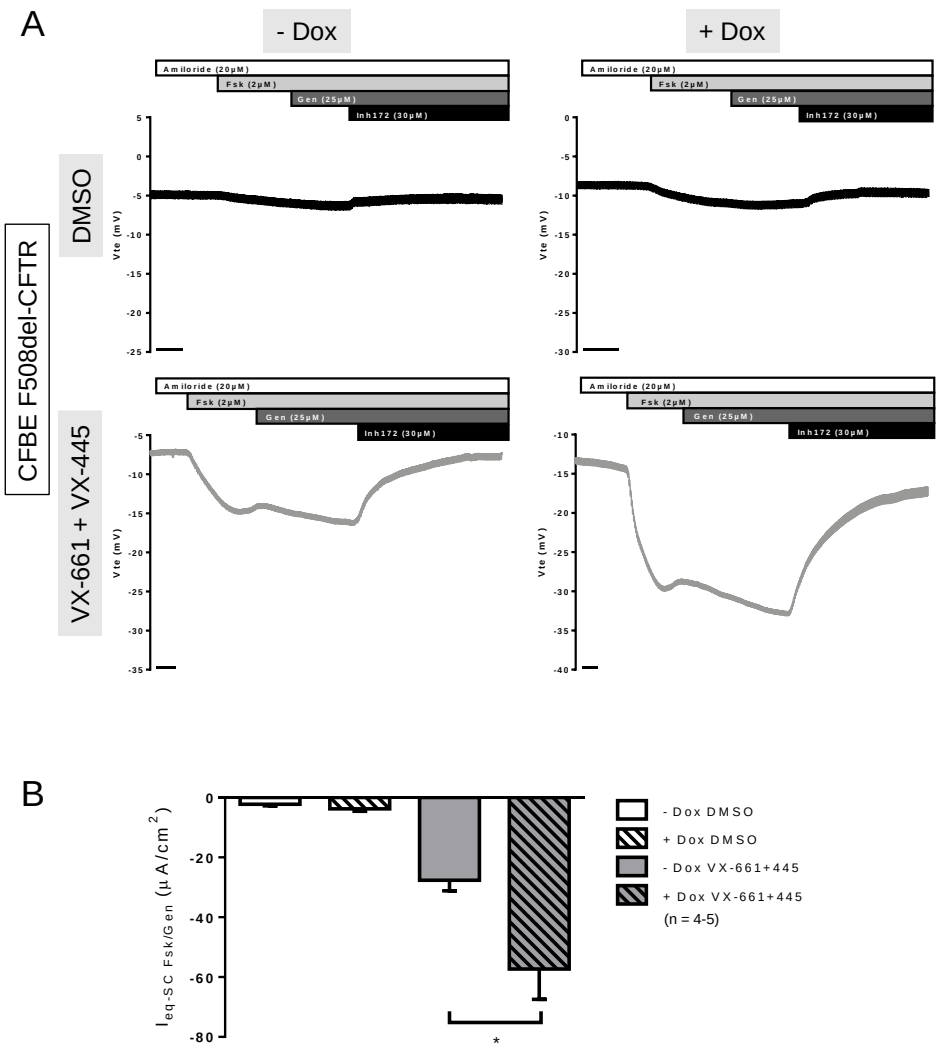

Figure 41 – SLC26A9 overexpression heightens F508del-CFTR correction by VX-661 + VX-445. (A) Original Ussing chamber tracings obtained for cAMP-induced Cl^- currents (Fsk + Gen) in the absence (top tracings, black) or in the presence (lower tracings, grey) of 5 μM VX-661 + 3 μM VX-445 for CFBE F508del-CFTR cells with (right) or without (left) SLC26A9 overexpression (+ Dox and – Dox, respectively); **(B)** Summary of $I_{sc\text{-}eq}$ currents of CFBE F508del-CFTR +/- Dox and treated with DMSO vs VX661+VX-445. Data are represented by mean ± SEM. (*) indicates significant statistical difference between cells treated or untreated with Dox (unpaired t-test, $p < 0.05$). The number of filters (n) used in the statistical analyses is indicated in the graph. Scale bars in (A) represent 1 min. Data in collaboration with Iris Silva.

Similar data were obtained in 16HBE cells overexpressing SLC26A9 thus further validating these results and demonstrating that SLC26A9 enhances total and PM expression of endogenous wt-CFTR (Fig. S29A,C – Appendix 3) and rescue of F508del-CFTR by all the correctors tested (VX-809, VX-661, VX-445 and the combination of VX-661 with VX-445) (Fig. S29A,B – Appendix 3). These data are of particular relevance, as we show here that the clinically approved therapies for people carrying the F508del mutation can be improved by increasing SLC26A9 expression.

Interestingly, lowering SLC26A9 expression (by KD through shRNA transfection) resulted in a delay in cell polarization of CFBE wt-CFTR cells, as seen by the lower values of transepithelial resistance (TEER) on day 3, eventually reaching the levels of the control cells on day 5 (Fig. S30A – Appendix 3). No differences were observed in CFBE F508del-CFTR cells (Fig. S30B – Appendix 3). However, CFBE F508del-CFTR cells overexpressing SLC26A9 showed a significant increase in TEER after Dox induction (Fig. S30C – Appendix 3). Remarkably, CFBE cells transduced with the inducible SLC26A9 construct have – even without adding Dox – a higher TEER when compared to non-transfected cells or transfected with control shRNAs. This result might be explained by the leaky expression of SLC26A9 in the absence of Dox (Fig. 40A, Fig. S30C – Appendix 3).

Overexpression of SLC26A9 does not alter the PM expression of other CFTR traffic mutants

Since F508del is classified as a class II mutation, i.e., has impaired trafficking[19], we decided to investigate the impact of SLC26A9 overexpression in cells expressing other class II CFTR mutations, namely G85E, R560S, and N1303K (Fig. 42). None of these CFTR mutants was rescued by VX-661 + VX-445, as observed by the absence of band C, i.e., mature form of CFTR (Fig. 42) after treatment with these drugs. Similarly, SLC26A9 overexpression did not alter the expression levels of any of the mutants, although there is a trend to slightly higher CFTR expression levels for these mutants upon SLC26A9 overexpression (Fig. 42). Thus, these results indicate that SLC26A9 contributes to increasing CFTR levels at the PM only when it is able to exit the ER, namely wt-CFTR and F508del-CFTR when rescued by HEMT. Notwithstanding SLC26A9 overexpression seems to contribute to some ER-retained stabilization, at least for F508del-CFTR and possibly also some other class II mutants. Notably, it has been demonstrated that SLC26A9 interacts with CFTR bearing other rare mutations, being its expression also enhanced after the rescue of these mutants by CFTR modulators[305].

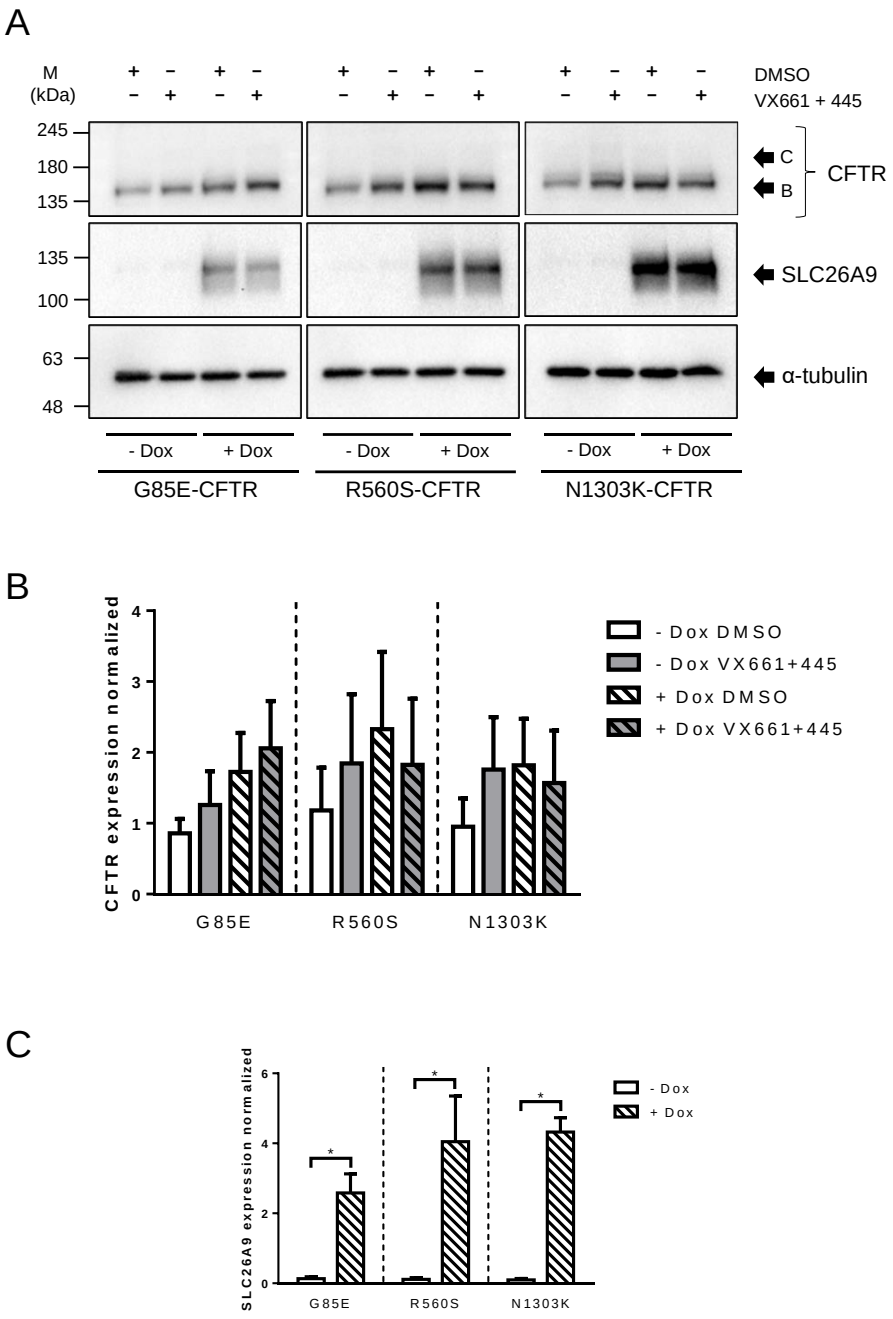

Figure 42 – Overexpression of SLC26A9 does not alter the PM expression of other class II CFTR mutants. (A) Western Blot showing CFTR and SLC26A9 expression in CFBE cells transduced with SLC26A9 and stably expressing one of the following class II CFTR mutants: G85E, R560S, or N1303K. SLC26A9 expression is detectable after Doxycycline induction (+ Dox). α-tubulin was used as a loading control. **(B)** Quantification of CFTR protein expression detected by WB in (A). **(C)** Quantification of SLC26A9 overexpression after Dox induction, as shown in (A). Data are normalized to loading control and showed as mean ± SEM (n = 3). (*) indicates significant difference between cells in the absence or presence of Dox (unpaired t-test, $p < 0.05$).

Discussion

In the present work we demonstrated the synergistic effect of SLC26A9 expression levels on CFTR expression and function, and most importantly, on the rescue of F508del-CFTR by the HEMT currently available in the clinic (VX-661+VX-445). Consistently with previous data[149] our data show that SLC26A9 and CFTR seem to co-localize in native human bronchial epithelia, either in samples from a non-CF individual (control) at the PM or intracellularly in tissues from an individual with CF (F508del/F508del).

Although thus far, the co-localization of SLC26A9 and CFTR has been assessed mostly through their heterologous expression either in HEK293T or CFBE41o- cells transfected with tagged SLC26A9 constructs[155,301,302], recently the same was also shown in well-differentiated primary human bronchial epithelial (pHBE) cell cultures[149]. However, here we show for the first time that SLC26A9 and CFTR also appear to co-localize in native human bronchial epithelial CF (F508del/F508del) and non-CF tissue. Native bronchial tissues provide a unique insight into the pathological and molecular events of the disease and are good snapshots of the physiological situation. These data providing evidence of SLC26A9 and CFTR co-localization in human native lung epithelia (CF and healthy control) are in line with previous studies reporting that SLC26A9 and CFTR physically interact, both its wt and F508del forms[148,302]. Our results are also in agreement with studies showing that SLC26A9 expression levels are reduced in CF[149].

Importantly, it has been established that SLC26A9 and CFTR behave differently in polarized vs non-polarized cells[301], namely at the level of TJs, and that the negative effect of F508del-CFTR on SLC26A9 is more pronounced in well-differentiated epithelial cells endogenously expressing these proteins[149], evidencing the importance of studying physiologically relevant model systems. Here, we also observed that in control lung epithelia SLC26A9 localizes to the TJs as well as in the sub-apical compartment, as previously reported in pHBE cells[149]. However, we also show that in CF epithelia, the TJ protein ZO-1 shows intracellular and diffuse staining and, although SLC26A9 and ZO-1 still appear to co-localize, the integrity of TJ structures is compromised. This is in line with our previous findings (both in lung tissue and immortalized CFBE cells) demonstrating that the presence of mutant CFTR occurs with a shift in the localization of ZO-1 from a TJ/apical to a more intracellular one[306]. These data are also consistent with multiple reports of abnormal TJ formation caused by mutant CFTR[303,304,307], as well as with the proposal that functional CFTR interacts directly with ZO-1 to regulate TJ formation[303].

Also consistent with these data on diffuse SLC26A9 expression at the compromised TJ structures in CF[306], our results in CF (F508del/F508del) pHNE cells also suggest a delayed expression of SLC26A9 over the course of differentiation vs. control cells. Moreover, our data indicate that lower SLC26A9 expression levels may affect cell polarization. Indeed, these data show, similarly to those by other authors[149], that SLC26A9 KD resulted in a delay in cell polarization in CFBE wt-CFTR cells, as seen by a decrease in TEER values. In parallel, SLC26A9 KD had no effect on the TEER of CFBE F508del-CFTR cells, likely due to the fact that CF cells already have compromised TJs and low TEER values[306]. However, CFBE F508del-CFTR cells overexpressing SLC26A9 showed a significant increase in TEER, suggesting that a higher expression of SLC26A9 may potentiate cell polarization.

To further investigate the relationship between SLC26A9 and CFTR we used two different cell models: CFBE, which stably overexpress CFTR; and 16HBE, with endogenous CFTR expression. We took advantage of molecular biology tools to decrease (shRNA) or increase (cDNA) SLC26A9 expression levels in these cells. Consistently in both systems, SLC26A9 KD led to a reduction in wt- and F508del-CFTR protein expression and in CFTR-mediated Cl^- transport. F508del-CFTR rescue by the clinically available HEMT was also inhibited in both cell models by SLC26A9 KD. On the other hand, SLC26A9 overexpression increased F508del-CFTR rescue by HEMT (expression and function), confirming that it is possible to further improve the current best treatment for people with CF carrying F508del. Enhancing SLC26A9 expression could therefore increase Cl^- secretion in two ways: *i)* by its own function as a Cl^- transporter (and therefore bringing benefits for everyone with CF, regardless of their genotype), and *ii)* by its synergistic rescuing effect with the HEMT VX-661 + VX-445.

Given ours and previous data showing the effect of SLC26A9 expression in PM-localized CFTR (either wt, corrected F508del, or G551D[151]) and the failure to rescue other trafficking mutants (G85E, R560S and N1303K), we hypothesize that SLC26A9 plays a role in stabilizing some misfolded CFTR mutants at the ER which are then available to be rescued to the PM by modulators that act on these mutants. This hypothesis is consistent with previous reports which already suggested a stabilization of CFTR by SLC26A9 in the biogenesis/ maturation process[302]. Furthermore, the effect of SLC26A9 on CFTR stability appears to be rather specific, as SLC26A9 overexpression does not alter the expression levels of other membrane proteins such as Na^+/K^+ ATPase (data not shown).

Importantly, despite that some class II mutations tested here (namely G85E and N1303K) showed a significant – albeit modest – correction by Kaftrio in studies in primary nasal epithelial cultures from CF patients[308], we acknowledge the differences and limitations of immortalized cells and overexpressing systems. Nonetheless, we show here that the results in CFBE cells (overexpressing CFTR) were reproducible, and even more significant, in 16HBE cells which have endogenous expression of CFTR. In our view, the results obtained here and by other authors[308] indicate that SLC26A9 might actually improve the response to the correctors in people with CF carrying F508del-CFTR and possibly other class II mutations that respond to these drugs. Nonetheless, more studies are needed to confirm this hypothesis. An interesting approach would be to assess the effect of SLC26A9 overexpression on other trafficking mutations known to respond better to the treatment with Kaftrio, such as M1101K[308], or overexpressing SLC26A9 in primary cells.

In summary, our data revealed that SLC26A9 expression is crucial for enhanced CFTR PM expression and function, while also having a potential effect on TJ structures. Moreover, increasing SLC26A9 levels is a potential therapeutic option for CF, by providing an additional source of Cl^- secretion, and/or by enhancing the effect of the already clinically available HEMT.

2. Identification of SLC26A9 traffic regulators as novel targets for Cystic Fibrosis therapies

Introduction

Solute carrier family 26 member 9 (SLC26A9) is a constitutively active Cl^- transporter that has gained attention over the past years as a relevant modifier in respiratory disorders such as Cystic Fibrosis (CF), asthma and non-CF bronchiectasis[136,309]. CF is a genetic disease caused by mutations in the CFTR (Cystic Fibrosis Transmembrane Conductance Regulator) gene[6], which encodes a chloride (Cl^-) and bicarbonate (HCO_3^-) channel expressed at the apical plasma membrane (PM) of epithelial cells in the airways, intestine, pancreas, sweat glands and other organs[7]. Although CF has multi-organ involvement, respiratory disease is the major cause of morbidity and premature death. CF is characterized by a cycle of airways obstruction by a thick mucus, chronic inflammation and recurrent infections, that cause epithelial injury, tissue remodelling and progressive loss of lung function, ultimately leading to respiratory failure[12,19].

Life expectancy of individuals with CF has significantly increased with the evolution of CF therapies in the last decades, with many currently living into their 40s and beyond[310,311]. However, novel highly effective CFTR modulator therapies are not available for all individuals with CF, and even among the eligible patients, drug responsiveness is heterogeneous, with some showing no benefit at all. Moreover, the very high cost and delays in approval by regulatory agencies make these drugs inaccessible to a large group of patients. Importantly, even the ones with the higher responsiveness levels to available therapies never reach levels of individuals with no CF (or carriers). Therefore, an alternative therapeutic option, which would suit all CF patients, consists in the modulation of other (non-CFTR) Cl^- channels/transporters[102,140].

SLC26A9, a member of the SLC26 family of anion transporters[128], functions as a constitutively active Cl^- transporter[86,141] expressed in epithelial cells of the respiratory tract, stomach, duodenum, ileum, and pancreas[133,140]. The study of SLC26A9 as an alternative channel to bypass dysfunctional CFTR in CF has recently expanded due to its multiple effects on the pathophysiology of the disease. Firstly, SLC26A9 is a modifier of lung function[151]. Secondly, SLC26A9 polymorphisms have been associated with the level of response to CFTR modulator therapies[151,152], and correlate with the risk to

develop meconium ileus and early exocrine pancreatic disease in individuals with CF[137,153,154]. Thirdly, SLC26A9 is necessary for proper CFTR expression and function, as well as for the rescue of F508del-CFTR – the most common CF-causing mutation – by the most effective modulators to date (chapter 3.1). Finally, SLC26A9 was shown to contribute to epithelial Cl^- transport and to prevent mucus obstruction under inflammatory conditions[136].

SLC26A9 is predominantly localized at the tight junctions (TJ) as well as in the sub-apical compartment of lung epithelia. It co-localizes with CFTR and with the TJ marker zonula occludens-1 (ZO-1) in healthy and in CF tissue (chapter 3.1[149]). SLC26A9 interacts with CFTR via the STAS domain of SLC26A9 and the regulatory domain (RD) of CFTR[150], and possibly also by the PDZ-binding domains of both proteins[102]. When co-expressed with wt-CFTR, SLC26A9 and CFTR traffic together from the endoplasmic reticulum (ER) to the PM, while its co-expression with F508del-CFTR prevents SLC26A9 PM expression due to the ER-retention and premature degradation by the proteasome[149], as observed by the lower expression of SLC26A9 in CF tissue (chapter 3.1). Therefore, being SLC26A9 trafficking strongly dependent on CFTR, the exploitation of SLC26A9 as a pharmacological target for the treatment of CF would require improvement of its PM traffic in the absence of functional CFTR[86].

The lack of effective and selective SLC26A9 modulators has limited the therapeutic targeting of SLC26A9 in the context of CF. Hence, the identification of selective regulators of SLC26A9 traffic and function is important to further understand its cellular functions, its complex relationship with CFTR, and whether and how it may be used as a therapeutic target in lung disease. Given that SLC26A9 is constitutively active when localized at the PM[148], a good strategy to increase epithelial Cl^- secretion consists in targeting genes and/or using small molecules that increase or stabilize SLC26A9 expression at the PM. The goal of the present study was thus to identify SLC26A9 regulators as potential drug targets for CF. Using a novel screening platform in high-throughput (HT) microscopy screens, we discovered several modulators of SLC26A9 trafficking in a CFTR-null model, some of which also rescued F508del-CFTR trafficking in previous studies (Amaral lab, unpublished data).

Results

SLC26A9 traffic reporter

We have developed a novel microscopy-based traffic assay to quantify SLC26A9 traffic in the context of CF. CF Bronchial Epithelial (CFBE) cells, an established model for the study of CF which do not express CFTR[157,165], were stably transduced to express the SLC26A9 traffic reporter under an inducible promoter (Tet-On). The reporter contains an enhanced green fluorescent protein (eGFP) tag fused to its N-terminus and a triple hemagglutinin (3HA) tag at its putative second extracellular loop (Fig. S31 – Appendix 3). The latter allows for the detection of PM-localized SLC26A9 using an anti-HA antibody without cell permeabilization. Similarly to what was previously described for CFTR[165] and TMEM16A[226] (chapter 1.1), this double-tagged reporter allows for the quantification of either SLC26A9 traffic efficiency or total protein expressed at the PM on a single cell basis (see Methods).

The inducible expression of the eGFP-3HA-SLC26A9 traffic reporter is advantageous when screening for traffic modulator genes since it allows the cell transcriptome to be purged of selected gene transcripts using RNA interference before SLC26A9 synthesis can occur, thereby increasing the sensitivity to co-translational factors. Inducibility of the SLC26A9 traffic reporter by the tetracycline analogue doxycycline (Dox) was confirmed by Western Blot (WB) using an anti-SLC26A9 antibody which showed a very significant increase in the levels of SLC26A9 in Dox-induced vs non-induced cells (Fig. 43A,B). Endogenous protein is not detected since it is expressed at much lower levels. Nevertheless, it is possible to observe a negligeable, leaky expression of the double-tagged construct in the absence of Dox (Fig. 43A).

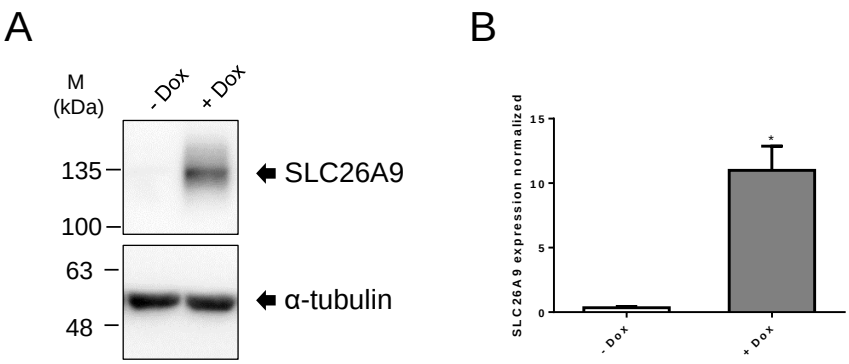

C

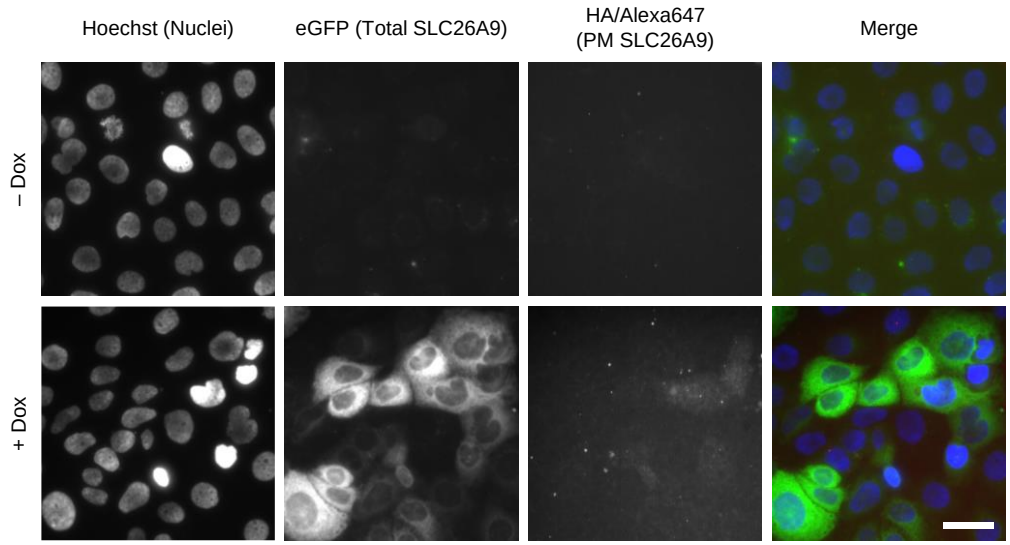

Figure 43 – Confirmation of double-tagged SLC26A9 expression levels after Dox induction and intracellular localization. CFBE cells expressing the eGFP-3HA-SLC26A9 construct grown in the absence (−Dox) or presence of 1 μg/mL Dox for 48h (+Dox) to induce double-tagged SLC26A9 expression were analysed by: **(A)** Western Blot (WB) where SLC26A9 was detected by the anti-SLC26A9 antibody (1:500) being α-tubulin used as a loading control and quantified in **(B)**; or **(C)** immunofluorescence to detect SLC26A9 expression in non-permeabilized CFBE cells. From left to right: nuclei (Hoescht); total amount of expressed SLC26A9, represented by eGFP fluorescence; Alexa Fluor® 647 (immuno) fluorescence of anti-HA antibody detecting 3HA tags exposed extracellularly, i.e., SLC26A9 molecules present at the PM (very low levels in CFTR-null cells); merged image of the fluorescence channels. Images were acquired using a Leica DMI 6000B widefield microscope (objective: 40x water, NA 1.1; exposure times: Hoechst: 50 ms, GFP: 350 ms, Alexa647: 1 s). Scale bar = 50 μm.

Given its localization at a putative extracellular loop (Fig. S31 – Appendix 3), the 3HA-tag only becomes exposed to the extracellular environment when the double-tagged protein is located at the PM. Thus – as previously demonstrated for mutant CFTR (Amaral lab, unpublished data) and TMEM16A[226] (chapter 1.1) – the cell surface pool of the traffic reporter can be detected through HA immunodetection (with an Alexa Fluor® 647 secondary antibody) in cells which have not been permeabilized. No eGFP nor Alexa647 fluorescence were detected in the non-induced cells, while in the presence of Dox there was a significant expression of the construct, with only a very modest PM expression (Fig. 43C). This result is, however, expected given the known reduction in SLC26A9 PM expression in the absence of CFTR as it is the case here[149]. The CFBE eGFP-3HA-SLC26A9 cells were sorted to obtain a cell population with an enriched and more homogeneous expression of the construct (Fig. S32 – Appendix 3).

High throughput siRNA screen to identify SLC26A9 traffic regulators

The SLC26A9 traffic reporter was used to screen a library containing 826 siRNAs targeting 414 genes (Fig. 44) known to interact with CFTR, to increase F508del-CFTR expression at the PM, or to be involved in protein trafficking (Amaral lab, unpublished data), with the goal of identifying SLC26A9 traffic regulators and potential drug targets for CF.

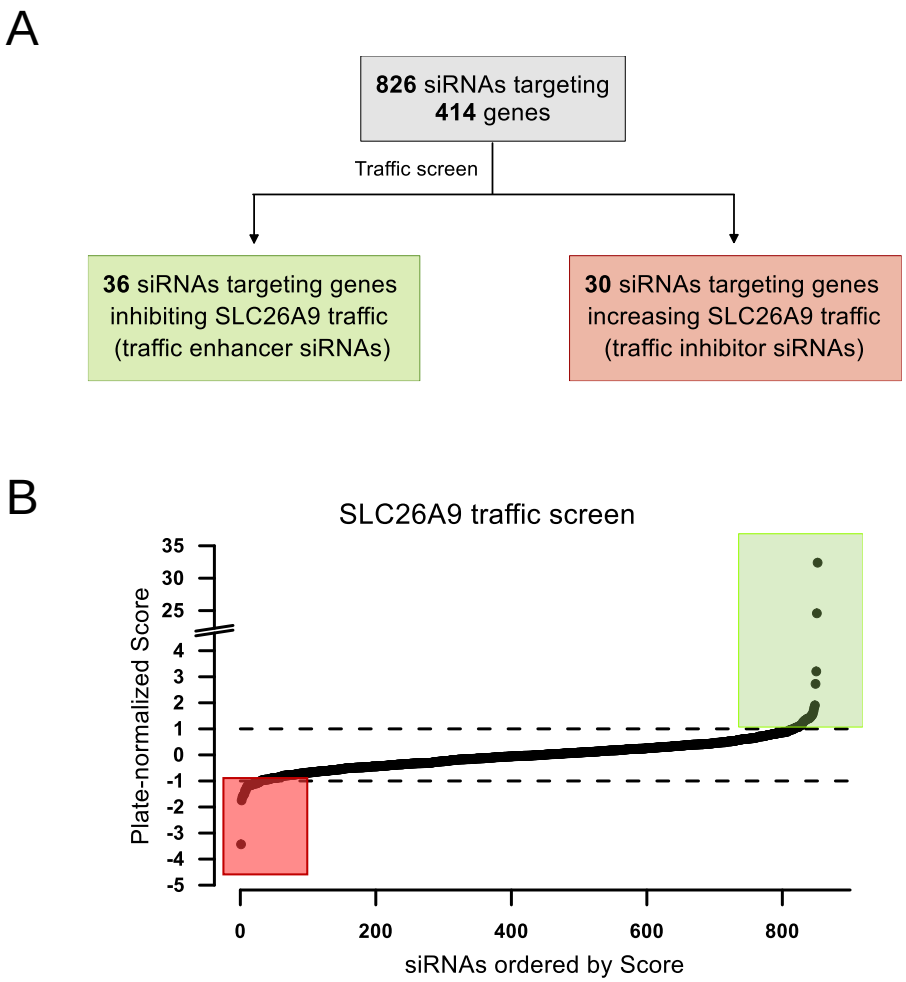

Figure 44 – Overview of the screen data. (A) Workflow showing the number of hit genes found in the traffic screen (1 siRNA per gene). **(B)** Distribution of averaged scores obtained for every siRNA in the SLC26A9 traffic screen. siRNAs with scores above +1 (green shade) were considered as SLC26A9 traffic enhancers and with scores below -1 (red shade) were considered SLC26A9 traffic inhibitors.

The traffic assay consisted in the reverse transfection of reporter cells in siRNA pre-coated microscopy plates for 72h, of which the last 48h included the incubation with Dox to induce the expression of the eGFP-3HA-SLC26A9 construct. Following PM HA

immunostaining and imaging, image analysis was performed with CellProfiler as previously described[226].

All results were normalized to same-plate negative control siRNA (siNEG1) treated cells and expressed as a Z-score. The screen revealed several siRNAs which significantly affected SLC26A9 traffic. We identified 36 siRNAs increasing SLC26A9 PM traffic (i.e., targeting putative traffic inhibitor genes, Table S11 – Appendix 5) and 30 siRNAs further inhibiting SLC26A9 traffic (i.e., targeting putative traffic enhancer genes) (Figs. 44 and 45). Treatment with a specific siRNA targeting SLC26A9 (siSLC26A9) significantly decreased the eGFP fluorescence (total SLC26A9) in most cells (Fig. 45), thus demonstrating efficient levels of siRNA transfection.

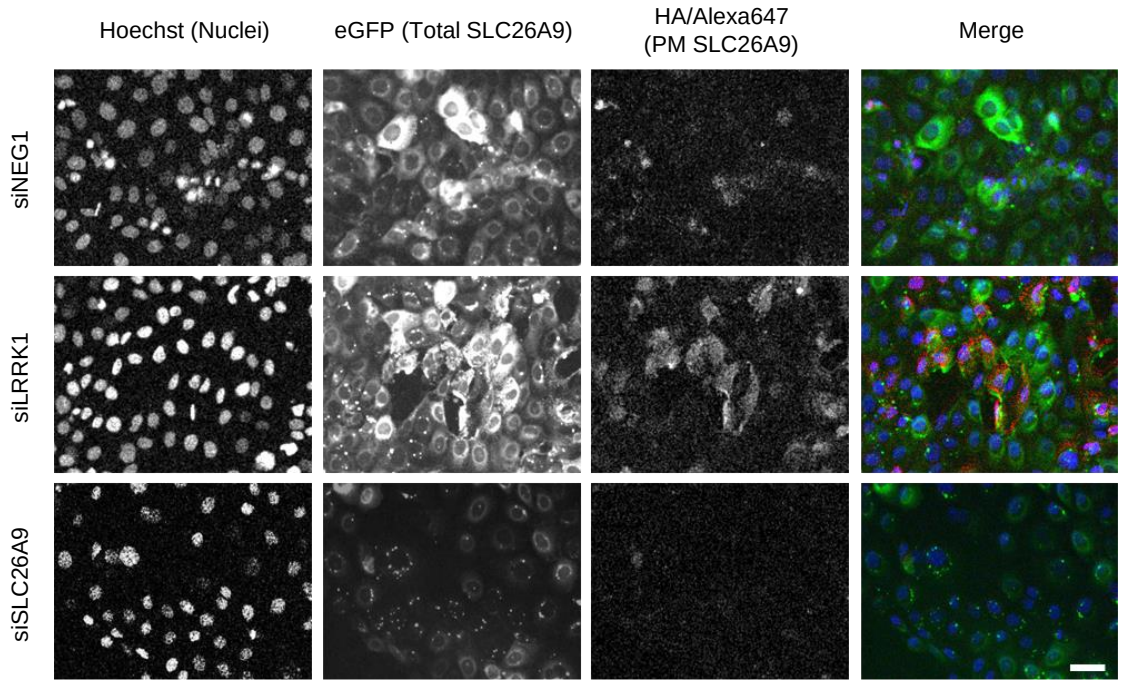

Figure 45 – Representative data of screen hits and controls. Widefield epifluorescence microscopy images obtained for the SLC26A9 traffic screen using siRNAs targeting one hit (LRRK1, Z-score: 1.03), SLC26A9 (transfection control) and non-targeting control siRNA siNEG1. Cell imaging was performed with a Leica TCS SP8 confocal microscope with a 20x (0.75 NA) dry objective. Scale bar: 30 µm. Data in collaboration with Hugo Botelho.

Bioinformatic analyses and classification of SLC26A9 hits

As our goal is to uncover strategies to increase the PM levels of SLC26A9, we focused on the 36 genes targeted by siRNAs that increase the HA/Alexa647 signal (Fig. 44) and sought to identify the pathways or protein networks that the hit genes are part

of. We analysed the 36 hits using STRING[312] to search for described interactions among them. CFTR and SLC26A9 were added to the pool of genes to anchor the network and provide information on interactions among these proteins and the hits (Fig. 46). Our analysis revealed that there are no reported interactions between SLC26A9 and any of the regulators identified in the current screen. We could, however, list 4 hits which have been previously shown to interact with CFTR (APOB, ARRB1, PSMD2 and SLC9A3R1).

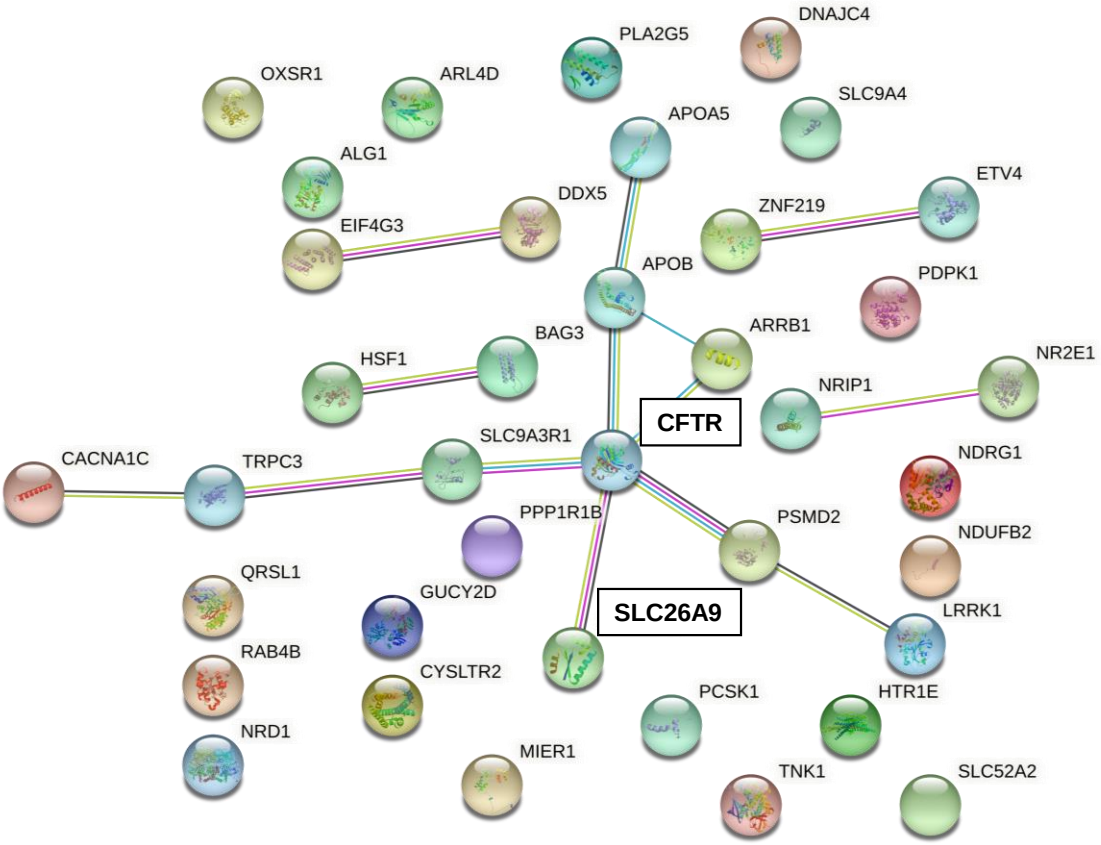

Figure 46 – Bioinformatic analysis of genes targeted by the traffic enhancer siRNA hits. Protein network of SLC26A9 traffic hits, showing reported interactions between some hits and CFTR.

We then analysed the 36 genes using the Gene Ontology (GO) Bioinformatics Resource[252,253], employing a high stringency, so as to identify the most important biological processes that were enriched in the primary hit list (Table 2). The identified most enriched pathways included: regulation of transcription, protein phosphorylation and signal transduction. Among these, we decided to focus on protein kinases (protein phosphorylation) for two main reasons: *i)* the design of specific small molecule kinase inhibitors is typically straightforward; *ii)* cell type-specific silencing or pharmacological blocking of kinases is achievable, so that using this strategy for SLC26A9 regulation is less likely to have pleiotropic and/or deleterious secondary effects. We thus selected

LRRK1 (Leucine-rich repeat serine/threonine-protein kinase 1) for further mechanistic validation, as it had already been identified as a CFTR interactor, with its knockdown rescuing F508del-CFTR traffic and function, while showing no harmful effects on cells (Amaral lab, unpublished data).

Table 2 – Bioinformatic analysis of genes targeted by the traffic enhancer siRNA hits. The most relevant biological processes identified by analysing SLC26A9 traffic hits using the Gene Ontology Bioinformatics Resource.

Biological Processes	Number of genes	% of hits
Regulation of transcription	7	19.4
Protein phosphorylation	6	16.6
Intracellular signal transduction	4	11.1

Regulation of SLC26A9 by Protein Kinase Hits

The identification of LRRK1 as a traffic regulator of both SLC26A9 and F508del-CFTR made us question whether LRRK1 regulates the traffic of both proteins through independent mechanisms or whether the coincidence is based on the known SLC26A9-CFTR interaction. SLC26A9 expression is known to be essential for CFTR PM expression and F508del-CFTR correction by modulators. Additionally, we can immediately exclude a CFTR-mediated effect of LRRK1 on SLC26A9 traffic since our screen was performed in a CFTR-null model.

We then aimed to determine the role of LRRK1 on the expression of these two proteins. We started by assessing how F508del-CFTR expression and maturation is modulated by the presence of SLC26A9 and LRRK1. We transiently transfected CFBE cells stably expressing F508del-CFTR with shRNAs targeting SLC26A9 or a non-expressed gene (Luciferase). The role of LRRK1 was then probed by transfecting CFBE cells with an siRNA targeting LRRK1 (or with a non-targeting siNEG1 siRNA). Through WB we could firstly observe that there is approximately 50% SLC26A9 knockdown in shSLC26A9 transfected cells (Fig. 47A,C). As expected, in these cells, due to a lower expression of SLC26A9, F508del-CFTR expression is significantly diminished (Fig. 47A,B). This result is observed for both the core-glycosylated form (band B) and the mature or fully glycosylated form of CFTR (band C). LRRK1 knockdown was confirmed by semi-quantitative PCR (Fig. S33 – Appendix 3). Interestingly, and confirming the SLC26A9 screen data for LRRK1, in siLRRK1-transfected shLuciferase-cells, there is a

tendency for an increase in SLC26A9 expression (Fig. 47A,D). Finally, F508del-CFTR trafficking is rescued by siLRRK1 as seen by an increase (although not statistically significant) in the mature form of CFTR (band C). However, even though the levels of PM F508del-CFTR are strongly decreased by the knockdown of SLC26A9, the CFTR PM rescue (i.e., increase in cell surface expression) observed under siLRRK1 is always ~50% (in cells with or without SLC26A9 KD). These data suggest that LRRK1 is independently regulating SLC26A9 and F508del-CFTR, thus holding the potential of being an efficient drug target for CF by increasing chloride (Cl^-) secretion through enhancement of both proteins PM traffic.

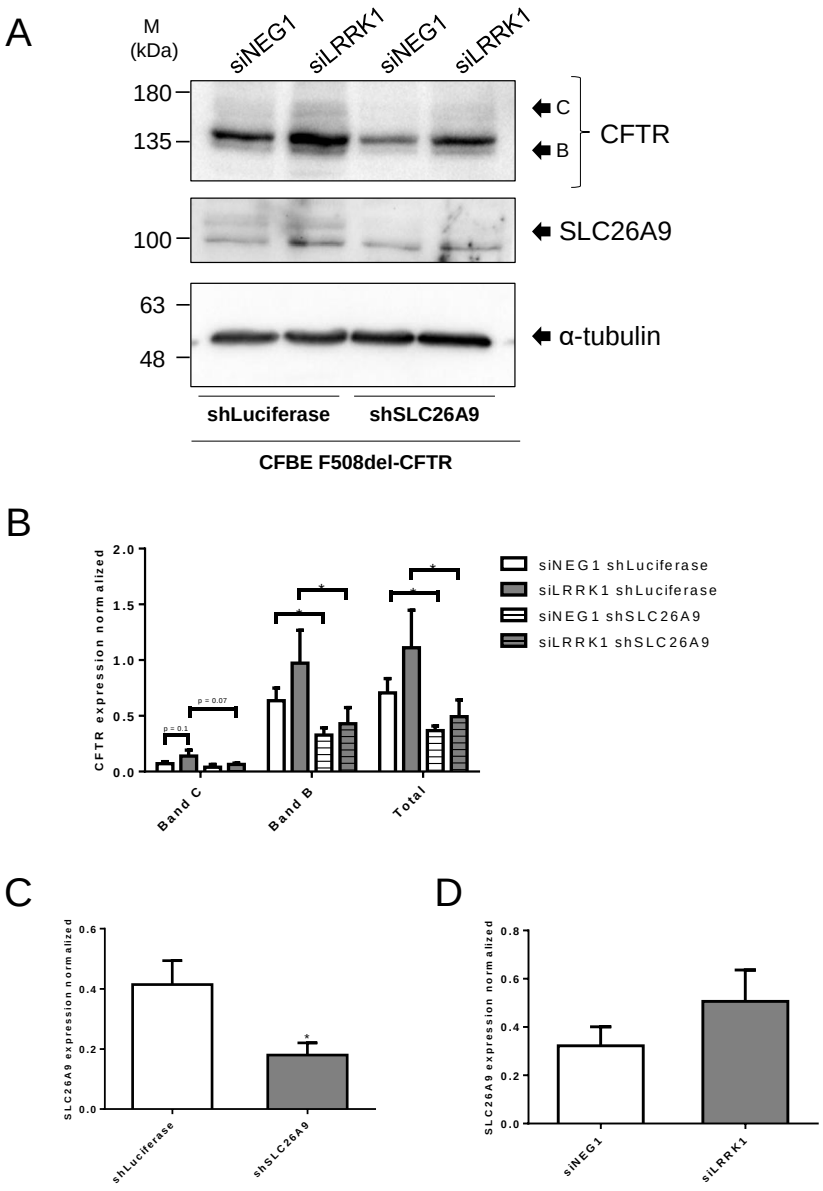

Figure 47 – siLRRK1 enhances traffic of both F508del-CFTR and SLC26A9. (A) Representative Western Blot of CFBE F508del-CFTR stably expressing shSLC26A9 or shLuciferase (control shRNA) and transiently transfected with a siRNA targeting a hit (siLRRK1) or the non-targeting negative control siRNA (siNEG1). **(B)** Quantification of F508del-CFTR expression (Band C – fully-glycosylated CFTR; Band B – core-

glycosylated CFTR; Total – total CFTR expression. **(C)** Quantification of SLC26A9 knockdown after shRNA transduction. **(D)** Quantification of SLC26A9 expression showing a small increase (not statistically significant) in total expression of SLC26A9 after siLRRK1 transfection, when compared to the negative control. Statistical analyses were performed by GraphPad Prism 6.0 using unpaired t-test where "*" indicates statistically significant differences ($p < 0.05$).

Discussion

SLC26A9 is a well-recognized gene modifier of CF disease and its polymorphisms have been associated with the severity of CF symptoms in many organs. These include the risk of developing meconium ileus, early exocrine pancreatic disease, and the age of onset of CF-related diabetes[137,138,153,154]. SLC26A9 is also a disease modifier in other respiratory disorders such as asthma and non-CF bronchiectasis[309]. Moreover, SLC26A9 polymorphisms have been demonstrated to differentially correlate with intensity of G551D and F508del-CFTR responses to modulator drugs[151,152]. Furthermore, since it also plays a role in epithelial Cl^- secretion[136], SLC26A9 appears to be an interesting alternative drug target in obstructive airway diseases, particularly in CF. Interestingly, two SLC26A9 missense mutations (R575W and V486I) that decrease SLC26A9 Cl^- conductance have been identified in patients with diffuse idiopathic bronchiectasis[309]. R575W-SLC26A9 was identified in a patient heterozygote for the F508del-CFTR mutation, which displayed CF-like symptoms. R575W is localized in the STAS domain, probably interfering with the interaction between SLC26A9 and CFTR[309]. These data suggest, once more, a potential role of SLC26A9 in CF-like diseases.

A concerted drug discovery effort has been made by the CF research community to identify potent CFTR correctors (i.e., small molecules that partially rescue CFTR mutants with a traffic defect, namely the most common CF-causing mutation F508del) and potentiators (i.e., compounds that increase CFTR channel open probability). However, the clinically approved modulators only partially reverse CFTR dysfunction, and provide variable clinical benefits. Moreover, a considerable number of individuals with CF carrying rare CFTR mutations remain without any effective CFTR modulator therapy. Accordingly, additional efforts have been pursued to identify novel therapies that may benefit a larger CF population. An example of such strategy includes the modulation of alternative ion channels/transporters that may restore epithelial Cl^- secretion in all individuals with CF. Due to the multiple above-mentioned studies reporting the important role of SLC26A9 in the pathogenesis of CF, this transporter is an attractive candidate for this mutation-agnostic therapeutic approach to CF.

To take advantage of SLC26A9 in the context of CF, however, we must keep in mind that the synergistic interaction between SLC26A9 and wt-CFTR traffic might be a significant obstacle in the absence of functional CFTR. Indeed, when co-expressed with the traffic incompetent F508del-CFTR mutant, SLC26A9 is also retained in the ER and degraded by the proteasome. Since this CFTR mutant is found in at least one allele of 80-85% of individuals with CF worldwide[313,314], research should focus on finding SLC26A9 potentiators (and correctors) that can work independently of CFTR. Moreover, being SLC26A9 activated once inserted into the PM[148], an interesting strategy would consist in increasing SLC26A9 PM expression in the absence of functional CFTR. Here we developed a platform to identify SLC26A9 traffic enhancers in a CFTR-null model. This traffic screen revealed 36 siRNAs that increase SLC26A9 PM expression, and consequently hold the promise of increasing Cl^- secretion in CF. The study of SLC26A9 in the context of CF has been limited by rather unspecific inhibitors and antibodies. This double-tagged construct constitutes a new tool for the study of the interactome of SLC26A9, allows for the identification of potentiators of SLC26A9 PM expression and function, and can be used in different cell models to study not only CF but also other obstructive airway diseases. Notably, as we have previously shown that the response to CFTR modulators is affected by SLC26A9 expression levels (chapter 3.1), CFTR modulators and drugs increasing SLC26A9 function may be combined for synergistic effects in enhancing fluid secretion in CF.

One of the most promising hits was LRRK1, a serine/threonine-protein kinase known to regulate endosomal trafficking of the epidermal growth factor receptor (EGFR) and osteoclast biology[315]. We had previously shown that the knockdown of LRRK1 partially rescues F508del-CFTR trafficking and function in CFBE cells (Amaral lab, unpublished data). Here we found that the knockdown of LRRK1 also increases SLC26A9 PM trafficking, while showing an increase (albeit not significant) in overall SLC26A9 expression. From our results shown here, this regulation of CFTR and SLC26A9 by LRRK1 appears to be independent, as SLC26A9 PM expression was assessed in a CFTR-null model, and the knockdown of LRRK1 led to a proportional increase in the rescue of F508del-CFTR in shSLC26A9 expressing cells vs control cells. Therefore, we can conclude that LRRK1 is an attractive drug target for CF being its inhibitors of interest to be further explored as potential therapies for CF, by causing an increase in both CFTR- and SLC26A9-mediated Cl^- secretion.

Even though there exist no specific LRRK1 inhibitors, significant pharmacological efforts have been directed at its close homologue LRRK2. Since several years LRRK2 has been implicated in immune disorders and infectious diseases, but its most relevant

pharmacological application is as a therapeutic target in Parkinson's disease, acting independently of α-synuclein[316,317]. This has led to the development and clinical deployment of LRRK2 inhibitors in Parkinson's patients, including compounds binding and inhibiting either the open or closed conformation of the LRRK2 kinase domain[318]. Nevertheless, there is high resolution structural information on LRRK1 currently available[319] which may potentially be used for the development of LRRK1 inhibitors with relevance in CF biomedicine or clinical practice.

Finally, the hits identified in the present traffic screen constitute a valuable resource to be used in future studies to expand our mechanistic knowledge on the role of SLC26A9 in CF pathophysiology.

IV. General Discussion and Future Perspectives

Despite remarkable progress in developing highly effective CFTR modulator therapies that target the cellular/functional defects for different CFTR mutations, several issues still need to be addressed: 1) there are still ~15-20% of individuals with CF for whom the available CFTR modulator drugs are not suitable and require alternative CFTR-independent strategies; 2) among those who are eligible, benefit occurs at different degrees, never reaching the levels of individuals without CF (or carriers); 3) some individuals do not tolerate available modulators; 4) there is no equitable access to these drugs due to their very high cost and lack of international regulatory issues; 5) real-world and long-term benefits and sequelae are yet to be determined. Accordingly, there is an unmet need for alternative therapeutic approaches so as to increase the options available in the clinic to treat the basic defect underlying this disease.

One strategy that gained increasing attention over the last few years consists in the modulation of other (non-CFTR) ion channels/transporters which are already expressed at the PM of secretory epithelial cells[102,140]. The main allure of this approach is that it applies to all individuals with CF, regardless of their CF genotypes, thus being a “mutation-agnostic” approach. Notably, CFTR modulators and drugs targeting distinct alternative channels/transporters may also be combined for additive effects in improving fluid secretion in CF. The present work was focused on the study of two of these alternative targets: TMEM16A and SLC26A9, so as to explore their therapeutic potential for CF.

TMEM16A/ANO1 is a calcium (Ca^{2+})-activated Cl^- channel (CaCC) expressed in various epithelia common to CFTR, including the airways, large intestine, salivary glands, pancreas, kidney and liver[70,102]. Notwithstanding, it is also expressed in the nervous system[89], smooth muscle[91] and tumour cells[92]. Such a broad tissue expression justifies its multiple physiological roles, which include airway and exocrine gland secretion, smooth muscle contraction, neuronal signalling control and peristalsis regulation of gastrointestinal system[93]. Furthermore, TMEM16A expression has been found to be upregulated in various types of cancer[123,124].

Targeting TMEM16A for the treatment of CF has been a matter of debate. While several research groups support the need to activate TMEM16A in the context of CF to compensate for the absence of functional CFTR in order to increase airway hydration and MCC, others consider the opposite and suggest that inhibition of TMEM16A might decrease mucus secretion and prevent bronchoconstriction. Efforts have been carried out in both directions to discover TMEM16A modulators (activators and inhibitors) and in parallel, multiple studies progress to better understand the role of TMEM16A in epithelial

physiology in general, and in CF, in particular. However, despite the existence of various TMEM16A modulator drugs, the potency and selectivity of these compounds is questionable, thus constituting a considerable limitation. The development of effective and selective molecules that target either TMEM16A itself or TMEM16A regulator proteins may provide valuable information on the role of this channel in CF and TMEM16A-related disorders, namely CF, and bring about significant insight for its therapeutic potential.

In this work we first developed a novel screening platform to assess the effects of silencing multiple genes on the PM traffic of TMEM16A (**Chapter 1**). Regardless of the final goal – activating or inhibiting TMEM16A – this screening platform allows for the identification of TMEM16A traffic regulators on a large scale, while also shedding light on its cellular roles. The traffic assay reported here is an improvement over current strategies for TMEM16A-based drug development for CF by allowing a direct study of TMEM16A and its regulators in a relevant cellular model without resorting to compounds with low potency and specificity which may have off target effects. Moreover, other cell types can be transduced with the double tagged TMEM16A construct to identify TMEM16A modulators of relevance for other disorders (e.g., asthma or cancer). Importantly, even though our assay employed a double-tagged construct expressed at high levels, i.e., not in a physiological context, our data demonstrate that the screen hits have similar effects on cells with endogenous TMEM16A, thus validating its applicability. Thus, such platform is a bona fide model to identify physiologically relevant genes and/or compounds that regulate TMEM16A PM traffic and function.

Next, we used this platform to identify and mechanistically validate genes which enhance (targeted by inhibitory siRNAs) or inhibit (targeted by activator siRNAs) TMEM16A trafficking and function. The knockdown (KD) of ESYT1, a member of the extended synaptotagmins family of proteins with a role in tethering the ER to the PM in a Ca^{2+}- and PIP_2-dependent manner, led to a significant reduction in the trafficking and function of TMEM16A. This is consistent with the localization of TMEM16A yeast analogue Ist2 at the ER-PM junctions and the role of TMEM16 proteins in generating compartmentalized Ca^{2+} signals. Hence, these data reveal once more how the traffic screening platform developed here can be valuable for determining TMEM16A cellular functions and unveiling its regulators.

Negative regulation of TMEM16A expression and function might be useful for the treatment of conditions where TMEM16A appears to be upregulated or have deleterious effects, such as muscular contraction, bronchoconstriction, intestinal contraction,

diarrhoea, and perhaps also cancer. In fact, our studies with head and neck cancer cells suggest that TMEM16A KD and channel inhibition contribute to reducing cancer cell proliferation. Accordingly, silencing CK2 decreased TMEM16A PM expression and function, and the knockdown or inhibition of both proteins had an additive effect on blocking cancer cell proliferation. It should nevertheless be said that CK2 has pleiotropic effects, besides regulating TMEM16A PM expression, thus a direct causal relationship is difficult to establish.

On the other hand, blocking the traffic inhibitors of TMEM16A might be an interesting way of increasing Cl^- secretion and ASL hydration in CF. We identified ADRA2C and CXCR3, two GPCRs, as TMEM16A traffic inhibitors, with their KD increasing TMEM16A PM expression and function while showing no cytotoxicity nor raising Ca^{2+} levels. Their MoA appears to be through destabilization of TMEM16A at the PM, and therefore their inhibition results in a new way to boost TMEM16A PM expression. Accordingly, it would be of interest to carry out follow-up experiments that include studying the effect of silencing ADRA2C or CXCR3 in primary human bronchial epithelial cells to confirm their effects not only on TMEM16A, but also on Cl^- secretion and ASL hydration in a more physiological model. Additionally, the use of (yet unidentified) selective chemical inhibitors of these GPCRs would confirm if their effect on TMEM16A is dependent on their activity, and if so, thereof potential new drugs could be developed to enhance Cl^- secretion in individuals with CF.

TMEM16A is as interesting therapeutic target for CF not only because of its role in Cl^- secretion, but also because of its close functional interaction with CFTR. This was the focus of our next investigation (**Chapter 2**) where we concentrated on deepening our knowledge on this relationship by studying their common activation pathways and their functional interaction in several cell types.

Our data show that cAMP-dependent and Ca^{2+}-activated Cl^- currents in airway epithelial cells strongly overlap due to the crosstalk of intracellular signalling molecules. This signalling/functional overlap probably takes places in shielded membrane compartments – membrane microdomains (lipid raft-like compartments) – and is mediated by EPAC1 and ADCY1. Future studies may provide additional details on this functional interaction, namely on how phosphodiesterases or other possible intermediaries contribute to this tight regulation.

In parallel, we demonstrated that TMEM16A or TMEM16F – another PM expressed TMEM16 family member – are required for exocytosis and expression of CFTR at the PM, in several human cell lines with either endogenous or heterologous

protein expression. Furthermore, we have also reported that the rescue of F508del-CFTR by CFTR correctors is significantly less efficient in the absence of functional TMEM16A/F.

These data further reinforce the hypothesis of TMEM16A activation (rather than its inhibition) will be beneficial for CF. Indeed, considering this close functional interaction between TMEM16A and CFTR, one can assume that inhibiting TMEM16A in the airways of individuals with CF would cause additional problems, especially to those with residual function mutations or taking CFTR modulator drugs, as TMEM16A inhibition/silencing would most likely also inhibit the already the existing/rescued CFTR function. Nevertheless, given the possible adverse effects of TMEM16A overexpression, TMEM16A potentiators (such as ETX001, currently under clinical trial) or traffic enhancers may constitute interesting alternatives for CF therapeutic strategies. More studies are needed to finally understand the potential of modulating this channel in human diseases, CF in particular.

The SLC26A9 Cl^- transporter is another promising alternative candidate to compensate for the lack of CFTR function in CF. It has been proposed to function as a constitutively active Cl^- transporter[86,141], predominantly expressed in epithelial cells of the respiratory tract, stomach, duodenum, ileum and pancreas[133,140]. In human airways, SLC26A9 contributes to constitutive Cl^- secretion and MCC[136], and, in contrast to CFTR and TMEM16A, its activation is not regulated, i.e., it is spontaneously active once inserted into the PM of airway epithelial cells[148]. The importance of investigating SLC26A9 in the context of CF has been highlighted by its identification as a CF modifier gene, the association of SLC26A9 polymorphisms to more severe CF symptoms, as well as to lower responses to CFTR modulator drugs, as also above described for TMEM16A.

Indeed, there is a consensus in that the currently available data support a clinically relevant role of SLC26A9 as a disease modifier and promising therapeutic target to circumvent deficient/absent Cl^- secretion in CF. In fact, in contrast to TMEM16A, SLC26A9 modulation as a strategy in CF therapies is consensual in that it will be beneficial for CF to increase SLC26A9 PM expression and function. Nevertheless, the study of SLC26A9 has been somehow limited by the lack of sensitive and selective pharmacological modulators. Some compounds that have been demonstrated to inhibit SLC26A9 are non-selective Cl^- channel inhibitors (i.e., NFA, and GlyH101) with different degrees of potency. Accordingly, identification of selective modulators of SLC26A9 is necessary to further understand if and how it can be used as a therapeutic target. Also, the mechanisms of the functional interaction between CFTR and SLC26A9 are not fully

understood. Due to its constitutive activation when located at the PM, increasing or stabilizing SLC26A9 PM expression may contribute to increase epithelial Cl^- secretion. Thus, here we studied the functional interaction between SLC26A9 and CFTR and searched for modulators of SLC26A9 PM expression through HTS (**Chapter 3**).

We show here that SLC26A9 expression enhances CFTR PM traffic and function, as well as CFTR response to highly effective modulator drugs. Our data indicate that SLC26A9 stabilizes CFTR at the ER level and that the efficacy of CFTR modulator drugs is further enhanced by SLC26A9 increased expression. Accordingly, and because SLC26A9 polymorphisms have been correlated with the response to CFTR modulator drugs, it will be interesting to carry out follow-up experiments that include genotyping (for SLC26A9) individuals with CF homozygous for the F508del mutation which do not respond adequately in the clinic to the approved drugs, as done before for the in vitro responses to these drugs in primary human respiratory cells. Additionally, it would be of great interest to know if SLC26A9 overexpression also potentiates the effects of the CFTR modulators on other mutations which do not affect CFTR trafficking, i.e., when CFTR is already at the PM (e.g., G551D).

Considering the positive effects of enhancing SLC26A9 expression for CF, we performed a HTS where we identified several genes targeted by siRNAs that increase SLC26A9 expression at the PM. One of the most promising hits is LRRK1, which also enhances F508del-CFTR traffic and function. Thus, inhibiting/silencing LRRK1 is an appealing strategy for alternative CF therapies suitable for all patients, which will probably be even more efficient for the ones carrying the F508del mutation by increasing Cl^- secretion via both SLC26A9 and CFTR. The development of specific and potent LRRK1 inhibitors would be important for the validation of this protein as a therapeutic target.

In summary, the work developed here contributed to better understand the complex relationship between CFTR and other alternative Cl^- channels/transporters, and how the latter may be used as potential therapeutic targets for the development of drugs applying to all people with CF, regardless of their CFTR mutations.

Finally, the significance of the current findings for the CF field is three-fold. Firstly, we have developed new cellular models and HTS platforms to identify the regulators of TMEM16A and SLC26A9 on a global scale. These platforms are useful to identify modulators of TMEM16A and/or SLC26A9 PM expression (and function) with possible therapeutic applications for CF and other diseases. Secondly, we have deepened the current knowledge on the mechanisms of interaction between TMEM16A and CFTR, as

well as those of SLC26A9 and CFTR. Thirdly, we have discovered that even the most effective clinically available CF therapies can be further enhanced, namely by increasing SLC26A9 (and possibly also TMEM16A) expression levels.

V. References

1. Collins, F. S. Cystic Fibrosis: Molecular Biology and Therapeutic Implications. *Science (80-.).* **1992**, *256*, 774–779.

2. Amaral, M. D. Novel personalized therapies for cystic fibrosis: treating the basic defect in all patients. *J. Intern. Med.* **2015**, *277*, 155–166. doi:10.1111/joim.12314.

3. Bobadilla, J. L., Macek, M., Fine, J. P. & Farrell, P. M. Cystic fibrosis: A worldwide analysis of CFTR mutations - Correlation with incidence data and application to screening. *Hum. Mutat.* **2002**, *19*, 575–606. doi:10.1002/humu.10041.

4. O'Sullivan, B. P. & Freedman, S. D. Cystic fibrosis. *Lancet* **2009**, *373*, 1891–1904. doi:10.1016/S0140-6736(09)60327-5.

5. Andersen, H. . Cystic Fibrosis of the pancreas and its relation to celiac disease. *Am J Dis Child* **1938**, *56*, 344–399.

6. Riordan, J. R. *et al.* Identification the Cystic Fibrosis Gene : Cloning and Characterization of Complementary DNA. *Science (80-.).* **1989**, *245*, 1066–73.

7. Hug, M. J., Tamada, T. & Bridges, R. J. CFTR and bicarbonate secretion by epithelial cells. *News Physiol. Sci.* **2003**, *18*, 38–42.

8. Sheppard, D. N. & Welsh, M. J. Structure and function of the CFTR chloride channel. *Physiol. Rev.* **1999**, *79*, S23–S45.

9. Cutting, G. R. Cystic fibrosis genetics: from molecular understanding to clinical application. *Nat. Rev. Genet.* **2014**, *16*, 45–56. doi:10.1038/nrg3849.

10. Zielenski, J. Genotype and phenotype in cystic fibrosis. *Respiration* **2000**, *67*, 117–133. doi:29497.

11. Cystic Fibrosis Mutation Database. http://www.genet.sickkids.on.ca/cftr/ (Accessed: 11 August 2021).

12. De Boeck, K. & Amaral, M. D. Progress in therapies for cystic fibrosis. *Lancet Respir. Med.* **2016**, *4*, 662–674. doi:10.1016/S2213-2600(16)00023-0.

13. Kunzelmann, K., Kathöfer, S. & Greger, R. Na+ and Cl- conductances in airway epithelial cells: increased Na+ conductance in cystic fibrosis. *Pflügers Arch. Eur. J. Physiol.* **1995**, *431*, 1–9. doi:10.1007/BF00374371.

14. Reddy, M. M., Light, M. J. & Quinton, P. M. Activation of the epithelial Na+ channel (ENaC) requires CFTR Cl- channel function. *Nature* **1999**, *402*, 301–304. doi:10.1038/46297.

15. Verkman, A. S., Song, Y. & Thiagarajah, J. R. Role of airway surface liquid and submucosal glands in cystic fibrosis lung disease. *Am J Physiol Cell Physiol* **2003**, *284*, C2–C15. doi:10.1152/ajpcell.00417.2002.

16. Davies, J. C. & Bilton, D. Bugs, biofilms, and resistance in cystic fibrosis. *Respir. Care* **2009**, *54*, 628–638. doi:10.4187/aarc0492.

17. Perrem, L. & Ratjen, F. Anti-inflammatories and mucociliary clearance therapies in the age of CFTR modulators. *Pediatr. Pulmonol.* **2019**, *54*, S46–S55. doi:10.1002/ppul.24364.

18. Turcios, N. L. Cystic Fibrosis Lung Disease: An Overview. *Respir. Care* **2020**, *65*, 233–251. doi:10.4187/respcare.06697.

19. Lopes-Pacheco, M. CFTR modulators: Shedding light on precision medicine for cystic fibrosis. *Front. Pharmacol.* **2016**, *7*, 1–20. doi:10.3389/fphar.2016.00275.

20. Wilschanski, M. *et al.* Correlation of sweat chloride concentration with classes of the cystic fibrosis transmembrane conductance regulator gene mutations. *J. Pediatr.* **1995**, *127*, 705–710. doi:10.1016/S0022-3476(95)70157-5.

21. Gibson-Corley, K. N., Meyerholz, D. K. & Engelhardt, J. F. Pancreatic Pathophysiology in Cystic Fibrosis. *J Pathol.* **2016**, *238*, 311–320. doi:10.1002/path.4634.

22. Al Sinani, S., Al-Mulaabed, S., Naamani, K. Al & Sultan, R. Cystic fibrosis liver disease: Know more. *Oman Med. J.* **2019**, *34*, 482–489. doi:10.5001/omj.2019.90.

23. Plant, B. J., Goss, C. H., Plant, W. D. & Bell, S. C. Management of comorbidities in older patients with cystic fibrosis. *Lancet Respir. Med.* **2013**, *1*, 164–174. doi:10.1016/S2213-2600(13)70025-0.

24. McCarthy, V. a. & Harris, A. The CFTR gene and regulation of its expression. *Pediatr. Pulmonol.* **2005**, *40*, 1–8. doi:10.1002/ppul.20199.

25. CFTR2 Variant List History. https://cftr2.org/mutations_history (Accessed: 11 August 2021).

26. CF Foundation Patient Registry Data. https://www.cff.org/2018_CFF_Patient_Registry_Annual_Data_Report.pdf (Accessed: 14 September 2020).

27. Amaral, M. D. & Kunzelmann, K. Molecular targeting of CFTR as a therapeutic approach to cystic fibrosis. *Trends Pharmacol. Sci.* **2007**, *28*, 334–341. doi:10.1016/j.tips.2007.05.004.

28. Dalemans, W. *et al.* Altered chloride ion channel kinetics associated with the F508del cystic fibrosis mutation. *Nature* **1991**, *354*, 526–528.

29. Bell, S. C., De Boeck, K. & Amaral, M. D. New pharmacological approaches for cystic fibrosis: Promises, progress, pitfalls. *Pharmacol. Ther.* **2014**, *145*, 19–34. doi:10.1016/j.pharmthera.2014.06.005.

30. Li, C. & Naren, A. P. Macromolecular complexes of cystic fibrosis transmembrane conductance regulator and its interacting partners. *Pharmacol. Ther.* **2005**, *108*, 208–223. doi:10.1016/j.pharmthera.2005.04.004.

31. Liu, F., Zhang, Z., Csanády, L., Gadsby, D. C. & Chen, J. Molecular Structure of the Human CFTR Ion Channel. *Cell* **2017**, *169*, 85-95.e8. doi:10.1016/j.cell.2017.02.024.

32. Rowe, Steven; Miller, Stacey; Sorscher, E. Cystic fibrosis. *N Engl J Med* **2005**, *352*, 1992–2001.

33. Gadsby, D. C., Vergani, P. & Csanády, L. The ABC protein turned chloride channel whose failure causes cystic fibrosis. *Nature* **2006**, *440*, 477–483. doi:10.1038/nature04712.

34. Riordan, J. R. Assembly of functional CFTR chloride channels. *Annu. Rev. Physiol.* **2005**, *67*, 701–718. doi:10.1146/annurev.physiol.67.032003.154107.

35. Raghuram, V., Mak, D. O. D. & Foskett, J. K. Regulation of cystic fibrosis transmembrane conductance regulator single-channel gating by bivalent PDZ-domain-mediated interaction. *Proc. Natl. Acad. Sci. U. S. A.* **2001**, *98*, 1300–1305. doi:10.1073/pnas.98.3.1300.

36. Guggino, W. B. The cystic fibrosis transmembrane regulator forms

macromolecular complexes with PDZ domain scaffold proteins. *Proc. Am. Thorac. Soc.* **2004**, *1*, 28–32. doi:10.1513/pats.2306011.

37. Farinha, C. M. & Amaral, M. D. Most F508del-CFTR Is Targeted to Degradation at an Early Folding Checkpoint and Independently of Calnexin. *Mol. Cell. Biol.* **2005**, *25*, 5242–5252. doi:10.1128/mcb.25.12.5242-5252.2005.

38. Farinha, C. M. & Canato, S. From the endoplasmic reticulum to the plasma membrane: mechanisms of CFTR folding and trafficking. *Cell. Mol. Life Sci.* **2017**, *74*, 39–55. doi:10.1007/s00018-016-2387-7.

39. Riordan, J. R. CFTR function and prospects for therapy. *Annu. Rev. Biochem.* **2008**, *77*, 701–726. doi:10.1146/annurev.biochem.75.103004.142532.

40. Farinha, C. M., Matos, P. & Amaral, M. D. Control of cystic fibrosis transmembrane conductance regulator membrane trafficking: Not just from the endoplasmic reticulum to the Golgi. *FEBS J.* **2013**, *280*, 4396–4406. doi:10.1111/febs.12392.

41. Yoo, J. S. *et al.* Non-conventional trafficking of the cystic fibrosis transmembrane conductance regulator through the early secretory pathway. *J. Biol. Chem.* **2002**, *277*, 11401–11409. doi:10.1074/jbc.M110263200.

42. Grieve, A. G. & Rabouille, C. Golgi bypass: Skirting around the heart of classical secretion. *Cold Spring Harb. Perspect. Biol.* **2011**, *3*, 1–15. doi:10.1101/cshperspect.a005298.

43. Riordan, J. R. The cystic fibrosis transmembrane conductance regulator. *Annu. Rev. Physiol.* **1993**, *55*, 609–630.

44. Vergani, P., Lockless, S. W., Nairn, A. C. & Gadsby, D. C. CFTR channel opening by ATP-driven tight dimerization of its nucleotide-binding domains. *Nature* **2005**, *433*, 876–880. doi:10.1038/nature03313.

45. Linsdell, P., Evagelidis, A. & Hanrahan, J. W. Molecular determinants of anion selectivity in the cystic fibrosis transmembrane conductance regulator chloride channel pore. *Biophys. J.* **2000**, *78*, 2973–2982. doi:10.1016/S0006-3495(00)76836-6.

46. Hwang, T. C. & Kirk, K. L. The CFTR Ion channel: Gating, regulation, and anion permeation. *Cold Spring Harb. Perspect. Med.* **2013**, *3*, 1–15. doi:10.1101/cshperspect.a009498.

47. Kunzelmann, K. & Schreiber, R. CFTR, a regulator of channels. *J. Membr. Biol.* **1999**, *168*, 1–8. doi:10.1007/s002329900492.

48. Vankeerberghen, A., Cuppens, H. & Cassiman, J. J. The cystic fibrosis transmembrane conductance regulator: An intriguing protein with pleiotropic functions. *J. Cyst. Fibros.* **2002**, *1*, 13–29. doi:10.1016/S1569-1993(01)00003-0.

49. Amaral, M. D., Quaresma, M. C. & Pankonien, I. What Role Does CFTR Play in Development, Differentiation, Regeneration and Cancer. *Int. J. Mol. Sci.* **2020**, Accepted for Publication.

50. Stern, M. *et al.* European cystic fibrosis society standards of care: Quality management in cystic fibrosis. *J. Cyst. Fibros.* **2014**, *13*, S43–S59. doi:10.1016/j.jcf.2014.03.011.

51. Ramos, K. J. *et al.* Lung transplant referral for individuals with cystic fibrosis: Cystic Fibrosis Foundation consensus guidelines. *J. Cyst. Fibros.* **2019**, *18*, 321–333. doi:10.1016/j.jcf.2019.03.002.

52. Regard, L., Martin, C., Chassagnon, G. & Burgel, P. R. Acute and chronic non-pulmonary complications in adults with cystic fibrosis. *Expert Rev. Respir. Med.* **2019**, *13*, 23–38. doi:10.1080/17476348.2019.1552832.

53. Joshi, D., Ehrhardt, A., Hong, J. S. & Sorscher, E. J. Cystic fibrosis precision therapeutics: Emerging considerations. *Pediatr. Pulmonol.* **2019**, *54*, S13–S17. doi:10.1002/ppul.24547.

54. Amaral, M. D. & Farinha, C. M. Rescuing mutant CFTR: a multi-task approach to a better outcome in treating cystic fibrosis. *Curr. Pharm. Des.* **2013**, *19*, 3497–508. doi:10.2174/13816128113199990318.

55. Howard, M., Frizzell, R. A. & Bedwell, D. M. Aminoglycoside antibiotics restore CFTR function by overcoming premature stop mutations. *Nat. Med.* **1996**, *2*, 467–469.

56. Wilschanski, M. *et al.* Gentamicin-induced correction of CFTR, function in patients with cystic fibrosis and CFTR stop mutations. *N. Engl. J. Med.* **2003**, *349*, 1433–1441. doi:10.1056/NEJMoa022170.

57. Van Goor, F. *et al.* Rescue of CF airway epithelial cell function in vitro by a CFTR potentiator, VX-770. *Proc. Natl. Acad. Sci. U. S. A.* **2009**, *106*, 18825–18830. doi:10.1073/pnas.0904709106.

58. Yu, H. *et al.* Ivacaftor potentiation of multiple CFTR channels with gating mutations. *J. Cyst. Fibros.* **2012**, *11*, 237–245. doi:10.1016/j.jcf.2011.12.005.

59. Van Goor, F. *et al.* Correction of the F508del-CFTR protein processing defect in vitro by the investigational drug VX-809. *Proc. Natl. Acad. Sci. U. S. A.* **2011**, *108*, 18843–18848. doi:10.1073/pnas.1105787108.

60. Pranke, I. M. *et al.* Correction of CFTR function in nasal epithelial cells from cystic fibrosis patients predicts improvement of respiratory function by CFTR modulators. *Sci. Rep.* **2017**, *7*, 1–11. doi:10.1038/s41598-017-07504-1.

61. Heijerman, H. G. M. *et al.* Efficacy and safety of the elexacaftor plus tezacaftor plus ivacaftor combination regimen in people with cystic fibrosis homozygous for the F508del mutation: a double-blind, randomised, phase 3 trial. *Lancet* **2019**, *394*, 1940–1948. doi:10.1016/S0140-6736(19)32597-8.

62. Middleton, P. G. *et al.* Elexacaftor-tezacaftor-ivacaftor for cystic fibrosis with a single Phe508del allele. *N. Engl. J. Med.* **2019**, *381*, 1809–1819. doi:10.1056/NEJMoa1908639.

63. Molinski, S. V *et al.* Orkambi® and amplifier co-therapy improves function from a rare CFTR mutation in gene-edited cells and patient tissue. *EMBO Mol. Med.* **2017**, *9*, 1224–1243. doi:10.15252/emmm.201607137.

64. Igreja, S., Clarke, L. A., Botelho, H. M., Marques, L. & Amaral, M. D. Correction of a cystic fibrosis splicing mutation by antisense oligonucleotides. *Hum. Mutat.* **2015**, *37*, 209–215. doi:10.1002/humu.22931.

65. Donaldson, S. H. *et al.* Pharmacokinetics and safety of cavosonstat (N91115) in healthy and cystic fibrosis adults homozygous for F508DEL-CFTR. *J. Cyst. Fibros.* **2017**, *16*, 371–379. doi:10.1016/j.jcf.2017.01.009.

66. Pranke, I., Golec, A., Hinzpeter, A., Edelman, A. & Sermet-Gaudelus, I. Emerging therapeutic approaches for cystic fibrosis. From gene editing to personalized medicine. *Front. Pharmacol.* **2019**, *10*, 1–21. doi:10.3389/fphar.2019.00121.

67. Christopher Boyd, A. *et al.* New approaches to genetic therapies for cystic fibrosis. *J. Cyst. Fibros.* **2020**, *19*, S54–S59. doi:10.1016/j.jcf.2019.12.012.

68. Milenkovic, V. M., Brockmann, M., Stöhr, H., Weber, B. H. & Strauss, O. Evolution and functional divergence of the anoctamin family of membrane proteins. *BMC Evol. Biol.* **2010**, *10*, 319. doi:10.1186/1471-2148-10-319.

69. Brunner, J. D., Lim, N. K., Schenck, S., Duerst, A. & Dutzler, R. X-ray structure of a calcium-activated TMEM16 lipid scramblase. *Nature* **2014**, *516*, 207–212. doi:10.1038/nature13984.

70. Kunzelmann, K. *et al.* Anoctamins. *Pflugers Arch. Eur. J. Physiol.* **2011**, *462*, 195–208. doi:10.1007/s00424-011-0975-9.

71. Pedemonte, N. & Galietta, L. J. V. Structure and function of TMEM16 proteins (anoctamins). *Physiol. Rev.* **2014**, *94*, 419–59. doi:10.1152/physrev.00039.2011.

72. Whitlock, J. M. & Hartzell, H. C. Anoctamins/TMEM16 Proteins: Chloride Channels Flirting with Lipids and Extracellular Vesicles. *Annu. Rev. Physiol.* **2017**, *79*, 119–143. doi:10.1146/annurev-physiol-022516-034031.

73. Yang, Y. D. *et al.* TMEM16A confers receptor-activated calcium-dependent chloride conductance. *Nature* **2008**, *455*, 1210–1215. doi:10.1038/nature07313.

74. Caputo, A. *et al.* TMEM16A, a membrane protein associated with calcium-dependent chloride channel activity. *Science* **2008**, *322*, 590–594. doi:10.1126/science.1163518.

75. Schroeder, B. C., Cheng, T., Jan, Y. N. & Jan, L. Y. Expression Cloning of TMEM16A as a Calcium-Activated Chloride Channel Subunit. *Cell* **2008**, *134*, 1019–1029.

76. Stephan, A. B. *et al.* ANO2 is the cilial calcium-activated chloride channel that may mediate olfactory amplification. *Proc. Natl. Acad. Sci. U. S. A.* **2009**, *106*, 11776–11781. doi:10.1073/pnas.0903304106.

77. Suzuki, J. & Nagata, S. Calcium-dependent phospholipid scrambling by TMEM16F. *Nature* **2010**, *468*, 834–840. doi:10.1038/nature09583.

78. Grubb, S. *et al.* TMEM16F (Anoctamin 6), an anion channel of delayed Ca(2+) activation. *J. Gen. Physiol.* **2013**, *141*, 585–600. doi:10.1085/jgp.201210861.

79. Yang, H. *et al.* TMEM16F Forms a Ca2+-Activated Cation Channel Required for Lipid Scrambling in Platelets during Blood Coagulation. *Cell* **2012**, *151*, 111–122. doi:10.1016/j.cell.2012.07.036.

80. Whitlock, J. M. & Hartzell, H. C. A Pore Idea: the ion conduction pathway of TMEM16/ANO proteins is composed partly of lipid. *Pflugers Arch. Eur. J. Physiol.* **2016**, *468*, 455–473. doi:10.1007/s00424-015-1777-2.

81. Paulino, C., Kalienkova, V., Lam, A. K. M., Neldner, Y. & Dutzler, R. Activation mechanism of the calcium-activated chloride channel TMEM16A revealed by cryo-EM. *Nature* **2017**, *552*, 421–425. doi:10.1038/nature24652.

82. Paulino, C. *et al.* Structural basis for anion conduction in the calcium-activated chloride channel TMEM16A. *Elife* **2017**, *6*, 1–23. doi:10.7554/eLife.26232.

83. Dang, S. *et al.* Cryo-EM structures of the TMEM16A calcium-activated chloride channel. *Nature* **2017**, *552*, 426–429. doi:10.1038/nature25024.

84. Peters, C. J. *et al.* The Sixth Transmembrane Segment Is a Major Gating

Component of the TMEM16A Calcium-Activated Chloride Channel. *Neuron* **2018**, *97*, 1063-1077.e4. doi:10.1016/j.neuron.2018.01.048.

85. Benedetto, R. *et al.* Epithelial Chloride Transport by CFTR Requires TMEM16A. *Sci. Rep.* **2017**, *7*, 1–13. doi:10.1038/s41598-017-10910-0.

86. Quesada, R. & Dutzler, R. Alternative chloride transport pathways as pharmacological targets for the treatment of cystic fibrosis. *J. Cyst. Fibros.* **2020**, *19*, S37–S41. doi:10.1016/j.jcf.2019.10.020.

87. Alvadia, C. *et al.* Cryo-EM structures and functional characterization of the murine lipid scramblase TMEM16F. *Elife* **2019**, *8*, 1–28. doi:10.7554/eLife.44365.

88. Feng, S. *et al.* Cryo-EM Studies of TMEM16F Calcium-Activated Ion Channel Suggest Features Important for Lipid Scrambling. *Cell Rep.* **2019**, *28*, 567-579.e4. doi:10.1016/j.celrep.2019.06.023.

89. Cho, H. *et al.* The calcium-activated chloride channel anoctamin 1 acts as a heat sensor in nociceptive neurons. *Nat. Neurosci.* **2012**, *15*, 1015–1021. doi:10.1038/nn.3111.

90. Hong, G. S. *et al.* ANO1/TMEM16A regulates process maturation in radial glial cells in the developing brain. *Proc. Natl. Acad. Sci. U. S. A.* **2019**, *116*, 12494–12499. doi:10.1073/pnas.1901067116.

91. Huang, F. *et al.* Calcium-activated chloride channel TMEM16A modulates mucin secretion and airway smooth muscle contraction. *Proc. Natl. Acad. Sci. U. S. A.* **2012**, *109*, 16354–16359. doi:10.1073/pnas.1214596109.

92. Crottès, D. & Jan, L. Y. The multifaceted role of TMEM16A in cancer. *Cell Calcium* **2019**, *82*, 102050. doi:10.1016/j.ceca.2019.06.004.

93. Shi, S. *et al.* Recent progress in structural studies on TMEM16A channel. *Comput. Struct. Biotechnol. J.* **2020**, *18*, 714–722. doi:10.1016/j.csbj.2020.03.015.

94. Ni, Y. L., Kuan, A. S. & Chen, T. Y. Activation and inhibition of TMEM16A calcium-activated chloride channels. *PLoS One* **2014**, *9*, 4–6. doi:10.1371/journal.pone.0086734.

95. Le, S. C., Jia, Z., Chen, J. & Yang, H. Molecular basis of PIP2-dependent regulation of the Ca2+-activated chloride channel TMEM16A. *Nat. Commun.* **2019**, *10*, doi:10.1038/s41467-019-11784-8.

96. Tembo, M., Wozniak, K. L., Bainbridge, R. E. & Carlson, A. E. Phosphatidylinositol 4,5-bisphosphate (PIP2) and Ca2 are both required to open the Cl channel TMEM16A. *J. Biol. Chem.* **2019**, *294*, 12556–12564. doi:10.1074/jbc.RA118.007128.

97. Martins, J. R. *et al.* Anoctamin 6 is an essential component of the outwardly rectifying chloride channel. *Proc. Natl. Acad. Sci.* **2011**, *108*, 18168–18172. doi:10.1073/pnas.1108094108.

98. Ye, W. *et al.* Phosphatidylinositol-(4, 5)-bisphosphate regulates calcium gating of small-conductance cation channel TMEM16F. *Proc. Natl. Acad. Sci. U. S. A.* **2018**, *115*, E1667–E1674. doi:10.1073/pnas.1718728115.

99. Schreiber, R. *et al.* Expression and function of epithelial anoctamins. *J. Biol. Chem.* **2010**, *285*, 7838–7845. doi:10.1074/jbc.M109.065367.

100. Lin, J. *et al.* TMEM16A mediates the hypersecretion of mucus induced by

Interleukin-13. *Exp. Cell Res.* **2015**, *334*, 260–269. doi:10.1016/j.yexcr.2015.02.026.

101. Benedetto, R., Cabrita, I., Schreiber, R. & Kunzelmann, K. TMEM16A is indispensable for basal mucus secretion in airways and intestine. *FASEB J.* **2019**, *33*, 4502–4512. doi:10.1096/fj.201801333RRR.

102. Kunzelmann, K. *et al.* TMEM16A in cystic fibrosis: Activating or inhibiting? *Front. Pharmacol.* **2019**, *9*, 1–18. doi:10.3389/fphar.2019.00003.

103. Miner, K. *et al.* Drug repurposing: The anthelmintics niclosamide and nitazoxanide are potent TMEM16A antagonists that fully bronchodilate airways. *Front. Pharmacol.* **2019**, *10*, doi:10.3389/fphar.2019.00051.

104. Smith, S. & Edwards, C. T. Long-acting inhaled bronchodilators for cystic fibrosis. *Paediatr. Respir. Rev.* **2018**, *28*, 31–32. doi:10.1016/j.prrv.2018.04.002.

105. Ousingsawat, J. *et al.* Loss of TMEM16A causes a defect in epithelial Ca2+ -dependent chloride transport. *J. Biol. Chem.* **2009**, *284*, 28698–28703. doi:10.1074/jbc.M109.012120.

106. Rock, J. R. *et al.* Transmembrane protein 16A (TMEM16A) is a Ca2+ -regulated Cl- secretory channel in mouse airways. *J. Biol. Chem.* **2009**, *284*, 14875–14880. doi:10.1074/jbc.C109.000869.

107. He, M. *et al.* Chloride channels regulate differentiation and barrier functions of the mammalian airway. *Elife* **2020**, *9*, 1–23. doi:10.7554/eLife.53085.

108. Simões, F. B. *et al.* TMEM16A chloride channel does not drive mucus production. *Life Sci. Alliance* **2019**, *2*, 1–13. doi:10.26508/LSA.201900462.

109. Danahay, H. L. *et al.* TMEM16A Potentiation: A Novel Therapeutic Approach for the Treatment of Cystic Fibrosis. *Am. J. Respir. Crit. Care Med.* **2020**, *201*, 946–954. doi:10.1164/rccm.201908-1641OC.

110. Ousingsawat, J., Kongsuphol, P., Schreiber, R. & Kunzelmann, K. CFTR and TMEM16A are separate but functionally related Cl - channels. *Cell. Physiol. Biochem.* **2011**, *28*, 715–724. doi:10.1159/000335765.

111. Sondo, E., Caci, E. & Galietta, L. J. V. The TMEM16A chloride channel as an alternative therapeutic target in cystic fibrosis. *Int. J. Biochem. Cell Biol.* **2014**, *52*, 73–76. doi:10.1016/j.biocel.2014.03.022.

112. Zwaal, R. F. A., Comfurius, P. & Bevers, E. M. Scott syndrome, a bleeding disorder caused by defective scrambling of membrane phospholipids. *Biochim. Biophys. Acta - Mol. Cell Biol. Lipids* **2004**, *1636*, 119–128. doi:10.1016/j.bbalip.2003.07.003.

113. Kunzelmann, K. *et al.* Molecular functions of anoctamin 6 (TMEM16F): A chloride channel, cation channel, or phospholipid scramblase? *Pflugers Arch. Eur. J. Physiol.* **2014**, *466*, 407–414. doi:10.1007/s00424-013-1305-1.

114. Rock, J. R., Futtner, C. R. & Harfe, B. D. The transmembrane protein TMEM16A is required for normal development of the murine trachea. *Dev. Biol.* **2008**, *321*, 141–149. doi:10.1016/j.ydbio.2008.06.009.

115. Ornoy, A. *et al.* Pathological confirmation of cystic fibrosis in the fetus following prenatal diagnosis. *Am. J. Med. Genet.* **1987**, *28*, 935–947. doi:10.1002/ajmg.1320280420.

116. Bonvin, E. *et al.* Congenital tracheal malformation in cystic fibrosis transmembrane conductance regulator-deficient mice. *J. Physiol.* **2008**, *586*, 3231–3243. doi:10.1113/jphysiol.2008.150763.

117. Tuggle, K. L. *et al.* Characterization of defects in ion transport and tissue development in Cystic Fibrosis Transmembrane Conductance Regulator (CFTR)-knockout rats. *PLoS One* **2014**, *9*, 1–14. doi:10.1371/journal.pone.0091253.

118. Meyerholz, D. K. *et al.* Lack of cystic fibrosis transmembrane conductance regulator disrupts fetal airway development in pigs. *Lab. Investig.* **2018**, *98*, 825–838. doi:10.1038/s41374-018-0026-7.

119. Park, J. H. *et al.* TMEM16A deficiency: a potentially fatal neonatal disease resulting from impaired chloride currents. *J. Med. Genet.* **2020**, jmedgenet-2020-106978. doi:10.1136/jmedgenet-2020-106978.

120. West, R. B. *et al.* The novel marker, DOG1, is expressed ubiquitously in gastrointestinal stromal tumors irrespective of KIT or PDGFRA mutation status. *Am. J. Pathol.* **2004**, *165*, 107–113. doi:10.1016/S0002-9440(10)63279-8.

121. Carles, A. *et al.* Head and neck squamous cell carcinoma transcriptome analysis by comprehensive validated differential display. *Oncogene* **2006**, *25*, 1821–1831. doi:10.1038/sj.onc.1209203.

122. Britschgi, A. *et al.* Calcium-activated chloride channel ANO1 promotes breast cancer progression by activating EGFR and CAMK signaling. *Proc. Natl. Acad. Sci. U. S. A.* **2013**, *110*, doi:10.1073/pnas.1217072110.

123. Jia, L., Liu, W., Guan, L., Lu, M. & Wang, K. W. Inhibition of calcium-activated chloride channel ANO1/TMEM16A suppresses tumor growth and invasion in human lung cancer. *PLoS One* **2015**, *10*, 1–17. doi:10.1371/journal.pone.0136584.

124. Duvvuri, U. *et al.* TMEM16A induces MAPK and contributes directly to tumorigenesis and cancer progression. *Cancer Res.* **2012**, *72*, 3270–3281. doi:10.1158/0008-5472.CAN-12-0475-T.

125. Huang, X., Godfrey, T. E., Gooding, W. E., McCarty Jr., K. S. & Gollin, S. M. Comprehensive Genome and Transcriptome Analysis of the 11q13 Amplicon in Human Oral Cancer and Synteny to the 7F5 Amplicon in Murine Oral Carcinoma. *Genes. Chromosomes Cancer* **2006**, *45*, 1058–1069. doi:10.1002/gcc.20371.

126. Peters, G., Fantl, V., Smith, R., Brookes, S. & Dickson, C. Chromosome 11q13 markers and D-type cyclins in breast cancer. *Breast Cancer Res. Treat.* **1995**, *33*, 125–135. doi:10.1007/BF00682720.

127. Wang, H. *et al.* Cell-specific mechanisms of TMEM16A Ca2+-activated chloride channel in cancer. *Mol. Cancer* **2017**, *16*, 1–17. doi:10.1186/s12943-017-0720-x.

128. Mount, D. B. & Romero, M. F. The SLC26 gene family of multifunctional anion exchangers. *Pflugers Arch. Eur. J. Physiol.* **2004**, *447*, 710–721. doi:10.1007/s00424-003-1090-3.

129. Kere, J. Overview of the SLC26 family and associated diseases. *Novartis Found. Symp.* **2006**, *273*, 2–11.

130. Alper, S. L. & Sharma, A. K. The SLC26 gene family of anion transporters and channels. *Mol. Aspects Med.* **2013**, *34*, 494–515. doi:10.1016/j.mam.2012.07.009.

131. Geertsma, E. R. *et al.* Structure of a prokaryotic fumarate transporter reveals the architecture of the SLC26 family. *Nat. Struct. Mol. Biol.* **2015**, *22*, 803–808. doi:10.1038/nsmb.3091.

132. Chang, Y. N. *et al.* Structural basis for functional interactions in dimers of SLC26 transporters. *Nat. Commun.* **2019**, *10*, doi:10.1038/s41467-019-10001-w.

133. Dorwart, M. R., Shcheynikov, N., Yang, D. & Muallem, S. The solute carrier 26 family of proteins in epithelial ion transport. *Physiology* **2008**, *23*, 104–114. doi:10.1152/physiol.00037.2007.

134. Höglund, P. *et al.* Mutations of the Down-regulated in adenoma (DRA) gene cause congenital chloride diarrhoea. *Nat. Genet.* **1996**, *14*, 316–319.

135. Sheffield, V. C. *et al.* Pendred syndrome maps to chromosome 7q21-34 and is caused by an intrinsic defect in thyroid iodine organification. *Nat. Genet.* **1996**, *12*, 424–426. doi:10.1038/ng0496-424.

136. Anagnostopoulou, P. *et al.* SLC26A9-mediated chloride secretion prevents mucus obstruction in airway inflammation. *J. Clin. Invest.* **2012**, *122*, 3629–3634. doi:10.1172/JCI60429.

137. Miller, M. R. *et al.* Variants in solute carrier SLC26A9 modify prenatal exocrine pancreatic damage in cystic fibrosis. *J. Pediatr.* **2015**, *166*, 1152-1157.e6. doi:10.1016/j.jpeds.2015.01.044.

138. Lam, A. T. N. *et al.* Increased expression of anion transporter SLC26A9 delays diabetes onset in cystic fibrosis. *J. Clin. Invest.* **2020**, *130*, 272–286. doi:10.1172/JCI129833.

139. Seidler, U. & Nikolovska, K. Slc26 family of anion transporters in the gastrointestinal tract: Expression, function, regulation, and role in disease. *Compr. Physiol.* **2019**, *9*, 839–872. doi:10.1002/cphy.c180027.

140. Balázs, A. & Mall, M. A. Role of the SLC26A9 chloride channel as disease modifier and potential therapeutic target in cystic fibrosis. *Front. Pharmacol.* **2018**, *9*, 1–9. doi:10.3389/fphar.2018.01112.

141. Walter, J. D., Sawicka, M. & Dutzler, R. Cryo-EM structures and functional characterization of murine Slc26a9 reveal mechanism of uncoupled chloride transport. *Elife* **2019**, *8*, 1–31. doi:10.7554/eLife.46986.

142. Chang, Y. N. & Geertsma, E. R. The novel class of seven transmembrane segment inverted repeat carriers. *Biol. Chem.* **2017**, *398*, 165–174. doi:10.1515/hsz-2016-0254.

143. Chang, M. H. *et al.* Slc26a9-Anion exchanger, channel and Na+ transporter. *J. Membr. Biol.* **2009**, *228*, 125–140. doi:10.1007/s00232-009-9165-5.

144. Chi, X. *et al.* Structural insights into the gating mechanism of human SLC26A9 mediated by its C-terminal sequence. *Cell Discov.* **2020**, *6*, doi:10.1038/s41421-020-00193-7.

145. Dorwart, M. R., Shcheynikov, N., Wang, Y., Stippec, S. & Muallem, S. SLC26A9 is a Cl- channel regulated by the WNK kinases. *J. Physiol.* **2007**, *584*, 333–345. doi:10.1113/jphysiol.2007.135855.

146. Xu, J. *et al.* Deletion of the chloride transporter Slc26a9 causes loss of tubulovesicles in parietal cells and impairs acid secretion in the stomach. *Proc. Natl. Acad. Sci. U. S. A.* **2008**, *105*, 17955–17960. doi:10.1073/pnas.0800616105.

147. Liu, X. *et al.* Loss of Slc26a9 anion transporter alters intestinal electrolyte and HCO3- transport and reduces survival in CFTR-deficient mice. *Pflugers Arch. Eur. J. Physiol.* **2015**, *467*, 1261–1275. doi:10.1007/s00424-014-1543-x.

148. Bertrand, C. A., Zhang, R., Pilewski, J. M. & Frizzell, R. A. SLC26A9 is a constitutively active, CFTR-regulated anion conductance in human bronchial epithelia. *J. Gen. Physiol.* **2009**, *133*, 421–438. doi:10.1085/jgp.200810097.

149. Sato, Y., Thomas, D. Y. & Hanrahan, J. W. The anion transporter SLC26A9 localizes to tight junctions and is degraded by the proteasome when co-expressed with F508del-CFTR. *J. Biol. Chem.* **2019**, *294*, 18269–18284. doi:10.1074/jbc.RA119.010192.

150. El Khouri, E. & Touré, A. Functional interaction of the cystic fibrosis transmembrane conductance regulator with members of the SLC26 family of anion transporters (SLC26A8 and SLC26A9): Physiological and pathophysiological relevance. *Int. J. Biochem. Cell Biol.* **2014**, *52*, 58–67. doi:10.1016/j.biocel.2014.02.001.

151. Strug, L. J. *et al.* Cystic fibrosis gene modifier SLC26A9 modulates airway response to CFTR-directed therapeutics. *Hum. Mol. Genet.* **2016**, *25*, 4590–4600. doi:10.1093/hmg/ddw290.

152. Corvol, H. *et al.* SLC26A9 gene is associated with lung function response to ivacaftor in patients with cystic fibrosis. *Front. Pharmacol.* **2018**, *9*, 1–11. doi:10.3389/fphar.2018.00828.

153. Sun, L. *et al.* Multiple apical plasma membrane constituents are associated with susceptibility to meconium ileus in individuals with cystic fibrosis. *Nat. Genet.* **2012**, *44*, 562–569. doi:10.1038/ng.2221.

154. Li, W. *et al.* Unraveling the complex genetic model for cystic fibrosis: Pleiotropic effects of modifier genes on early cystic fibrosis-related morbidities. *Hum. Genet.* **2014**, *133*, 151–161. doi:10.1007/s00439-013-1363-7.

155. Bertrand, C. A. *et al.* The CFTR trafficking mutation F508del inhibits the constitutive activity of SLC26A9. *Am. J. Physiol. - Lung Cell. Mol. Physiol.* **2017**, *312*, L12–L925. doi:10.1152/ajplung.00178.2016.

156. Pinto, M. C., Silva, I. A. L., Figueira, M. F., Amaral, M. D. & Lopes-Pacheco, M. Pharmacological Modulation of Ion Channels for the Treatment of Cystic Fibrosis. *J. Exp. Pharmacol.* **2021**, *13*, 693–723. doi:10.2147/JEP.S255377.

157. Ehrhardt, C. *et al.* Towards an in vitro model of cystic fibrosis small airway epithelium: Characterisation of the human bronchial epithelial cell line CFBE41o-. *Cell Tissue Res.* **2006**, *323*, 405–415. doi:10.1007/s00441-005-0062-7.

158. Amatngalim, G. D. *et al.* CFTR modulator response measurements in subjects with cystic fibrosis using 2D differentiated nasal epithelia converted into spheroids. *bioRxiv* **2021**, 2021.07.20.453105. doi:10.1101/2021.07.20.453105.

159. Schindelin, J. *et al.* Fiji: An open-source platform for biological-image analysis. *Nat. Methods* **2012**, *9*, 676–682. doi:10.1038/nmeth.2019.

160. Carpenter, A. E. *et al.* CellProfiler: Image analysis software for identifying and quantifying cell phenotypes. *Genome Biol.* **2006**, *7*, doi:10.1186/gb-2006-7-10-r100.

161. Klarenbeek, J., Goedhart, J., Van Batenburg, A., Groenewald, D. & Jalink, K.

Fourth-generation Epac-based FRET sensors for cAMP feature exceptional brightness, photostability and dynamic range: Characterization of dedicated sensors for FLIM, for ratiometry and with high affinity. *PLoS One* **2015**, *10*, 1–11. doi:10.1371/journal.pone.0122513.

162. Storch, U., Straub, J., Erdogmus, S., Gudermann, T. & Mederos y Schnitzler, M. Dynamic monitoring of Gi/o-protein-mediated decreases of intracellular cAMP by FRET-based Epac sensors. *Pflugers Arch. Eur. J. Physiol.* **2017**, *469*, 725–737. doi:10.1007/s00424-017-1975-1.

163. Ponsioen, B. *et al.* Detecting cAMP-induced Epac activation by fluorescence resonance energy transfer: Epac as a novel cAMP indicator. *EMBO Rep.* **2004**, *5*, 1176–1180. doi:10.1038/sj.embor.7400290.

164. Erfle, H. *et al.* Work flow for multiplexing siRNA assays by solid-phase reverse transfection in multiwell plates. *J. Biomol. Screen.* **2008**, *13*, 575–580. doi:10.1177/1087057108320133.

165. Botelho, H. M. *et al.* Protein Traffic Disorders: An Effective High-Throughput Fluorescence Microscopy Pipeline for Drug Discovery. *Sci. Rep.* **2015**, *5*, 1–8. doi:10.1038/srep09038.

166. Simpson, J. C. *et al.* Genome-wide RNAi screening identifies human proteins with a regulatory function in the early secretory pathway. *Nat. Cell Biol.* **2012**, *14*, 764–774. doi:10.1038/ncb2510.

167. Suzuki, J. *et al.* Calcium-dependent phospholipid scramblase activity of TMEM 16 protein family members. *J. Biol. Chem.* **2013**, *288*, 13305–13316. doi:10.1074/jbc.M113.457937.

168. Picollo, A., Malvezzi, M. & Accardi, A. TMEM16 proteins: unknown structure and confusing functions. *J. Mol. Biol.* **2015**, *427*, 94–105. doi:10.1016/j.jmb.2014.09.028.

169. Romanenko, V. G. *et al.* Tmem16A encodes the Ca2+-activated Cl- channel in mouse submandibular salivary gland acinar cells. *J. Biol. Chem.* **2010**, *285*, 12990–13001. doi:10.1074/jbc.M109.068544.

170. Scudieri, P. *et al.* Association of TMEM16A chloride channel overexpression with airway goblet cell metaplasia. *J. Physiol.* **2012**, *590*, 6141–6155. doi:10.1113/jphysiol.2012.240838.

171. Jung, J. *et al.* Dynamic modulation of ANO1/TMEM16A HCO3- permeability by Ca2+/calmodulin. *Proc. Natl. Acad. Sci. U. S. A.* **2013**, *110*, 360–365. doi:10.1073/pnas.1211594110.

172. Jun, I. *et al.* Pore dilatation increases the bicarbonate permeability of CFTR, ANO1 and glycine receptor anion channels. *J. Physiol.* **2016**, *594*, 2929–2955. doi:10.1113/JP271311.

173. Jin, X. *et al.* Activation of the Cl- Channel ANO1 by localized calcium signals in nociceptive sensory neurons requires coupling with the IP3 receptor. *Sci. Signal.* **2013**, *6*, 1–12. doi:10.1126/scisignal.2004184.

174. Kunzelmann, K. TMEM16, LRRC8A, bestrophin: Chloride channels controlled by Ca2+ and cell volume. *Trends Biochem. Sci.* **2015**, *40*, 535–543. doi:10.1016/j.tibs.2015.07.005.

175. Kunzelmann, K. *et al.* Modulating Ca2+ signals: a common theme for TMEM16,

Ist2, and TMC. *Pflugers Arch. Eur. J. Physiol.* **2016**, *468*, 475–490. doi:10.1007/s00424-015-1767-4.

176. Yu, K., Duran, C., Qu, Z., Cui, Y. Y. & Hartzell, H. C. Explaining calcium-dependent gating of anoctamin-1 chloride channels requires a revised topology. *Circ. Res.* **2012**, *110*, 990–999. doi:10.1161/CIRCRESAHA.112.264440.

177. Almaça, J. *et al.* High-content siRNA screen reveals global ENaC regulators and potential cystic fibrosis therapy targets. *Cell* **2013**, *154*, 1390. doi:10.1016/j.cell.2013.08.045.

178. Perez-Cornejo, P. *et al.* Anoctamin 1 (Tmem16A) Ca2+-activated chloride channel stoichiometrically interacts with an ezrin-radixin-moesin network. *Proc. Natl. Acad. Sci. U. S. A.* **2012**, *109*, 10376–10381. doi:10.1073/pnas.1200174109.

179. De La Fuente, R., Namkung, W., Mills, A. & Verkman, A. S. Small-molecule screen identifies inhibitors of a human intestinal calcium-activated chloride channel. *Mol. Pharmacol.* **2008**, *73*, 758–768. doi:10.1124/mol.107.043208.

180. Namkung, W., Yao, Z., Finkbeiner, W. E. & Verkman, A. S. Small-molecule activators of TMEM16A, a calcium-activated chloride channel, stimulate epithelial chloride secretion and intestinal contraction. *FASEB J.* **2011**, *25*, 4048–4062. doi:10.1096/fj.11-191627.

181. Seo, Y. *et al.* Inhibition of ANO1/TMEM16A chloride channel by idebenone and its cytotoxicity to cancer cell lines. *PLoS One* **2015**, *10*, 7–9. doi:10.1371/journal.pone.0133656.

182. Lee, Y. S. *et al.* Surface expression of the Anoctamin-1 (ANO1) channel is suppressed by protein-protein interactions with β-COP. *Biochem. Biophys. Res. Commun.* **2016**, *475*, 216–222. doi:10.1016/j.bbrc.2016.05.077.

183. Giordano, F. *et al.* PI(4,5)P2-Dependent and Ca2+-Regulated ER-PM interactions mediated by the extended synaptotagmins. *Cell* **2013**, *153*, 1494. doi:10.1016/j.cell.2013.05.026.

184. Manford, A. G., Stefan, C. J., Yuan, H. L., MacGurn, J. A. & Emr, S. D. ER-to-Plasma Membrane Tethering Proteins Regulate Cell Signaling and ER Morphology. *Dev. Cell* **2012**, *23*, 1129–1140. doi:10.1016/j.devcel.2012.11.004.

185. Schauder, C. M. *et al.* Structure of a lipid-bound extended synaptotagmin indicates a role in lipid transfer. *Nature* **2014**, *510*, 552–555. doi:10.1038/nature13269.

186. Amaya, M. J. *et al.* Apical localization of inositol 1,4,5-trisphosphate receptors is independent of extended synaptotagmins in hepatocytes. *PLoS One* **2014**, *9*, 1–18. doi:10.1371/journal.pone.0114043.

187. Sclip, A., Bacaj, T., Giam, L. R. & Südhof, T. C. Extended Synaptotagmin (ESyt) triple knock-out mice are viable and fertile without obvious endoplasmic reticulum dysfunction. *PLoS One* **2016**, *11*, 1–17. doi:10.1371/journal.pone.0158295.

188. Tremblay, M. G. & Moss, T. Loss of all 3 Extended Synaptotagmins does not affect normal mouse development, viability or fertility. *Cell Cycle* **2016**, *15*, 2360–2366. doi:10.1080/15384101.2016.1203494.

189. Saheki, Y. *et al.* Control of plasma membrane lipid homeostasis by the extended synaptotagmins. *Nat. Cell Biol.* **2016**, *18*, 504–515. doi:10.1038/ncb3339.

190. Gallos, G. *et al.* Functional expression of the TMEM16 family of calcium-activated

chloride channels in airway smooth muscle. *Am. J. Physiol. - Lung Cell. Mol. Physiol.* **2013**, *305*, 625–634. doi:10.1152/ajplung.00068.2013.

191. Zhang, C. H. *et al.* The transmembrane protein 16A Ca2+-activated Cl channel in airway smooth muscle contributes to airway hyperresponsiveness. *Am. J. Respir. Crit. Care Med.* **2013**, *187*, 374–381. doi:10.1164/rccm.201207-1303OC.

192. Li, H. *et al.* Increased TMEM16A Involved in Alveolar Fluid Clearance After Lipopolysaccharide Stimulation. *Inflammation* **2016**, *39*, 881–890. doi:10.1007/s10753-016-0320-8.

193. Litchfield, D. W. Protein kinase CK2: Structure, regulation and role in cellular decisions of life and death. *Biochem. J.* **2003**, *369*, 1–15. doi:10.1042/BJ20021469.

194. Borgo, C. & Ruzzene, M. Role of protein kinase CK2 in antitumor drug resistance. *J. Exp. Clin. Cancer Res.* **2019**, *38*, doi:10.1186/s13046-019-1292-y.

195. Trembley, J. H., Wang, G., Unger, G., Slaton, J. & Ahmed, K. Protein kinase CK2 in health and disease: CK2: a key player in cancer biology. *Cell. Mol. Life Sci.* **2009**, *66*, 1858–67. doi:10.1007/s00018-009-9154-y.

196. Ruzzene, M., Penzo, D. & Pinna, L. A. Protein kinase CK2 inhibitor 4,5,6,7-tetrabromobenzotriazole (TBB) induces apoptosis and caspase-dependent degradation of haematopoietic lineage cell-specific protein 1 (HS1) in Jurkat cells. *Biochem. J.* **2002**, *364*, 41–47. doi:10.1042/bj3640041.

197. Siddiqui-Jain, A. *et al.* CX-4945, an orally bioavailable selective inhibitor of protein kinase CK2, inhibits prosurvival and angiogenic signaling and exhibits antitumor efficacy. *Cancer Res.* **2010**, *70*, 10288–10298. doi:10.1158/0008-5472.CAN-10-1893.

198. Zheng, Y. *et al.* Targeting protein kinase CK2 suppresses prosurvival signaling pathways and growth of glioblastoma. *Clin. Cancer Res.* **2013**, *19*, 6484–6494. doi:10.1158/1078-0432.CCR-13-0265.

199. Almaça, J. *et al.* TMEM16 proteins produce volume-regulated chloride currents that are reduced in mice lacking TMEM16A. *J. Biol. Chem.* **2009**, *284*, 28571–28578. doi:10.1074/jbc.M109.010074.

200. Ayoub, C. *et al.* ANO1 amplification and expression in HNSCC with a high propensity for future distant metastasis and its functions in HNSCC cell lines. *Br. J. Cancer* **2010**, *103*, 715–726. doi:10.1038/sj.bjc.6605823.

201. Stanich, J. E. *et al.* Ano1 as a regulator of proliferation. *Am. J. Physiol. - Gastrointest. Liver Physiol.* **2011**, *301*, 1044–1051. doi:10.1152/ajpgi.00196.2011.

202. Wang, M. *et al.* Downregulation of TMEM16A calcium-activated chloride channel contributes to cerebrovascular remodeling during hypertension by promoting basilar smooth muscle cell proliferation. *Circulation* **2012**, *125*, 697–707. doi:10.1161/CIRCULATIONAHA.111.041806.

203. Ruiz, C. *et al.* Enhanced expression of ANO1 in head and neck squamous cell carcinoma causes cell migration and correlates with poor prognosis. *PLoS One* **2012**, *7*, doi:10.1371/journal.pone.0043265.

204. Mazzone, A. *et al.* Inhibition of Cell Proliferation by a Selective Inhibitor of the Ca2+-activated Cl− Channel, Ano1. *Biochem. Biophys. Res. Commun.* **2012**, *427*,

248–253. doi:10.1016/j.bbrc.2012.09.022.

205. Buchholz, B. *et al.* Anoctamin 1 induces calcium-activated chloride secretion and proliferation of renal cyst-forming epithelial cells. *Kidney Int.* **2014**, *85*, 1058–1067. doi:10.1038/ki.2013.418.

206. Guan, L., Song, Y., Gao, J., Gao, J. & Wang, K. W. Inhibition of calcium-activated chloride channel ANO1 suppresses proliferation and induces apoptosis of epithelium originated cancer cells. *Oncotarget* **2016**, *7*, 78619–78630. doi:10.18632/oncotarget.12524.

207. Allawzi, A. M. *et al.* Activation of anoctamin-1 limits pulmonary endothelial cell proliferation via p38–Mitogen-activated protein Kinase–dependent apoptosis. *Am. J. Respir. Cell Mol. Biol.* **2018**, *58*, 658–667. doi:10.1165/rcmb.2016-0344OC.

208. Wang, A. M. *et al.* The autonomous notch signal pathway is activated by baicalin and baicalein but is suppressed by niclosamide in K562 cells. *J. Cell. Biochem.* **2009**, *106*, 682–692. doi:10.1002/jcb.22065.

209. Meurette, O. & Mehlen, P. Notch Signaling in the Tumor Microenvironment. *Cancer Cell* **2018**, *34*, 536–548. doi:10.1016/j.ccell.2018.07.009.

210. Kim, S.-Y. *et al.* Role of the IL-6-JAK1-STAT3-Oct-4 pathway in the conversion of non-stem cancer cells into cancer stem-like cells. *Cell Signal.* **2013**, *25*, 961–969. doi:10.1016/j.cellsig.2013.01.007.

211. Jin, Y. *et al.* Antineoplastic mechanisms of niclosamide in acute myelogenous leukemia stem cells: Inactivation of the NF-κB pathway and generation of reactive oxygen species. *Cancer Res.* **2010**, *70*, 2516–2527. doi:10.1158/0008-5472.CAN-09-3950.

212. Ren, X. *et al.* Identification of niclosamide as a new small-molecule inhibitor of the STAT3 signaling pathway. *ACS Med. Chem. Lett.* **2010**, *1*, 454–459. doi:10.1021/ml100146z.

213. Osada, T. *et al.* Anti-helminth compound niclosamide downregulates Wnt Signaling and elicits antitumor responses in tumors with activating APC mutations. *Cancer Res.* **2011**, *71*, 4172–4182. doi:10.1158/0008-5472.CAN-10-3978.

214. Wang, L. H., Xu, M., Fu, L. Q., Chen, X. Y. & Yang, F. The Antihelminthic Niclosamide Inhibits Cancer Stemness, Extracellular Matrix Remodeling, and Metastasis through Dysregulation of the Nuclear β-catenin/c-Myc axis in OSCC. *Sci. Rep.* **2018**, *8*, 1–13. doi:10.1038/s41598-018-30692-3.

215. Arend, R. C. *et al.* Niclosamide and its analogs are potent inhibitors of Wnt/ß-catenin, mTOR and STAT3 signaling in ovarian cancer. *Oncotarget* **2016**, *7*, 86803–86815. doi:10.18632/oncotarget.13466.

216. Ahn, S. Y. *et al.* Anti-helminthic niclosamide inhibits Ras-driven oncogenic transformation via activation of GSK-3. *Oncotarget* **2017**, *8*, 31856–31863. doi:10.18632/oncotarget.16255.

217. Chen, B. *et al.* Computational Discovery of Niclosamide Ethanolamine, A Repurposed Drug Candidate That Reduces Growth of Hepatocellular Carcinoma Cells in Vitro and in Mice by Inhibiting CDC37 Signaling. *Gastroenterology* **2017**, *152*, 2022–2036. doi:10.1053/j.gastro.2017.02.039.

218. Li, Y. *et al.* Multi-targeted therapy of cancer by niclosamide: a new application for an old drug. *Cancer Lett* **2014**, *349*, 8–14. doi:10.1016/j.canlet.2014.04.003.

219. Han, Z. *et al.* Niclosamide induces cell cycle arrest in G1 phase in head and neck squamous cell carcinoma through let-7d/Cdc34 axis. *Front. Pharmacol.* **2019**, *9*, 1–12. doi:10.3389/fphar.2018.01544.

220. Wang, Y. *et al.* Suppression of the growth and invasion of human head and neck squamous cell carcinomas via regulating STAT3 signaling and the miR-21/β-catenin axis with HJC0152. *Mol. Cancer Ther.* **2017**, *16*, 578–590. doi:10.1158/1535-7163.MCT-16-0606.

221. Liu, C. *et al.* Niclosamide inhibits androgen receptor variants expression and overcomes enzalutamide resistance in castration resistant prostate cancer. *Clin. Cancer Res.* **2014**, *20*, 3198–3210. doi:10.1158/1078-0432.CCR-13-3296.

222. Wieland, A. *et al.* Anticancer effects of niclosamide in human glioblastoma. *Clin. Cancer Res.* **2013**, *19*, 4124–4136. doi:10.1158/1078-0432.CCR-12-2895.

223. Schweizer, M. T. *et al.* A phase I study of niclosamide in combination with enzalutamide in men with castration- resistant prostate cancer. *PLoS One* **2018**, *13*, doi:10.1371/journal.pone.0198389.

224. Burock, S. *et al.* Phase II trial to investigate the safety and efficacy of orally applied niclosamide in patients with metachronous or sychronous metastases of a colorectal cancer progressing after therapy: The NIKOLO trial. *BMC Cancer* **2018**, *18*, 1–7. doi:10.1186/s12885-018-4197-9.

225. Kunzelmann, K., Ousingsawat, J., Benedetto, R., Cabrita, I. & Schreiber, R. Contribution of anoctamins to cell survival and cell death. *Cancers (Basel).* **2019**, *11*, 1–24. doi:10.3390/cancers11030382.

226. Lérias, J. R. *et al.* A novel microscopy-based assay identifies extended synaptotagmin-1 (ESYT1) as a positive regulator of anoctamin 1 traffic. *Biochim. Biophys. Acta - Mol. Cell Res.* **2018**, *1865*, 421–431. doi:10.1016/j.bbamcr.2017.11.009.

227. Yu, M., Yeh, J. & Van Waes, C. Protein kinase casein kinase 2 mediates inhibitor-κB kinase and aberrant nuclear factor-κB activation by serum factor(s) in head and neck squamous carcinoma cells. *Cancer Res.* **2006**, *66*, 6722–6731. doi:10.1158/0008-5472.CAN-05-3758.

228. Schreiber, R. *et al.* Regulation of TMEM16A/ANO1 and TMEM16F/ANO6 ion currents and phospholipid scrambling by Ca 2+ and plasma membrane lipid. *J. Physiol.* **2018**, *596*, 217–229. doi:10.1113/JP275175.

229. Cabrita, I. *et al.* Differential effects of anoctamins on intracellular calcium signals. *FASEB J.* **2017**, *31*, 2123–2134. doi:10.1096/fj.201600797RR.

230. Treharne, K. J. *et al.* Inhibition of protein kinase CK2 closes the CFTR Cl channel, but has no effect on the cystic fibrosis mutant Δf508-CFTR. *Cell. Physiol. Biochem.* **2009**, *24*, 347–360. doi:10.1159/000257427.

231. Pagano, M. A. *et al.* Modulation of protein kinase CK2 activity by fragments of CFTR encompassing F508 may reflect functional links with cystic fibrosis pathogenesis. *Biochemistry* **2008**, *47*, 7925–7936. doi:10.1021/bi800316z.

232. Tosoni, K. *et al.* CFTR mutations altering CFTR fragmentation. *Biochem. J.* **2013**, *449*, 295–305. doi:10.1042/BJ20121240.

233. Kunzelmann, K. & Mehta, A. CFTR: A hub for kinases and crosstalk of cAMP and Ca2+. *FEBS J.* **2013**, *280*, 4417–4429. doi:10.1111/febs.12457.

234. Bachhuber, T. *et al.* Regulation of the epithelial Na+ channel by the protein kinase CK2. *J. Biol. Chem.* **2008**, *283*, 13225–13232. doi:10.1074/jbc.M704532200.

235. Berman, J. M., Mironova, E. & Stockand, J. D. Physiological regulation of the epithelial Na + channel by casein kinase II. *Am. J. Physiol. - Ren. Physiol.* **2018**, *314*, F367–F372. doi:10.1152/ajprenal.00469.2017.

236. Tian, Y. *et al.* Calmodulin-dependent activation of the epithelial calcium-dependent chloride channel TMEM16A. *FASEB J.* **2011**, *25*, 1058–1068. doi:10.1096/fj.10-166884.

237. Kunzelmann, K. *et al.* Bestrophin and TMEM16-Ca2+ activated Cl- channels with different functions. *Cell Calcium* **2009**, *46*, 233–241. doi:10.1016/j.ceca.2009.09.003.

238. Adelman, J. P., Maylie, J. & Sah, P. Small-conductance Ca 2+-activated K + channels: Form and function. *Annu. Rev. Physiol.* **2012**, *74*, 245–269. doi:10.1146/annurev-physiol-020911-153336.

239. Ibrahim, S. H. *et al.* CK2 is a key regulator of SLC4A2-mediated Cl−/HCO3− exchange in human airway epithelia. *Pflugers Arch. Eur. J. Physiol.* **2017**, *469*, 1073–1091. doi:10.1007/s00424-017-1981-3.

240. Luz, S. *et al.* Contribution of Casein Kinase 2 and Spleen Tyrosine Kinase to CFTR Trafficking and Protein Kinase A-Induced Activity. *Mol. Cell. Biol.* **2011**, *31*, 4392–4404. doi:10.1128/mcb.05517-11.

241. Koreishi, M., Yu, S., Oda, M., Honjo, Y. & Satoh, A. CK2 Phosphorylates Sec31 and Regulates ER-To-Golgi Trafficking. *PLoS One* **2013**, *8*, 1–9. doi:10.1371/journal.pone.0054382.

242. Gerst, J. E. SNAREs and SNARE regulators in membrane fusion and exocytosis. *Cell. Mol. Life Sci.* **1999**, *55*, 707–734. doi:10.1007/s000180050328.

243. Mazzone, A. *et al.* Identification and characterization of a novel promoter for the human ANO1 gene regulated by the transcription factor signal transducer and activator of transcription 6 (STAT6). *FASEB J.* **2015**, *29*, 152–163. doi:10.1096/fj.14-258541.

244. Chen, Y. *et al.* Casein Kinase 2 Interacting Protein-1 regulates M1 and M2 inflammatory macrophage polarization. *Cell. Signal.* **2017**, *33*, 107–121. doi:10.1016/j.cellsig.2017.02.015.

245. Lee, M. C., Chen, Y. K., Hsu, Y. J. & Lin, B. R. Niclosamide inhibits the cell proliferation and enhances the responsiveness of esophageal cancer cells to chemotherapeutic agents. *Oncol. Rep.* **2020**, *43*, 549–561. doi:10.3892/or.2019.7449.

246. Bill, A. *et al.* Small molecule-facilitated degradation of ANO1 protein: A new targeting approach for anticancer therapeutics. *J. Biol. Chem.* **2014**, *289*, 11029–11041. doi:10.1074/jbc.M114.549188.

247. *ECFS Patient Registry Annual Data Report 2018*.

248. Gentzsch, M. & Mall, M. A. Ion Channel Modulators in Cystic Fibrosis. *Chest* **2018**, *154*, 383–393. doi:10.1016/j.chest.2018.04.036.

249. Mall, M. A., Mayer-Hamblett, N. & Rowe, S. M. Cystic fibrosis: Emergence of highly effective targeted therapeutics and potential clinical implications. *Am. J. Respir. Crit. Care Med.* **2020**, *201*, 1193–1208. doi:10.1164/rccm.201910-

1943SO.

250. Danahay, H. *et al.* Potentiating TMEM16A does not stimulate airway mucus secretion or bronchial and pulmonary arterial smooth muscle contraction. *FASEB BioAdvances* **2020**, *2*, 464–477. doi:10.1096/fba.2020-00035.

251. Lérias, J. *et al.* Compartmentalized crosstalk of CFTR and TMEM16A (ANO1) through EPAC1 and ADCY1. *Cell. Signal.* **2018**, *44*, 10–19. doi:10.1016/j.cellsig.2018.01.008.

252. Ashburner, M. *et al.* Gene Ontology: tool for the unification of biology. *Nat. Genet.* **2000**, *25*, 25–29.

253. Carbon, S. *et al.* The Gene Ontology Resource: 20 years and still GOing strong. *Nucleic Acids Res.* **2019**, *47*, D330–D338. doi:10.1093/nar/gky1055.

254. Civantos Calzada, B. & Aleixandre De Artiñano, A. Alpha-adrenoceptor subtypes. *Pharmacol. Res.* **2001**, *44*, 195–208. doi:10.1006/phrs.2001.0857.

255. Rossi, D. & Zlotnik, A. The Biology of Chemokines and Their Receptors. *Annu. Rev. Immunol.* **2000**, *18*, 217–242. doi:10.1146/annurev.immunol.18.1.217.

256. Hepler, J. R. & Gilman, A. G. G-proteins. *Trends Biochem. Sci.* **1992**, *17*, 383–387. doi:10.1016/0968-0004(92)90005-T.

257. Carbonetti, N. H. Pertussis toxin and adenylate cyclase toxin: key virulence factors of Bordetella pertussis and cell biology tools. *Futur. Microbiol.* **2010**, 455–469. doi:10.2217/fmb.09.133.

258. Boucrot, E., Saffarian, S., Zhang, R. & Kirchhausen, T. Roles of AP-2 in clathrin-mediated endocytosis. *PLoS One* **2010**, *5*, doi:10.1371/journal.pone.0010597.

259. Pinto, M. C. *et al.* Regulation of TMEM16A by CK2 and Its Role in Cellular Proliferation. *Cells* **2020**, *9*, doi:10.3390/cells9051138.

260. Benedetto, R. *et al.* Plasma membrane–localized TMEM16 proteins are indispensable for expression of CFTR. *J. Mol. Med.* **2019**, doi:10.1007/s00109-019-01770-4.

261. Neumann, B. *et al.* Phenotypic profiling of the human genome by time-lapse microscopy reveals cell division genes. *Nature* **2010**, *464*, 721–727. doi:10.1038/nature08869.

262. Dibner, M. D. & Insel, P. A. Serum catecholamines desensitize β-adrenergic receptors of cultured C6 glioma cells. *J. Biol. Chem.* **1981**, *256*, 7343–7346. doi:10.1016/s0021-9258(19)68968-4.

263. Dorn, G. W., Oswald, K. J., McCluskey, T. S., Kuhel, D. G. & Liggett, S. B. α(2A)-Adrenergic receptor stimulated calcium release is transduced by G(i)-associated G(βγ)-mediated activation of phospholipase C. *Biochemistry* **1997**, *36*, 6415–6423. doi:10.1021/bi970080s.

264. Smit, M. J. *et al.* CXCR3-mediated chemotaxis of human T cells is regulated by a G i-and phospholipase C-dependent pathway and not via activation of MEK/p44/p42 MAPK nor Akt/PI-3 kinase. *Blood* **2003**, *102*, 1959–1965. doi:10.1182/blood-2002-12-3945.

265. Cuíñas, A., García-Morales, V., Viña, D., Gil-Longo, J. & Campos-Toimil, M. Activation of PKA and Epac proteins by cyclic AMP depletes intracellular calcium stores and reduces calcium availability for vasoconstriction. *Life Sci.* **2016**, *155*,

102–109. doi:10.1016/j.lfs.2016.03.059.

266. Ferguson, S. S. G. *et al.* Role of β-arrestin in mediating agonist-promoted G protein-coupled receptor internalization. *Science (80-.).* **1996**, *271*, 363–366. doi:10.1126/science.271.5247.363.

267. Zhang, J., Barak, L. S., Winkler, K. E., Caron, M. G. & Ferguson, S. S. G. A central role for β-arrestins and clathrin-coated vesicle-mediated endocytosis in β2-adrenergic receptor resensitization. Differential regulation of receptor resensitization in two distinct cell types. *J. Biol. Chem.* **1997**, *272*, 27005–27014. doi:10.1074/jbc.272.43.27005.

268. Olli-Lähdesmäki, T., Scheinin, M., Pohjanoksa, K. & Kallio, J. Agonist-dependent trafficking of α2-adrenoceptor subtypes: Dependence on receptor subtype and employed agonist. *Eur. J. Cell Biol.* **2003**, *82*, 231–239. doi:10.1078/0171-9335-00311.

269. Meiser, A. *et al.* The Chemokine Receptor CXCR3 Is Degraded following Internalization and Is Replenished at the Cell Surface by De Novo Synthesis of Receptor. *J. Immunol.* **2008**, *180*, 6713–6724. doi:10.4049/jimmunol.180.10.6713.

270. Ameen, N., Silvis, M. & Bradbury, N. A. Endocytic Trafficking of CFTR in Health and Disease. *J. Cyst. Fibros.* **2007**, *6*, 1–14.

271. Pley, U., Parham, P. & Brodsky, F. M. Clathrin: Its role in receptor-mediated vesicular transport and specialized functions in neurons. *Crit. Rev. Biochem. Mol. Biol.* **1993**, *28*, 431–464. doi:10.3109/10409239309078441.

272. Lau, A. W. & Chou, M. M. The adaptor complex AP-2 regulates post-endocytic trafficking through the non-clathrin Arf6-dependent endocytic pathway. *J. Cell Sci.* **2008**, *121*, 4008–4017. doi:10.1242/jcs.033522.

273. Kunzelmann, K. *et al.* Expression and function of epithelial anoctamins. *Exp. Physiol.* **2012**, *97*, 184–192. doi:10.1113/expphysiol.2011.058206.

274. Faria, D., Schreiber, R. & Kunzelmann, K. CFTR is activated through stimulation of purinergic P2Y2 receptors. *Pflugers Arch. Eur. J. Physiol.* **2009**, *457*, 1373–1380. doi:10.1007/s00424-008-0606-2.

275. Namkung, W., Finkbeiner, W. E. & Verkman, A. S. CFTR-Adenylyl Cyclase I Association Responsible for UTP Activation of CFTR in Well-Differentiated Primary Human Bronchial Cell Cultures. *Mol. Biol. Cell* **2010**, *21*, 2639–2648. doi:10.1091/mbc.E09–12–1004.

276. Billet, A., Luo, Y., Balghi, H. & Hanrahan, J. W. Role of tyrosine phosphorylation in the muscarinic activation of the cystic fibrosis transmembrane conductance regulator (CFTR). *J. Biol. Chem.* **2013**, *288*, 21815–21823. doi:10.1074/jbc.M113.479360.

277. Broadbent, D. *et al. Roles of NHERF Family of PDZ-Binding Proteins in Regulating GPCR Functions*. *Advances in Immunology* (Elsevier Inc., 2017). vol. 136 doi:10.1016/bs.ai.2017.05.008.

278. Lobo, M. J., Amaral, M. D., Zaccolo, M. & Farinha, C. M. EPAC1 activation by cAMP stabilizes CFTR at the membrane by promoting its interaction with NHERF1. *J. Cell Sci.* **2016**, *129*, 2599–2612. doi:10.1242/jcs.185629.

279. Ostrom, R. S. & Insel, P. A. The evolving role of lipid rafts and caveolae in G

protein-coupled receptor signaling: Implications for molecular pharmacology. *Br. J. Pharmacol.* **2004**, *143*, 235–245. doi:10.1038/sj.bjp.0705930.

280. Kowalski, M. P. & Pier, G. B. Localization of Cystic Fibrosis Transmembrane Conductance Regulator to Lipid Rafts of Epithelial Cells Is Required for Pseudomonas aeruginosa -Induced Cellular Activation. *J. Immunol.* **2004**, *172*, 418–425. doi:10.4049/jimmunol.172.1.418.

281. Hoque, K. M. *et al.* Epac1 mediates protein kinase A-independent mechanism of forskolinactivated intestinal chloride secretion. *J. Gen. Physiol.* **2010**, *135*, 43–58. doi:10.1085/jgp.200910339.

282. Domingue, J. C., Ao, M., Sarathy, J. & Rao, M. C. Chenodeoxycholic acid requires activation of EGFR, EPAC, and Ca2+ to stimulate CFTR-dependent Cl- secretion in human colonic T84 cells. *Am. J. Physiol. - Cell Physiol.* **2016**, *311*, C777–C792. doi:10.1152/ajpcell.00168.2016.

283. Nascimbeni, A. C. *et al.* ER–plasma membrane contact sites contribute to autophagosome biogenesis by regulation of local PI 3P synthesis. *EMBO J.* **2017**, *36*, 2018–2033. doi:10.15252/embj.201797006.

284. Maléth, J., Choi, S., Muallem, S. & Ahuja, M. Translocation between PI(4,5)P 2 -poor and PI(4,5)P 2 -rich microdomains during store depletion determines STIM1 conformation and Orai1 gating. *Nat. Commun.* **2014**, *5*, 1–10. doi:10.1038/ncomms6843.

285. Fallah, G. *et al.* TMEM16A(a)/anoctamin-1 shares a homodimeric architecture with CLC chloride channels. *Mol. Cell. Proteomics* **2011**, *10*, 1–11. doi:10.1074/mcp.M110.004697.

286. Greger, R. *et al.* Cystic fibrosis and CFTR. *Pflugers Arch. Eur. J. Physiol.* **2001**, *443*, 3–7. doi:10.1007/s004240100635.

287. Schreiber, R. *et al.* Anoctamins support calcium-dependent chloride secretion by facilitating calcium signaling in adult mouse intestine. *Pflugers Arch. Eur. J. Physiol.* **2015**, *467*, 1203–1213. doi:10.1007/s00424-014-1559-2.

288. Kmit, A. *et al.* Calcium-activated and apoptotic phospholipid scrambling induced by Ano6 can occur independently of Ano6 ion currents. *Cell Death Dis.* **2013**, *4*, 1–8. doi:10.1038/cddis.2013.135.

289. Son, M. *et al.* Apical and Basolateral ATP-Induced Anion Secretion in Polarized Human Airway Epithelia. *Am. J. Respir. Cell Mol. Biol.* **2004**, *30*, 411–419. doi:10.1165/rcmb.2003-0183OC.

290. Ousingsawat, J. *et al.* Anoctamin 6 mediates effects essential for innate immunity downstream of P2X7 receptors in macrophages. *Nat. Commun.* **2015**, *6*, 1–10. doi:10.1038/ncomms7245.

291. Ousingsawat, J. *et al.* Anoctamin-6 controls bone mineralization by activating the calcium transporter NCX1. *J. Biol. Chem.* **2015**, *290*, 6270–6280. doi:10.1074/jbc.M114.602979.

292. Ousingsawat, J. *et al.* Ca2+ signals, cell membrane disintegration, and activation of TMEM16F during necroptosis. *Cell. Mol. Life Sci.* **2017**, *74*, 173–181. doi:10.1007/s00018-016-2338-3.

293. Ammar, M. R., Kassas, N., Chasserot-Golaz, S., Bader, M. F. & Vitale, N. Lipids in regulated exocytosis: What are they doing? *Front. Endocrinol. (Lausanne).*

2013, *4*, 1–6. doi:10.3389/fendo.2013.00125.

294. Ory, S. *et al.* Phospholipid scramblase-1-induced lipid reorganization regulates compensatory endocytosis in neuroendocrine cells. *J. Neurosci.* **2013**, *33*, 3545–3556. doi:10.1523/JNEUROSCI.3654-12.2013.

295. Yeung, T. *et al.* Membrane phosphatidylserine regulates surface charge and protein localization. *Science (80-.).* **2008**, *319*, 210–213. doi:10.1126/science.1152066.

296. Chernomordik, L. V. & Kozlov, M. M. Membrane hemifusion: Crossing a chasm in two leaps. *Cell* **2005**, *123*, 375–382. doi:10.1016/j.cell.2005.10.015.

297. He, M. *et al.* Cytoplasmic Cl- couples membrane remodeling to epithelial morphogenesis. *Proc. Natl. Acad. Sci. U. S. A.* **2017**, *114*, E11161–E11169. doi:10.1073/pnas.1714448115.

298. Henkel, B. *et al.* Co-expression of anoctamins in cilia of olfactory sensory neurons. *Chem. Senses* **2015**, *40*, 73–87. doi:10.1093/chemse/bju061.

299. Bricogne, C. *et al.* TMEM16F activation by Ca2+ triggers plasma membrane expansion and directs PD-1 trafficking. *Sci. Rep.* **2019**, *9*, 1–13. doi:10.1038/s41598-018-37056-x.

300. Kmit, A. *et al.* Extent of rescue of F508del-CFTR function by VX-809 and VX-770 in human nasal epithelial cells correlates with SNP rs7512462 in SLC26A9 gene in F508del/F508del Cystic Fibrosis patients. *Biochim. Biophys. Acta - Mol. Basis Dis.* **2019**, *1865*, 1323–1331. doi:10.1016/j.bbadis.2019.01.029.

301. Ousingsawat, J., Schreiber, R. & Kunzelmann, K. Differential contribution of SLC26A9 to Cl - conductance in polarized and non-polarized epithelial cells. *J. Cell. Physiol.* **2012**, *227*, 2323–2329. doi:10.1002/jcp.22967.

302. Avella, M., Loriol, C., Boulukos, K., Borgese, F. & Ehrenfeld, J. SLC26A9 stimulates CFTR expression and function in human bronchial cell lines. *J. Cell. Physiol.* **2011**, *226*, 212–223. doi:10.1002/jcp.22328.

303. Ruan, Y. C. *et al.* CFTR interacts with ZO-1 to regulate tight junction assembly and epithelial differentiation through the ZONAB pathway. *J. Cell Sci.* **2014**, *127*, 4396–4408. doi:10.1242/jcs.148098.

304. De Lisle, R. C. Disrupted tight junctions in the small intestine of cystic fibrosis mice. *Cell Tissue Res.* **2014**, *355*, 131–142. doi:10.1007/s00441-013-1734-3.

305. Laselva, O. *et al.* Emerging preclinical modulators developed for F508del-CFTR have the potential to be effective for ORKAMBI resistant processing mutants. *J. Cyst. Fibros.* **2021**, *20*, 106–119. doi:10.1016/j.jcf.2020.07.015.

306. Quaresma, M. C. *et al.* Mutant CFTR Drives TWIST1 mediated epithelial–mesenchymal transition. *Cell Death Dis.* **2020**, *11*, doi:10.1038/s41419-020-03119-z.

307. LeSimple, P., Liao, J., Robert, R., Gruenert, D. C. & Hanrahan, J. W. Cystic fibrosis transmembrane conductance regulator trafficking modulates the barrier function of airway epithelial cell monolayers. *J. Physiol.* **2010**, *588*, 1195–1209. doi:10.1113/jphysiol.2009.182246.

308. Laselva, O. *et al.* Rescue of multiple class II CFTR mutations by elexacaftor+tezacaftor+ ivacaftor mediated in part by the dual activities of elexacaftor as both corrector and potentiator. *Eur. Respir. J.* **2021**, *57*,

doi:10.1183/13993003.02774-2020.

309. Bakouh, N. *et al.* Characterization of SLC26A9 in patients with CF-like lung disease. *Hum. Mutat.* **2013**, *34*, 1404–1414. doi:10.1002/humu.22382.

310. Castellani, C. *et al.* ECFS best practice guidelines: the 2018 revision. *J. Cyst. Fibros.* **2018**, *17*, 153–178. doi:10.1016/j.jcf.2018.02.006.

311. Bell, S. C. *et al.* The future of cystic fibrosis care: a global perspective. *Lancet Respir. Med.* **2020**, *8*, 65–124. doi:10.1016/S2213-2600(19)30337-6.

312. Szklarczyk, D. *et al.* STRING v11: Protein-protein association networks with increased coverage, supporting functional discovery in genome-wide experimental datasets. *Nucleic Acids Res.* **2019**, *47*, D607–D613. doi:10.1093/nar/gky1131.

313. Lopes-Pacheco, M. CFTR Modulators: The Changing Face of Cystic Fibrosis in the Era of Precision Medicine. *Front. Pharmacol.* **2020**, *10*, 1662. doi:10.3389/fphar.2019.01662.

314. Lopes-Pacheco, M., Pedemonte, N. & Veit, G. Discovery of CFTR modulators for the treatment of cystic fibrosis. *Expert Opin. Drug Discov.* **2021**, 1–17. doi:10.1080/17460441.2021.1912732.

315. Malik, A. U. *et al.* Deciphering the LRRK code: LRRK1 and LRRK2 phosphorylate distinct Rab proteins and are regulated by diverse mechanisms. *Biochem. J.* **2021**, *478*, 553–578. doi:10.1042/BCJ20200937.

316. Zimprich, A. *et al.* Mutations in LRRK2 cause autosomal-dominant parkinsonism with pleomorphic pathology. *Neuron* **2004**, *44*, 601–607. doi:10.1016/j.neuron.2004.11.005.

317. Taymans, J. M. & Cookson, M. R. Mechanisms in dominant parkinsonism: The toxic triangle of LRRK2, α-synuclein, and tau. *BioEssays* **2010**, *32*, 227–235. doi:10.1002/bies.200900163.

318. Wojewska, D. N. & Kortholt, A. Lrrk2 targeting strategies as potential treatment of parkinson's disease. *Biomolecules* **2021**, *11*, doi:10.3390/biom11081101.

319. Sejwal, K. *et al.* Cryo-EM analysis of homodimeric full-length LRRK2 and LRRK1 protein complexes. *Sci. Rep.* **2017**, *7*, 1–12. doi:10.1038/s41598-017-09126-z.

VI. Appendices

Appendix 1 – Supplementary data of Chapter 1

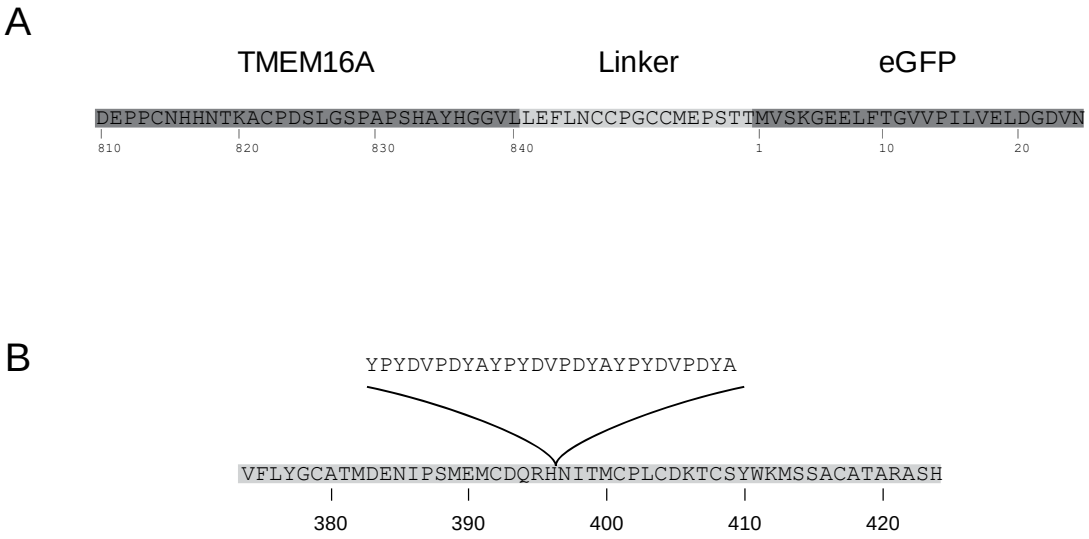

Figure S 1 – The 3HA-TMEM16A-eGFP traffic reporter construct. (A) Amino acid sequence showing the linker (light grey shadow) connecting eGFP and TMEM16A (dark grey shadows). **(B)** TMEM16A amino acid sequences showing the insertion of the 3HA peptide between His^{396} and Asn^{397}. The numbering corresponds to TMEM16A isoform X5 (NCBI Reference Sequence: XP_011543427.1). Data in collaboration with Hugo Botelho.

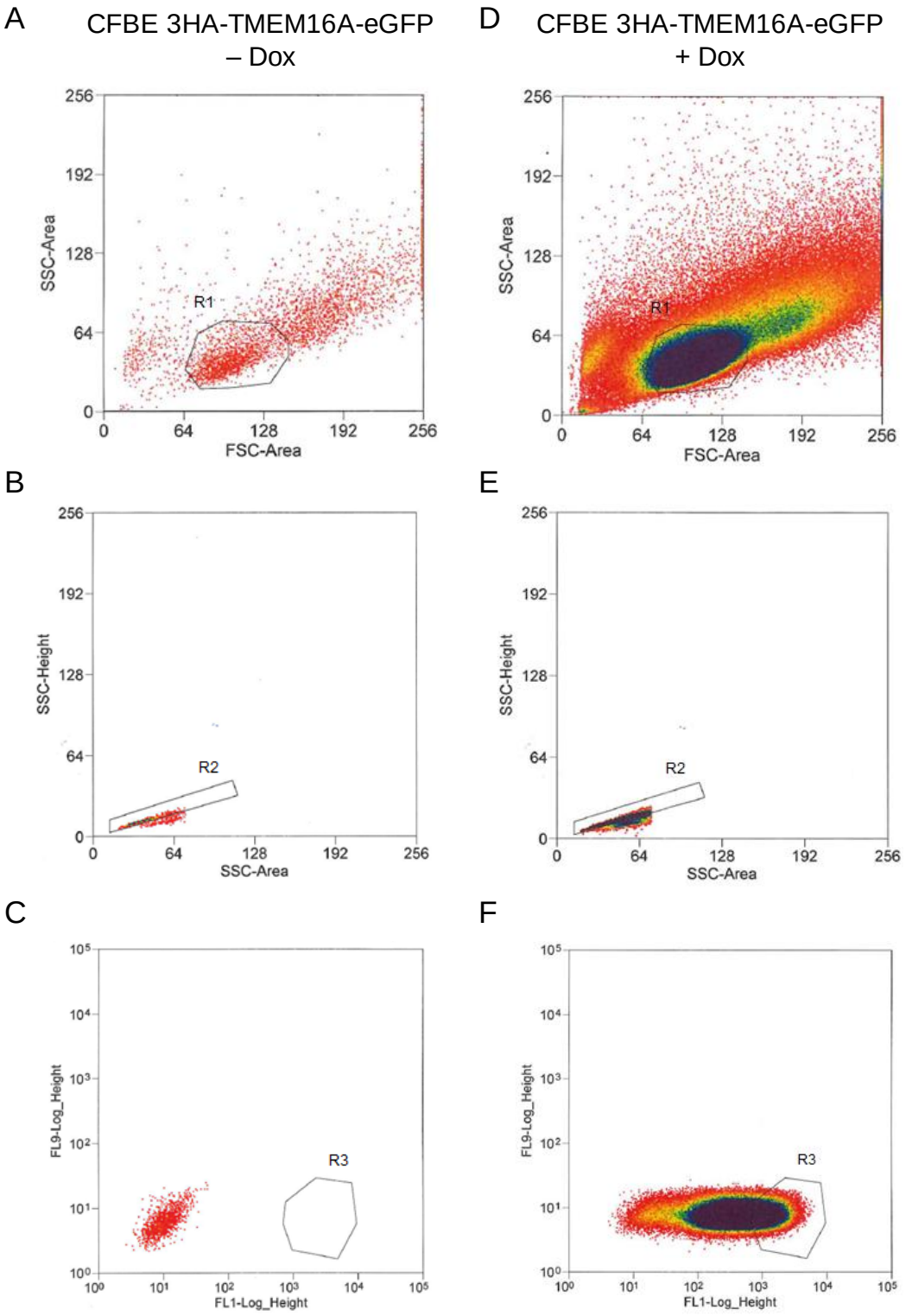

Figure S 2 – Fluorescence-activated cell sorting (FACS) of CFBE 3HA-TMEM16A-eGFP cells. CFBE cells induced with Dox to express the 3HA-TMEM16A-eGFP construct (D-F) were sorted by FACS using non-induced cells (-Dox) (A-C) as controls to set the gating parameters. Among the induced cells only the ones with the highest TMEM16A expression (GFP fluorescence) were selected. **(A,D)** Selection of relevant and living cells in region R1 by the area of the side scatter (SSC-Area) and the area of the forward scatter (FSC-Area). **(B,E)** Discrimination of single cells from aggregates in region R2 by SSC-Height and SSC-Area. **(F)** Selection of GFP-positive cells with the highest GFP fluorescence, using **(C)** as a control (auto-fluorescence of non-induced cells). Experiments were performed using a BC MoFlo Cell Sorter. Scale in arbitrary units provided by the instrument.

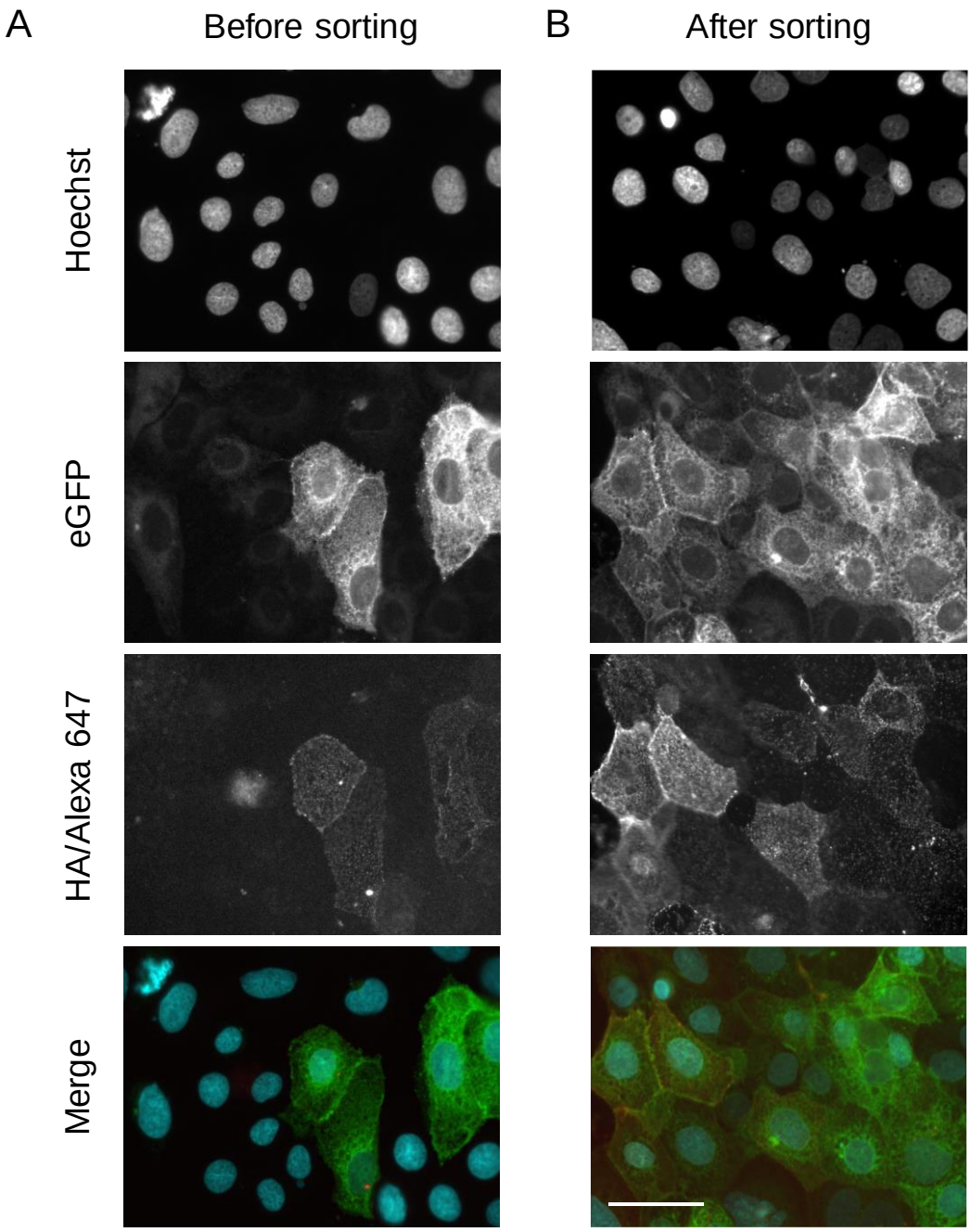

Figure S 3 – Effect of cell sorting on the expression of the 3HA-TMEM16A-eGFP construct in CFBE cells. CFBE cells were induced with Dox to express the 3HA-TMEM16A-eGFP construct and stained with anti-HA Ab (see Methods) before **(A)** and after **(B)** sorting. Images show that after sorting the cell population is more homogeneous and expresses a higher amount of TMEM16A (measured through its GFP fluorescence). Images were acquired in Olympus Scan^R microscope (objective: 20x dry, NA 0.7; exposure times: Hoechst: 50 ms, GFP: 350 ms, Cy5: 750 ms). Scale bar=50 µm.

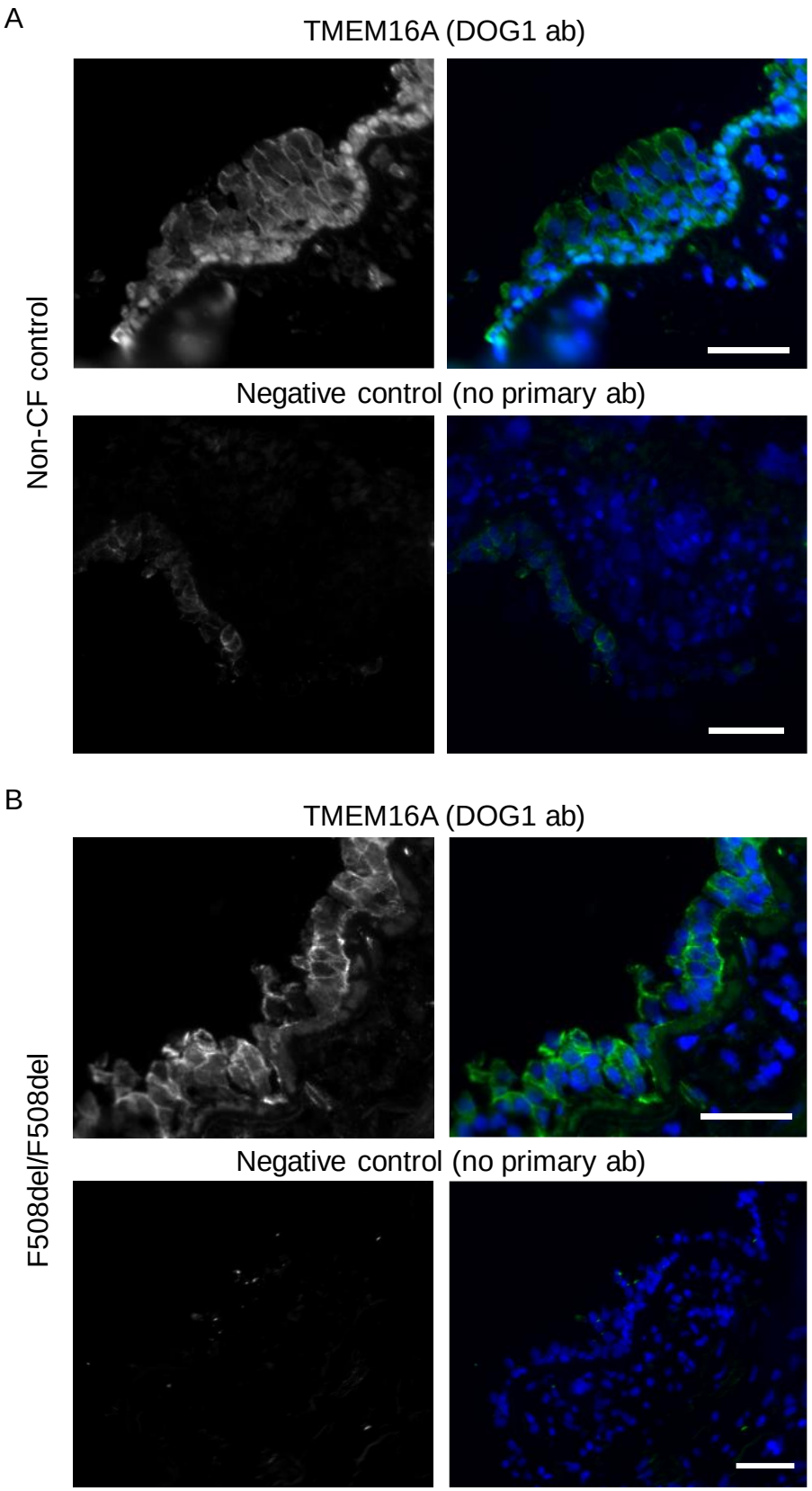

Figure S 4 – Localization of TMEM16A in human bronchial epithelia. In non-CF bronchial epithelia **(A)**, TMEM16A detected by the anti DOG-1 antibody (shown in green) localizes mostly to the apical surface, whereas in CF epithelia **(B)** it remains largely intracellularly located. Negative controls performed on adjacent tissues slices (no primary antibody) are shown. Nuclei staining is shown in blue. Scale bars = 50 µm. Experiments performed by Margarida Quaresma.

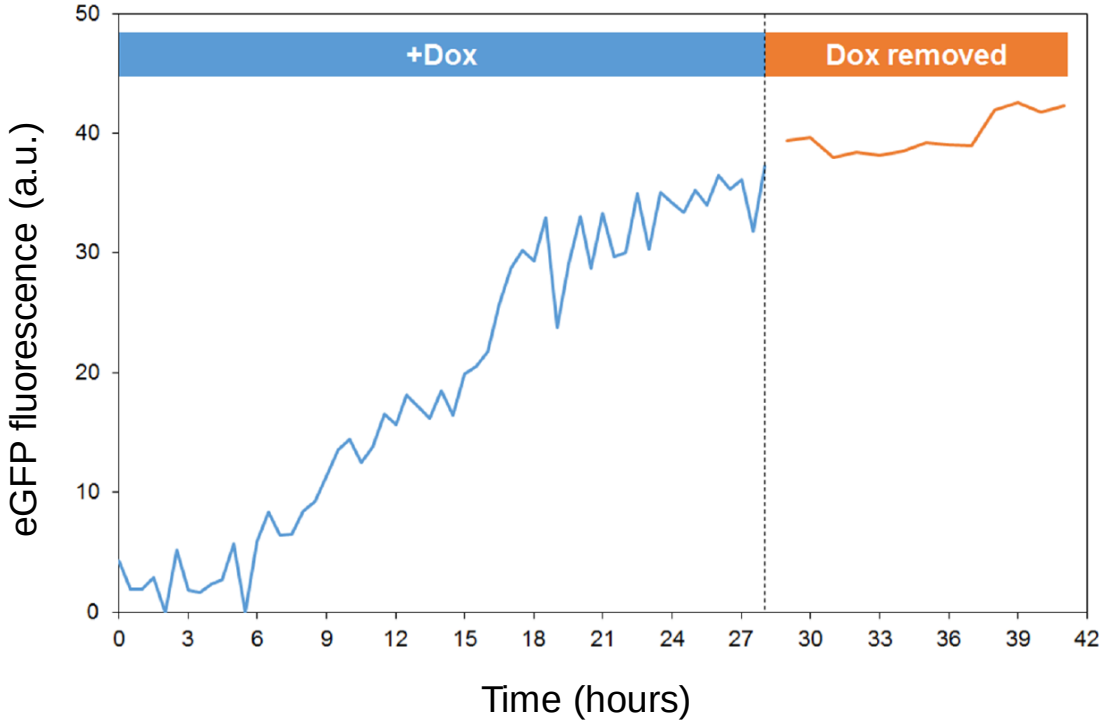

Figure S 5 – Time-course of 3HA-TMEM16A-eGFP induction by doxycycline (Dox) in CFBE cells. Levels of 3HA-TMEM16A-eGFP expression were quantified by image processing of time-lapse microscopy after induction with 1 µg/mL doxycycline (Dox), time=0 until 28h post-induction in CFBE cells and until 13h after removal of Dox. Expression of the 3HA-TMEM16A-eGFP construct starts to be noticeable after 6h of Dox induction and its plasma membrane (PM) localization after 13h of Dox, becoming quite distinct from 20h onwards. After Dox removal, for shutdown of 3HA-TMEM16A-eGFP transcription, no reduction was observed for the TMEM16A steady-state levels at least up to 13h after Dox removal. Data in collaboration with Hugo Botelho.

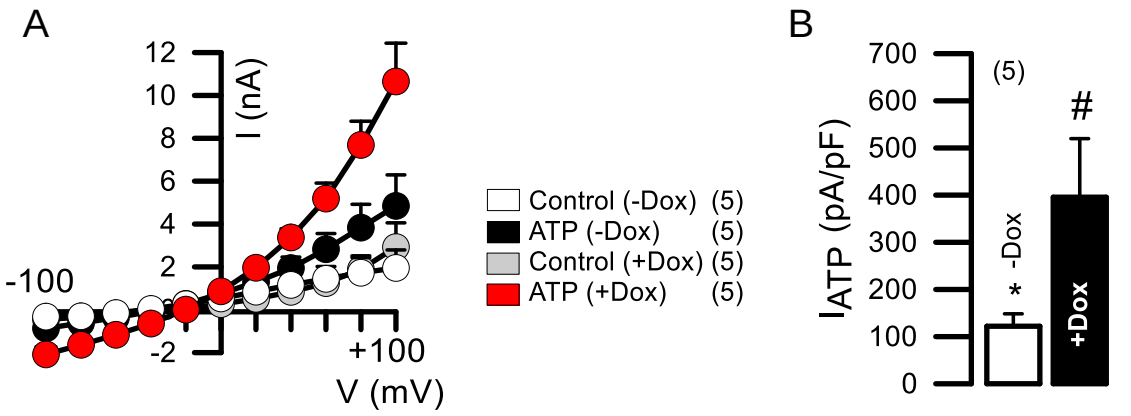

Figure S 6 – Demonstration of function for the 3HA-TMEM16A-eGFP construct by transfection into HEK-293 cells, which are null for endogenous TMEM16A expression. (A) Whole-cell patch-clamp data obtained for HEK 293T cells transfected with the 3HA-TMEM16A-eGFP-pLVX-TRE3G construct without (-Dox; white, black) or with (+Dox, grey, red) induction shown as current/voltage (I/V) curves -100mV to +100mV in Ringer (white, grey) or after stimulation by 100 µM ATP (black, red); **(B)** Delta of the average of ATP-induced current densities. '#' indicates statistical significance of ATP stimulated currents in induced vs non-induced cells ($p < 0.05$ in unpaired t-test) (number of experiments). Experiments performed by Joana Lérias.

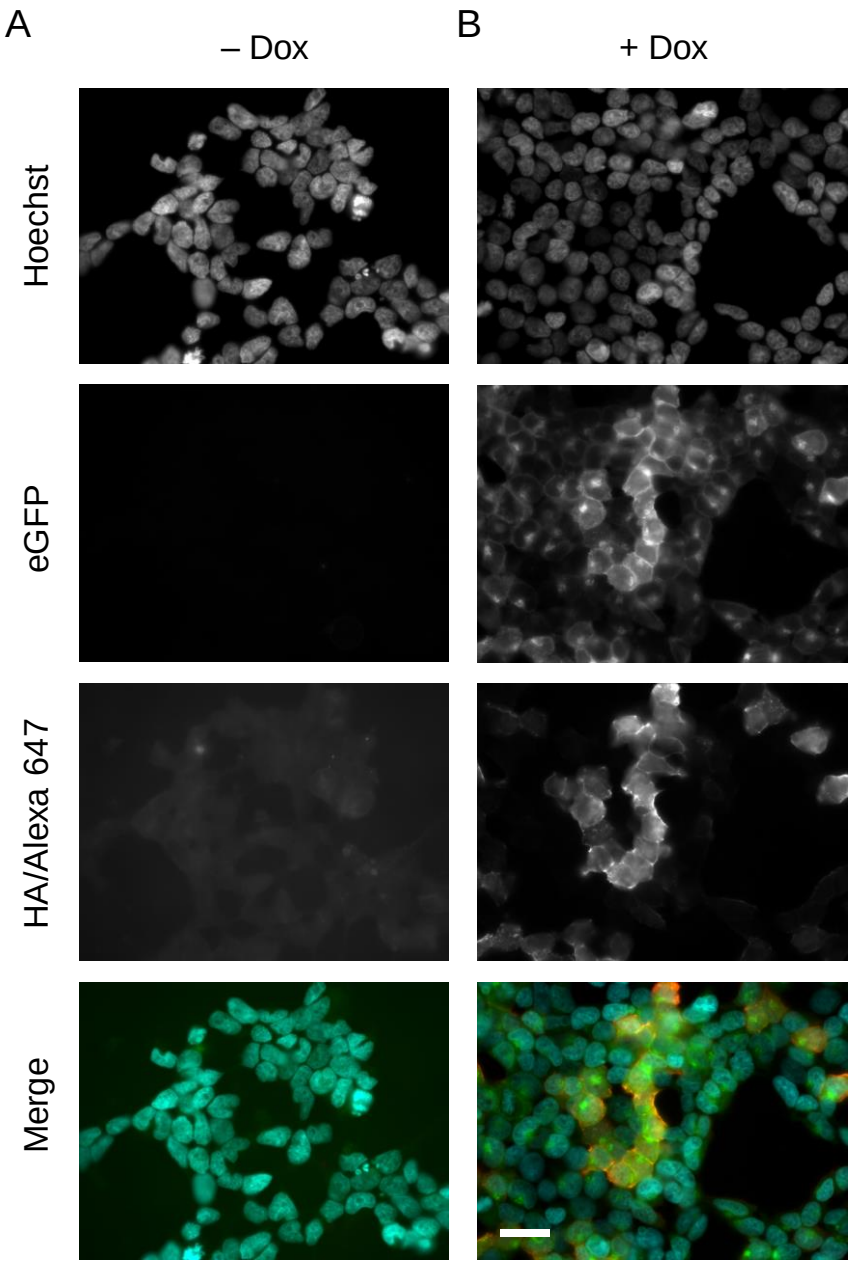

Figure S 7 – Membrane localization of the 3HA-TMEM16A-eGFP construct in HEK cells. Representative widefield epifluorescence microscopy images of HEK293 cells transfected with 3HA-TMEM16A-eGFP. Cells were either non-induced **(A)**, (-Dox, left panels) or induced with doxycycline **(B)**, (+Dox, right panels) for 48 h, 24 h after transfection. Cells were then stained with the anti-HA antibody without cell permeabilization as for CFBE cells (see Methods). Images were acquired with the fluorescence microscope Leica DMI6000B, using a 40x objective. Scale bar = 30µm.

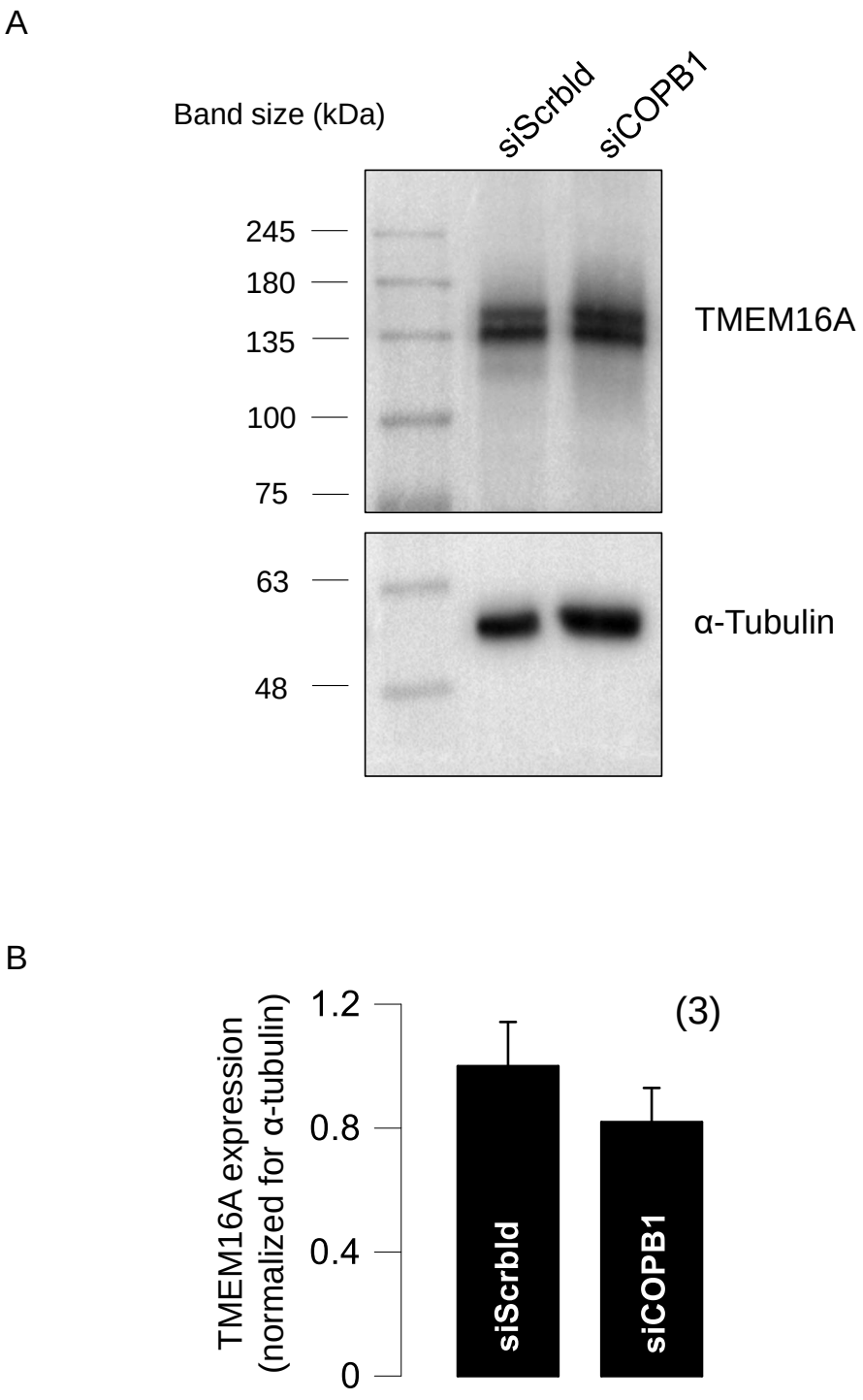

Figure S 8 – TMEM16A expression levels after siCOPB1 transfection. (A) Western blot of CFBE 3HA-TMEM16A-eGFP cells transfected with siScrbld (negative control) or with siCOPB1 for 72 h, where TMEM16A was detected by the primary antibody DOG1 (1:500). 3HA-TMEM16A-eGFP expression was induced with 1 µg/mL doxycycline for 48 h (24 h after siRNA transfection). α-Tubulin was used as a loading control and molecular mass markers are shown on the left. **(B)** The knockdown of COPB1 does not change the expression of double-tagged TMEM16A in CFBE 3HA-TMEM16A-eGFP cells. 3HA-TMEM16A-eGFP expression was normalized for α-Tubulin levels. Data are represented as means ± SEM (number of experiments).

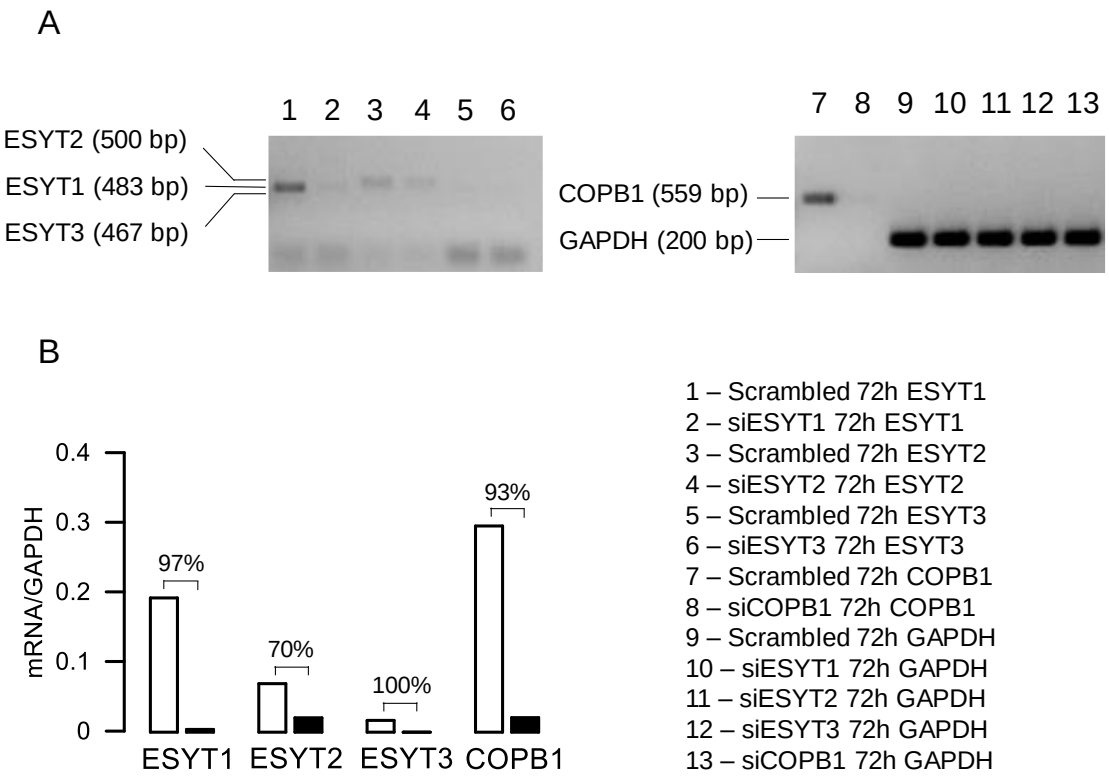

Figure S 9 – Endogenous levels of extended synaptotagmins (ESYT1, 2 and 3) in CFBE 3HA-TMEM16A-eGFP cells and effect of siRNA knockdown. (A) Products of RT-PCR performed in CFBE 3HA-TMEM16A-eGFP cells induced with doxycycline for 48h to assess endogenous levels of ESYT1, ESYT2, ESYT3 and COPB1. Cells were transfected for 72h with either with Scrambled siRNA (left) or with siRNAs targeting those genes (right). **(B)** Summary of data in (A), where knockdown efficiencies (shown as numbers above bars) were determined by comparing the mRNA levels of ESYT1-3 or COPB1 in the siRNA transfected cells with those in cells transfected with Scrambled siRNA. Experiments performed by Rainer Schreiber.

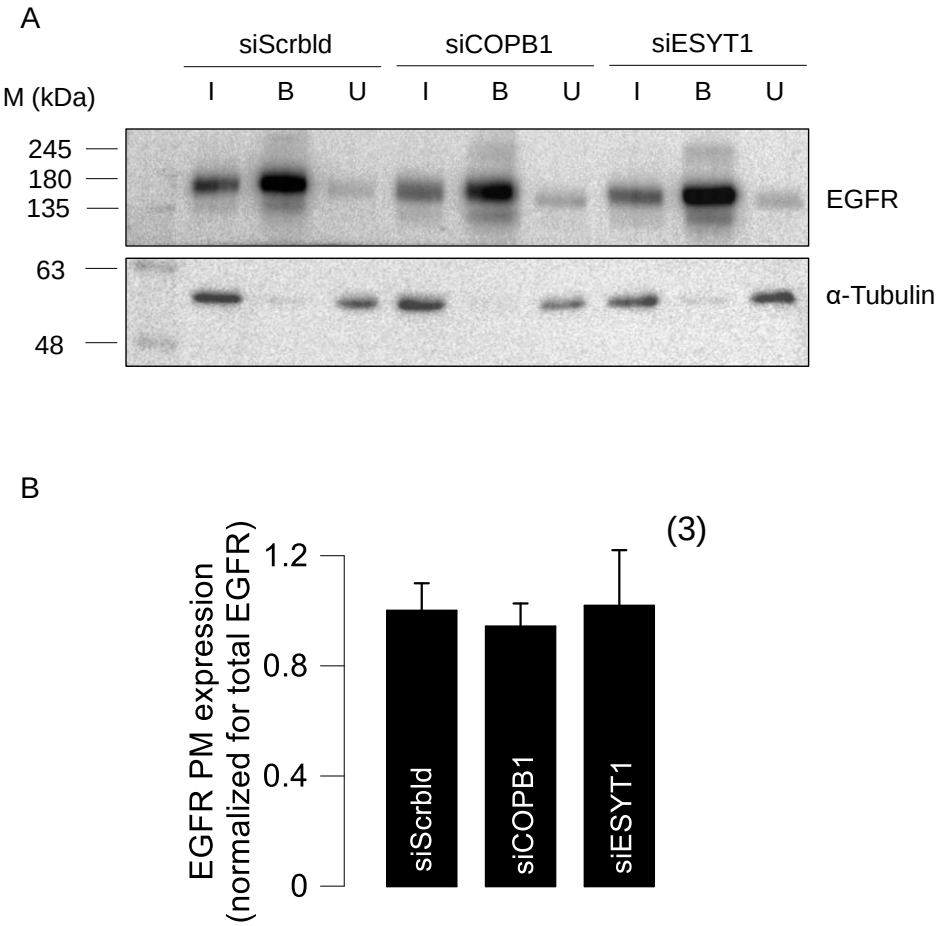

Figure S 10 – EGF receptor expression levels at the PM after siCOPB1 or siESYT1 transfection. (A) Biotinylation assay in CFBE wt-CFTR cells transfected for 72 h either with siScrbld (negative control), siCOPB1 or siESYT1 using the primary antibody anti-EGFR (1:500). α-Tubulin was used as a loading control and molecular mass markers are shown on the left. I – Input (whole-cell lysate), B – Biotinylated samples, U – Unbound (protein fraction that did not bind to the streptavidin beads). **(B)** The knockdown of siCOPB1 or siESYT1 does not alter membrane expression of EGFR. EGFR expression at the PM was normalized for total EGFR levels (whole-cell lysate). Data are represented as means ± SEM (number of experiments).

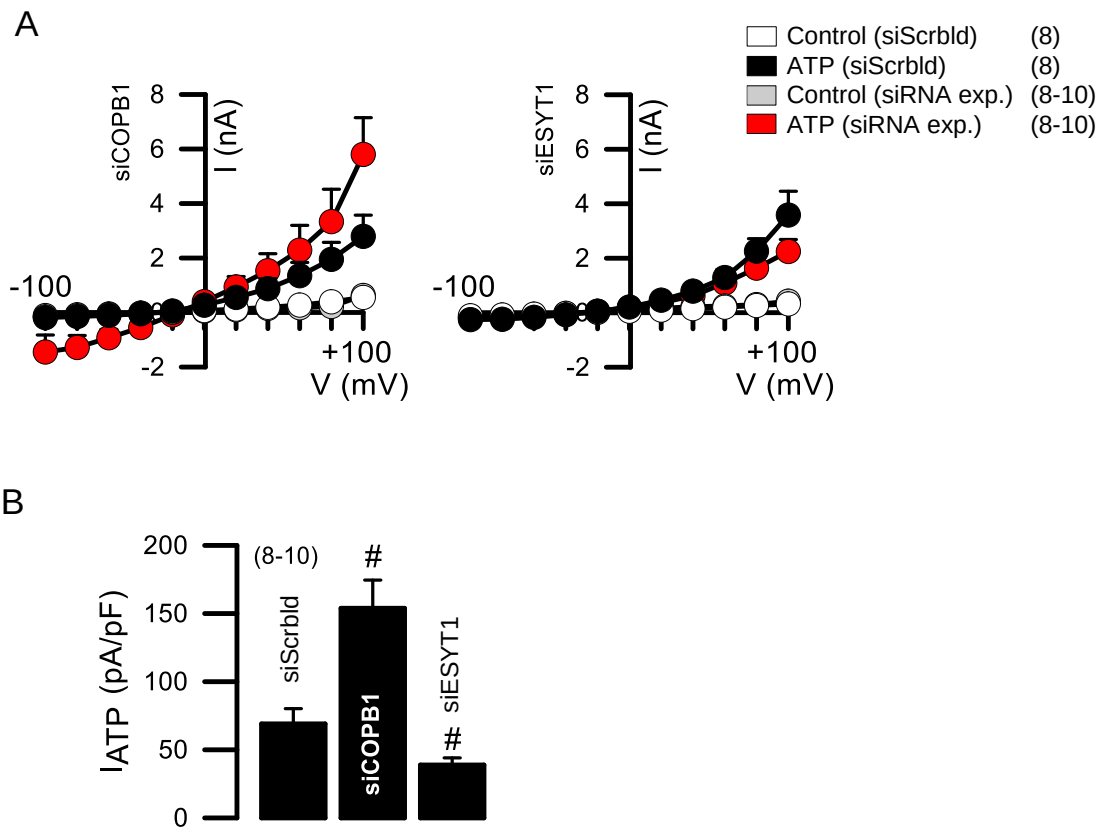

Figure S 11 – Impact of screen hits COPB1 and ESYT1 on endogenous TMEM16A function. (A) Whole-cell patch-clamp data, shown as current/voltage (I/V) curves -100mV to +100mV, obtained for CFBE parental cells transfected with siRNAs targeting screen hits COPB1 (left; grey, red) or ESYT1 (right; grey, red) as well as Scrambled siRNA as a control (white, black) in Ringer (white, grey) or after stimulation by 100 µM ATP (black, red). All solutions contained 50 nM TRAM 34, and the number (n) of experiments is indicated in front of each label. **(B)** Delta of the average of ATP-induced current densities. '#' indicates statistical significance of ATP-stimulated currents of siRNA transfected cells vs Scrambled ($p < 0.05$ in unpaired t-test). Experiments performed by Joana Lérias.

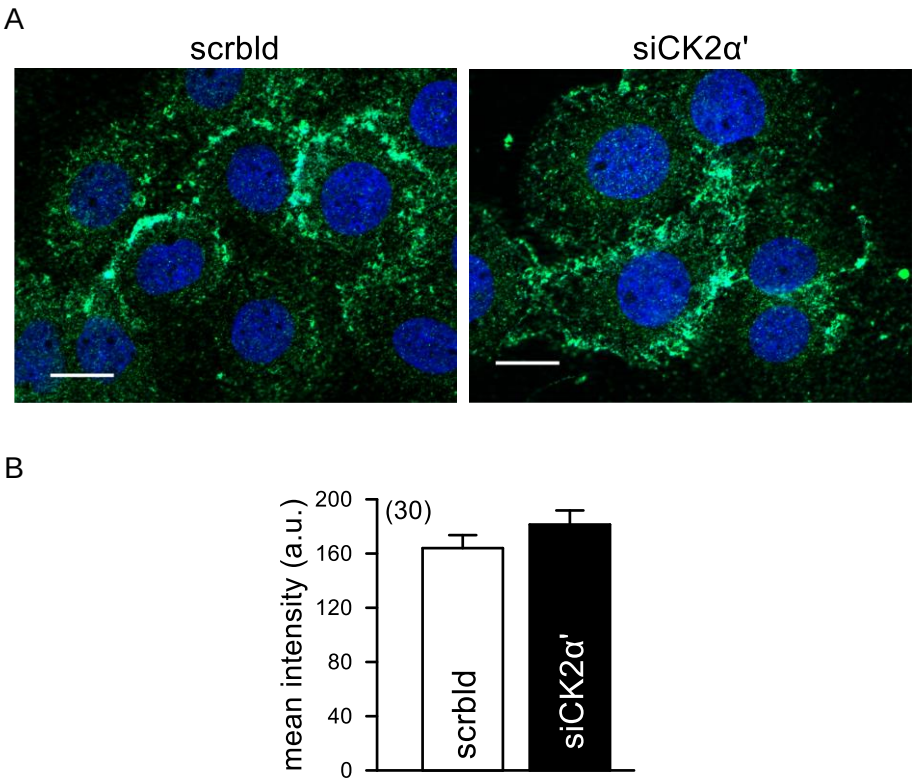

Figure S 12 – CK2 does not affect membrane expression of Na^+/K^+-ATPase. (A) CFBE cells were exposed to siRNA for CK2α' for 48 hrs. Successful knockdown of CK2α' is demonstrated in Fig. 13 – Chapter 1.2. **(B)** Knockdown of CK2α' did not affect membrane expression of the Na^+/K^+-ATPase. Primary antibody: rabbit anti-human Na^+/K^+-ATPase (1:150, Santa Cruz, sc-28800). Secondary antibody: donkey anti-rabbit Alexa 488 (1:300); Hoechst 33342 (10 µM). 40.000 cells/coverslip were transfected. Cover slips were mounted on slides using fluorescence mounting medium (DAKO). Mean ± SEM (number of cells analyzed). Experiments performed by Rainer Schreiber.

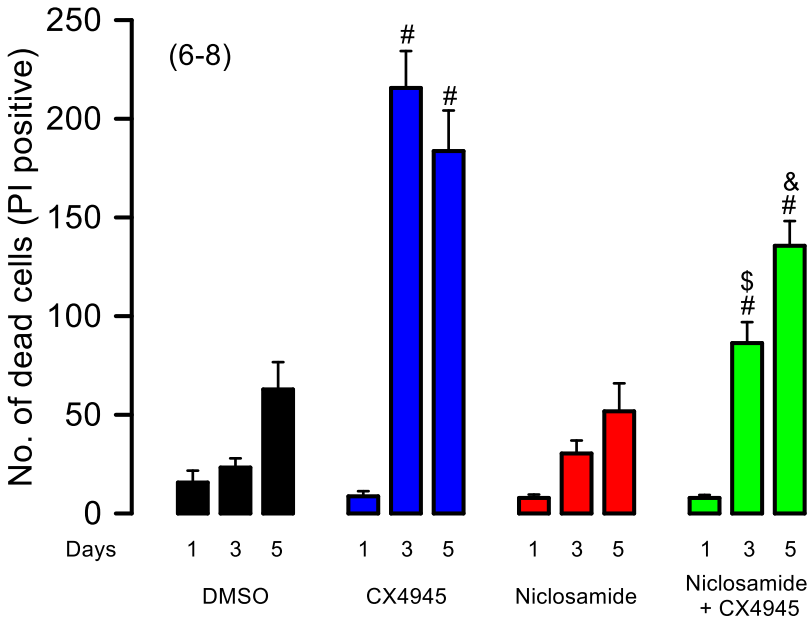

Figure S 13 – CX4945 but not niclosamide induces cell death. Cell death was assessed by propidium iodide (PI) positivity. Cell death was induced by 1-20 µM CX4945 (but not below 1 µM) while no cell death was induced by niclosamide up to 5 µM. Values are shown for 20 µM CX4945 (#significant difference compared to DMSO, unpaired t-tests; $p < 0.05$) and 0.5 µM niclosamide. Notably, while additional niclosamide further increases inhibition of proliferation by CX4945 (chapter 1.2), it significantly lowered cell death (&significant inhibition, unpaired t-tests; $p< 0.05$). Mean ± SEM (number of experiments). Data in collaboration with Aires Duarte.

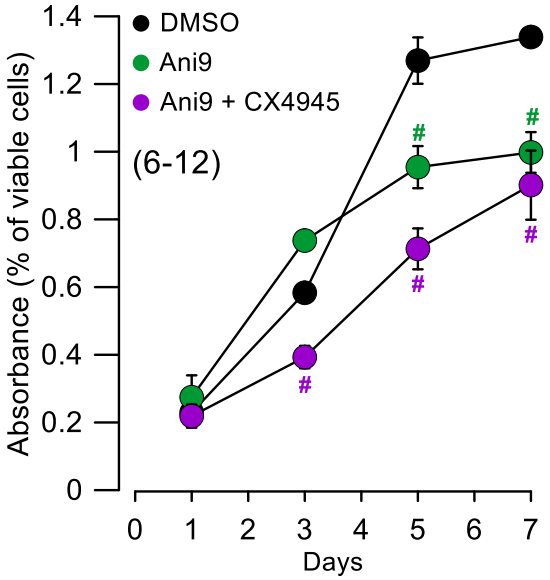

Figure S 14 – The TMEM16A inhibitor Ani9 inhibits proliferation. Blocking TMEM16A by Ani9 (1 µM) and simultaneous inhibition of CK2 by CX4945 (20 µM) inhibited proliferation of Cal33 cells. #Significant difference compared to DMSO, unpaired t-tests; $p < 0.05$. Mean ± SEM (number of experiments). Experiments performed by Rainer Schreiber.

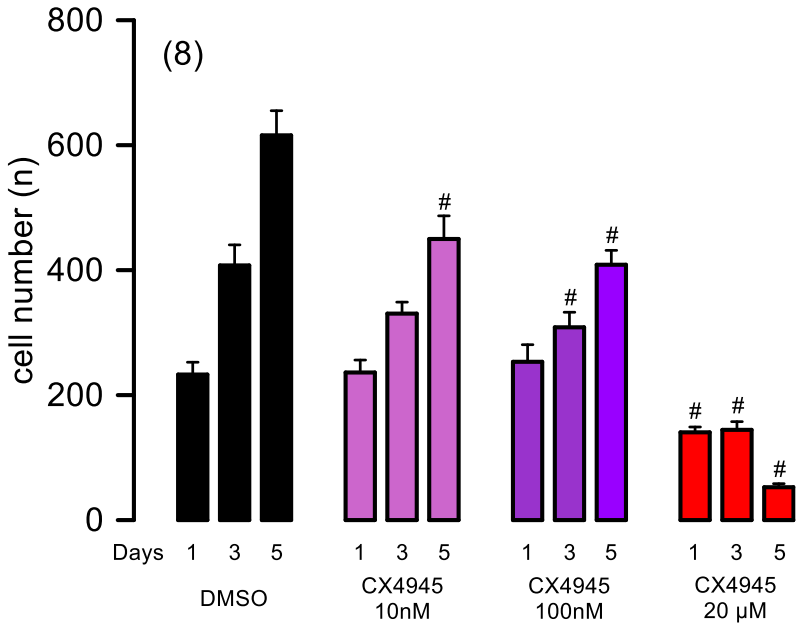

Figure S 15 – Inhibition of cell proliferation by different concentrations of CX4945: 10 nM, 100 nM, and 20 µM (#Significant inhibition, unpaired t-tests; $p < 0.05$). Mean ± SEM (number of experiments). Data in collaboration with Aires Duarte.

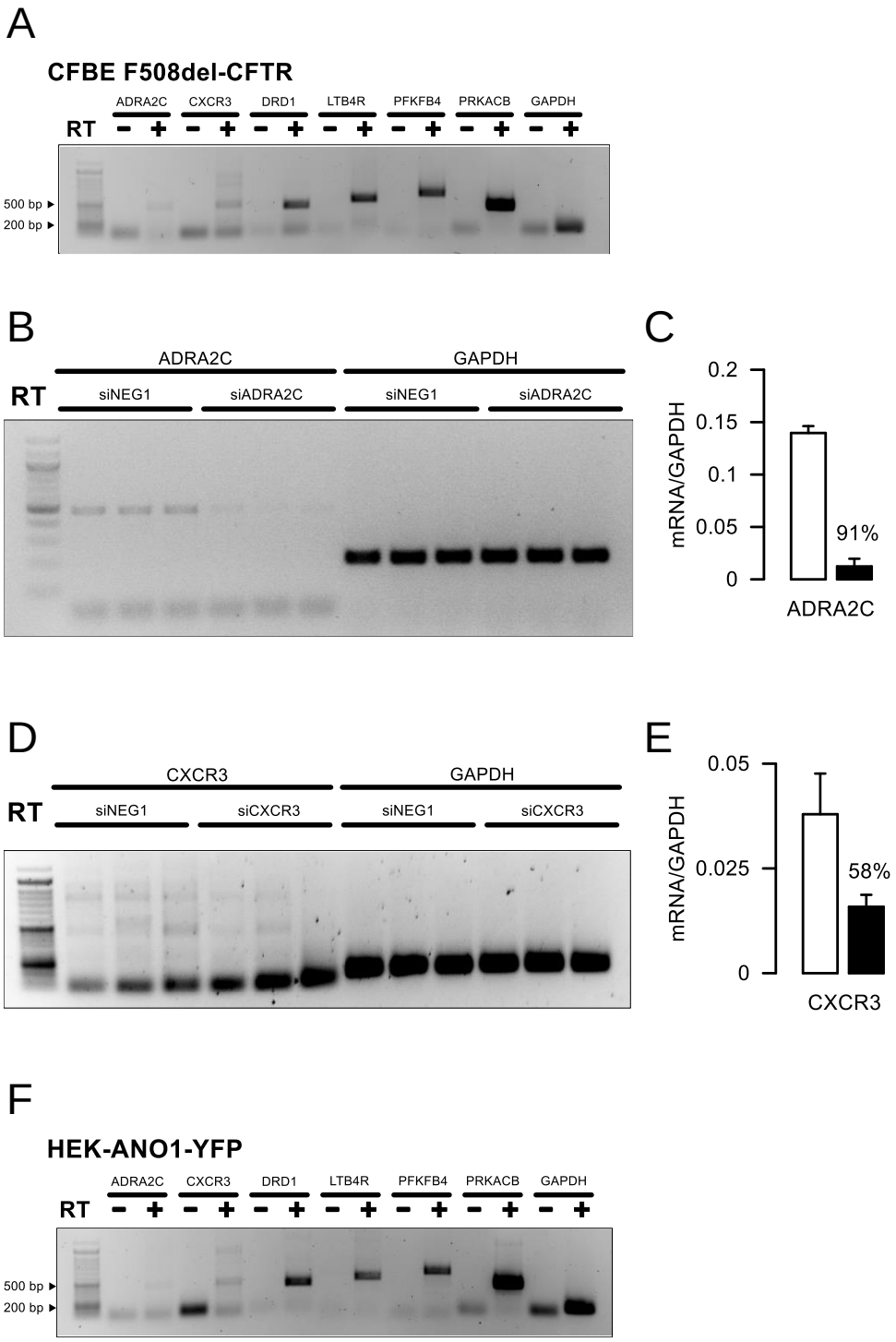

Figure S 16 – Expression of the selected hit genes in CFBE and HEK cells. (A) Expression of the 6 genes selected for further validation in CFBE cells. **(B)** RT-PCR analysis of the knockdown of ADRA2C, when CFBE cells were transfected with the targeting siRNA (compared with siNEG1-transfected cells), and its quantification **(C)**. **(D)** RT-PCR analysis of CXCR3 knockdown in CFBE cells and its quantification **(E)**. **(F)** Expression of hits in HEK-TMEM16A-YFP cells.

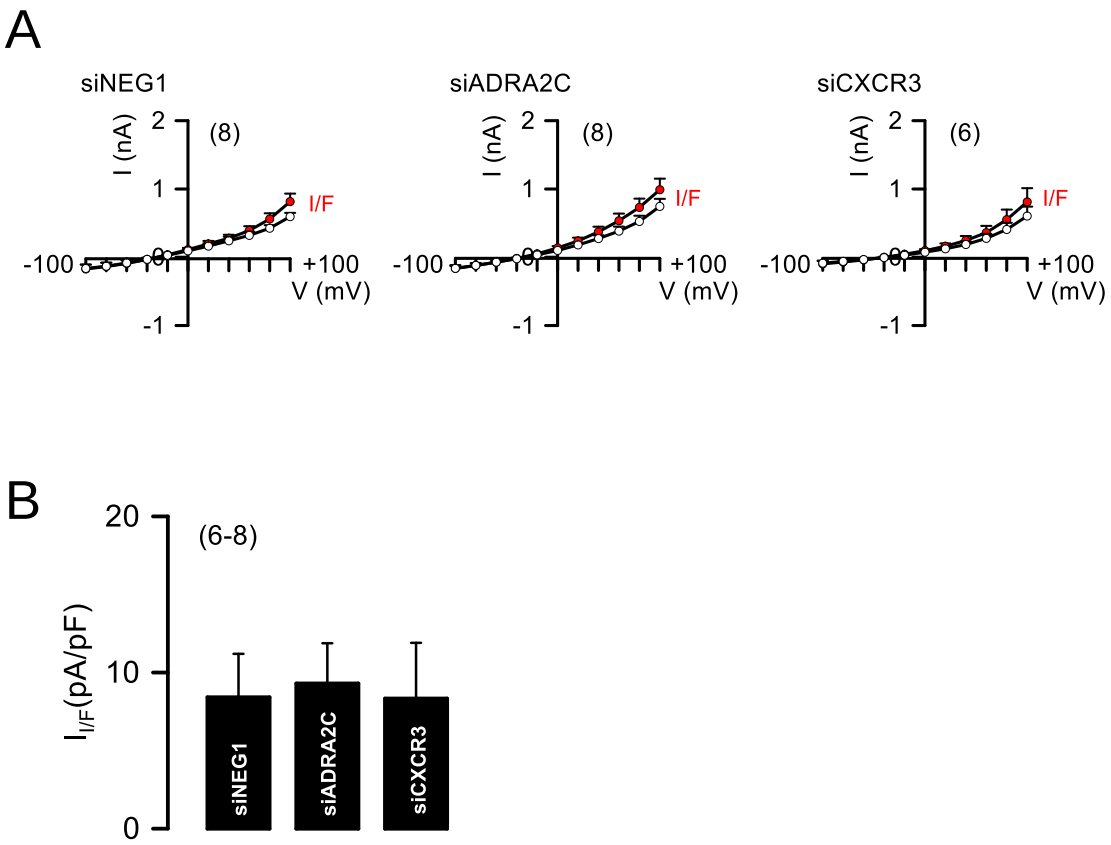

Figure S 17 – The knockdown of TMEM16A hits has no effect on F508del-CFTR function. (A) Whole cell currents obtained in siRNA-transfected cells (current/voltage (I/V) curves) activated by IBMX (100 μM) and Forskolin (2 μM) – I/F. **(B)** Summary of I/F-induced currents with different siRNA treatments. Mean ± SEM (number of cells measured). *Significant current activation ($p < 0.05$; paired t-test). #Significant difference when compared with the negative control siNEG1 ($p < 0.05$; unpaired t-test).

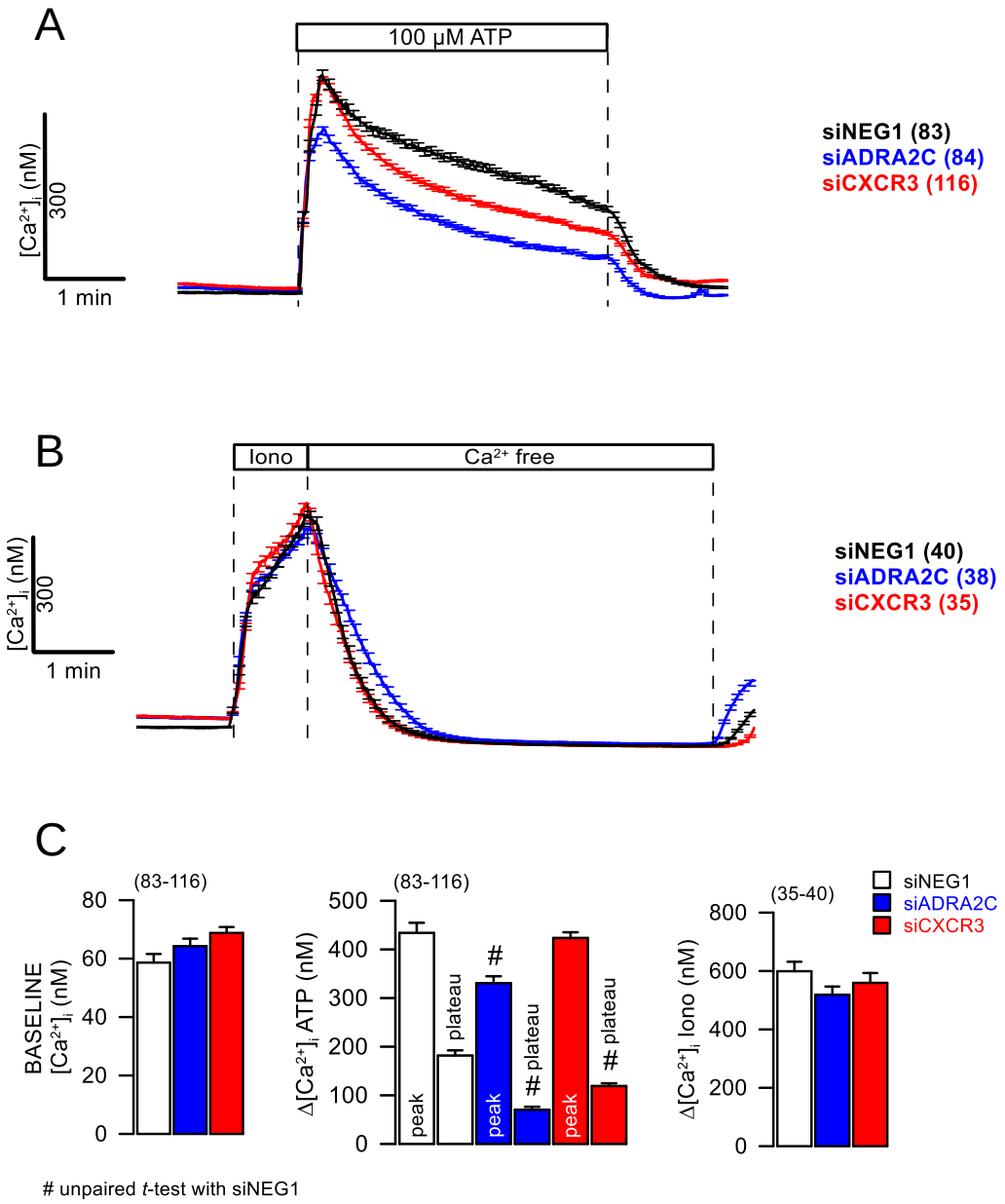

Figure S 18 – TMEM16A regulators do not increase receptor-mediated Ca^{2+} signalling. (A) Intracellular Ca^{2+} measurements using Fura2-AM in CFBE F508del-CFTR cells treated with non-targeting siRNA (siNEG1) or siRNAs targeting ADRA2C or CXCR3. Original recordings for basal and ATP-induced intracellular Ca^{2+} concentrations. **(B)** Original recordings for basal and Ionomycin (Iono)-induced intracellular Ca^{2+} concentrations. Increase of intracellular Ca^{2+} by 100 µM ATP, and 1 µM Iono respectively. **(C)** Summaries of basal, ATP-induced and Iono-induced Ca^{2+} levels. Data represented as mean ± SEM (number of cells measured). #Significant difference when compared with the negative control siNEG1 ($p < 0.05$; unpaired t-test).

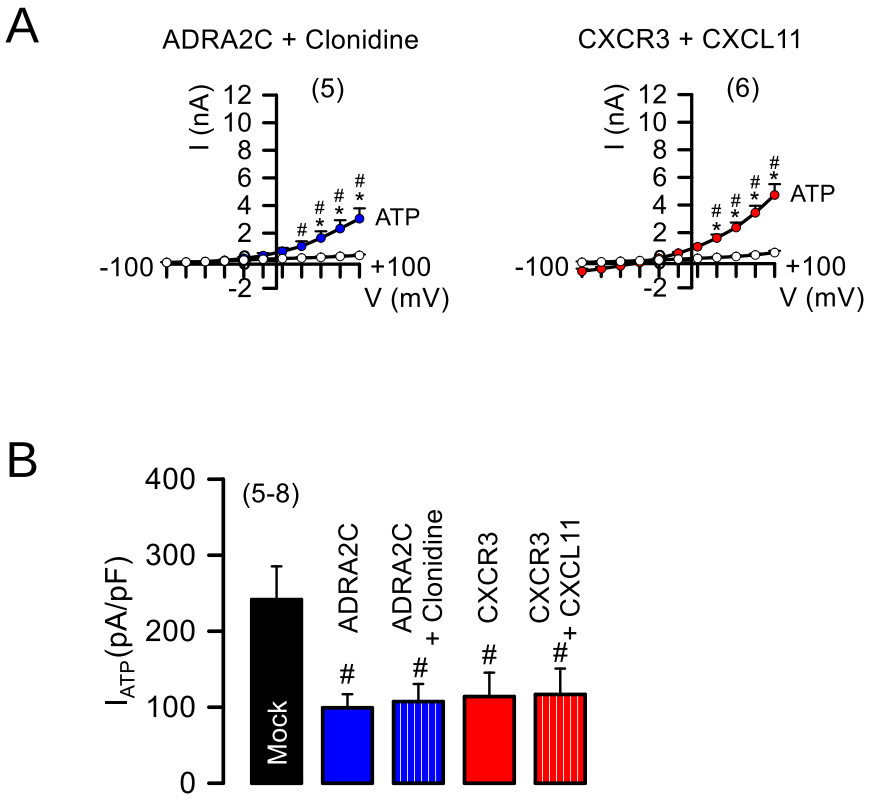

Figure S 19 – Effect of receptor agonists on ATP-activated whole cell currents in CFBE F508del-CFTR cells overexpressing ADRA2C or CXCR3. (A) Current/voltage curves and corresponding summary **(B)** of ATP-induced currents in CFBE F508del-CFTR cells transfected with ADRA2C, CXCR3 or an empty vector, with or without treatment with receptor agonists (10 µM clonidine or 100 ng/mL CXCL11). Mean ± SEM (number of cells measured). *Significant current activation ($p < 0.05$; paired t-test). #Significant difference when compared with the negative control Mock ($p < 0.05$; unpaired t-test).

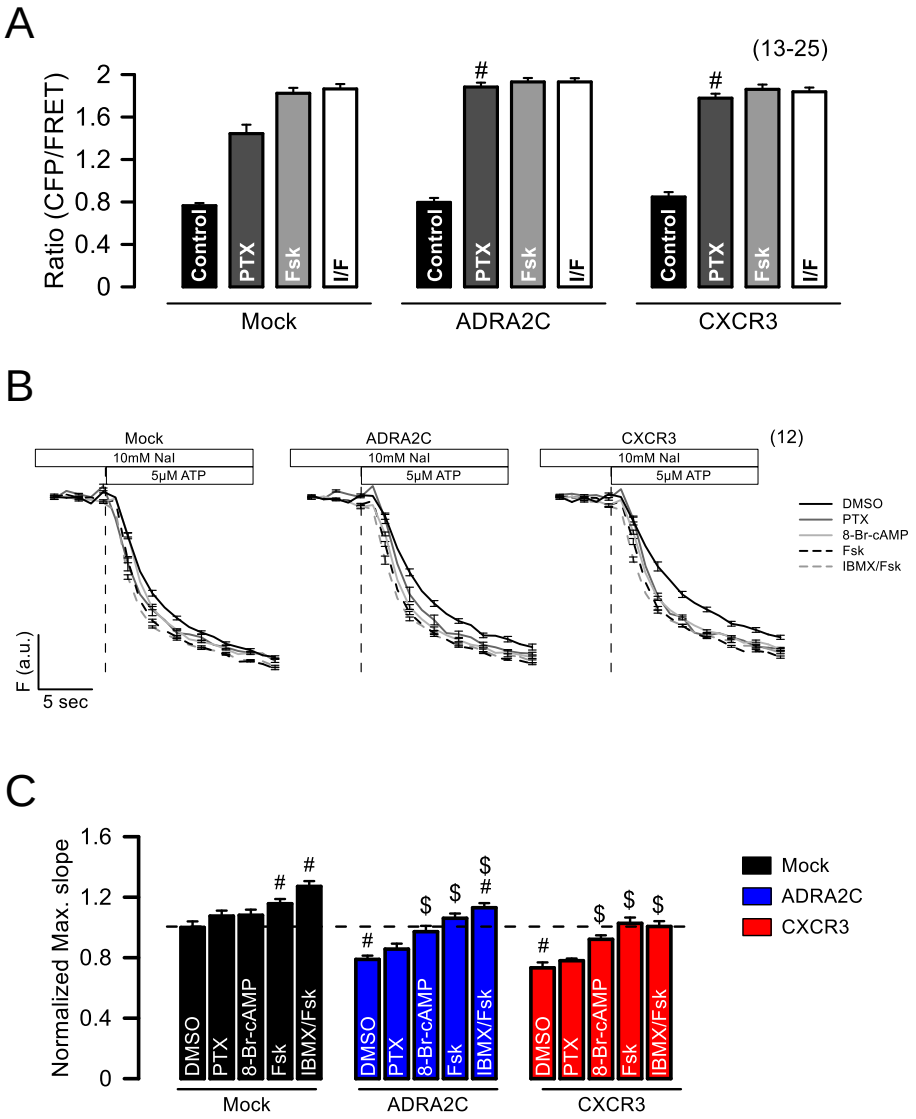

Figure S 20 – Measurement of intracellular cAMP levels and effect of increasing intracellular cAMP concentration on TMEM16A function. (A) Intracellular cAMP levels measured by FRET using HEK cells transiently transfected with an Epac cAMP sensor (YFP-Epac-CFP) co-transfected with ADRA2C or CXCR3. cAMP concentration was increased by incubation with 100 ng/mL pertussis toxin (PTX), 10 μM forskolin (Fsk) and 100 μM IBMX. **(B)** Original tracings of ATP-induced YFP quenching in HEK-TMEM16A-YFP cells transfected with an empty vector or with ADRA2C/CXCR3 and incubated for 2 h with 100 ng/mL PTX, 100 μM 8-bromo-cAMP, 25 μM Fsk, and/or 100 μM IBMX. **(C)** Maximum slope of the curves obtained in (B). The dashed line represents TMEM16A function under control conditions (mock-transfected cells treated with DMSO). #Significant difference when compared with the control ($p < 0.05$; unpaired t-test). $Significant difference when compared with cells transfected with the same cDNA but with different treatments (DMSO vs cAMP increasing agent).

Appendix 2 – Supplementary data of Chapter 2

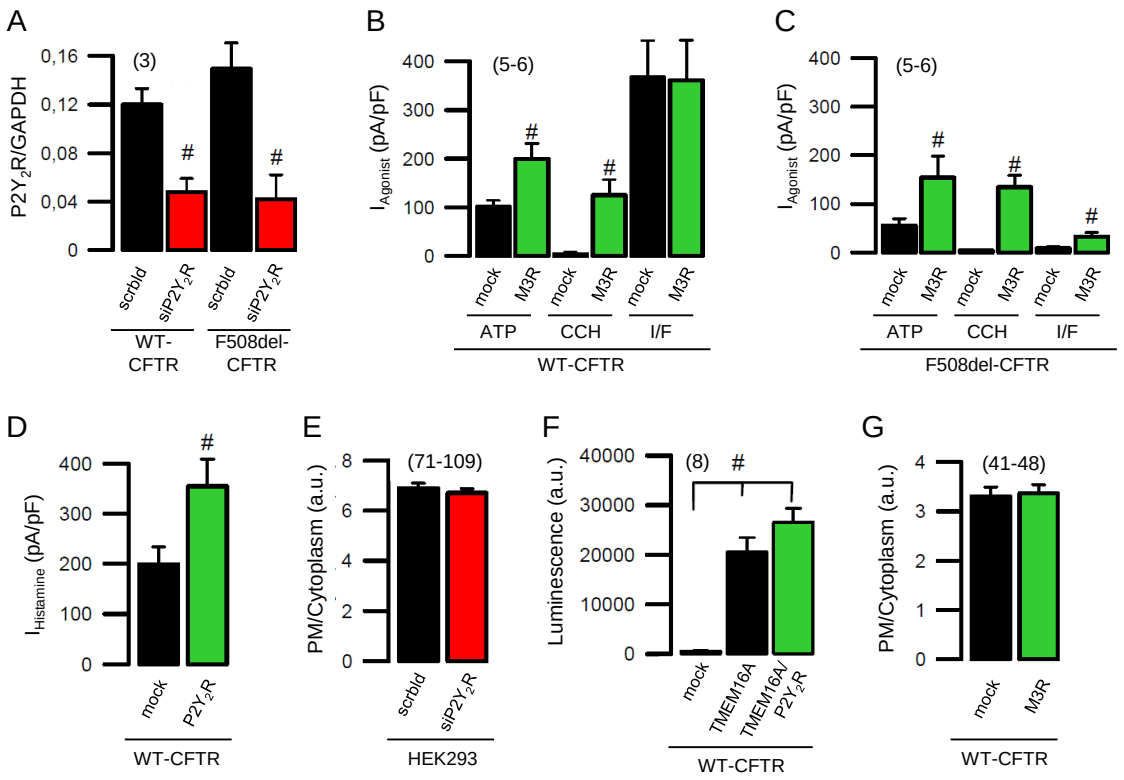

Figure S 21 – Activation of TMEM16A by GPCR. (A) siRNA knockdown of $P2Y_2R$ detected by semiquantitative RT-PCR in wt-CFTR and F508del-CFTR expressing CFBE cells. **(B,C)** Summary of whole cell currents activated by ATP (100 µM), carbachol (CCH; 100 µM) and IBMX/forskolin (100 µM/2 µM). Summaries are shown for cells expressing empty plasmid (mock) or M3 receptors (M3R) in CFBE wt-CFTR (B) and CFBE F508del-CFTR (C) cells. **(D)** Summary of current densities activated by histamine (50 µM) in mock transfected CFBE cells and cells overexpressing $P2Y_2R$. **(E)** Ratio of PM to cytoplasmic expression of TMEM16A in HEK293 cells by analysis of fluorescence intensities in regions of interest. Knockdown of $P2Y_2$ receptors does not change membrane expression. **(F)** Membrane expression of TMEM16A in CFBE cells measured by chemiluminescence. CFBE cells expressed a TMEM16A construct that contained an extracellularly accessible HA tag in the first extracellular loop of TMEM16A. Cells were labelled using an anti-HA antibody and a secondary horseradish peroxidase conjugated antibody. Additional expression of $P2Y_2R$ did not change membrane expression of TMEM16A. **(G)** Ratio of PM to cytoplasmic expression of TMEM16A in CFBE cells. Expression of M3R does not change membrane expression. Mean ± SEM (number of experiments). #Significant difference when compared to mock or scrambled RNA (Scrbld) or mock transfected cells (unpaired Student's t test). Experiments performed by Rainer Schreiber and Joana Lérias.

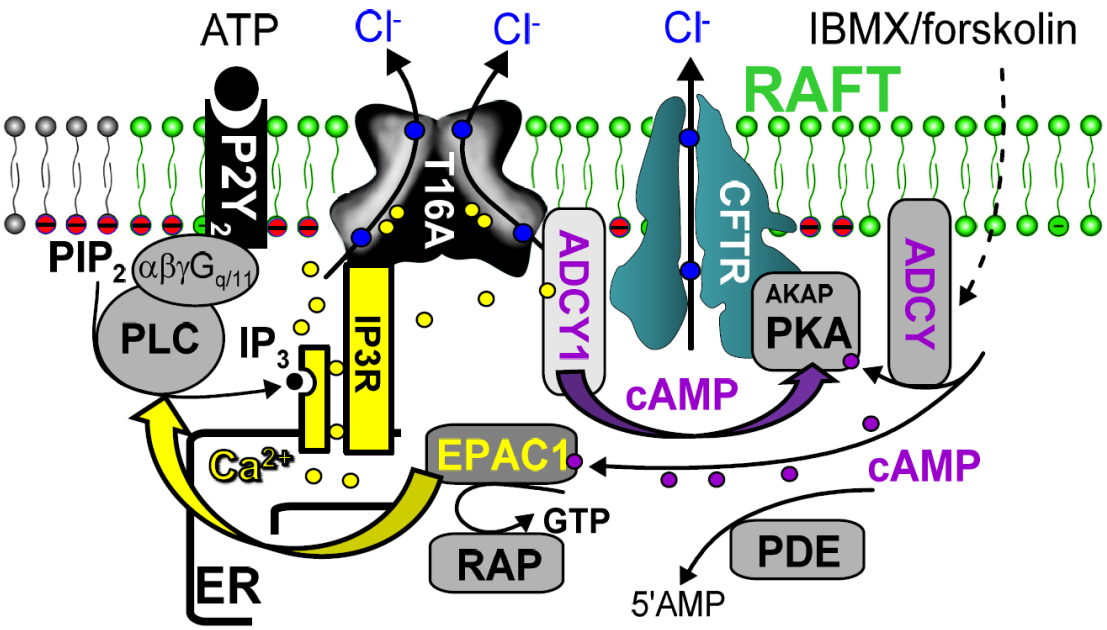

Figure S 22 – cAMP/Ca^{2+}-crosstalk activates CFTR and TMEM16A. Stimulation of purinergic receptors leads to endoplasmic reticulum (ER) Ca^{2+} store release through IP_3 receptors (IP_3R). Ca^{2+} not only activates TMEM16A (T16A) but also stimulates adenylate cyclase type 1 (ADCY1) to produce cAMP and to activate CFTR via protein kinase A (PKA). Vice versa, activation of adenylate cyclases by IBMX/forskolin (or through ß-adrenergic stimulation) generates cAMP and activates not only CFTR but also TMEM16A via exchange protein directly activated by cAMP (EPAC1), small GTP-binding protein RAP, phospholipase C (PLC) and local increase in intracellular Ca^{2+}. Receptor, TMEM16A, CFTR and signalling molecules are probably colocalized in a raft-like PM microdomain.

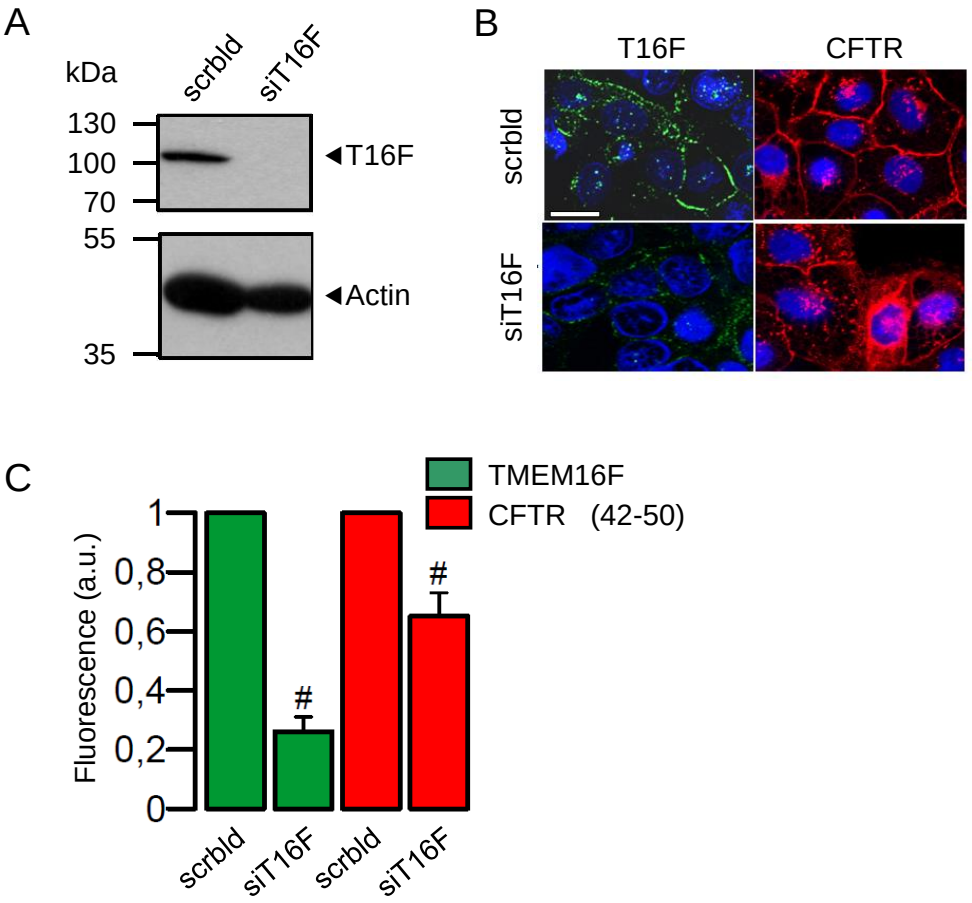

Figure S 23 – Role of TMEM16F for membrane expression of CFTR in CFBE cells. (A) Western blotting indicating knockdown of TMEM16F by siRNA-TMEM16F in CFBE human airway epithelial cells. Densitometry analysis revealed a knockdown of 91%. **(B)** Knockdown of TMEM16F attenuated expression of TMEM16F (green fluorescence) and membrane expression of mCherry-CFTR (red fluorescence). **(C)** Fluorescence intensity of PM staining. Data are represented as means ± SEM (number of cells measured). #Indicates significant difference when compared to scrambled (Scrbld; $p < 0.05$, unpaired t-test). Scale bar = 20 µm. Experiments performed by Jiraporn Ousingsawat and Podchanart Wanitchakool.

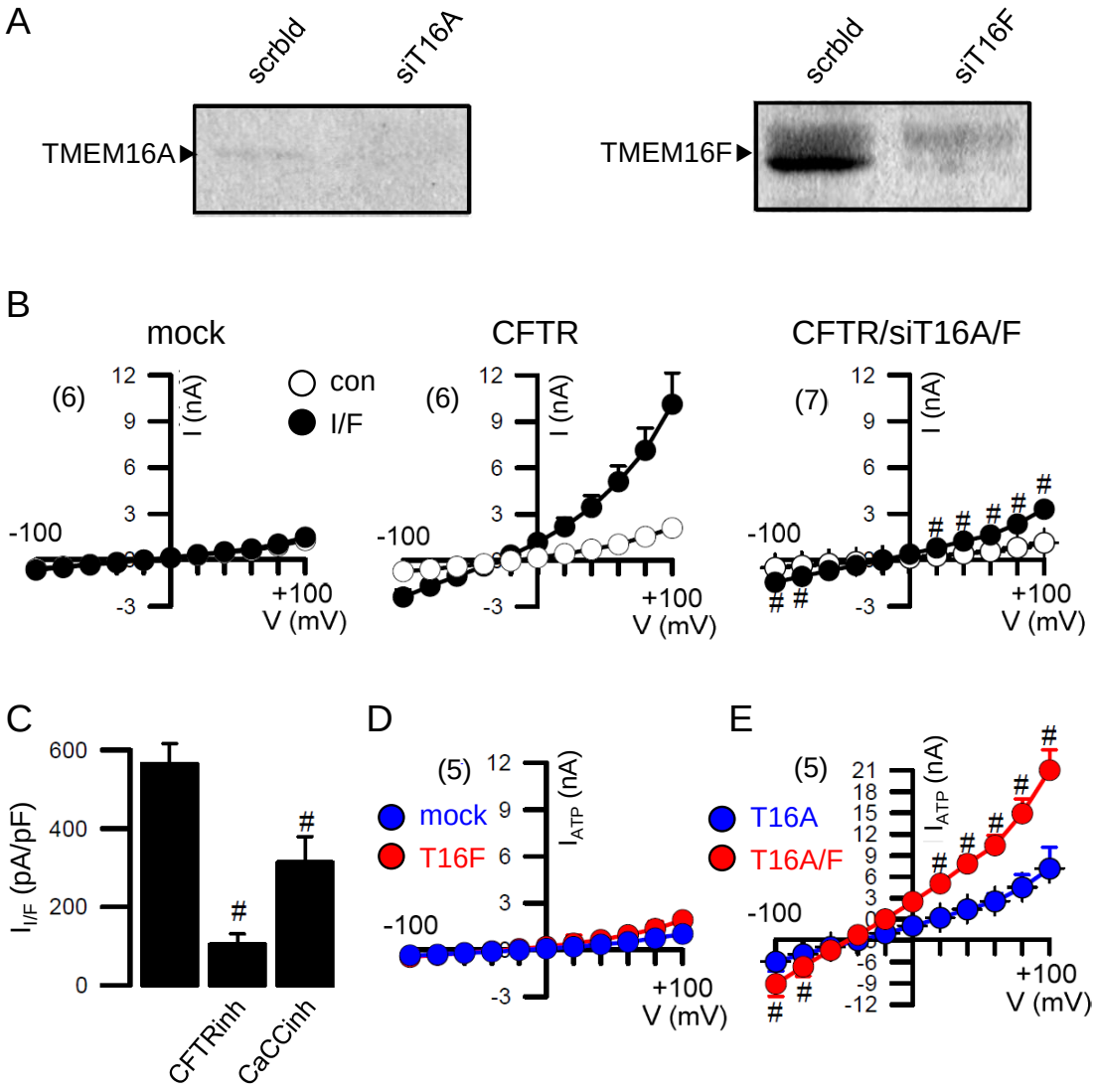

Figure S 24 – Cooperativity of CFTR, TMEM16A and TMEM16F in HEK293 cells. (A) Western blot indicating knockdown of (faintly expressed) endogenous TMEM16A and (more strongly expressed) endogenous TMEM16F in HEK293 cells. **(B)** IBMX (100 µM) and forskolin (2 µM) (I/F) induced CFTR currents in HEK293 cells and effect of knockdown of TMEM16A/F (siT16A/F) on activation of CFTR currents. **(C)** Inhibition of I/F-activated whole cell currents by CFTRinh172 (30 µM) and CaCCinh-A01 (30 µM). **(D)** ATP (100 µM) activated whole cell currents in mock transfected and TMEM16F-overexpressing HEK293 cells. **(E)** ATP activated whole cell currents in cells expressing TMEM16A (T16A) or co-expressing both TMEM16A and TMEM16F (T16A/F). Augmentation of ATP-activated TMEM16A whole cell currents suggests positive cooperativity between TMEM16A and TMEM16F. Mean ± SEM (number of cells measured). #Significant difference when compared to the absence of inhibitors or siRNA or compared to T16A only ($p < 0.05$; unpaired t-test). Experiments performed by Joana Lérias and Podchanart Wanitchakool.

Appendix 3 – Supplementary data of Chapter 3

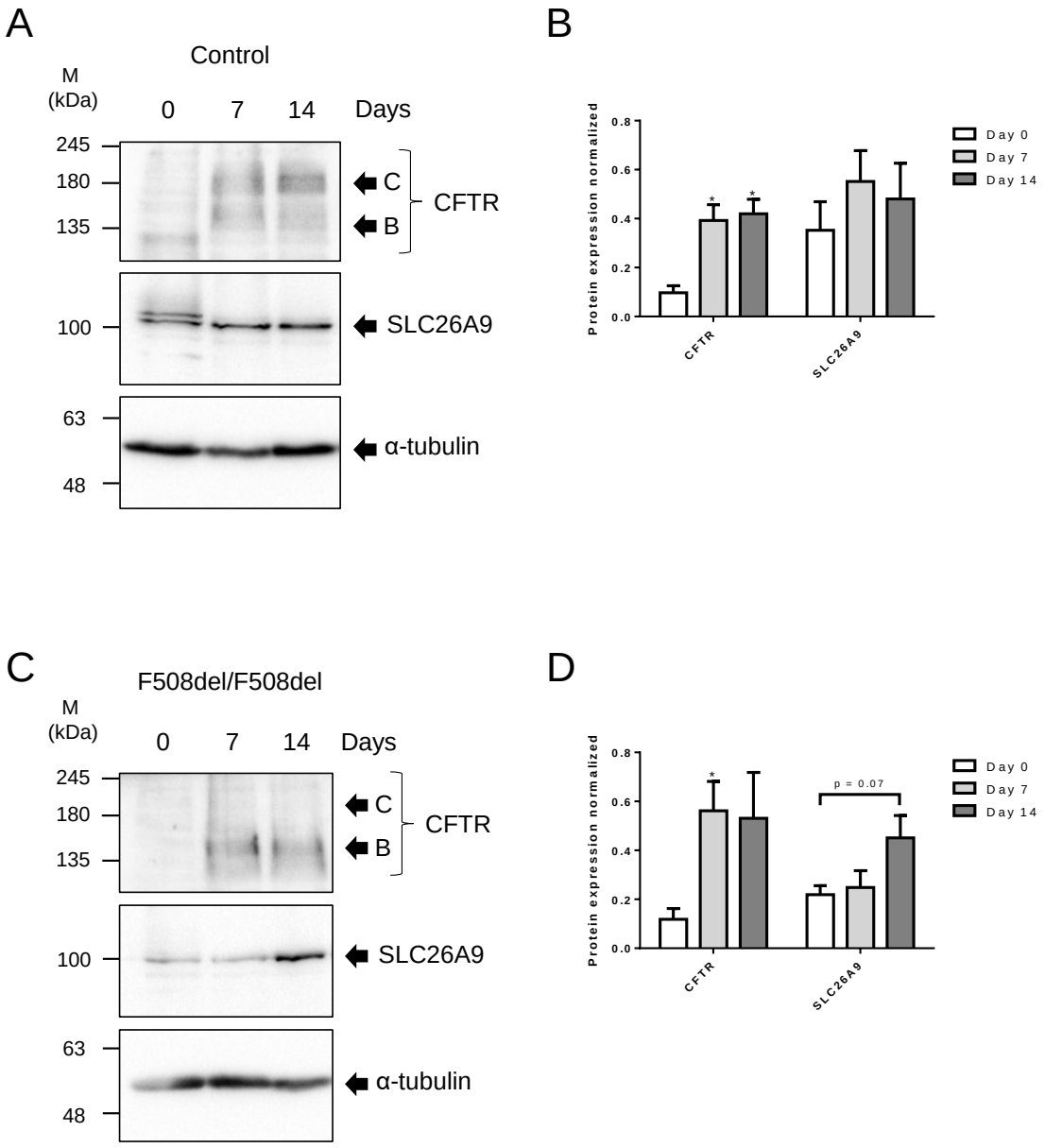

Figure S 25 – SLC26A9 expression is delayed over the course of differentiation in CF (F508del/F508del) vs. control pHNE cells. (A) Western Blot showing wt-CFTR and SLC26A9 expression during differentiation (days 0, 7 and 14 in air-liquid interface) in primary human nasal epithelial (pHNE) cells derived from a healthy control. **(B)** Quantification of CFTR and SLC26A9 protein expression detected by WB in (A). **(C)** F508del-CFTR and SLC26A9 expression in CF pHNE cells over differentiation and its quantification in **(D)**. Data are normalized to loading control and showed as arbitrary units, mean ± SEM (number of experiments (n) = 3 experiments with cells from the same donors but with different passage numbers). "*" indicates statistically significant differences (unpaired t-test, $p < 0.05$). Data in collaboration with Violeta Railean.

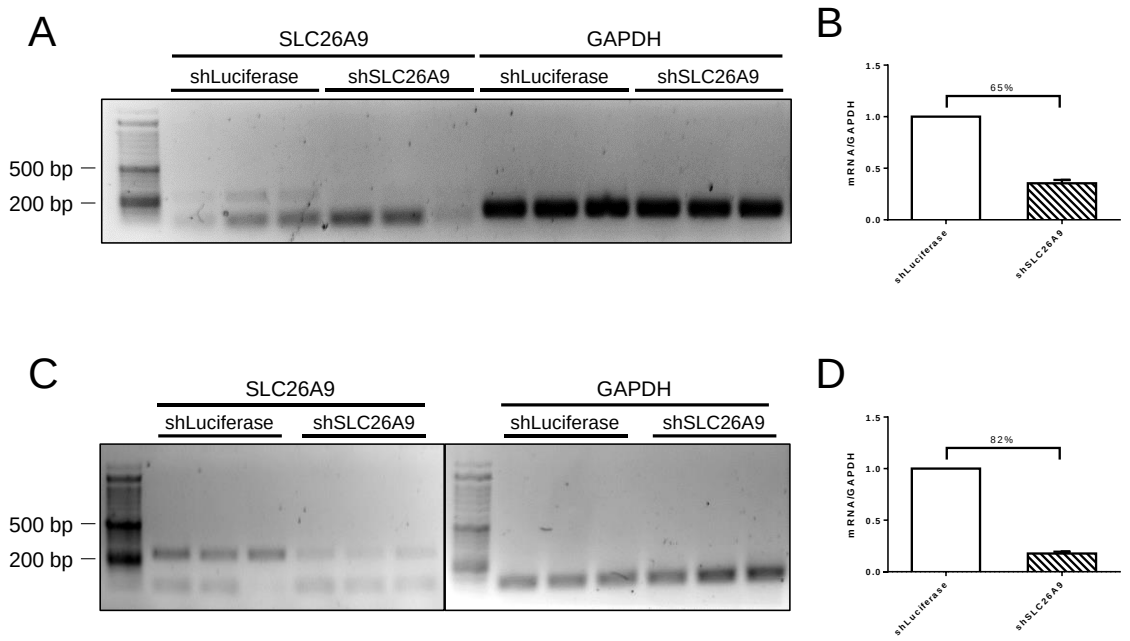

Figure S 26 – Semi-quantitative PCR to assess SLC26A9 knockdown. (A) Semi-quantitative RT-PCR performed in CFBE F508del-CFTR or **(C)** 16HBE F508del-CFTR cells stably transfected with either shLuciferase (left) or shSLC26A9 (right). **(B, D)** Summary of data in (A, C), respectively, where knockdown efficiencies (shown in percentages above bars) were determined by comparing the mRNA levels of SLC26A9 normalized to GAPDH mRNA in the shRNA transfected cells with those in cells transfected with the control shRNA (shLuciferase). Data are presented as mean ± SEM (n = 3).

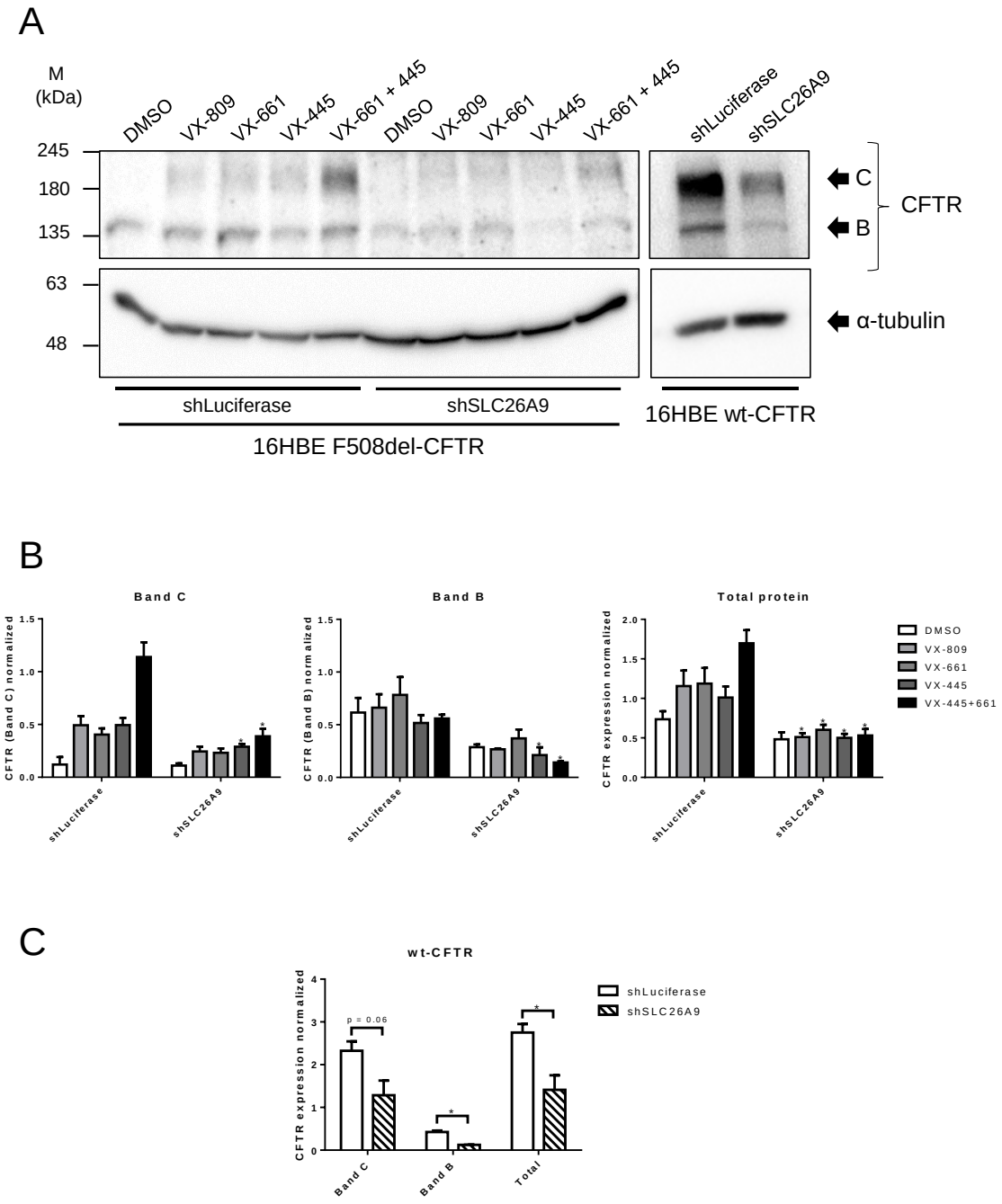

Figure S 27 – SLC26A9 knockdown lowers both wt- and F508del-CFTR expression in 16HBE cells. (A) Western Blot showing CFTR expression changes due to SLC26A9 knockdown in the presence or absence of different CFTR correctors (VX-809, VX-661, VX-445 or the combination VX-661+VX-445). α-tubulin was used as a loading control. **(B)** Quantification of F508del-CFTR protein expression obtained in (A), with SLC26A9 knockdown and in the presence of different correctors. From left to right: Band C – fully glycosylated CFTR; Band B – core-glycosylated CFTR; and total protein expression. **(C)** Quantification of wt-CFTR total protein expression, as well as band B and C, in cells transfected with shSLC26A9. Data are normalized to the loading control and presented as mean ± SEM (n = 3). (*) indicates statistical significance when comparing the same treatment in the presence or absence of shSLC26A9 (unpaired t-test, $p < 0.05$).

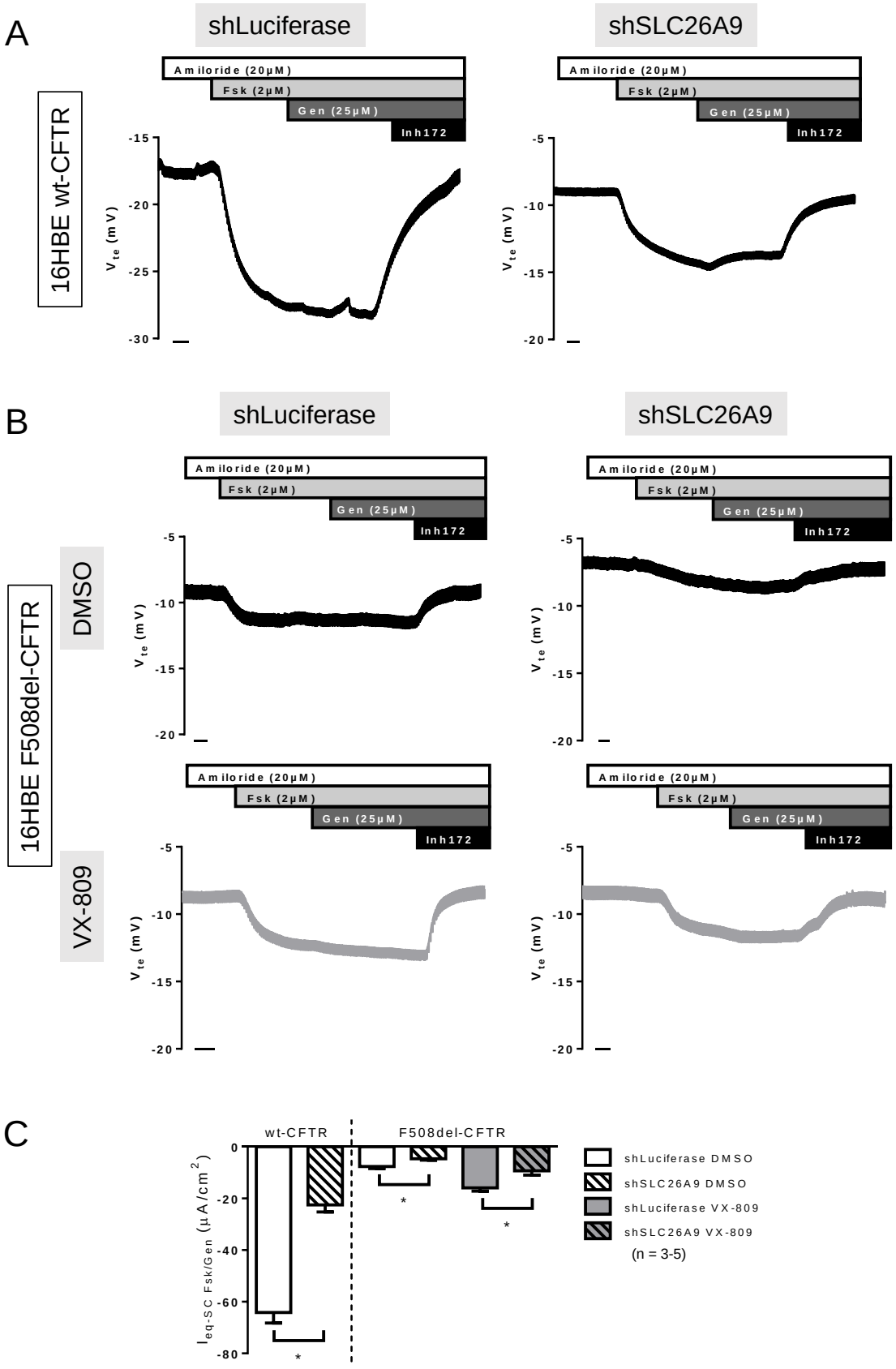

Figure S 28 – SLC26A9 knockdown inhibits endogenous wt-CFTR function and the correction of F508del-CFTR by VX-809 in 16HBE cells. (A) Original Ussing chamber tracings obtained for 16HBE wt-CFTR cells transduced with the control shRNA shLuciferase (left) or shSLC26A9 (right). CFTR was activated by 2 µM Forskolin (Fsk) and 25 µM Genistein (Gen) in the presence of the epithelial sodium channel (ENaC)

inhibitor (Amiloride 20 µM) and was inhibited by CFTR-inhibitor 172 (30 µM) added to the luminal side. **(B)** Original Ussing chamber tracings obtained for cAMP-induced Cl^- currents activated and inhibited as in (A) in the absence (top tracings, black) or in the presence (lower tracings, grey) of 3 µM VX-809 for 16HBE F508del-CFTR cells transfected with shLuciferase (left) or shSLC26A9 (right); **(C)** Summary of $I_{sc\text{-}eq}$ currents of 16HBE wt-/F508del-CFTR transfected with shLuciferase vs shSLC26A9 and treated with DMSO vs VX-809. Data are represented by mean ± SEM and "*" indicates statistically significant differences (unpaired t-test, $p < 0.05$). The number of filters (n) used in the statistical analyses is indicated in the graph. Scale bars in (A) and (B) represent 1 min. Data in collaboration with Iris Silva.

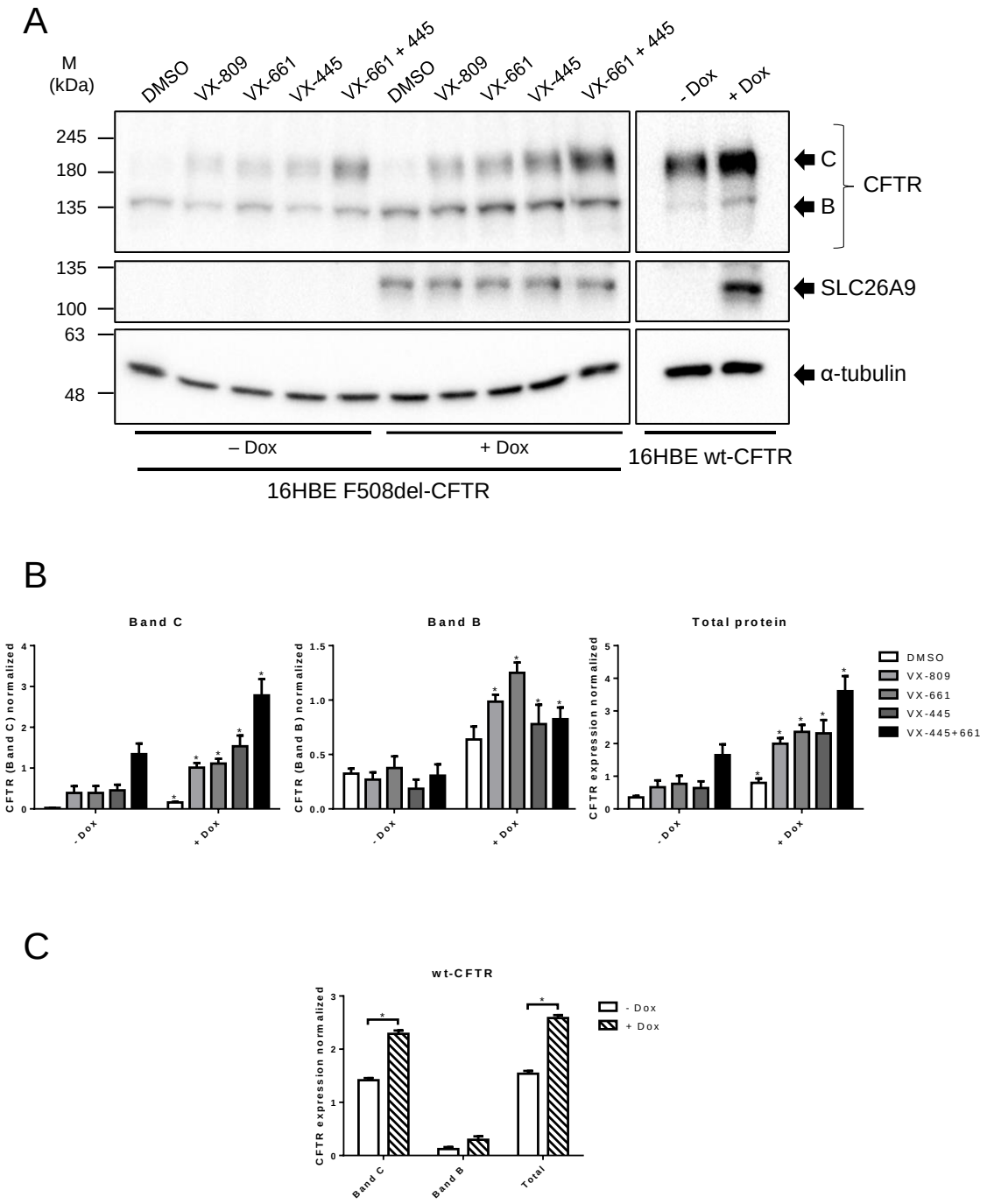

Figure S 29 – SLC26A9 overexpression increases both wt- and F508del-CFTR expression in 16HBE cells. (A) Western Blot showing CFTR expression changes due to SLC26A9 overexpression in the presence or absence of different CFTR correctors (VX-809, VX-661, VX-445 or the combination VX-661+VX-445). α-

tubulin was used as a loading control. **(B)** Quantification of F508del-CFTR protein expression obtained in (A), with and without SLC26A9 overexpression (+ Dox, and - Dox, respectively) and in the presence of different correctors. From left to right: Band C, Band B, and total protein expression. **(C)** Quantification of wt-CFTR expression in cells transfected with SLC26A9 under an inducible promoter. Data are normalized to the loading control and presented as mean ± SEM (n = 3). (*) indicates statistical significance when comparing the same treatment in the presence or absence of Dox (unpaired t-test, $p < 0.05$).

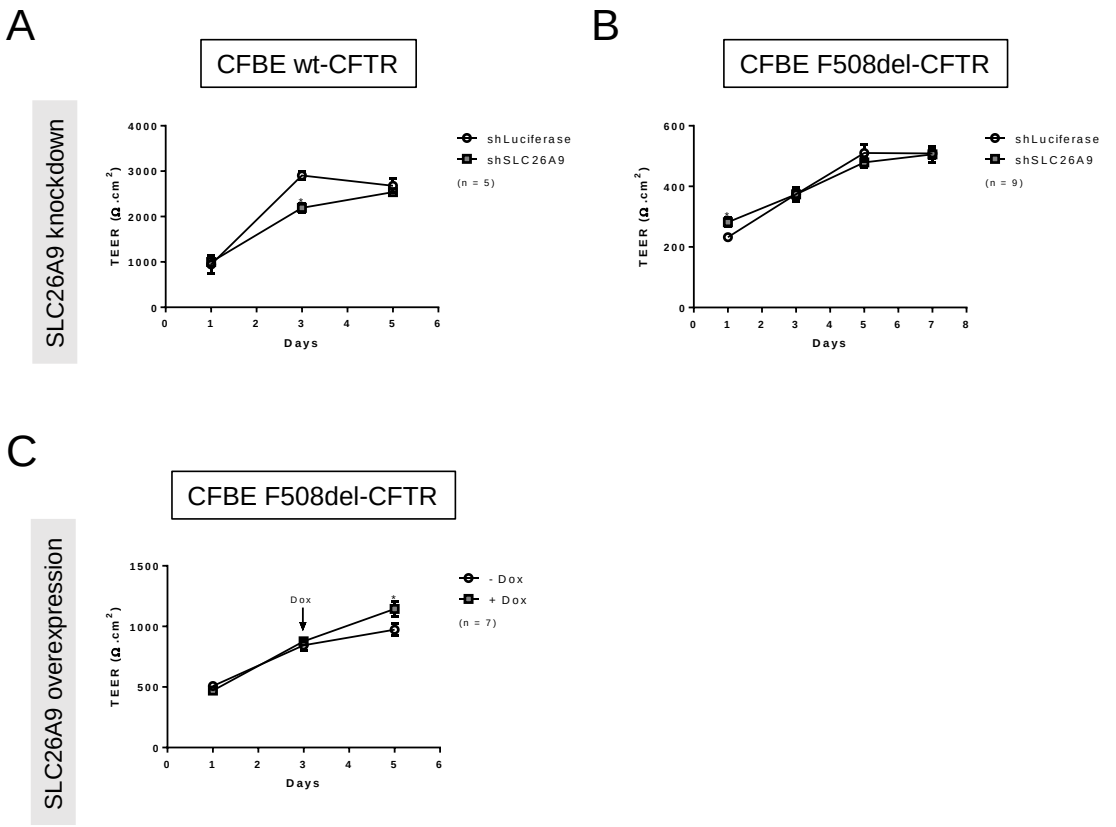

Figure S 30 – SLC26A9 expression levels affect the polarization of CFBE cells. Transepithelial resistance (TEER) measurements of CFBE cells with different levels of SLC26A9 expression over 5 to 7 days in liquid-liquid interface (LLI). TEER of CFBE wt-CFTR **(A)** or CFBE F508del-CFTR **(B)** stably expressing shLuc (control) vs shSLC26A9. **(C)** TEER of SLC26A9 overexpressing CFBE F508del-CFTR cells in the presence or absence of Dox. (*) indicates significant difference (unpaired t-test, $p < 0.05$). The number of filters used in the statistical analyses is indicated in each graph.

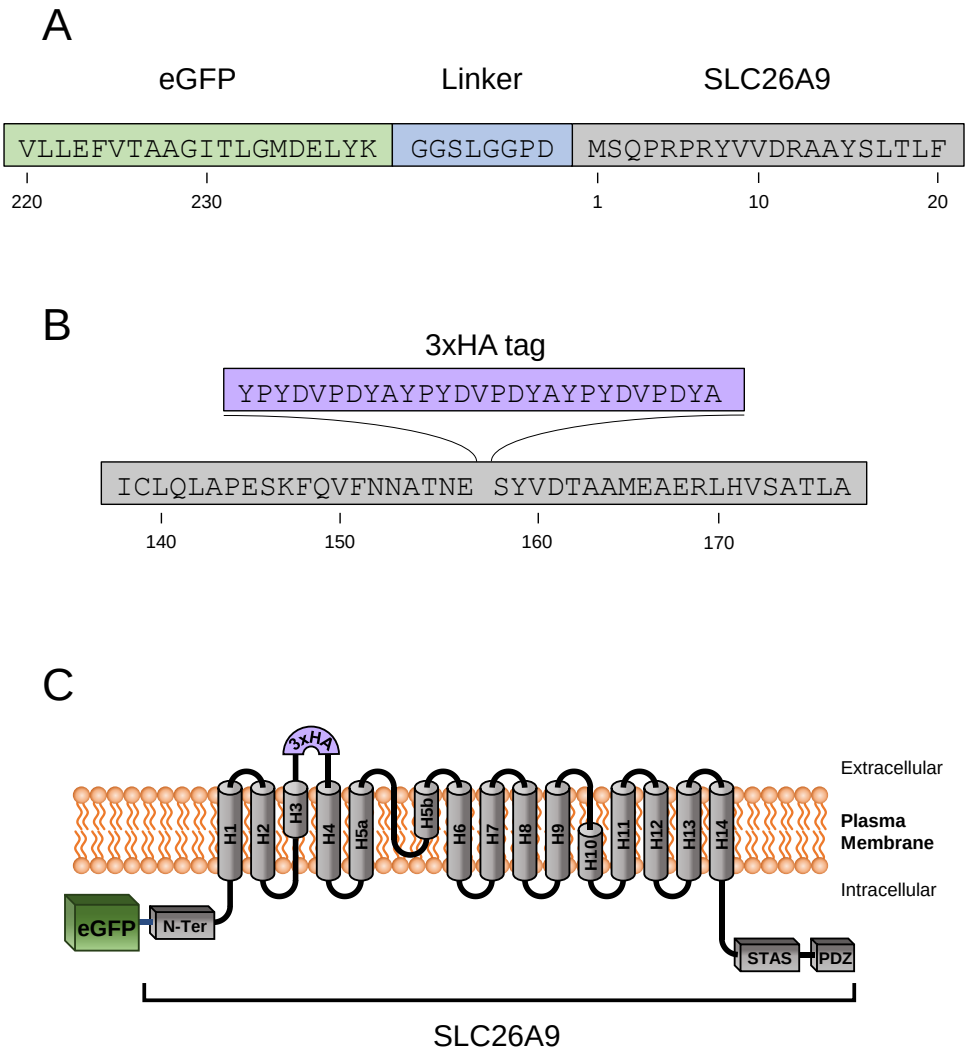

Figure S 31 – The eGFP-3HA-SLC26A9 traffic reporter construct. (A) Amino acid sequence of eGFP-3HA-SLC26A9, showing the linker (light blue shadow) connecting eGFP (light green shadow) and SLC26A9 (light grey shadow). **(B)** SLC26A9 amino acid sequence (light grey shadow) showing the insertion of the 3HA peptide (light purple shadow) between Glu^{157} and Ser^{158}. The numbering corresponds to human SLC26A9 isoform a (NCBI Reference Sequence: NP_443166.1). **(C)** Topology of the eGFP-3HA-SLC26A9 construct, showing the location of the 3xHA tag on the second extracellular loop, which is exposed to the extracellular environment when the construct is embedded in the plasma membrane. Data in collaboration with Hugo Botelho.

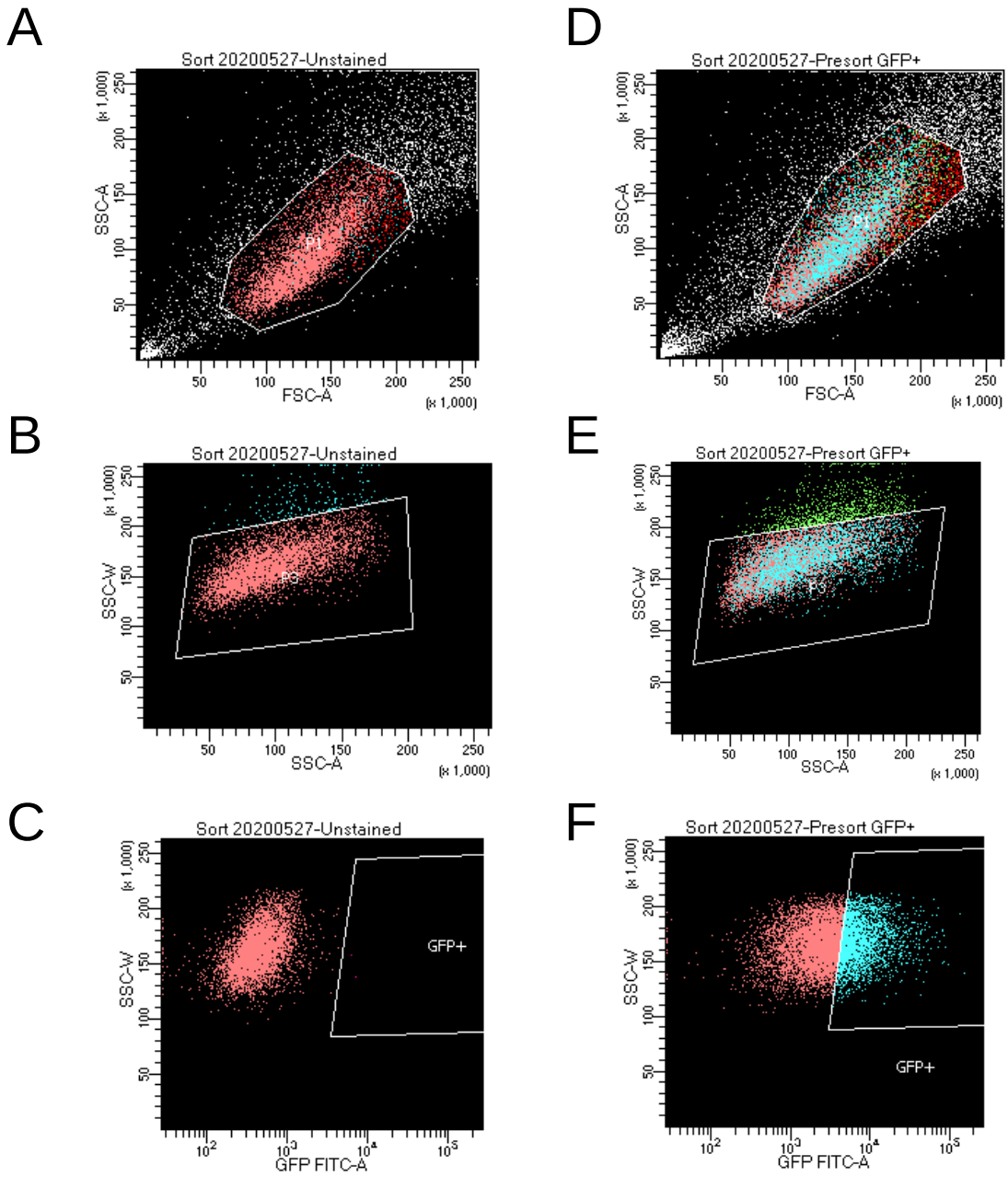

Figure S 32 – Fluorescence-activated cell sorting (FACS) of CFBE eGFP-3HA-SLC26A9 cells. CFBE cells induced with Dox to express the eGFP-3HA-SLC26A9 construct (D-F) were sorted by FACS using non-induced cells (-Dox) (A-C) as controls to set the gating parameters. Among the induced cells only the ones with the highest SLC26A9 expression (eGFP fluorescence) were selected. **(A,D)** Selection of relevant and living cells in region P1 by the area of the side scatter (SSC-Area) and the area of the forward scatter (FSC-Area). **(B,E)** Discrimination of single cells from aggregates in region P3 by SSC-Height and SSC-Area. **(F)** Selection of eGFP-positive cells with the highest GFP fluorescence, using **(C)** as a control (auto-fluorescence of non-induced cells). Experiments were performed using a BD FACSAria III (IMM Lisboa). Scale in arbitrary units provided by the instrument.

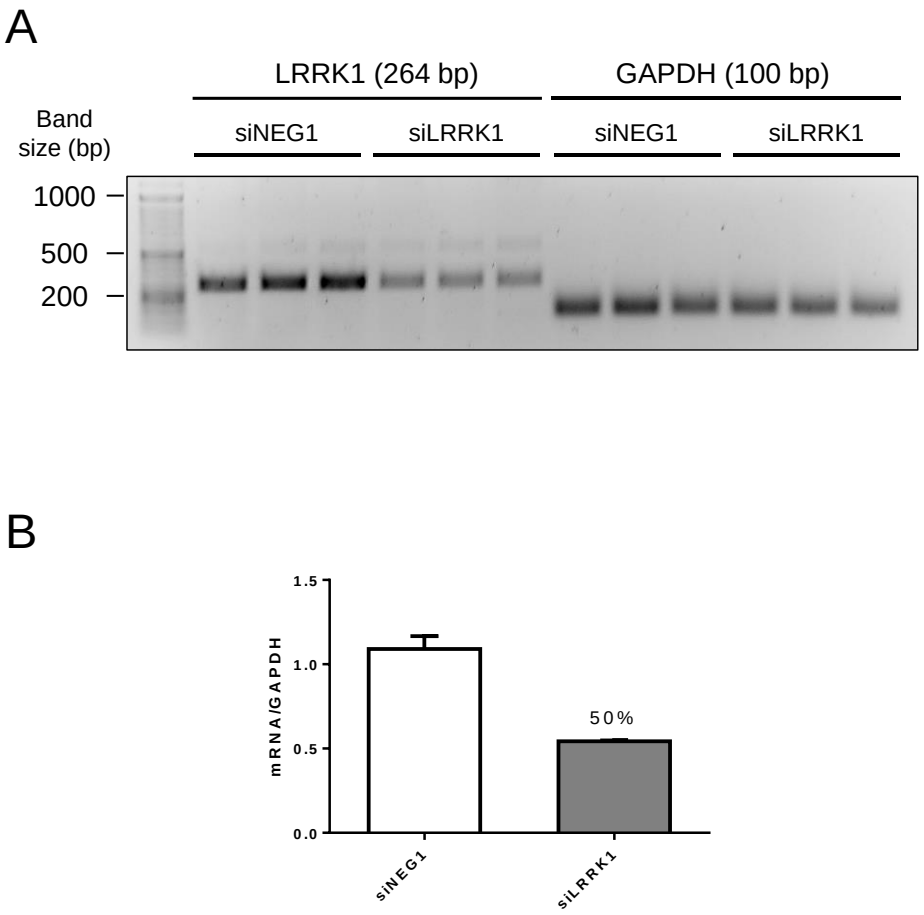

Figure S 33 – Quantification of LRRK1 knockdown by semi-quantitative PCR. (A) Agarose gel showing a decrease in LRRK1 mRNA when transfected with siLRRK1 vs siNEG1 (negative control). **(B)** Quantification of LRRK1 knockdown from the samples in (A), normalized to GAPDH.

Appendix 4 – Antibodies, dyes, siRNAs, and primers

Table S 1 – Antibodies used for Western Blot/Chemiluminescence.

Type of Antibody	Antigen	Host	Cat.No. (Brand)	Application (Dilution)
Primary Antibodies	ADRA2C	Mouse	ab167433 (Abcam)	WB (1:500)
	α-tubulin	Mouse	T5168 (Sigma-Aldrich)	WB (1:3000)
	β-actin	Rabbit	A2066 (Sigma-Aldrich)	WB (1:10000)
	Calnexin	Mouse	610523 (BD Transduction Laboratories)	WB (1:3000)
	CFTR	Mouse	#596, kindly provided by the North American CF foundation	WB (1:3000)
	CSNK2A2 (CK2α')	Mouse	sc-514403 (SantaCruz)	WB (1:1000)
	CXCR3	Mouse	sc-137140 (SantaCruz)	WB (1:500)
	DOG1 (TMEM16A)	Rabbit	NP060513 (Novus Biologicals)	WB (1:500)
	EGFR	Rabbit	sc-03 (SantaCruz)	WB (1:1000)
	$P2Y_2R$	Mouse	sc-518019 (SantaCruz)	WB (1:1000)
	SLC26A9	Mouse	H00115019-MO2 (BioTechne)	WB (1:250)
	SLC26A9	Rabbit	NBP2-30425 (BioTechne)	WB (1:250)
	TMEM16A	Rabbit	ab64085 (Abcam)	WB (1:500)
	TMEM16F	Rabbit	Davids Biotechnology, Germany	WB (1:1000)
HRP-Conjugated Antibodies	Anti-FLAG M2-Peroxidase	Mouse	A8592 (Sigma-Aldrich)	Chemi-luminescence (1:1000)
Secondary Antibodies	Anti-mouse IgG – HRP conjugated	Goat	170-6516 (Bio-Rad)	WB (1:3000)
	Anti-rabbit IgG – HRP conjugated	Goat	170-6515 (Bio-Rad)	WB (1:3000)

Table S 2 – Antibodies used for Immunofluorescence.

Type of Antibody	Antigen	Host	Cat.No. (Brand)	Application (Dilution)
Primary Antibodies	CFTR	Mouse	#570, kindly provided by the North American CF foundation	IF (1:200)
	DOG1 (TMEM16A)	Rabbit	NP060513 (Novus Biologicals)	IF (1:100)
	EPAC1	Mouse	sc-28366 (SantaCruz)	IF (1:100)
	HA	Mouse	901502 (Biolegend)	IF (1:200)
	Na^+/K^+ ATPase	Mouse	sc-48345 (SantaCruz)	IF (1:200)
	$P2Y_2R$	Mouse	sc-518019 (SantaCruz)	IF (1:100)
	SLC26A9	Rabbit	NBP2-30425 (BioTechne)	IF (1:100)
	TMEM16F	Rabbit	Davids Biotechnology, Germany	IF (1:100)
	ZO-1	Mouse	33-9100 (Invitrogen)	IF (1:200)
Secondary Antibodies	Anti-mouse Alexa Fluor 488	Donkey	A-21202 (Invitrogen)	IF (1:500)
	Anti-rabbit Alexa Fluor 488	Donkey	A-21206 (Invitrogen)	IF (1:500)
	Anti-mouse Alexa Fluor 546	Donkey	A-10036 (Invitrogen)	IF (1:500)
	Anti-mouse Alexa Fluor 647	Donkey	A-31571 (Invitrogen)	IF (1:500)

Table S 3 – Dyes used for nuclear staining, staining of dead cells, and measurements of cell proliferation by absorbance.

Dye	Cat.No. (Brand)	Final Concentration
Hoechst 33342 Solution	B2261 (Sigma-Aldrich)	200 ng/mL
3-(4,5-Dimethylthiazol-2-Yl)-2,5-Diphenyl-2h-Tetrazolium Bromide (MTT)	M2128 (Sigma-Aldrich)	0.5 mg/mL
Propidium Iodide	P4170 (Sigma-Aldrich)	1 µg/mL

Table S 4 – Primers used for semi-quantitative RT-PCR.

Target	Primer sequence	PCR Product
ADCY1	FW: 5’ – GTATTCTGCATCTGCTTCCTG – 3’ RV: 5’ – GAGAAGAGCAGGATGGCCAC – 3’	461 bp
ADCY3	FW: 5’ – GTGGAGAAGGAGAAGCAGAG – 3’ RV: 5’ – CATCAAAGACGGGACGCCAG – 3’	526 bp
ADCY8	FW: 5’ – GTCCTCATCACCACAGCAGA – 3’ RV: 5’ – ACACAGCCAGGAGGAACATG – 3’	472 bp
ADCY10	FW: 5’ – CAAGACAAAGCAGAAGAGATAG – 3’ RV: 5’ – CTCATACATTAAGACTTGGCTG – 3’	636 bp
ADRA2C	FW: 5’ – CGAGCTCATGGCCTACTGG – 3’ RV: 5’ – CCCAGCCCGTTTTCGGTAG – 3’	462 bp
CFTR	FW: 5’ – CATCTTTGGTGTTTCCTATG – 3’ RV: 5’ – GGAGTCTTTTGCACAATGG – 3’	636 bp
COPB1	FW: 5’ – CTCCAGATGGGAGACTTTTAC – 3’ RV: 5’ – GGTGCACTAGAGAGTGTCAC – 3’	559 bp
CSNK2A2 (CK2α’)	FW: 5’ – AAGATGATTACCAACTGGTTCG – 3’ RV: 5’ – AGTCGCAGCTTTTTCTGTTGG – 3’	411 bp
CXCR3	FW: 5’ – CCACCTAGCTGTAGCAGACAC – 3’ RV: 5’ – GCAGTAGGCCATGACCAGC – 3’	424 bp
DRD1	FW: 5’ – TGCTGCCGTTATCAGGTTCC – 3’ RV: 5’ – GTCACAGTTGTCTATGGTCTCAG – 3’	427 bp
EPAC1	FW: 5’ – GCGGCTGTTCTGCTCTTTG – 3’ RV: 5’ – GTCATGAGCACTGGAATCTG – 3’	465 bp
ESYT1	FW: 5’ – GCCACAGCTACAGCCACAG – 3’ RV: 5’ – GGTCTGTCTCAGCTAGGTCC – 3’	483 bp
ESYT2	FW: 5’ – CTAACAGACATCAAAGCTGAC – 3’ RV: 5’ – GATGTTTTCCTCCCCTCTTTG – 3’	500 bp
ESYT3	FW: 5’ – GAAGGGGCTGGATCTGACC – 3’ RV: 5’ – CGAGAATGGCAGTGGAAAGG – 3’	467 bp

GAPDH	FW.1: 5’ – GTATTGGGCGCCTGGTCAC – 3’ RV.1: 5’ – CTCCTGGAAGATGGTGATGG – 3’	200 bp
	FW.2: 5’ – ATGGGGAAGGTGAAGGTCG – 3’ RV.2: 5’ – GGGGTCATTGATGGCAACAATA – 3’	110 bp
LRRK1	FW: 5’ – CTGGCCTACCTGCACAAGAA – 3’ RV: 5’ – CTGTCCTGACAGCAACTCGT – 3’	264 bp
LTB4R	FW: 5’ – AGCTTTGTGGTGTGGAGTATCC – 3’ RV: 5’ – CGCCCTATGTCCGAGTAGC – 3’	509 bp
P2Y2R	FW: 5’ – GGCCCCTGGAATGACACC – 3’ RV: 5’ – CTGGTGGTGACAAAGTAGAG – 3’	509 bp
PFKFB4	FW: 5’ – TCCCCACGGGAATTGACAC – 3’ RV: 5’ – GACTCGTAGGAGTTCTCATAGCA – 3’	605 bp
PRKACB	FW: 5’ – CCCTTGGAACAGGTTCATTTGG – 3’ RV: 5’ – GTCTGTGACCTGGATATAGCCTT – 3’	410 bp
SLC26A9	FW: 5’ – CTGGCCCCAGAGTCGAAATTC – 3’ RV: 5’ – CTTGAGCACCGAAATCAGGAT – 3’	240 bp
TMEM16A	FW: 5’ – CGACTACGTGTACATTTTCCG – 3’ RV: 5’ – GATTCCGATGTCTTTGGCTC – 3’	445 bp
TMEM16F	FW: 5’ – GTATTTGTAAAAGTACACGCACC – 3’ RV: 5’ – GAGGATGAGCCCATTCTCTG – 3’	463 bp

Table S 5 – Primers used for TMEM16A sequencing (plasmids).

Primer Name	Primer Sequence
CMV-F	FW: 5’ – CGCAAATGGGCGGTAGGCGTG – 3’
ANO1_seq1	FW: 5’ – GTGGCTGAGCACAGGC – 3’
ANO1_ seq2	FW: 5’ – CTTCATGGAGCACTGG – 3’
ANO1_ seq3	FW: 5’ – CTGAAGCTGAAGCAGC – 3’
ANO1_ seq4	FW: 5’ – CATGCGGGAGGAGC – 3’

Table S 6 – Primers used for TMEM16A/SLC26A9 mutagenesis and cloning.

Application	Primer Sequence
3HA Insertion TMEM16A	5’ – CCCAGCATGGAGATGTGTGACCAGAGACACTACCCATACGATGTTCCAGATTACGCTTACCCATACGATGTTCCAGATTACGCTTACCCATACGATGTTCCAGATTACGCTAATATTACCATGTGCCCGCTTTGCGACAAGACC – 3’
3HA Insertion SLC26A9	5’ – CTTCAACAATGCCACCAATGAGTACCCATACGATGTTCCAGATTACGCTTACCCATACGATGTTCCAGATTACGCTTACCCATACGATGTTCCAGATTACGCTAGCTATGTGGACACAGCAGCCATG – 3’

Cloning TMEM16A into pLVX-TRE3G	FW: 5’ – TCTTATACTTGGATCCATGAGGGTCAACGAGAAGTACTCG – 3’ RV: 5’ – ATTCCATATGACGCGTTTACTTGTACAGCTCGTCCATGCC – 3’

Table S 7 – siRNAs used for liquid transfections.

Target	siRNA No.	Sense sequence (5’ → 3’)
ADRA2C	s194275 s194276	CCUCGUCGAUCGUGCAUCUtt GCAUCUACCGAGUGGCCAAtt
CFTR	s2947	GCAUAGAUGUGGAUAGCUUtt
COPB1	s3371	GGUCUGUCAUGCUAAUCCAtt
COPZ1	s22428	GCCUGACAGUGGUAUACAAtt
CSNK2A2 (CK2α')	s3640	GAUCCACACUUCAACGAUAtt
CXCR3	s6013 s6014	GACUAUGGAGAAAACGAGAtt GCUUUGACCGCUACCUGAAtt
DRD1	s4281 s4282	GGACCUUGUCUGUACUCAUtt CCCUAUCAGUCAUAUUGGAtt
ESYT1	s23605 s23606 s23607	GGACUUGAACAUCAGCUAUtt CCAUGAUCAUGGACUCCAUtt GGGAAGGUGUUACAGGCUAtt
ESYT2	s33137	GCACCUUUAGUUUCACGAAtt
ESYT3	s38210	CGAAUUCCUUGACAAUGAAtt
LRRK1	s36138	GGCCUCGCAUUGUAUAUGAtt
LTB4R	s194337 s194338	GCUUUGUGGUGUGGAGUAUtt UCACGGCCAUGAGUCUAGAtt
NEG1	s813	UAACGACGCGACGACGUAAtt
P2RY2	HSS143206	UAACCUUGUAGGCCAUGUUGAUGGC GCCAUCAACAUGGCCUACAAGGUUA
PFKFB4	s10361 s10362	GUAUAUUACCUCAUGAACAtt GGAGAGCGACCAUCUUUAAtt
PRKACB	s11068 s11070	GCUAUAUCCAGGUCACAGAtt CGAGUACCUCCAUUCACUAtt
Scrbld	s229174	UUCUCCGAACGUGUCACGUtt

SLC26A9	s41749 s41751	GCACGUCUUUCCCAGCAUAtt UGAUUUCGGUGCUCAAGUAtt
TMEM16A	s30184 HSS182856	GGAGCACGAUUGUCUAUGAtt GGUUCCCAGCCUACCUCACUAACUU
TMEM16F	s225826 HSS153251	GGAUCAACAGACUUGUAAAtt CCUCCAUCAUCAGCUUUAUAAUUAU

Appendix 5 – TMEM16A and SLC26A9 traffic screen data

Table S 8 – TMEM16A traffic enhancer siRNAs.

Ensembl ID (v. 92)	siRNA IDs	Targeted gene	Average PM score	Targeted gene name	Function of targeted gene
ENSG00000111481	s22428	COPZ1	5.176085973	coatomer protein complex subunit zeta 1	The coatomer is a cytosolic protein complex that binds to dilysine motifs and reversibly associates with Golgi non- clathrin-coated vesicles, which further mediate biosynthetic protein transport from the ER, via the Golgi up to the trans Golgi network. Coatomer complex is required for budding from Golgi membranes, and is essential for the retrograde Golgi-to-ER transport of dilysine-tagged proteins. In mammals, the coatomer can only be recruited by membranes associated to ADP-ribosylation factors (ARFs), which are small GTP-binding proteins; the complex also influences the Golgi structural integrity, as well as the processing, activity, and endocytic recycling of LDL receptors (By similarity). The zeta subunit may be involved in regulating the coat assembly and, hence, the rate of biosynthetic protein transport due to its association-dissociation properties with the coatomer complex.
ENSG00000204611	s40325	ZNF616	4.73506243	zinc finger protein 616	May be involved in transcriptional regulation.
ENSG00000163884	s26387	KLF15	3.877581294	Kruppel like factor 15	Transcriptional regulator that binds to the GA element of the CLCNKA promoter. Binds to the KCNIP2 promoter and regulates KCNIP2 circadian expression in the heart (By similarity). Is a repressor of CTGF expression, involved in the control of cardiac fibrosis. It is also involved in the control of cardiac hypertrophy acting through the inhibition of MEF2A and GATA4 (By similarity). Involved in podocyte differentiation (By similarity). Inhibits MYOCD activity. Is a negative regulator of TP53 acetylation. Inhibits NF-kappa-B activation through repression of EP300-dependent RELA acetylation.
ENSG00000159346	s27411	ADIPOR1	3.789358726	adiponectin receptor 1	Receptor for ADIPOQ, an essential hormone secreted by adipocytes that regulates glucose and lipid metabolism 25855295, PubMed:12802337). Required for normal glucose and fat homeostasis and for maintaining a normal body weight. ADIPOQ-binding activates a signaling cascade that leads to increased AMPK activity, and ultimately to increased fatty acid oxidation, increased glucose uptake and decreased gluconeogenesis. Has high affinity for globular adiponectin and low affinity for full-length adiponectin (By similarity).
ENSG00000120322	s31952	PCDHB8	3.500763927	protocadherin beta 8	Calcium-dependent cell-adhesion protein involved in cells self-recognition and non-self discrimination. Thereby, it is involved in the establishment and maintenance of specific neuronal connections in the brain.
ENSG00000146950	s1513	SHROOM2	3.480774717	shroom family member 2	May be involved in endothelial cell morphology changes during cell spreading. In the retinal pigment epithelium, may regulate the biogenesis of melanosomes and promote their association with the apical cell surface by inducing gamma-tubulin redistribution (By similarity).

Ensembl ID (v. 92)	siRNA IDs	Targeted gene	Average PM score	Targeted gene name	Function of targeted gene
ENSG00000134569	s8287	LRP4	3.344527228	LDL receptor related protein 4	Mediates SOST-dependent inhibition of bone formation. Functions as a specific facilitator of SOST-mediated inhibition of Wnt signaling. Plays a key role in the formation and the maintenance of the neuromuscular junction (NMJ), the synapse between motor neuron and skeletal muscle. Directly binds AGRIN and recruits it to the MUSK signaling complex. Mediates the AGRIN- induced phosphorylation of MUSK, the kinase of the complex. The activation of MUSK in myotubes induces the formation of NMJ by regulating different processes including the transcription of specific genes and the clustering of AChR in the postsynaptic membrane. Alternatively, may be involved in the negative regulation of the canonical Wnt signaling pathway, being able to antagonize the LRP6-mediated activation of this pathway. More generally, has been proposed to function as a cell surface endocytic receptor binding and internalizing extracellular ligands for degradation by lysosomes. May play an essential role in the process of digit differentiation (By similarity).
ENSG00000128683	s5521	GAD1	3.15455757	glutamate decarboxylase 1	Catalyzes the production of GABA.
ENSG00000180269	s42721	GPR139	3.115286985	G protein-coupled receptor 139	Orphan receptor. Seems to act through a G(q/11)-mediated pathway.
ENSG00000166603	s8566	MC4R	3.022686802	melanocortin 4 receptor	Receptor specific to the heptapeptide core common to adrenocorticotropic hormone and alpha-, beta-, and gamma-MSH. Plays a central role in energy homeostasis and somatic growth. This receptor is mediated by G proteins that stimulate adenylate cyclase (cAMP).
ENSG00000198478	s38125	SH3BGRL2	2.981059133	SH3 domain binding glutamate rich protein like 2	Gene Ontology (GO) annotations related to this gene include SH3 domain binding and protein disulfide oxidoreductase activity. An important paralog of this gene is SH3BGR.

Ensembl ID (v. 92)	siRNA IDs	Targeted gene	Average PM score	Targeted gene name	Function of targeted gene
ENSG00000129083	s3371	COPB1	2.942563197	coatomer protein complex subunit beta 1	The coatomer is a cytosolic protein complex that binds to dilysine motifs and reversibly associates with Golgi non- clathrin-coated vesicles, which further mediate biosynthetic protein transport from the ER, via the Golgi up to the trans Golgi network. Coatomer complex is required for budding from Golgi membranes, and is essential for the retrograde Golgi-to-ER transport of dilysine-tagged proteins. In mammals, the coatomer can only be recruited by membranes associated to ADP-ribosylation factors (ARFs), which are small GTP-binding proteins; the complex also influences the Golgi structural integrity, as well as the processing, activity, and endocytic recycling of LDL receptors. Plays a functional role in facilitating the transport of kappa-type opioid receptor mRNAs into axons and enhances translation of these proteins. Required for limiting lipid storage in lipid droplets. Involved in lipid homeostasis by regulating the presence of perilipin family members PLIN2 and PLIN3 at the lipid droplet surface and promoting the association of adipocyte surface triglyceride lipase (PNPLA2) with the lipid droplet to mediate lipolysis (By similarity). Involved in the Golgi disassembly and reassembly processes during cell cycle. Involved in autophagy by playing a role in early endosome function. Plays a role in organellar compartmentalization of secretory compartments including endoplasmic reticulum (ER)-Golgi intermediate compartment (ERGIC), Golgi, trans-Golgi network (TGN) and recycling endosomes, and in biosynthetic transport of CAV1. Promotes degradation of Nef cellular targets CD4 and MHC class I antigens by facilitating their trafficking to degradative compartments.
ENSG00000167306	s9209	MYO5B	2.80603761	myosin VB	May be involved in vesicular trafficking via its association with the CART complex. The CART complex is necessary for efficient transferrin receptor recycling but not for EGFR degradation. Required in a complex with RAB11A and RAB11FIP2 for the transport of NPC1L1 to the plasma membrane. Together with RAB11A participates in CFTR trafficking to the plasma membrane and TF (transferrin) recycling in nonpolarized cells. Together with RAB11A and RAB8A participates in epithelial cell polarization. Together with RAB25 regulates transcytosis.

Ensembl ID (v. 92)	siRNA IDs	Targeted gene	Average PM score	Targeted gene name	Function of targeted gene
ENSG00000173083	s21305	HPSE	2.765740832	heparanase	Endoglycosidase that cleaves heparan sulfate proteoglycans (HSPGs) into heparan sulfate side chains and core proteoglycans. Participates in extracellular matrix (ECM) degradation and remodeling. Selectively cleaves the linkage between a glucuronic acid unit and an N-sulfo glucosamine unit carrying either a 3-O-sulfo or a 6-O-sulfo group. Can also cleave the linkage between a glucuronic acid unit and an N-sulfo glucosamine unit carrying a 2-O-sulfo group, but not linkages between a glucuronic acid unit and a 2-O-sulfated iduronic acid moiety. It is essentially inactive at neutral pH but becomes active under acidic conditions such as during tumor invasion and in inflammatory processes. Facilitates cell migration associated with metastasis, wound healing and inflammation. Enhances shedding of syndecans, and increases endothelial invasion and angiogenesis in myelomas. Acts as procoagulant by increasing the generation of activation factor X in the presence of tissue factor and activation factor VII. Increases cell adhesion to the extracellular matrix (ECM), independent of its enzymatic activity. Induces AKT1/PKB phosphorylation via lipid rafts increasing cell mobility and invasion. Heparin increases this AKT1/PKB activation. Regulates osteogenesis. Enhances angiogenesis through up- regulation of SRC-mediated activation of VEGF. Implicated in hair follicle inner root sheath differentiation and hair homeostasis.
ENSG00000120949	s2630	TNFRSF8	2.587751249	TNF receptor superfamily member 8	Receptor for TNFSF8/CD30L. May play a role in the regulation of cellular growth and transformation of activated lymphoblasts. Regulates gene expression through activation of NF-kappa-B.
ENSG00000185483	s9755	ROR1	2.571446929	receptor tyrosine kinase like orphan receptor 1	Has very low kinase activity in vitro and is unlikely to function as a tyrosine kinase in vivo. Receptor for ligand WNT5A which activate downstream NFkB signaling pathway and may result in the inhibition of WNT3A-mediated signaling. In inner ear, crucial for spiral ganglion neurons to innervate auditory hair cells.
ENSG00000069974	s11693	RAB27A	2.533893429	RAB27A, member RAS oncogene family	Plays a role in cytotoxic granule exocytosis in lymphocytes. Required for both granule maturation and granule docking and priming at the immunologic synapse.
ENSG00000184845	s4282	DRD1	2.512901229	dopamine receptor D1	Dopamine receptor whose activity is mediated by G proteins which activate adenylyl cyclase.
ENSG00000117906	s11887	RCN2	2.490244952	reticulocalbin 2	Not known. Binds calcium.
ENSG00000171408	s25844	PDE7B	2.479649382	phosphodiesterase 7B	Hydrolyzes the second messenger cAMP, which is a key regulator of many important physiological processes. May be involved in the control of cAMP-mediated neural activity and cAMP metabolism in the brain.
ENSG00000128881	s44814	TTBK2	2.395681767	tau tubulin kinase 2	Serine/threonine kinase that acts as a key regulator of ciliogenesis: controls the initiation of ciliogenesis by binding to the distal end of the basal body and promoting the removal of CCP110, which caps the mother centriole, leading to the recruitment of IFT proteins, which build the ciliary axoneme. Has some substrate preference for proteins that are already phosphorylated on a Tyr residue at the +2 position relative to the phosphorylation site. Able to phosphorylate tau on serines in vitro.
ENSG00000029559	s7081	IBSP	2.393689107	integrin binding sialoprotein	Binds tightly to hydroxyapatite. Appears to form an integral part of the mineralized matrix. Probably important to cell-matrix interaction. Promotes Arg-Gly-Asp-dependent cell attachment.

Ensembl ID (v. 92)	siRNA IDs	Targeted gene	Average PM score	Targeted gene name	Function of targeted gene
ENSG00000165804	s27703	ZNF219	2.385127142	zinc finger protein 219	Transcriptional regulator. Recognizes and binds 2 copies of the core DNA sequence motif 5'-GGGGG-3'. Binds to the HMGN1 promoter and may repress HMGN1 expression. Regulates SNCA expression in primary cortical neurons. Binds to the COL2A1 promoter and activates COL2A1 expression, as part of a complex with SOX9 (By similarity). Plays a role in chondrocyte differentiation (By similarity).
ENSG00000115904	s13285	SOS1	2.352878528	SOS Ras/Rac guanine nucleotide exchange factor 1	Promotes the exchange of Ras-bound GDP by GTP. Probably by promoting Ras activation, regulates phosphorylation of MAP kinase MAPK3 in response to EGF. Catalytic component of a trimeric complex that participates in transduction of signals from Ras to Rac by promoting the Rac-specific guanine nucleotide exchange factor (GEF) activity (By similarity).
ENSG00000160683	s2003	CXCR5	2.349999904	C-X-C motif chemokine receptor 5	Cytokine receptor that binds to B-lymphocyte chemoattractant (BLC). Involved in B-cell migration into B-cell follicles of spleen and Peyer patches but not into those of mesenteric or peripheral lymph nodes. May have a regulatory function in Burkitt lymphoma (BL) lymphomagenesis and/or B-cell differentiation.
ENSG00000184160	s194275	ADRA2C	2.300936657	adrenoceptor alpha 2C	Alpha-2 adrenergic receptors mediate the catecholamine- induced inhibition of adenylate cyclase through the action of G proteins.
ENSG00000168702	s28716	LRP1B	2.290154461	LDL receptor related protein 1B	Potential cell surface proteins that bind and internalize ligands in the process of receptor-mediated endocytosis.
ENSG00000036054	s31476	TBC1D23	2.245511115	TBC1 domain family member 23	Putative Rab GTPase-activating protein which plays a role in vesicular trafficking. Involved in endosome-to-Golgi trafficking. Acts as a bridging protein by binding simultaneously to golgins, including GOLGA1 and GOLGA4, located at the trans-Golgi, and to the WASH complex, located on endosome-derived vesicles. Plays a role in brain development, including in cortical neuron positioning (By similarity). May also be important for neurite outgrowth, possibly through its involvement in membrane trafficking and cargo delivery, 2 processes that are essential for axonal and dendritic growth (By similarity). May act as a general inhibitor of innate immunity signaling, strongly inhibiting multiple TLR and dectin/CLEC7A-signaling pathways. Does not alter initial activation events, but instead affects maintenance of inflammatory gene expression several hours after bacterial lipopolysaccharide (LPS) challenge (By similarity).
ENSG00000214013	s5568	GANC	2.191845129	glucosidase alpha, neutral C	Has alpha-glucosidase activity.
ENSG00000184939	s44826	ZFP90	2.171505389	ZFP90 zinc finger protein	Inhibits the transcriptional repressor activity of REST by inhibiting its binding to DNA, thereby derepressing transcription of REST target genes. . Isoform 2: Acts as a bridge between FOXP3 and the corepressor TRIM28, and is required for the transcriptional repressor activity of FOXP3 in regulatory T-cells (Treg).

Ensembl ID (v. 92)	siRNA IDs	Targeted gene	Average PM score	Targeted gene name	Function of targeted gene
ENSG00000100714	s9033	MTHFD1	2.14214116	methylenetetrahydrofolate dehydrogenase, cyclohydrolase and formyltetrahydrofolate synthetase 1	Diseases associated with MTHFD1 include Neural Tube Defects, Folate-Sensitive and Combined Immunodeficiency And Megaloblastic Anemia With Or Without Hyperhomocysteinemia. Among its related pathways are One carbon pool by folate and histidine degradation. Gene Ontology (GO) annotations related to this gene include formate-tetrahydrofolate ligase activity and methylenetetrahydrofolate dehydrogenase (NADP+) activity. An important paralog of this gene is MTHFD1L.
ENSG00000141194	s25597	OR4D1	2.115962692	olfactory receptor family 4 subfamily D member 1	Odorant receptor.
ENSG00000128918	s16907	ALDH1A2	2.115319693	aldehyde dehydrogenase 1 family member A2	Recognizes as substrates free retinal and cellular retinol-binding protein-bound retinal. Does metabolize octanal and decanal but does not metabolize citral, benzaldehyde, acetaldehyde and propanal efficiently (By similarity).
ENSG00000143320	s3484; s3485	CRABP2	2.108555362	cellular retinoic acid binding protein 2	Transports retinoic acid to the nucleus. Regulates the access of retinoic acid to the nuclear retinoic acid receptors.
ENSG00000198033	s194842	TUBA3C	2.076979601	tubulin alpha 3c	Tubulin is the major constituent of microtubules. It binds two moles of GTP, one at an exchangeable site on the beta chain and one at a non-exchangeable site on the alpha chain.
ENSG00000179163	s5395	FUCA1	2.0680311	fucosidase, alpha-L- 1, tissue	Alpha-L-fucosidase is responsible for hydrolyzing the alpha-1,6-linked fucose joined to the reducing-end N- acetylglucosamine of the carbohydrate moieties of glycoproteins.
ENSG00000071909	s44292	MYO3B	2.067568664	myosin IIIB	Probable actin-based motor with a protein kinase activity. Required for normal cochlear hair bundle development and hearing. Plays an important role in the early steps of cochlear hair bundle morphogenesis. Influences the number and lengths of stereocilia to be produced and limits the growth of microvilli within the forming auditory hair bundles thereby contributing to the architecture of the hair bundle, including its staircase pattern. Involved in the elongation of actin in stereocilia tips by transporting the actin regulatory factor ESPN to the plus ends of actin filaments.
ENSG00000070831	s2765	CDC42	2.061026792	cell division cycle 42	Plasma membrane-associated small GTPase which cycles between an active GTP-bound and an inactive GDP-bound state. In active state binds to a variety of effector proteins to regulate cellular responses. Involved in epithelial cell polarization processes. Regulates the bipolar attachment of spindle microtubules to kinetochores before chromosome congression in metaphase. Plays a role in the extension and maintenance of the formation of thin, actin-rich surface projections called filopodia. Mediates CDC42-dependent cell migration. Required for DOCK10-mediated spine formation in Purkinje cells and hippocampal neurons. Facilitates filopodia formation upon DOCK11-activation (By similarity). Also plays a role in phagocytosis through organization of the F-actin cytoskeleton associated with forming phagocytic cups.

Ensembl ID (v. 92)	siRNA IDs	Targeted gene	Average PM score	Targeted gene name	Function of targeted gene
ENSG00000111432	s22128	FZD10	2.022552876	frizzled class receptor 10	Receptor for Wnt proteins. Functions in the canonical Wnt/beta-catenin signaling pathway (By similarity). The canonical Wnt/beta-catenin signaling pathway leads to the activation of disheveled proteins, inhibition of GSK-3 kinase, nuclear accumulation of beta-catenin and activation of Wnt target genes. A second signaling pathway involving PKC and calcium fluxes has been seen for some family members, but it is not yet clear if it represents a distinct pathway or if it can be integrated in the canonical pathway, as PKC seems to be required for Wnt-mediated inactivation of GSK-3 kinase. Both pathways seem to involve interactions with G-proteins. May be involved in transduction and intercellular transmission of polarity information during tissue morphogenesis and/or in differentiated tissues (Probable).
ENSG00000151846	s9986	PABPC3	2.016669732	poly(A) binding protein cytoplasmic 3	Binds the poly(A) tail of mRNA. May be involved in cytoplasmic regulatory processes of mRNA metabolism. Binds poly(A) with a slightly lower affinity as compared to PABPC1.
ENSG00000196411	s243	EPHB4	2.005984784	EPH receptor B4	Receptor tyrosine kinase which binds promiscuously transmembrane ephrin-B family ligands residing on adjacent cells, leading to contact-dependent bidirectional signaling into neighboring cells. The signaling pathway downstream of the receptor is referred to as forward signaling while the signaling pathway downstream of the ephrin ligand is referred to as reverse signaling. Together with its cognate ligand/functional ligand EFNB2 plays a central role in heart morphogenesis and angiogenesis through regulation of cell adhesion and cell migration. EPHB4-mediated forward signaling controls cellular repulsion and segregation form EFNB2-expressing cells. Plays also a role in postnatal blood vessel remodeling, morphogenesis and permeability and is thus important in the context of tumor angiogenesis.
ENSG00000153201	s11773	RANBP2	1.984863703	RAN binding protein 2	E3 SUMO-protein ligase which facilitates SUMO1 and SUMO2 conjugation by UBE2I. Involved in transport factor (Ran-GTP, karyopherin)-mediated protein import via the F-G repeat-containing domain which acts as a docking site for substrates. Binds single-stranded RNA (in vitro). May bind DNA. Component of the nuclear export pathway. Specific docking site for the nuclear export factor exportin-1. Sumoylates PML at 'Lys-490' which is essential for the proper assembly of PML-NB. Recruits BICD2 to the nuclear envelope and cytoplasmic stacks of nuclear pore complex known as annulate lamellae during G2 phase of cell cycle.
ENSG00000124788	s12489; s12490	ATXN1	1.974868471	ataxin 1	Chromatin-binding factor that repress Notch signaling in the absence of Notch intracellular domain by acting as a CBF1 corepressor. Binds to the HEY promoter and might assist, along with NCOR2, RBPJ-mediated repression. Binds RNA in vitro. May be involved in RNA metabolism. In concert with CIC and ATXN1L, involved in brain development (By similarity).
ENSG00000268089	s425	GABRQ	1.963561008	gamma-aminobutyric acid type A receptor theta subunit	GABA, the major inhibitory neurotransmitter in the vertebrate brain, mediates neuronal inhibition by binding to the GABA/benzodiazepine receptor and opening an integral chloride channel.
ENSG00000131910	s15997	NR0B2	1.955162028	nuclear receptor subfamily 0 group B member 2	Acts as a transcriptional regulator. Acts as a negative regulator of receptor-dependent signaling pathways. Specifically inhibits transactivation of the nuclear receptor with whom it interacts. Inhibits transcriptional activity of NEUROD1 on E-box- containing promoter by interfering with the coactivation function of the p300/CBP-mediated transcription complex for NEUROD1.

Ensembl ID (v. 92)	siRNA IDs	Targeted gene	Average PM score	Targeted gene name	Function of targeted gene
ENSG00000115415	s278	STAT1	1.951766364	signal transducer and activator of transcription 1	Signal transducer and transcription activator that mediates cellular responses to interferons (IFNs), cytokine KITLG/SCF and other cytokines and other growth factors. Following type I IFN (IFN-alpha and IFN-beta) binding to cell surface receptors, signaling via protein kinases leads to activation of Jak kinases (TYK2 and JAK1) and to tyrosine phosphorylation of STAT1 and STAT2. The phosphorylated STATs dimerize and associate with ISGF3G/IRF-9 to form a complex termed ISGF3 transcription factor, that enters the nucleus. ISGF3 binds to the IFN stimulated response element (ISRE) to activate the transcription of IFN-stimulated genes (ISG), which drive the cell in an antiviral state. In response to type II IFN (IFN-gamma), STAT1 is tyrosine- and serine-phosphorylated. It then forms a homodimer termed IFN-gamma-activated factor (GAF), migrates into the nucleus and binds to the IFN gamma activated sequence (GAS) to drive the expression of the target genes, inducing a cellular antiviral state. Becomes activated in response to KITLG/SCF and KIT signaling. May mediate cellular responses to activated FGFR1, FGFR2, FGFR3 and FGFR4.
ENSG00000151366	s9379; s9380	NDUFC2	1.917882624	NADH:ubiquinone oxidoreductase subunit C2	Accessory subunit of the mitochondrial membrane respiratory chain NADH dehydrogenase (Complex I), that is believed not to be involved in catalysis. Complex I functions in the transfer of electrons from NADH to the respiratory chain. The immediate electron acceptor for the enzyme is believed to be ubiquinone.
ENSG00000182885	s48199	GPR97	1.916672795	adhesion G protein-coupled receptor G3	Among its related pathways are Innate Immune System. Gene Ontology (GO) annotations related to this gene include G-protein coupled receptor activity and transmembrane signaling receptor activity. An important paralog of this gene is ADGRG1.
ENSG00000127080	s34896	IPPK	1.912752365	inositol-pentakisphosphate 2-kinase	Phosphorylates Ins(1,3,4,5,6)P5 at position 2 to form Ins(1,2,3,4,5,6)P6 (InsP6 or phytate). InsP6 is involved in many processes such as mRNA export, non-homologous end-joining, endocytosis, ion channel regulation. It also protects cells from TNF-alpha-induced apoptosis.
ENSG00000102572	s15993	STK24	1.910747967	serine/threonine kinase 24	Serine/threonine-protein kinase that acts on both serine and threonine residues and promotes apoptosis in response to stress stimuli and caspase activation. Mediates oxidative-stress-induced cell death by modulating phosphorylation of JNK1-JNK2 (MAPK8 and MAPK9), p38 (MAPK11, MAPK12, MAPK13 and MAPK14) during oxidative stress. Plays a role in a staurosporine-induced caspase- independent apoptotic pathway by regulating the nuclear translocation of AIFM1 and ENDOG and the DNase activity associated with ENDOG. Phosphorylates STK38L on 'Thr-442' and stimulates its kinase activity. In association with STK26 negatively regulates Golgi reorientation in polarized cell migration upon RHO activation. Regulates also cellular migration with alteration of PTPN12 activity and PXN phosphorylation: phosphorylates PTPN12 and inhibits its activity and may regulate PXN phosphorylation through PTPN12. May act as a key regulator of axon regeneration in the optic nerve and radial nerve.
ENSG00000115758	s9821	ODC1	1.895924488	ornithine decarboxylase 1	Catalyzes the first and rate-limiting step of polyamine biosynthesis that converts ornithine into putrescine, which is the precursor for the polyamines, spermidine and spermine. Polyamines are essential for cell proliferation and are implicated in cellular processes, ranging from DNA replication to apoptosis.

Ensembl ID (v. 92)	siRNA IDs	Targeted gene	Average PM score	Targeted gene name	Function of targeted gene
ENSG00000221983	s14556	UBA52	1.869345147	ubiquitin A-52 residue ribosomal protein fusion product 1	Ubiquitin: Exists either covalently attached to another protein, or free (unanchored). When covalently bound, it is conjugated to target proteins via an isopeptide bond either as a monomer (monoubiquitin), a polymer linked via different Lys residues of the ubiquitin (polyubiquitin chains) or a linear polymer linked via the initiator Met of the ubiquitin (linear polyubiquitin chains). Polyubiquitin chains, when attached to a target protein, have different functions depending on the Lys residue of the ubiquitin that is linked: Lys-6-linked may be involved in DNA repair; Lys-11-linked is involved in ERAD (endoplasmic reticulum-associated degradation) and in cell-cycle regulation; Lys-29-linked is involved in lysosomal degradation; Lys-33-linked is involved in kinase modification; Lys-48-linked is involved in protein degradation via the proteasome; Lys-63-linked is involved in endocytosis, DNA-damage responses as well as in signaling processes leading to activation of the transcription factor NF-kappa-B. Linear polymer chains formed via attachment by the initiator Met lead to cell signaling. Ubiquitin is usually conjugated to Lys residues of target proteins, however, in rare cases, conjugation to Cys or Ser residues has been observed. When polyubiquitin is free (unanchored-polyubiquitin), it also has distinct roles, such as in activation of protein kinases, and in signaling.60S ribosomal protein L40: Component of the 60S subunit of the ribosome. Ribosomal protein L40 is essential for translation of a subset of cellular transcripts, and especially for cap-dependent translation of vesicular stomatitis virus mRNAs.
ENSG00000064933	s229951	PMS1	1.855396778	PMS1 homolog 1, mismatch repair system component	Probably involved in the repair of mismatches in DNA.
ENSG00000124493	s6200	GRM4	1.849047222	glutamate metabotropic receptor 4	G-protein coupled receptor for glutamate. Ligand binding causes a conformation change that triggers signaling via guanine nucleotide-binding proteins (G proteins) and modulates the activity of down-stream effectors. Signaling inhibits adenylate cyclase activity. .
ENSG00000048828	s23257	FAM120A	1.846914006	family with sequence similarity 120A	May participate in mRNA transport in the cytoplasm (By similarity). Critical component of the oxidative stress-induced survival signaling. Activates src family kinases and acts as a scaffolding protein enabling src family kinases to phosphorylate and activate PI3-kinase. Binds RNA and promotes the secretion of IGF-II. May play a pivotal role in the progression of scirrhous- type gastric cancer by supporting cancer cell survival in environments with various oxidative stresses.
ENSG00000185803	s35852; s35853	GPR172A	1.844631648	solute carrier family 52 member 2	Diseases associated with SLC52A2 include Brown-Vialetto-Van Laere Syndrome 2 and Spinocerebellar Ataxia, Autosomal Recessive 3. Among its related pathways are Metabolism and Metabolism of water-soluble vitamins and cofactors. Gene Ontology (GO) annotations related to this gene include virus receptor activity and riboflavin transmembrane transporter activity. An important paralog of this gene is SLC52A1.

Ensembl ID (v. 92)	siRNA IDs	Targeted gene	Average PM score	Targeted gene name	Function of targeted gene
ENSG00000011243	s25667	AKAP8L	1.841667989	A-kinase anchoring protein 8 like	Could play a role in constitutive transport element (CTE)-mediated gene expression by association with DHX9. Increases CTE-dependent nuclear unspliced mRNA export. Proposed to target PRKACA to the nucleus but does not seem to be implicated in the binding of regulatory subunit II of PKA. May be involved in nuclear envelope breakdown and chromatin condensation. May be involved in anchoring nuclear membranes to chromatin in interphase and in releasing membranes from chromating at mitosis. May regulate the initiation phase of DNA replication when associated with TMPO isoform Beta. Required for cell cycle G2/M transition and histone deacetylation during mitosis. In mitotic cells recruits HDAC3 to the vicinity of chromatin leading to deacetylation and subsequent phosphorylation at 'Ser-10' of histone H3; in this function seems to act redundantly with AKAP8. May be involved in regulation of pre-mRNA splicing.(Microbial infection) In case of EBV infection, may target PRKACA to EBNA-LP-containing nuclear sites to modulate transcription from specific promoters. .(Microbial infection) Can synergize with DHX9 to activate the CTE-mediated gene expression of type D retroviruses. .(Microbial infection) In case of HIV-1 infection, involved in the DHX9-promoted annealing of host tRNA(Lys3) to viral genomic RNA as a primer in reverse transcription; in vitro negatively regulates DHX9 annealing activity.
ENSG00000108840	s19463	HDAC5	1.838397353	histone deacetylase 5	Responsible for the deacetylation of lysine residues on the N-terminal part of the core histones (H2A, H2B, H3 and H4). Histone deacetylation gives a tag for epigenetic repression and plays an important role in transcriptional regulation, cell cycle progression and developmental events. Histone deacetylases act via the formation of large multiprotein complexes. Involved in muscle maturation by repressing transcription of myocyte enhancer MEF2C. During muscle differentiation, it shuttles into the cytoplasm, allowing the expression of myocyte enhancer factors. Involved in the MTA1-mediated epigenetic regulation of ESR1 expression in breast cancer.
ENSG00000117971	s3066	CHRNB4	1.785940117	cholinergic receptor nicotinic beta 4 subunit	After binding acetylcholine, the AChR responds by an extensive change in conformation that affects all subunits and leads to opening of an ion-conducting channel across the plasma membrane.
ENSG00000134817	s1186	APLNR	1.779701654	apelin receptor	Receptor for apelin receptor early endogenous ligand (APELA) and apelin (APLN) hormones coupled to G proteins that inhibit adenylate cyclase activity. Plays a key role in early development such as gastrulation, blood vessels formation and heart morphogenesis by acting as a receptor for APELA hormone (By similarity). May promote angioblast migration toward the embryonic midline, i.e. the position of the future vessel formation, during vasculogenesis (By similarity). Promotes sinus venosus (SV)- derived endothelial cells migration into the developing heart to promote coronary blood vessel development (By similarity). Plays also a role in various processes in adults such as regulation of blood vessel formation, blood pressure, heart contractility and heart failure. (Microbial infection) Alternative coreceptor with CD4 for HIV-1 infection; may be involved in the development of AIDS dementia.

Ensembl ID (v. 92)	siRNA IDs	Targeted gene	Average PM score	Targeted gene name	Function of targeted gene
ENSG00000167165	s200526	UGT1A6	1.770735876	UDP glucuronosyltransferase family 1 member A6	UDPGT is of major importance in the conjugation and subsequent elimination of potentially toxic xenobiotics and endogenous compounds. This isoform has specificity for phenols. Isoform 3 lacks transferase activity but acts as a negative regulator of isoform 1 (By similarity).
ENSG00000187626	s51828	ZKSCAN4	1.76875056	zinc finger with KRAB and SCAN domains 4	May be involved in the transcriptional activation of MDM2 and EP300 genes.
ENSG00000134308	s21597	YWHAQ	1.767854402	tyrosine 3-monooxygenase/tryptophan 5-monooxygenase activation protein theta	Adapter protein implicated in the regulation of a large spectrum of both general and specialized signaling pathways. Binds to a large number of partners, usually by recognition of a phosphoserine or phosphothreonine motif. Binding generally results in the modulation of the activity of the binding partner. Negatively regulates the kinase activity of PDPK1.
ENSG00000100902	s626	PSMA6	1.76551013	proteasome subunit alpha 6	Component of the 20S core proteasome complex involved in the proteolytic degradation of most intracellular proteins. This complex plays numerous essential roles within the cell by associating with different regulatory particles. Associated with two 19S regulatory particles, forms the 26S proteasome and thus participates in the ATP-dependent degradation of ubiquitinated proteins. The 26S proteasome plays a key role in the maintenance of protein homeostasis by removing misfolded or damaged proteins that could impair cellular functions, and by removing proteins whose functions are no longer required. Associated with the PA200 or PA28, the 20S proteasome mediates ubiquitin-independent protein degradation. This type of proteolysis is required in several pathways including spermatogenesis (20S-PA200 complex) or generation of a subset of MHC class I-presented antigenic peptides (20S-PA28 complex).
ENSG00000115318	s39344	LOXL3	1.755484693	lysyl oxidase like 3	Protein-lysine 6-oxidase that mediates the oxidation of peptidyl lysine residues to allysine in target proteins. Catalyzes the post- translational oxidative deamination of peptidyl lysine residues in precursors of elastin and different types of collagens, a prerequisite in the formation of cross-links between collagens and elastin. Required for somite boundary formation by catalyzing oxidation of fibronectin (FN1), enhancing integrin signaling in myofibers and their adhesion to the myotendinous junction (MTJ) (By similarity). Acts as a regulator of inflammatory response by inhibiting differentiation of naive CD4(+) T-cells into T-helper Th17 or regulatory T-cells (Treg): acts by interacting with STAT3 in the nucleus and catalyzing both deacetylation and oxidation of lysine residues on STAT3, leading to disrupt STAT3 dimerization and inhibit STAT3 transcription activity. Oxidation of lysine residues to allysine on STAT3 preferentially takes place on lysine residues that are acetylated. Also able to catalyze deacetylation of lysine residues on STAT3. Isoform 1: Shows protein-lysine 6-oxidase activity toward elastin and different types of collagens, with the highest activity toward collagen type VIII. Isoform 2: Shows protein-lysine 6-oxidase activity toward elastin and different types of collagens, with the highest activity toward collagen type IV.
ENSG00000128710	s6858	HOXD10	1.725411155	homeobox D10	Sequence-specific transcription factor which is part of a developmental regulatory system that provides cells with specific positional identities on the anterior-posterior axis.
ENSG00000182983	s52361	ZNF662	1.708661545	zinc finger protein 662	May be involved in transcriptional regulation.

Ensembl ID (v. 92)	siRNA IDs	Targeted gene	Average PM score	Targeted gene name	Function of targeted gene
ENSG00000171051	s5351	FPR1	1.697883963	formyl peptide receptor 1	High affinity receptor for N-formyl-methionyl peptides (fMLP), which are powerful neutrophil chemotactic factors. Binding of fMLP to the receptor stimulates intracellular calcium mobilization and superoxide anion release. This response is mediated via a G-protein that activates a phosphatidylinositol- calcium second messenger system.
ENSG00000163545	s37780	NUAK2	1.667786642	NUAK family kinase 2	Stress-activated kinase involved in tolerance to glucose starvation. Induces cell-cell detachment by increasing F-actin conversion to G-actin. Expression is induced by CD95 or TNF-alpha, via NF-kappa-B. Protects cells from CD95-mediated apoptosis and is required for the increased motility and invasiveness of CD95- activated tumor cells. Able to phosphorylate 'Ser-464' of LATS1.
ENSG00000118046	s13579	STK11	1.65686714	serine/threonine kinase 11	Tumor suppressor serine/threonine-protein kinase that controls the activity of AMP-activated protein kinase (AMPK) family members, thereby playing a role in various processes such as cell metabolism, cell polarity, apoptosis and DNA damage response. Acts by phosphorylating the T-loop of AMPK family proteins, thus promoting their activity: phosphorylates PRKAA1, PRKAA2, BRSK1, BRSK2, MARK1, MARK2, MARK3, MARK4, NUAK1, NUAK2, SIK1, SIK2, SIK3 and SNRK but not MELK. Also phosphorylates non- AMPK family proteins such as STRADA, PTEN and possibly p53/TP53. Acts as a key upstream regulator of AMPK by mediating phosphorylation and activation of AMPK catalytic subunits PRKAA1 and PRKAA2 and thereby regulates processes including: inhibition of signaling pathways that promote cell growth and proliferation when energy levels are low, glucose homeostasis in liver, activation of autophagy when cells undergo nutrient deprivation, and B-cell differentiation in the germinal center in response to DNA damage. Also acts as a regulator of cellular polarity by remodeling the actin cytoskeleton. Required for cortical neuron polarization by mediating phosphorylation and activation of BRSK1 and BRSK2, leading to axon initiation and specification. Involved in DNA damage response: interacts with p53/TP53 and recruited to the CDKN1A/WAF1 promoter to participate in transcription activation. Able to phosphorylate p53/TP53; the relevance of such result in vivo is however unclear and phosphorylation may be indirect and mediated by downstream STK11/LKB1 kinase NUAK1. Also acts as a mediator of p53/TP53-dependent apoptosis via interaction with p53/TP53: translocates to the mitochondrion during apoptosis and regulates p53/TP53-dependent apoptosis pathways. In vein endothelial cells, inhibits PI3K/Akt signaling activity and thus induces apoptosis in response to the oxidant peroxynitrite (in vitro). Regulates UV radiation-induced DNA damage response mediated by CDKN1A. In association with NUAK1, phosphorylates CDKN1A in response to UV radiation and contributes to its degradation which is necessary for optimal DNA repair.Isoform 2: Has a role in spermiogenesis.
ENSG00000138594	s26568; s26569	TMOD3	1.656228836	tropomodulin 3	Blocks the elongation and depolymerization of the actin filaments at the pointed end. The Tmod/TM complex contributes to the formation of the short actin protofilament, which in turn defines the geometry of the membrane skeleton (By similarity).
ENSG00000188060	s41782	RAB42	1.650482576	RAB42, member RAS oncogene family	Among its related pathways are Metabolism of proteins and RAB geranylgeranylation. Gene Ontology (GO) annotations related to this gene include GTP binding and GTPase activity. An important paralog of this gene is RAB39A.

Ensembl ID (v. 92)	siRNA IDs	Targeted gene	Average PM score	Targeted gene name	Function of targeted gene
ENSG00000168653	s9398	NDUFS5	1.636015598	NADH:ubiquinone oxidoreductase subunit S5	Accessory subunit of the mitochondrial membrane respiratory chain NADH dehydrogenase (Complex I), that is believed not to be involved in catalysis. Complex I functions in the transfer of electrons from NADH to the respiratory chain. The immediate electron acceptor for the enzyme is believed to be ubiquinone.
ENSG00000100038	s17097	TOP3B	1.600631999	topoisomerase (DNA) III beta	Releases the supercoiling and torsional tension of DNA introduced during the DNA replication and transcription by transiently cleaving and rejoining one strand of the DNA duplex. Introduces a single-strand break via transesterification at a target site in duplex DNA. The scissile phosphodiester is attacked by the catalytic tyrosine of the enzyme, resulting in the formation of a DNA-(5'-phosphotyrosyl)-enzyme intermediate and the expulsion of a 3'-OH DNA strand. The free DNA strand than undergoes passage around the unbroken strand thus removing DNA supercoils. Finally, in the religation step, the DNA 3'-OH attacks the covalent intermediate to expel the active-site tyrosine and restore the DNA phosphodiester backbone (By similarity). Possesses negatively supercoiled DNA relaxing activity.
ENSG00000197217	s18413	ENTPD4	1.592831137	ectonucleoside triphosphate diphosphohydrolase 4	Hydrolyzes preferentially nucleoside 5'-diphosphates, nucleoside 5'-triphosphates are hydrolyzed only to a minor extent. The order of activity with different substrates is UDP >> GDP = CDP = TDP, AMP, ADP, ATP and UMP are not substrates. Preferred substrates for isoform 2 are CTP, UDP, CDP, GTP and GDP, while isoform 1 utilizes UTP and TTP.
ENSG00000153936	s230106	HS2ST1	1.585672026	heparan sulfate 2-O-sulfotransferase 1	Catalyzes the transfer of sulfate to the C2-position of selected hexuronic acid residues within the maturing heparan sulfate (HS). 2-O-sulfation within HS, particularly of iduronate residues, is essential for HS to participate in a variety of high- affinity ligand-binding interactions and signaling processes. Mediates 2-O-sulfation of both L-iduronyl and D-glucuronyl residues (By similarity).
ENSG00000161133	s51518	USP41	1.566903125	ubiquitin specific peptidase 41	May recognize and hydrolyze the peptide bond at the C- terminal Gly of ubiquitin. Involved in the processing of poly- ubiquitin precursors as well as that of ubiquitinated proteins (By similarity).
ENSG00000152256	s10254	PDK1	1.566396979	pyruvate dehydrogenase kinase 1	Kinase that plays a key role in regulation of glucose and fatty acid metabolism and homeostasis via phosphorylation of the pyruvate dehydrogenase subunits PDHA1 and PDHA2. This inhibits pyruvate dehydrogenase activity, and thereby regulates metabolite flux through the tricarboxylic acid cycle, down-regulates aerobic respiration and inhibits the formation of acetyl-coenzyme A from pyruvate. Plays an important role in cellular responses to hypoxia and is important for cell proliferation under hypoxia. Protects cells against apoptosis in response to hypoxia and oxidative stress.
ENSG00000255095	s15913; s15914	OR1D4	1.566237412	olfactory receptor family 1 subfamily D member 4 (gene/pseudogene)	Among its related pathways are Signaling by GPCR and Olfactory Signaling Pathway. Gene Ontology (GO) annotations related to this gene include G-protein coupled receptor activity and olfactory receptor activity.

Ensembl ID (v. 92)	siRNA IDs	Targeted gene	Average PM score	Targeted gene name	Function of targeted gene
ENSG00000116833	s5382	NR5A2	1.553877377	nuclear receptor subfamily 5 group A member 2	Nuclear receptor that acts as a key metabolic sensor by regulating the expression of genes involved in bile acid synthesis, cholesterol homeostasis and triglyceride synthesis. Together with the oxysterol receptors NR1H3/LXR-alpha and NR1H2/LXR-beta, acts as an essential transcriptional regulator of lipid metabolism. Plays an anti-inflammatory role during the hepatic acute phase response by acting as a corepressor: inhibits the hepatic acute phase response by preventing dissociation of the N-Cor corepressor complex. Binds to the sequence element 5'-AACGACCGACCTTGAG-3' of the enhancer II of hepatitis B virus genes, a critical cis-element of their expression and regulation. May be responsible for the liver-specific activity of enhancer II, probably in combination with other hepatocyte transcription factors. Key regulator of cholesterol 7-alpha- hydroxylase gene (CYP7A) expression in liver. May also contribute to the regulation of pancreas-specific genes and play important roles in embryonic development.
ENSG00000104290	s15505	FZD3	1.54506761	frizzled class receptor 3	Receptor for Wnt proteins. Most of frizzled receptors are coupled to the beta-catenin canonical signaling pathway, which leads to the activation of disheveled proteins, inhibition of GSK- 3 kinase, nuclear accumulation of beta-catenin and activation of Wnt target genes. A second signaling pathway involving PKC and calcium fluxes has been seen for some family members, but it is not yet clear if it represents a distinct pathway or if it can be integrated in the canonical pathway, as PKC seems to be required for Wnt-mediated inactivation of GSK-3 kinase. Both pathways seem to involve interactions with G-proteins. Activation by Wnt5A stimulates PKC activity via a G-protein-dependent mechanism. Involved in transduction and intercellular transmission of polarity information during tissue morphogenesis and/or in differentiated tissues. Plays a role in controlling early axon growth and guidance processes necessary for the formation of a subset of central and peripheral major fiber tracts. Required for the development of major fiber tracts in the central nervous system, including: the anterior commissure, the corpus callosum, the thalamocortical, corticothalamic and nigrostriatal tracts, the corticospinal tract, the fasciculus retroflexus, the mammillothalamic tract, the medial lemniscus, and ascending fiber tracts from the spinal cord to the brain. In the peripheral nervous system, controls axon growth in distinct populations of cranial and spinal motor neurons, including the facial branchimotor nerve, the hypoglossal nerve, the phrenic nerve, and motor nerves innervating dorsal limbs. Involved in the migration of cranial neural crest cells. May also be implicated in the transmission of sensory information from the trunk and limbs to the brain. Controls commissural sensory axons guidance after midline crossing along the anterior-posterior axis in the developing spinal cord in a Wnt-dependent signaling pathway. Together with FZD6, is involved in the neural tube closure and plays a role in the regulation of the establishment of planar cell polarity (PCP), particularly in the orientation of asymmetric bundles of stereocilia on the apical faces of a subset of auditory and vestibular sensory cells located in the inner ear. Promotes neurogenesis by maintaining sympathetic neuroblasts within the cell cycle in a beta-catenin-dependent manner (By similarity).
ENSG00000133256	s10239	PDE6B	1.512592611	phosphodiesterase 6B	This protein participates in processes of transmission and amplification of the visual signal. Necessary for the formation of a functional phosphodiesterase holoenzyme.

Ensembl ID (v. 92)	siRNA IDs	Targeted gene	Average PM score	Targeted gene name	Function of targeted gene
ENSG00000151491	s4772	EPS8	1.499192545	epidermal growth factor receptor pathway substrate 8	Signaling adapter that controls various cellular protrusions by regulating actin cytoskeleton dynamics and architecture. Depending on its association with other signal transducers, can regulate different processes. Together with SOS1 and ABI1, forms a trimeric complex that participates in transduction of signals from Ras to Rac by activating the Rac- specific guanine nucleotide exchange factor (GEF) activity. Acts as a direct regulator of actin dynamics by binding actin filaments and has both barbed-end actin filament capping and actin bundling activities depending on the context. Displays barbed-end actin capping activity when associated with ABI1, thereby regulating actin-based motility process: capping activity is auto-inhibited and inhibition is relieved upon ABI1 interaction. Also shows actin bundling activity when associated with BAIAP2, enhancing BAIAP2- dependent membrane extensions and promoting filopodial protrusions. Involved in the regulation of processes such as axonal filopodia growth, stereocilia length, dendritic cell migration and cancer cell migration and invasion. Acts as a regulator of axonal filopodia formation in neurons: in the absence of neurotrophic factors, negatively regulates axonal filopodia formation via actin-capping activity. In contrast, it is phosphorylated in the presence of BDNF leading to inhibition of its actin-capping activity and stimulation of filopodia formation. Component of a complex with WHRN and MYO15A that localizes at stereocilia tips and is required for elongation of the stereocilia actin core. Indirectly involved in cell cycle progression; its degradation following ubiquitination being required during G2 phase to promote cell shape changes.
ENSG00000143252	s55037; s55038	SDHC	1.485760443	succinate dehydrogenase complex subunit C	Membrane-anchoring subunit of succinate dehydrogenase (SDH) that is involved in complex II of the mitochondrial electron transport chain and is responsible for transferring electrons from succinate to ubiquinone (coenzyme Q).
ENSG00000105568	s10965	PPP2R1A	1.4841666	protein phosphatase 2 scaffold subunit Aalpha	The PR65 subunit of protein phosphatase 2A serves as a scaffolding molecule to coordinate the assembly of the catalytic subunit and a variable regulatory B subunit. Upon interaction with GNA12 promotes dephosphorylation of microtubule associated protein TAU/MAPT. Required for proper chromosome segregation and for centromeric localization of SGO1 in mitosis.
ENSG00000160789	s8222	LMNA	1.463821477	lamin A/C	Lamins are components of the nuclear lamina, a fibrous layer on the nucleoplasmic side of the inner nuclear membrane, which is thought to provide a framework for the nuclear envelope and may also interact with chromatin. Lamin A and C are present in equal amounts in the lamina of mammals. Plays an important role in nuclear assembly, chromatin organization, nuclear membrane and telomere dynamics. Required for normal development of peripheral nervous system and skeletal muscle and for muscle satellite cell proliferation. Required for osteoblastogenesis and bone formation. Also prevents fat infiltration of muscle and bone marrow, helping to maintain the volume and strength of skeletal muscle and bone. Required for cardiac homeostasis. Prelamin-A/C can accelerate smooth muscle cell senescence. It acts to disrupt mitosis and induce DNA damage in vascular smooth muscle cells (VSMCs), leading to mitotic failure, genomic instability, and premature senescence.

Ensembl ID (v. 92)	siRNA IDs	Targeted gene	Average PM score	Targeted gene name	Function of targeted gene
ENSG00000186810	s6013	CXCR3	1.457908213	C-X-C motif chemokine receptor 3	Isoform 1: Receptor for the C-X-C chemokine CXCL9, CXCL10 and CXCL11 and mediates the proliferation, survival and angiogenic activity of human mesangial cells (HMC) through a heterotrimeric G-protein signaling pathway. Binds to CCL21. Probably promotes cell chemotaxis response. . Isoform 2: Receptor for the C-X-C chemokine CXCL4 and also mediates the inhibitory activities of CXCL9, CXCL10 and CXCL11 on the proliferation, survival and angiogenic activity of human microvascular endothelial cells (HMVEC) through a cAMP- mediated signaling pathway. Does not promote cell chemotaxis respons. Interaction with CXCL4 or CXCL10 leads to activation of the p38MAPK pathway and contributes to inhibition of angiogenesis. Overexpression in renal cancer cells down-regulates expression of the anti-apoptotic protein HMOX1 and promotes apoptosis. . Isoform 3: Mediates the activity of CXCL11.
ENSG00000143761	s223968	ARF1	1.449179639	ADP ribosylation factor 1	GTP-binding protein that functions as an allosteric activator of the cholera toxin catalytic subunit, an ADP- ribosyltransferase. Involved in protein trafficking among different compartments. Modulates vesicle budding and uncoating within the Golgi complex. Deactivation induces the redistribution of the entire Golgi complex to the endoplasmic reticulum, suggesting a crucial role in protein trafficking. In its GTP-bound form, its triggers the association with coat proteins with the Golgi membrane. The hydrolysis of ARF1-bound GTP, which is mediated by ARFGAPs proteins, is required for dissociation of coat proteins from Golgi membranes and vesicles. The GTP-bound form interacts with PICK1 to limit PICK1-mediated inhibition of Arp2/3 complex activity; the function is linked to AMPA receptor (AMPAR) trafficking, regulation of synaptic plasicity of excitatory synapses and spine shrinkage during long-term depression (LTD).
ENSG00000105819	s18239	PMPCB	1.44723119	peptidase, mitochondrial processing beta subunit	Cleaves presequences (transit peptides) from mitochondrial protein precursors.
ENSG00000184984	s3035	CHRM5	1.444475878	cholinergic receptor muscarinic 5	The muscarinic acetylcholine receptor mediates various cellular responses, including inhibition of adenylate cyclase, breakdown of phosphoinositides and modulation of potassium channels through the action of G proteins. Primary transducing effect is Pi turnover.
ENSG00000049860	s223844	HEXB	1.440439497	hexosaminidase subunit beta	Responsible for the degradation of GM2 gangliosides, and a variety of other molecules containing terminal N-acetyl hexosamines, in the brain and other tissues.
ENSG00000133105	s42516; s42517	RXFP2	1.439200067	relaxin/insulin like family peptide receptor 2	Receptor for relaxin. The activity of this receptor is mediated by G proteins leading to stimulation of adenylate cyclase and an increase of cAMP. May also be a receptor for Leydig insulin-like peptide (INSL3).
ENSG00000196428	s18988	TSC22D2	1.434270331	TSC22 domain family member 2	Gene Ontology (GO) annotations related to this gene include DNA binding transcription factor activity. An important paralog of this gene is TSC22D1.
ENSG00000196433	s1673	ASMT	1.423532563	acetylserotonin O-methyltransferase	Isoform 1 catalyzes the transfer of a methyl group onto N-acetylserotonin, producing melatonin (N-acetyl-5- methoxytryptamine). Isoform 2 and isoform 3 lack enzyme activity.
ENSG00000158578	s1225	ALAS2	1.413233869	5'-aminolevulinate synthase 2	Gene Ontology (GO) annotations related to this gene include DNA binding transcription factor activity. An important paralog of this gene is TSC22D1.

Ensembl ID (v. 92)	siRNA IDs	Targeted gene	Average PM score	Targeted gene name	Function of targeted gene
ENSG00000164442	s223110	CITED2	1.4058591	Cbp/p300 interacting transactivator with Glu/Asp rich carboxy-terminal domain 2	Transcriptional coactivator of the p300/CBP-mediated transcription complex. Acts as a bridge, linking TFAP2 transcription factors and the p300/CBP transcriptional coactivator complex in order to stimulate TFAP2-mediated transcriptional activation. Positively regulates TGF-beta signaling through its association with the SMAD/p300/CBP-mediated transcriptional coactivator complex. Stimulates the peroxisome proliferator- activated receptors PPARA transcriptional activity. Enhances estrogen-dependent transactivation mediated by estrogen receptors. Acts also as a transcriptional corepressor; interferes with the binding of the transcription factors HIF1A or STAT2 and the p300/CBP transcriptional coactivator complex. Participates in sex determination and early gonad development by stimulating transcription activation of SRY. Plays a role in controlling left- right patterning during embryogenesis; potentiates transcriptional activation of NODAL-mediated gene transcription in the left lateral plate mesoderm (LPM). Plays an essential role in differentiation of the adrenal cortex from the adrenogonadal primordium (AGP); stimulates WT1-mediated transcription activation thereby up-regulating the nuclear hormone receptor NR5A1 promoter activity. Associates with chromatin to the PITX2 P1 promoter region.
ENSG00000185122	s6952	HSF1	1.403274491	heat shock transcription factor 1	Function as a stress-inducible and DNA-binding transcription factor that plays a central role in the transcriptional activation of the heat shock response (HSR), leading to the expression of a large class of molecular chaperones heat shock proteins (HSPs) that protect cells from cellular insults' damage. In unstressed cells, is present in a HSP90-containing multichaperone complex that maintains it in a non-DNA-binding inactivated monomeric form. Upon exposure to heat and other stress stimuli, undergoes homotrimerization and activates HSP gene transcription through binding to site-specific heat shock elements (HSEs) present in the promoter regions of HSP genes. Activation is reversible, and during the attenuation and recovery phase period of the HSR, returns to its unactivated form. Binds to inverted 5'-NGAAN-3' pentamer DNA sequences. Binds to chromatin at heat shock gene promoters. Plays also several other functions independently of its transcriptional activity. Involved in the repression of Ras-induced transcriptional activation of the c-fos gene in heat-stressed cells. Positively regulates pre-mRNA 3'-end processing and polyadenylation of HSP70 mRNA upon heat-stressed cells in a symplekin (SYMPK)-dependent manner. Plays a role in nuclear export of stress-induced HSP70 mRNA. Plays a role in the regulation of mitotic progression. Plays also a role as a negative regulator of non-homologous end joining (NHEJ) repair activity in a DNA damage- dependent manner. Involved in stress-induced cancer cell proliferation in a IER5-dependent manner. (Microbial infection) Plays a role in latent human immunodeficiency virus (HIV-1) transcriptional reactivation. Binds to the HIV-1 long terminal repeat promoter (LTR) to reactivate viral transcription by recruiting cellular transcriptional elongation factors, such as CDK9, CCNT1 and EP300.
ENSG00000142511	s6057	GPR32	1.398037766	G protein-coupled receptor 32	Orphan receptor.
ENSG00000142675	s20036; s20038	CNKSR1	1.396833846	connector enhancer of kinase suppressor of Ras 1	May function as an adapter protein or regulator of Ras signaling pathways.

Ensembl ID (v. 92)	siRNA IDs	Targeted gene	Average PM score	Targeted gene name	Function of targeted gene
ENSG00000114268	s10362	PFKFB4	1.395810953	6-phosphofructo-2-kinase/fructose-2,6-biphosphatase 4	Synthesis and degradation of fructose 2,6-bisphosphate.
ENSG00000138741	s14412	TRPC3	1.389495035	transient receptor potential cation channel subfamily C member 3	Thought to form a receptor-activated non-selective calcium permeant cation channel. Probably is operated by a phosphatidylinositol second messenger system activated by receptor tyrosine kinases or G-protein coupled receptors. Activated by diacylglycerol (DAG) in a membrane-delimited fashion, independently of protein kinase C, and by inositol 1,4,5- triphosphate receptors (ITPR) with bound IP3. May also be activated by internal calcium store depletion.
ENSG00000141012	s5548	GALNS	1.385243086	galactosamine (N-acetyl)-6-sulfatase	Gene Ontology (GO) annotations related to this gene include DNA binding transcription factor activity. An important paralog of this gene is TSC22D1.
ENSG00000104960	s28748	PTOV1	1.38351085	prostate tumor overexpressed 1	May activate transcription. Required for nuclear translocation of FLOT1. Promotes cell proliferation.
ENSG00000112164	s5827	GLP1R	1.355224017	glucagon like peptide 1 receptor	G-protein coupled receptor for glucagon-like peptide 1 (GLP-1). Ligand binding triggers activation of a signaling cascade that leads to the activation of adenylyl cyclase and increased intracellular cAMP levels. Plays a role in regulating insulin secretion in response to GLP-1 (By similarity).
ENSG00000048540	s31717	LMO3	1.353008215	LIM domain only 3	Gene Ontology (GO) annotations related to this gene include DNA binding transcription factor activity. An important paralog of this gene is TSC22D1.
ENSG00000160791	s3211	CCR5	1.339929006	C-C motif chemokine receptor 5 (gene/pseudogene)	Receptor for a number of inflammatory CC-chemokines including MIP-1-alpha, MIP-1-beta and RANTES and subsequently transduces a signal by increasing the intracellular calcium ion level. May play a role in the control of granulocytic lineage proliferation or differentiation. Acts as a coreceptor (CD4 being the primary receptor) for HIV-1 R5 isolates. . (Microbial infection) Acts as a receptor for human immunodeficiency virus-1/HIV-1.
ENSG00000071967	s230762	CYBRD1	1.33426963	cytochrome b reductase 1	Ferric-chelate reductase that reduces Fe(3+) to Fe(2+). Present at the brush border of duodenal enterocytes where it probably reduces dietary Fe(3+) thereby facilitating its transport into the mucosal cells. Uses ascorbate as electron donor. May be involved in extracellular ascorbate recycling in erythrocyte membranes. May also act as a ferrireductase in airway epithelial cells.
ENSG00000114554	s10696; s10697	PLXNA1	1.333694687	plexin A1	Coreceptor for SEMA3A, SEMA3C, SEMA3F and SEMA6D. Necessary for signaling by class 3 semaphorins and subsequent remodeling of the cytoskeleton. Plays a role in axon guidance, invasive growth and cell migration. Class 3 semaphorins bind to a complex composed of a neuropilin and a plexin. The plexin modulates the affinity of the complex for specific semaphorins, and its cytoplasmic domain is required for the activation of down- stream signaling events in the cytoplasm (By similarity).
ENSG00000204700	s25607	OR2J2	1.327414717	olfactory receptor family 2 subfamily J member 2	Odorant receptor.

Ensembl ID (v. 92)	siRNA IDs	Targeted gene	Average PM score	Targeted gene name	Function of targeted gene
ENSG00000110048	s9918	OSBP	1.318258459	oxysterol binding protein	Lipid transporter involved in lipid countertransport between the Golgi complex and membranes of the endoplasmic reticulum: specifically exchanges sterol with phosphatidylinositol 4-phosphate (PI4P), delivering sterol to the Golgi in exchange for PI4P, which is degraded by the SAC1/SACM1L phosphatase in the endoplasmic reticulum. Binds cholesterol and a range of oxysterols including 25-hydroxycholesterol. Cholesterol binding promotes the formation of a complex with PP2A and a tyrosine phosphatase which dephosphorylates ERK1/2, whereas 25-hydroxycholesterol causes its disassembly. Regulates cholesterol efflux by decreasing ABCA1 stability.
ENSG00000137713	s10966; s10968	PPP2R1B	1.317320144	protein phosphatase 2 scaffold subunit Abeta	The PR65 subunit of protein phosphatase 2A serves as a scaffolding molecule to coordinate the assembly of the catalytic subunit and a variable regulatory B subunit.
ENSG00000114956	s4072	DGUOK	1.311336512	deoxyguanosine kinase	Phosphorylates deoxyguanosine and deoxyadenosine in the mitochondrial matrix, with the highest efficiency for deoxyguanosine. In non-replicating cells, where cytosolic dNTP synthesis is down-regulated, mtDNA synthesis depends solely on DGUOK and TK2. Phosphorylates certain nucleoside analogs. Widely used as target of antiviral and chemotherapeutic agents.
ENSG00000135312	s7030	HTR1B	1.306298175	5-hydroxytryptamine receptor 1B	G-protein coupled receptor for 5-hydroxytryptamine (serotonin). Also functions as a receptor for ergot alkaloid derivatives, various anxiolytic and antidepressant drugs and other psychoactive substances, such as lysergic acid diethylamide (LSD). Ligand binding causes a conformation change that triggers signaling via guanine nucleotide-binding proteins (G proteins) and modulates the activity of down-stream effectors, such as adenylate cyclase. Signaling inhibits adenylate cyclase activity. Arrestin family members inhibit signaling via G proteins and mediate activation of alternative signaling pathways. Regulates the release of 5-hydroxytryptamine, dopamine and acetylcholine in the brain, and thereby affects neural activity, nociceptive processing, pain perception, mood and behavior. Besides, plays a role in vasoconstriction of cerebral arteries.
ENSG00000278570	s19433	NR2E3	1.301088316	nuclear receptor subfamily 2 group E member 3	Orphan nuclear receptor of retinal photoreceptor cells. Transcriptional factor that is an activator of rod development and repressor of cone development. Binds the promoter region of a number of rod- and cone-specific genes, including rhodopsin, M- and S-opsin and rod-specific phosphodiesterase beta subunit. Enhances rhodopsin expression. Represses M- and S-cone opsin expression.
ENSG00000126746	s46887	ZNF384	1.300643654	zinc finger protein 384	Transcription factor that binds the consensus DNA sequence [GC]AAAAA. Seems to bind and regulate the promoters of MMP1, MMP3, MMP7 and COL1A1 (By similarity).

Ensembl ID (v. 92)	siRNA IDs	Targeted gene	Average PM score	Targeted gene name	Function of targeted gene
ENSG00000126821	s37587	SGPP1	1.287707712	sphingosine-1-phosphate phosphatase 1	Specifically dephosphorylates sphingosine 1-phosphate (S1P), dihydro-S1P, and phyto-S1P. Does not act on ceramide 1- phoshate, lysophosphatidic acid or phosphatidic acid. Regulates the intracellular levels of the bioactive sphingolipid metabolite S1P that regulates diverse biological processes acting both as an extracellular receptor ligand or as an intracellular second messenger. Involved in efficient ceramide synthesis from exogenous sphingoid bases. Converts S1P to sphingosine, which is readily metabolized to ceramide via ceramide synthase. In concert with sphingosine kinase 2 (SphK2), recycles sphingosine into ceramide though a phosphorylation/dephosphorylation cycle. Regulates intracellular ceramide levels, which in turn regulate apoptosis (By similarity). Via S1P levels, modulates resting tone, intracellular Ca(2+) and myogenic vasoconstriction in resistance arteries. Also involved in unfolded protein response (UPR) and ER stress-induced autophagy via regulation of intracellular S1P levels.
ENSG00000105438	s547	KDELR1	1.274455847	KDEL endoplasmic reticulum protein retention receptor 1	Required for the retention of luminal endoplasmic reticulum resident proteins via vesicular recycling. This receptor recognizes the C-terminal K-D-E-L motif. COPI-coated transport intermediates, either in the form of round vesicles or as tubular processes, mediate retrograde traffic of the KDEL receptor-ligand complexes. Also required for normal vesicular traffic through the Golgi.
ENSG00000183484	s26736	GPR132	1.27037737	G protein-coupled receptor 132	May be a receptor for oxidized free fatty acids derived from linoleic and arachidonic acids such as 9- hydroxyoctadecadienoic acid (9-HODE). Activates a G alpha protein, most likely G alpha(q). May be involved in apoptosis. Functions at the G2/M checkpoint to delay mitosis. May function as a sensor that monitors the oxidative states and mediates appropriate cellular responses such as secretion of paracrine signals and attenuation of proliferation. May mediate ths accumulation of intracellular inositol phosphates at acidic pH through proton- sensing activity.
ENSG00000072041	s30211	SLC6A15	1.266055298	solute carrier family 6 member 15	Functions as a sodium-dependent neutral amino acid transporter. Exhibits preference for the branched-chain amino acids, particularly leucine, valine and isoleucine and methionine. Mediates the saturable, pH-sensitive and electrogenic cotransport of proline and sodium ions with a stoichiometry of 1:1. May have a role as transporter for neurotransmitter precursors into neurons. In contrast to other members of the neurotransmitter transporter family, does not appear to be chloride-dependent.
ENSG00000135597	s39846	REPS1	1.259613746	RALBP1 associated Eps domain containing 1	May coordinate the cellular actions of activated EGF receptors and Ral-GTPases.
ENSG00000142875	s11070	PRKACB	1.259064573	protein kinase cAMP-activated catalytic subunit beta	Mediates cAMP-dependent signaling triggered by receptor binding to GPCRs. PKA activation regulates diverse cellular processes such as cell proliferation, the cell cycle, differentiation and regulation of microtubule dynamics, chromatin condensation and decondensation, nuclear envelope disassembly and reassembly, as well as regulation of intracellular transport mechanisms and ion flux. Regulates the abundance of compartmentalized pools of its regulatory subunits through phosphorylation of PJA2 which binds and ubiquitinates these subunits, leading to their subsequent proteolysis. Phosphorylates GPKOW which regulates its ability to bind RNA.

Ensembl ID (v. 92)	siRNA IDs	Targeted gene	Average PM score	Targeted gene name	Function of targeted gene
ENSG00000213625	s29371	LEPROT	1.242790236	leptin receptor overlapping transcript	Negatively regulates leptin receptor (LEPR) cell surface expression, and thus decreases response to leptin. Negatively regulates growth hormone (GH) receptor cell surface expression in liver. May play a role in liver resistance to GH during periods of reduced nutrient availability.
ENSG00000101292	s43338	PROKR2	1.232336355	prokineticin receptor 2	Receptor for prokineticin 2. Exclusively coupled to the G(q) subclass of heteromeric G proteins. Activation leads to mobilization of calcium, stimulation of phosphoinositide turnover and activation of p44/p42 mitogen-activated protein kinase.
ENSG00000115170	s974	ACVR1	1.231356156	activin A receptor type 1	On ligand binding, forms a receptor complex consisting of two type II and two type I transmembrane serine/threonine kinases. Type II receptors phosphorylate and activate type I receptors which autophosphorylate, then bind and activate SMAD transcriptional regulators. Receptor for activin. May be involved for left-right pattern formation during embryogenesis (By similarity).
ENSG00000108799	s4913	EZH1	1.230583029	enhancer of zeste 1 polycomb repressive complex 2 subunit	Polycomb group (PcG) protein. Catalytic subunit of the PRC2/EED-EZH1 complex, which methylates 'Lys-27' of histone H3, leading to transcriptional repression of the affected target gene. Able to mono-, di- and trimethylate 'Lys-27' of histone H3 to form H3K27me1, H3K27me2 and H3K27me3, respectively. Required for embryonic stem cell derivation and self-renewal, suggesting that it is involved in safeguarding embryonic stem cell identity. Compared to EZH2-containing complexes, it is less abundant in embryonic stem cells, has weak methyltransferase activity and plays a less critical role in forming H3K27me3, which is required for embryonic stem cell identity and proper differentiation.
ENSG00000136560	s19454	TANK	1.227152164	TRAF family member associated NFKB activator	Adapter protein involved in I-kappa-B-kinase (IKK) regulation which constitutively binds TBK1 and IKBKE playing a role in antiviral innate immunity. Acts as a regulator of TRAF function by maintaining them in a latent state. Blocks TRAF2 binding to LMP1 and inhibits LMP1-mediated NF-kappa-B activation. Negatively regulates NF-kappaB signaling and cell survival upon DNA damage. Plays a role as an adapter to assemble ZC3H12A, USP10 in a deubiquitination complex which plays a negative feedback response to attenuate NF-kappaB activation through the deubiquitination of IKBKG or TRAF6 in response to interleukin-1-beta (IL1B) stimulation or upon DNA damage. Promotes UBP10-induced deubiquitination of TRAF6 in response to DNA damage. May control negatively TRAF2-mediated NF-kappa-B activation signaled by CD40, TNFR1 and TNFR2.
ENSG00000008018	s11345	PSMB1	1.22469366	proteasome subunit beta 1	Component of the 20S core proteasome complex involved in the proteolytic degradation of most intracellular proteins. This complex plays numerous essential roles within the cell by associating with different regulatory particles. Associated with two 19S regulatory particles, forms the 26S proteasome and thus participates in the ATP-dependent degradation of ubiquitinated proteins. The 26S proteasome plays a key role in the maintenance of protein homeostasis by removing misfolded or damaged proteins that could impair cellular functions, and by removing proteins whose functions are no longer required. Associated with the PA200 or PA28, the 20S proteasome mediates ubiquitin-independent protein degradation. This type of proteolysis is required in several pathways including spermatogenesis (20S-PA200 complex) or generation of a subset of MHC class I-presented antigenic peptides (20S-PA28 complex).

Ensembl ID (v. 92)	siRNA IDs	Targeted gene	Average PM score	Targeted gene name	Function of targeted gene
ENSG00000132518	s6381	GUCY2D	1.221524312	guanylate cyclase 2D, retinal	Probably plays a specific functional role in the rods and/or cones of photoreceptors. It may be the enzyme involved in the resynthesis of cGMP required for recovery of the dark state after phototransduction.
ENSG00000154678	s10180	PDE1C	1.216725877	phosphodiesterase 1C	Cyclic nucleotide phosphodiesterase with a dual- specificity for the second messengers cAMP and cGMP, which are key regulators of many important physiological processes. Has a high affinity for both cAMP and cGMP.
ENSG00000108654	s4007	DDX5	1.213431409	DEAD-box helicase 5	Involved in the alternative regulation of pre-mRNA splicing; its RNA helicase activity is necessary for increasing tau exon 10 inclusion and occurs in a RBM4-dependent manner. Binds to the tau pre-mRNA in the stem-loop region downstream of exon 10. The rate of ATP hydrolysis is highly stimulated by single-stranded RNA. Involved in transcriptional regulation; the function is independent of the RNA helicase activity. Transcriptional coactivator for androgen receptor AR but probably not ESR1. Synergizes with DDX17 and SRA1 RNA to activate MYOD1 transcriptional activity and involved in skeletal muscle differentiation. Transcriptional coactivator for p53/TP53 and involved in p53/TP53 transcriptional response to DNA damage and p53/TP53-dependent apoptosis. Transcriptional coactivator for RUNX2 and involved in regulation of osteoblast differentiation. Acts as transcriptional repressor in a promoter-specific manner; the function probably involves association with histone deacetylases, such as HDAC1. As component of a large PER complex is involved in the inhibition of 3' transcriptional termination of circadian target genes such as PER1 and NR1D1 and the control of the circadian rhythms.
ENSG00000166573	s5546	GALR1	1.210838583	galanin receptor 1	Receptor for the hormone galanin. The activity of this receptor is mediated by G proteins that inhibit adenylate cyclase activity.
ENSG00000182771	s6144	GRID1	1.208876324	glutamate ionotropic receptor delta type subunit 1	Receptor for glutamate. L-glutamate acts as an excitatory neurotransmitter at many synapses in the central nervous system. The postsynaptic actions of Glu are mediated by a variety of receptors that are named according to their selective agonists.
ENSG00000170558	s2772	CDH2	1.20687973	cadherin 2	Cadherins are calcium-dependent cell adhesion proteins. They preferentially interact with themselves in a homophilic manner in connecting cells; cadherins may thus contribute to the sorting of heterogeneous cell types. Acts as a regulator of neural stem cells quiescence by mediating anchorage of neural stem cells to ependymocytes in the adult subependymal zone: upon cleavage by MMP24, CDH2-mediated anchorage is affected, leading to modulate neural stem cell quiescence. CDH2 may be involved in neuronal recognition mechanism. In hippocampal neurons, may regulate dendritic spine density (By similarity).
ENSG00000168685	s7324	IL7R	1.202306373	interleukin 7 receptor	Receptor for interleukin-7. Also acts as a receptor for thymic stromal lymphopoietin (TSLP).
ENSG00000213903	s194337	LTB4R	1.200629277	leukotriene B4 receptor	Receptor for extracellular ATP > UTP and ADP. The activity of this receptor is mediated by G proteins which activate a phosphatidylinositol-calcium second messenger system. May be the cardiac P2Y receptor involved in the regulation of cardiac muscle contraction through modulation of L-type calcium currents. Is a receptor for leukotriene B4, a potent chemoattractant involved in inflammation and immune response.

Ensembl ID (v. 92)	siRNA IDs	Targeted gene	Average PM score	Targeted gene name	Function of targeted gene
ENSG00000159527	s41579; s41580	PGLYRP3	1.187827865	peptidoglycan recognition protein 3	Pattern receptor that binds to murein peptidoglycans (PGN) of Gram-positive bacteria. Has bactericidal activity towards Gram-positive bacteria. May kill Gram-positive bacteria by interfering with peptidoglycan biosynthesis. Binds also to Gram- negative bacteria, and has bacteriostatic activity towards Gram- negative bacteria. Plays a role in innate immunity.
ENSG00000278195	s13501	SSTR3	1.181298275	somatostatin receptor 3	Receptor for somatostatin-14 and -28. This receptor is coupled via pertussis toxin sensitive G proteins to inhibition of adenylyl cyclase.
ENSG00000100749	s14821	VRK1	1.180911292	vaccinia related kinase 1	Serine/threonine kinase involved in Golgi disassembly during the cell cycle: following phosphorylation by PLK3 during mitosis, required to induce Golgi fragmentation. Acts by mediating phosphorylation of downstream target protein. Phosphorylates 'Thr- 18' of p53/TP53 and may thereby prevent the interaction between p53/TP53 and MDM2. Phosphorylates casein and histone H3. Phosphorylates BANF1: disrupts its ability to bind DNA, reduces its binding to LEM domain-containing proteins and causes its relocalization from the nucleus to the cytoplasm. Phosphorylates ATF2 which activates its transcriptional activity.
ENSG00000180353	s6484	HCLS1	1.180135528	hematopoietic cell-specific Lyn substrate 1	Substrate of the antigen receptor-coupled tyrosine kinase. Plays a role in antigen receptor signaling for both clonal expansion and deletion in lymphoid cells. May also be involved in the regulation of gene expression.
ENSG00000180263	s31504	FGD6	1.179622328	FYVE, RhoGEF and PH domain containing 6	May activate CDC42, a member of the Ras-like family of Rho- and Rac proteins, by exchanging bound GDP for free GTP. May play a role in regulating the actin cytoskeleton and cell shape (By similarity).
ENSG00000175166	s11389	PSMD2	1.170478875	proteasome 26S subunit, non-ATPase 2	Component of the 26S proteasome, a multiprotein complex involved in the ATP-dependent degradation of ubiquitinated proteins. This complex plays a key role in the maintenance of protein homeostasis by removing misfolded or damaged proteins, which could impair cellular functions, and by removing proteins whose functions are no longer required. Therefore, the proteasome participates in numerous cellular processes, including cell cycle progression, apoptosis, or DNA damage repair. . Binds to the intracellular domain of tumor necrosis factor type 1 receptor. The binding domain of TRAP1 and TRAP2 resides outside the death domain of TNFR1.

Ensembl ID (v. 92)	siRNA IDs	Targeted gene	Average PM score	Targeted gene name	Function of targeted gene
ENSG00000104856	s11917	RELB	1.16628549	RELB proto-oncogene, NF-kB subunit	NF-kappa-B is a pleiotropic transcription factor which is present in almost all cell types and is involved in many biological processed such as inflammation, immunity, differentiation, cell growth, tumorigenesis and apoptosis. NF- kappa-B is a homo- or heterodimeric complex formed by the Rel-like domain-containing proteins RELA/p65, RELB, NFKB1/p105, NFKB1/p50, REL and NFKB2/p52. The dimers bind at kappa-B sites in the DNA of their target genes and the individual dimers have distinct preferences for different kappa-B sites that they can bind with distinguishable affinity and specificity. Different dimer combinations act as transcriptional activators or repressors, respectively. NF-kappa-B is controlled by various mechanisms of post-translational modification and subcellular compartmentalization as well as by interactions with other cofactors or corepressors. NF-kappa-B complexes are held in the cytoplasm in an inactive state complexed with members of the NF- kappa-B inhibitor (I-kappa-B) family. In a conventional activation pathway, I-kappa-B is phosphorylated by I-kappa-B kinases (IKKs) in response to different activators, subsequently degraded thus liberating the active NF-kappa-B complex which translocates to the nucleus. NF-kappa-B heterodimeric RelB-p50 and RelB-p52 complexes are transcriptional activators. RELB neither associates with DNA nor with RELA/p65 or REL. Stimulates promoter activity in the presence of NFKB2/p49. As a member of the NUPR1/RELB/IER3 survival pathway, may provide pancreatic ductal adenocarcinoma with remarkable resistance to cell stress, such as starvation or gemcitabine treatment. Regulates the circadian clock by repressing the transcriptional activator activity of the CLOCK-ARNTL/BMAL1 heterodimer in a CRY1/CRY2 independent manner. Increased repression of the heterodimer is seen in the presence of NFKB2/p52. Is required for both T and B lymphocyte maturation and function.
ENSG00000110799	s14832; s14834	VWF	1.165845064	von Willebrand factor	Important in the maintenance of hemostasis, it promotes adhesion of platelets to the sites of vascular injury by forming a molecular bridge between sub-endothelial collagen matrix and platelet-surface receptor complex GPIb-IX-V. Also acts as a chaperone for coagulation factor VIII, delivering it to the site of injury, stabilizing its heterodimeric structure and protecting it from premature clearance from plasma.
ENSG00000132286	s25485	TIMM10B	1.163781038	translocase of inner mitochondrial membrane 10B	Component of the TIM22 complex, a complex that mediates the import and insertion of multi-pass transmembrane proteins into the mitochondrial inner membrane. The TIM22 complex forms a twin- pore translocase that uses the membrane potential as the external driving force. In the TIM22 complex, it may act as a docking point for the soluble 70 kDa complex that guides the target proteins in transit through the aqueous mitochondrial intermembrane space.
ENSG00000107819	s37840	SFXN3	1.162800288	sideroflexin 3	Potential iron transporter.
ENSG00000180530	s15703	NRIP1	1.16218252	nuclear receptor interacting protein 1	Modulates transcriptional activation by steroid receptors such as NR3C1, NR3C2 and ESR1. Also modulates transcriptional repression by nuclear hormone receptors. Positive regulator of the circadian clock gene expression: stimulates transcription of ARNTL/BMAL1, CLOCK and CRY1 by acting as a coactivator for RORA and RORC.
ENSG00000197479	s31944	PCDHB11	1.14608909	protocadherin beta 11	Potential calcium-dependent cell-adhesion protein. May be involved in the establishment and maintenance of specific neuronal connections in the brain.

Ensembl ID (v. 92)	siRNA IDs	Targeted gene	Average PM score	Targeted gene name	Function of targeted gene
ENSG00000204628	s20342	GNB2L1	1.139366885	receptor for activated C kinase 1	Gene Ontology (GO) annotations related to this gene include DNA binding transcription factor activity. An important paralog of this gene is TSC22D1.
ENSG00000132825	s10948	PPP1R3D	1.138978597	protein phosphatase 1 regulatory subunit 3D	Seems to act as a glycogen-targeting subunit for PP1. PP1 is essential for cell division, and participates in the regulation of glycogen metabolism, muscle contractility and protein synthesis.
ENSG00000153933	s16207	DGKE	1.137958296	diacylglycerol kinase epsilon	Highly selective for arachidonate-containing species of diacylglycerol (DAG). May terminate signals transmitted through arachidonoyl-DAG or may contribute to the synthesis of phospholipids with defined fatty acid composition.
ENSG00000111679	s663	PTPN6	1.128237649	protein tyrosine phosphatase, non-receptor type 6	Modulates signaling by tyrosine phosphorylated cell surface receptors such as KIT and the EGF receptor/EGFR. The SH2 regions may interact with other cellular components to modulate its own phosphatase activity against interacting substrates. Together with MTUS1, induces UBE2V2 expression upon angiotensin II stimulation. Plays a key role in hematopoiesis.
ENSG00000169857	s32670; s32671	AVEN	1.106523616	apoptosis and caspase activation inhibitor	Protects against apoptosis mediated by Apaf-1.
ENSG00000170385	s15331	SLC30A1	1.104497393	solute carrier family 30 member 1	May be involved in zinc transport out of the cell.
ENSG00000136240	s21688	KDELR2	1.096317865	KDEL endoplasmic reticulum protein retention receptor 2	Required for the retention of luminal endoplasmic reticulum proteins. Determines the specificity of the luminal ER protein retention system. Also required for normal vesicular traffic through the Golgi. This receptor recognizes K-D-E-L.
ENSG00000167535	s2307	CACNB3	1.086123594	calcium voltage-gated channel auxiliary subunit beta 3	The beta subunit of voltage-dependent calcium channels contributes to the function of the calcium channel by increasing peak calcium current, shifting the voltage dependencies of activation and inactivation, modulating G protein inhibition and controlling the alpha-1 subunit membrane targeting.
ENSG00000130164	s4	LDLR	1.079407139	low density lipoprotein receptor	Binds LDL, the major cholesterol-carrying lipoprotein of plasma, and transports it into cells by endocytosis. In order to be internalized, the receptor-ligand complexes must first cluster into clathrin-coated pits. . (Microbial infection) Acts as a receptor for hepatitis C virus in hepatocytes, but not through a direct interaction with viral proteins. . (Microbial infection) Acts as a receptor for Vesicular stomatitis virus. . (Microbial infection) In case of HIV-1 infection, may function as a receptor for extracellular Tat in neurons, mediating its internalization in uninfected cells.
ENSG00000109062	s17920	SLC9A3R1	1.076705127	SLC9A3 regulator 1	Scaffold protein that connects plasma membrane proteins with members of the ezrin/moesin/radixin family and thereby helps to link them to the actin cytoskeleton and to regulate their surface expression. Necessary for recycling of internalized ADRB2. Was first known to play a role in the regulation of the activity and subcellular location of SLC9A3. Necessary for cAMP-mediated phosphorylation and inhibition of SLC9A3. May enhance Wnt signaling. May participate in HTR4 targeting to microvilli (By similarity). Involved in the regulation of phosphate reabsorption in the renal proximal tubules. Involved in sperm capacitation. May participate in the regulation of the chloride and bicarbonate homeostasis in spermatozoa.

Ensembl ID (v. 92)	siRNA IDs	Targeted gene	Average PM score	Targeted gene name	Function of targeted gene
ENSG00000160746	s30238	ANO10	1.072553856	anoctamin 10	Does not exhibit calcium-activated chloride channel (CaCC) activity. Can inhibit the activity of ANO1.
ENSG00000177283	s15844; s15845	FZD8	1.070816914	frizzled class receptor 8	Receptor for Wnt proteins. Component of the Wnt-Fzd- LRP5-LRP6 complex that triggers beta-catenin signaling through inducing aggregation of receptor-ligand complexes into ribosome-sized signalosomes. The beta-catenin canonical signaling pathway leads to the activation of disheveled proteins, inhibition of GSK- 3 kinase, nuclear accumulation of beta-catenin and activation of Wnt target genes. A second signaling pathway involving PKC and calcium fluxes has been seen for some family members, but it is not yet clear if it represents a distinct pathway or if it can be integrated in the canonical pathway, as PKC seems to be required for Wnt-mediated inactivation of GSK-3 kinase. Both pathways seem to involve interactions with G-proteins. May be involved in transduction and intercellular transmission of polarity information during tissue morphogenesis and/or in differentiated tissues. Coreceptor along with RYK of Wnt proteins, such as WNT1.
ENSG00000112763	s21927	BTN2A1	1.070045722	butyrophilin subfamily 2 member A1	Gene Ontology (GO) annotations related to this gene include DNA binding transcription factor activity. An important paralog of this gene is TSC22D1.
ENSG00000069345	s20123	DNAJA2	1.063202048	DnaJ heat shock protein family (Hsp40) member A2	Co-chaperone of Hsc70. Stimulates ATP hydrolysis and the folding of unfolded proteins mediated by HSPA1A/B (in vitro).
ENSG00000151067	s2285	CACNA1C	1.052469474	calcium voltage-gated channel subunit alpha1 C	Voltage-sensitive calcium channels (VSCC) mediate the entry of calcium ions into excitable cells and are also involved in a variety of calcium-dependent processes, including muscle contraction, hormone or neurotransmitter release, gene expression, cell motility, cell division and cell death. The isoform alpha-1C gives rise to L-type calcium currents. Long- lasting (L-type) calcium channels belong to the 'high-voltage activated' (HVA) group. They are blocked by dihydropyridines (DHP), phenylalkylamines, benzothiazepines, and by omega-agatoxin- IIIA (omega-Aga-IIIA). They are however insensitive to omega- conotoxin-GVIA (omega-CTx-GVIA) and omega-agatoxin-IVA (omega-Aga- IVA). Calcium channels containing the alpha-1C subunit play an important role in excitation-contraction coupling in the heart. The various isoforms display marked differences in the sensitivity to DHP compounds. Binding of calmodulin or CABP1 at the same regulatory sites results in opposite effects on the channel function. STAC3 strongly decreases the rate of channel inactivation.
ENSG00000243477	s24422	NAT6	1.051038889	N-acetyltransferase 6	Seems to be involved in N-acetylation. Acts on peptides with a N-terminal Met followed by Asp/Glu/Asn. May act as a tumor suppressor.
ENSG00000171700	s20107	RGS19	1.042461299	regulator of G-protein signaling 19	Inhibits signal transduction by increasing the GTPase activity of G protein alpha subunits thereby driving them into their inactive GDP-bound form. Binds to G-alpha subfamily 1 members, with the order G(i)a3 > G(i)a1 > G(o)a >> G(z)a/G(i)a2. Activity on G(z)-alpha is inhibited by phosphorylation and palmitoylation of the G-protein.
ENSG00000153064	s30014; s223197	BANK1	1.040194575	B-cell scaffold protein with ankyrin repeats 1	Involved in B-cell receptor (BCR)-induced Ca(2+) mobilization from intracellular stores. Promotes Lyn-mediated phosphorylation of IP3 receptors 1 and 2.
ENSG00000157680	s17511	DGKI	1.038975826	diacylglycerol kinase iota	Gene Ontology (GO) annotations related to this gene include DNA binding transcription factor activity. An important paralog of this gene is TSC22D1.

Ensembl ID (v. 92)	siRNA IDs	Targeted gene	Average PM score	Targeted gene name	Function of targeted gene
ENSG00000171180	s25283	OR2M4	1.038670932	olfactory receptor family 2 subfamily M member 4	Odorant receptor.
ENSG00000165832	s44503	TRUB1	1.038307831	TruB pseudouridine synthase family member 1	May be responsible for synthesis of pseudouridine from uracil in transfer RNAs.
ENSG00000130368	s8521	MAS1	1.036561186	MAS1 proto-oncogene, G protein-coupled receptor	Receptor for angiotensin 1-7 (By similarity). Acts specifically as a functional antagonist of AGTR1 (angiotensin-2 type 1 receptor), although it up-regulates AGTR1 receptor levels. Positive regulation of AGTR1 levels occurs through activation of the G-proteins GNA11 and GNAQ, and stimulation of the protein kinase C signaling cascade. The antagonist effect on AGTR1 function is probably due to AGTR1 being physically altered by MAS1.
ENSG00000180251	s52339	SLC9A4	1.028645836	solute carrier family 9 member A4	Involved in pH regulation to eliminate acids generated by active metabolism or to counter adverse environmental conditions. Major proton extruding system driven by the inward sodium ion chemical gradient. Plays an important role in signal transduction. May play a specialized role in the kidney in rectifying cell volume in response to extreme fluctuations of hyperosmolar-stimulated cell shrinkage. Is relatively amiloride and ethylisopropylamiloride (EIPA) insensitive. Can be activated under conditions of hyperosmolar-induced cell shrinkage in a sustained intracellular acidification-dependence manner. Activated by 4,4'-diisothiocyanostilbene-2,2'-disulfonic acid (DIDS) in a sustained intracellular acidification-dependence manner. Affects potassium/proton exchange as well as sodium/proton and lithium/proton exchange. In basolateral cell membrane, participates in homeostatic control of intracellular pH, and may play a role in proton extrusion in order to achieve transepithelial HCO3(-) secretion. In apical cell membrane may be involved in mediating sodium absorption. Requires for normal levels of gastric acid secretion, secretory membrane development, parietal cell maturation and/or differentiation and at least secondarily for chief cell differentiation (By similarity).

Ensembl ID (v. 92)	siRNA IDs	Targeted gene	Average PM score	Targeted gene name	Function of targeted gene
ENSG00000142208	s659	AKT1	1.022023843	AKT serine/threonine kinase 1	AKT1 is one of 3 closely related serine/threonine- protein kinases (AKT1, AKT2 and AKT3) called the AKT kinase, and which regulate many processes including metabolism, proliferation, cell survival, growth and angiogenesis. This is mediated through serine and/or threonine phosphorylation of a range of downstream substrates. Over 100 substrate candidates have been reported so far, but for most of them, no isoform specificity has been reported. AKT is responsible of the regulation of glucose uptake by mediating insulin-induced translocation of the SLC2A4/GLUT4 glucose transporter to the cell surface. Phosphorylation of PTPN1 at 'Ser-50' negatively modulates its phosphatase activity preventing dephosphorylation of the insulin receptor and the attenuation of insulin signaling. Phosphorylation of TBC1D4 triggers the binding of this effector to inhibitory 14-3-3 proteins, which is required for insulin-stimulated glucose transport. AKT regulates also the storage of glucose in the form of glycogen by phosphorylating GSK3A at 'Ser-21' and GSK3B at 'Ser-9', resulting in inhibition of its kinase activity. Phosphorylation of GSK3 isoforms by AKT is also thought to be one mechanism by which cell proliferation is driven. AKT regulates also cell survival via the phosphorylation of MAP3K5 (apoptosis signal-related kinase). Phosphorylation of 'Ser-83' decreases MAP3K5 kinase activity stimulated by oxidative stress and thereby prevents apoptosis. AKT mediates insulin-stimulated protein synthesis by phosphorylating TSC2 at 'Ser-939' and 'Thr-1462', thereby activating mTORC1 signaling and leading to both phosphorylation of 4E-BP1 and in activation of RPS6KB1. AKT is involved in the phosphorylation of members of the FOXO factors (Forkhead family of transcription factors), leading to binding of 14-3-3 proteins and cytoplasmic localization. In particular, FOXO1 is phosphorylated at 'Thr-24', 'Ser-256' and 'Ser-319'. FOXO3 and FOXO4 are phosphorylated on equivalent sites. AKT has an important role in the regulation of NF-kappa-B-dependent gene transcription and positively regulates the activity of CREB1 (cyclic AMP (cAMP)- response element binding protein). The phosphorylation of CREB1 induces the binding of accessory proteins that are necessary for the transcription of pro-survival genes such as BCL2 and MCL1. AKT phosphorylates 'Ser-454' on ATP citrate lyase (ACLY), thereby potentially regulating ACLY activity and fatty acid synthesis. Activates the 3B isoform of cyclic nucleotide phosphodiesterase (PDE3B) via phosphorylation of 'Ser-273', resulting in reduced cyclic AMP levels and inhibition of lipolysis. Phosphorylates PIKFYVE on 'Ser-318', which results in increased PI(3)P-5 activity. The Rho GTPase-activating protein DLC1 is another substrate and its phosphorylation is implicated in the regulation cell proliferation and cell growth. AKT plays a role as key modulator of the AKT-mTOR signaling pathway controlling the tempo of the process of newborn neurons integration during adult neurogenesis, including correct neuron positioning, dendritic development and synapse formation. Signals downstream of phosphatidylinositol 3-kinase (PI(3)K) to mediate the effects of various growth factors such as platelet-derived growth factor (PDGF), epidermal growth factor (EGF), insulin and insulin-like growth factor I (IGF-I). AKT mediates the antiapoptotic effects of IGF-I.
ENSG00000074855	s33673	ANO8	1.020860107	anoctamin 8	Does not exhibit calcium-activated chloride channel (CaCC) activity.

Ensembl ID (v. 92)	siRNA IDs	Targeted gene	Average PM score	Targeted gene name	Function of targeted gene
ENSG00000113812	s41202	ACTR8	1.020840693	ARP8 actin-related protein 8 homolog	Plays an important role in the functional organization of mitotic chromosomes. Exhibits low basal ATPase activity, and unable to polymerize. Proposed core component of the chromatin remodeling INO80 complex which is involved in transcriptional regulation, DNA replication and probably DNA repair. Required for the recruitment of INO80 (and probably the INO80 complex) to sites of DNA damage. Strongly prefer nucleosomes and H3-H4 tetramers over H2A-H2B dimers, suggesting it may act as a nucleosome recognition module within the complex.
ENSG00000087586	s197	AURKA	1.016866376	aurora kinase A	Mitotic serine/threonine kinase that contributes to the regulation of cell cycle progression. Associates with the centrosome and the spindle microtubules during mitosis and plays a critical role in various mitotic events including the establishment of mitotic spindle, centrosome duplication, centrosome separation as well as maturation, chromosomal alignment, spindle assembly checkpoint, and cytokinesis. Required for initial activation of CDK1 at centrosomes. Phosphorylates numerous target proteins, including ARHGEF2, BORA, BRCA1, CDC25B, DLGP5, HDAC6, KIF2A, LATS2, NDEL1, PARD3, PPP1R2, PLK1, RASSF1, TACC3, p53/TP53 and TPX2. Regulates KIF2A tubulin depolymerase activity. Required for normal axon formation. Plays a role in microtubule remodeling during neurite extension. Important for microtubule formation and/or stabilization. Also acts as a key regulatory component of the p53/TP53 pathway, and particularly the checkpoint-response pathways critical for oncogenic transformation of cells, by phosphorylating and stabilizing p53/TP53. Phosphorylates its own inhibitors, the protein phosphatase type 1 (PP1) isoforms, to inhibit their activity. Necessary for proper cilia disassembly prior to mitosis.
ENSG00000157426	s43742	AASDH	1.012713834	aminoadipate-semialdehyde dehydrogenase	Covalently binds beta-alanine in an ATP-dependent manner to form a thioester bond with its phosphopantetheine group and transfers it to an, as yet, unknown acceptor. May be required for a post-translational protein modification or for post- transcriptional modification of an RNA.
ENSG00000198873	s6089	GRK5	1.008597065	G protein-coupled receptor kinase 5	Serine/threonine kinase that phosphorylates preferentially the activated forms of a variety of G-protein- coupled receptors (GPCRs). Such receptor phosphorylation initiates beta-arrestin-mediated receptor desensitization, internalization, and signaling events leading to their down-regulation. Phosphorylates a variety of GPCRs, including adrenergic receptors, muscarinic acetylcholine receptors (more specifically Gi-coupled M2/M4 subtypes), dopamine receptors and opioid receptors. In addition to GPCRs, also phosphorylates various substrates: Hsc70-interacting protein/ST13, TP53/p53, HDAC5, and arrestin-1/ARRB1. Phosphorylation of ARRB1 by GRK5 inhibits G-protein independent MAPK1/MAPK3 signaling downstream of 5HT4-receptors. Phosphorylation of HDAC5, a repressor of myocyte enhancer factor 2 (MEF2) leading to nuclear export of HDAC5 and allowing MEF2- mediated transcription. Phosphorylation of TP53/p53, a crucial tumor suppressor, inhibits TP53/p53-mediated apoptosis. Phosphorylation of ST13 regulates internalization of the chemokine receptor. Phosphorylates rhodopsin (RHO) (in vitro) and a non G- protein-coupled receptor, LRP6 during Wnt signaling (in vitro).

Ensembl ID (v. 92)	siRNA IDs	Targeted gene	Average PM score	Targeted gene name	Function of targeted gene
ENSG00000078269	s16942	SYNJ2	1.006728228	synaptojanin 2	Inositol 5-phosphatase which may be involved in distinct membrane trafficking and signal transduction pathways. May mediate the inhibitory effect of Rac1 on endocytosis.
ENSG00000167508	s224074	MVD	1.00379844	mevalonate diphosphate decarboxylase	Performs the first committed step in the biosynthesis of isoprenes.
ENSG00000166856	s22314	GPR182	1.001821139	G protein-coupled receptor 182	Orphan receptor.

Table S 9 – TMEM16A traffic inhibitor siRNAs.

Ensembl ID (v. 92)	siRNA IDs	Targeted gene	Average PM score	Targeted gene name	Function of targeted gene
ENSG00000076248	s14680	UNG	-1.000559271	uracil DNA glycosylase	Excises uracil residues from the DNA which can arise as a result of misincorporation of dUMP residues by DNA polymerase or due to deamination of cytosine.
ENSG00000136573	s1996	BLK	-1.003988366	BLK proto-oncogene, Src family tyrosine kinase	Non-receptor tyrosine kinase involved in B-lymphocyte development, differentiation and signaling. B-cell receptor (BCR) signaling requires a tight regulation of several protein tyrosine kinases and phosphatases, and associated coreceptors. Binding of antigen to the B-cell antigen receptor (BCR) triggers signaling that ultimately leads to B-cell activation. Signaling through BLK plays an important role in transmitting signals through surface immunoglobulins and supports the pro-B to pre-B transition, as well as the signaling for growth arrest and apoptosis downstream of B-cell receptor. Specifically binds and phosphorylates CD79A at 'Tyr-188'and 'Tyr-199', as well as CD79B at 'Tyr-196' and 'Tyr- 207'. Phosphorylates also the immunoglobulin G receptors FCGR2A, FCGR2B and FCGR2C. With FYN and LYN, plays an essential role in pre-B-cell receptor (pre-BCR)-mediated NF-kappa-B activation. Contributes also to BTK activation by indirectly stimulating BTK intramolecular autophosphorylation. In pancreatic islets, acts as a modulator of beta-cells function through the up-regulation of PDX1 and NKX6-1 and consequent stimulation of insulin secretion in response to glucose.
ENSG00000007264	s585	MATK	-1.004198795	megakaryocyte-associated tyrosine kinase	Could play a significant role in the signal transduction of hematopoietic cells. May regulate tyrosine kinase activity of SRC-family members in brain by specifically phosphorylating their C-terminal regulatory tyrosine residue which acts as a negative regulatory site. It may play an inhibitory role in the control of T-cell proliferation.
ENSG00000100412	s923	ACO2	-1.007272912	aconitase 2	Catalyzes the isomerization of citrate to isocitrate via cis-aconitate.
ENSG00000156709	s17441	AIFM1	-1.008978844	apoptosis inducing factor, mitochondria associated 1	Functions both as NADH oxidoreductase and as regulator of apoptosis. In response to apoptotic stimuli, it is released from the mitochondrion intermembrane space into the cytosol and to the nucleus, where it functions as a proapoptotic factor in a caspase-independent pathway. In contrast, functions as an antiapoptotic factor in normal mitochondria via its NADH oxidoreductase activity. The soluble form (AIFsol) found in the nucleus induces 'parthanatos' i.e. caspase-independent fragmentation of chromosomal DNA. Interacts with EIF3G,and thereby inhibits the EIF3 machinery and protein synthesis, and activates casapse-7 to amplify apoptosis. Plays a critical role in caspase- independent, pyknotic cell death in hydrogen peroxide-exposed cells. Binds to DNA in a sequence-independent manner.
ENSG00000131724	s7372	IL13RA1	-1.027454113	interleukin 13 receptor subunit alpha 1	Binds with low affinity to interleukin-13 (IL13). Together with IL4RA can form a functional receptor for IL13. Also serves as an alternate accessory protein to the common cytokine receptor gamma chain for interleukin-4 (IL4) signaling, but cannot replace the function of IL2RG in allowing enhanced interleukin-2 (IL2) binding activity.
ENSG00000175344	s3053	CHRNA7	-1.030799379	cholinergic receptor nicotinic alpha 7 subunit	After binding acetylcholine, the AChR responds by an extensive change in conformation that affects all subunits and leads to opening of an ion-conducting channel across the plasma membrane. The channel is blocked by alpha-bungarotoxin.

Ensembl ID (v. 92)	siRNA IDs	Targeted gene	Average PM score	Targeted gene name	Function of targeted gene
ENSG00000140526	s21786	ABHD2	-1.039321547	abhydrolase domain containing 2	Progesterone-dependent acylglycerol lipase that catalyzes hydrolysis of endocannabinoid arachidonoylglycerol (AG) from cell membrane. Acts as a progesterone receptor: progesterone-binding activates the acylglycerol lipase activity, mediating degradation of 1-arachidonoylglycerol (1AG) and 2-arachidonoylglycerol (2AG) to glycerol and arachidonic acid (AA). Plays a key role in sperm capacitation in response to progesterone by mediating degradation of 2AG, an inhibitor of the sperm calcium channel CatSper, leading to calcium influx via CatSper and sperm activation. May also play a role in smooth muscle cells migration (By similarity).
ENSG00000126010	s6230	GRPR	-1.039862065	gastrin releasing peptide receptor	Receptor for gastrin-releasing peptide (GRP). Signals via association with G proteins that activate a phosphatidylinositol-calcium second messenger system, resulting in Akt phosphorylation. Contributes to the regulation of food intake. Contributes to the perception of prurient stimuli and transmission of itch signals in the spinal cord that promote scratching behavior, but does not play a role in the perception of pain. Contributes primarily to nonhistaminergic itch sensation. Contributes to long-term fear memory, but not normal spatial memory (By similarity).
ENSG00000204003	s46025	LCN6	-1.040576567	lipocalin 6	May play a role in male fertility.

Ensembl ID (v. 92)	siRNA IDs	Targeted gene	Average PM score	Targeted gene name	Function of targeted gene
ENSG00000118515	s741	SGK1	-1.043730206	serum/glucocorticoid regulated kinase 1	Serine/threonine-protein kinase which is involved in the regulation of a wide variety of ion channels, membrane transporters, cellular enzymes, transcription factors, neuronal excitability, cell growth, proliferation, survival, migration and apoptosis. Plays an important role in cellular stress response. Contributes to regulation of renal Na(+) retention, renal K(+) elimination, salt appetite, gastric acid secretion, intestinal Na(+)/H(+) exchange and nutrient transport, insulin-dependent salt sensitivity of blood pressure, salt sensitivity of peripheral glucose uptake, cardiac repolarization and memory consolidation. Up-regulates Na(+) channels: SCNN1A/ENAC, SCN5A and ASIC1/ACCN2, K(+) channels: KCNJ1/ROMK1, KCNA1-5, KCNQ1-5 and KCNE1, epithelial Ca(2+) channels: TRPV5 and TRPV6, chloride channels: BSND, CLCN2 and CFTR, glutamate transporters: SLC1A3/EAAT1, SLC1A2 /EAAT2, SLC1A1/EAAT3, SLC1A6/EAAT4 and SLC1A7/EAAT5, amino acid transporters: SLC1A5/ASCT2, SLC38A1/SN1 and SLC6A19, creatine transporter: SLC6A8, Na(+)/dicarboxylate cotransporter: SLC13A2/NADC1, Na(+)-dependent phosphate cotransporter: SLC34A2/NAPI-2B, glutamate receptor: GRIK2/GLUR6. Up-regulates carriers: SLC9A3/NHE3, SLC12A1/NKCC2, SLC12A3/NCC, SLC5A3/SMIT, SLC2A1/GLUT1, SLC5A1/SGLT1 and SLC15A2/PEPT2. Regulates enzymes: GSK3A/B, PMM2 and Na(+)/K(+) ATPase, and transcription factors: CTNNB1 and nuclear factor NF-kappa-B. Stimulates sodium transport into epithelial cells by enhancing the stability and expression of SCNN1A/ENAC. This is achieved by phosphorylating the NEDD4L ubiquitin E3 ligase, promoting its interaction with 14-3-3 proteins, thereby preventing it from binding to SCNN1A/ENAC and targeting it for degradation. Regulates store-operated Ca(+2) entry (SOCE) by stimulating ORAI1 and STIM1. Regulates KCNJ1/ROMK1 directly via its phosphorylation or indirectly via increased interaction with SLC9A3R2/NHERF2. Phosphorylates MDM2 and activates MDM2-dependent ubiquitination of p53/TP53. Phosphorylates MAPT/TAU and mediates microtubule depolymerization and neurite formation in hippocampal neurons. Phosphorylates SLC2A4/GLUT4 and up-regulates its activity. Phosphorylates APBB1/FE65 and promotes its localization to the nucleus. Phosphorylates MAPK1/ERK2 and activates it by enhancing its interaction with MAP2K1/MEK1 and MAP2K2/MEK2. Phosphorylates FBXW7 and plays an inhibitory role in the NOTCH1 signaling. Phosphorylates FOXO1 resulting in its relocalization from the nucleus to the cytoplasm. Phosphorylates FOXO3, promoting its exit from the nucleus and interference with FOXO3-dependent transcription. Phosphorylates BRAF and MAP3K3/MEKK3 and inhibits their activity. Phosphorylates SLC9A3/NHE3 in response to dexamethasone, resulting in its activation and increased localization at the cell membrane. Phosphorylates CREB1. Necessary for vascular remodeling during angiogenesis. Sustained high levels and activity may contribute to conditions such as hypertension and diabetic nephropathy. Isoform 2 exhibited a greater effect on cell plasma membrane expression of SCNN1A/ENAC and Na(+) transport than isoform 1.

Ensembl ID (v. 92)	siRNA IDs	Targeted gene	Average PM score	Targeted gene name	Function of targeted gene
ENSG00000142875	s11068	PRKACB	-1.051991267	protein kinase cAMP-activated catalytic subunit beta	Mediates cAMP-dependent signaling triggered by receptor binding to GPCRs. PKA activation regulates diverse cellular processes such as cell proliferation, the cell cycle, differentiation and regulation of microtubule dynamics, chromatin condensation and decondensation, nuclear envelope disassembly and reassembly, as well as regulation of intracellular transport mechanisms and ion flux. Regulates the abundance of compartmentalized pools of its regulatory subunits through phosphorylation of PJA2 which binds and ubiquitinates these subunits, leading to their subsequent proteolysis. Phosphorylates GPKOW which regulates its ability to bind RNA.
ENSG00000204695	s54504	OR14J1	-1.055881512	olfactory receptor family 14 subfamily J member 1	Odorant receptor.
ENSG00000170683	s25452	OR10A3	-1.067913494	olfactory receptor family 10 subfamily A member 3	Odorant receptor.
ENSG00000114268	s10361	PFKFB4	-1.068510021	6-phosphofructo-2-kinase/fructose-2,6-biphosphatase 4	Synthesis and degradation of fructose 2,6-bisphosphate.
ENSG00000134986	s17796	NREP	-1.072946052	neuronal regeneration related protein	May have roles in neural function. Ectopic expression augments motility of gliomas. Promotes also axonal regeneration (By similarity). May also have functions in cellular differentiation (By similarity). Induces differentiation of fibroblast into myofibroblast and myofibroblast ameboid migration. Increases retinoic-acid regulation of lipid-droplet biogenesis (By similarity). Down-regulates the expression of TGFB1 and TGFB2 but not of TGFB3 (By similarity). May play a role in the regulation of alveolar generation.
ENSG00000104960	s28750	PTOV1	-1.076300147	prostate tumor overexpressed 1	May activate transcription. Required for nuclear translocation of FLOT1. Promotes cell proliferation.

Ensembl ID (v. 92)	siRNA IDs	Targeted gene	Average PM score	Targeted gene name	Function of targeted gene
ENSG00000185122	s6951	HSF1	-1.085468379	heat shock transcription factor 1	Function as a stress-inducible and DNA-binding transcription factor that plays a central role in the transcriptional activation of the heat shock response (HSR), leading to the expression of a large class of molecular chaperones heat shock proteins (HSPs) that protect cells from cellular insults' damage. In unstressed cells, is present in a HSP90-containing multichaperone complex that maintains it in a non-DNA-binding inactivated monomeric form. Upon exposure to heat and other stress stimuli, undergoes homotrimerization and activates HSP gene transcription through binding to site-specific heat shock elements (HSEs) present in the promoter regions of HSP genes. Activation is reversible, and during the attenuation and recovery phase period of the HSR, returns to its unactivated form. Binds to inverted 5'-NGAAN-3' pentamer DNA sequences. Binds to chromatin at heat shock gene promoters. Plays also several other functions independently of its transcriptional activity. Involved in the repression of Ras-induced transcriptional activation of the c-fos gene in heat-stressed cells. Positively regulates pre-mRNA 3'-end processing and polyadenylation of HSP70 mRNA upon heat-stressed cells in a symplekin (SYMPK)-dependent manner. Plays a role in nuclear export of stress-induced HSP70 mRNA. Plays a role in the regulation of mitotic progression. Plays also a role as a negative regulator of non-homologous end joining (NHEJ) repair activity in a DNA damage- dependent manner. Involved in stress-induced cancer cell proliferation in a IER5-dependent manner. (Microbial infection) Plays a role in latent human immunodeficiency virus (HIV-1) transcriptional reactivation. Binds to the HIV-1 long terminal repeat promoter (LTR) to reactivate viral transcription by recruiting cellular transcriptional elongation factors, such as CDK9, CCNT1 and EP300.
ENSG00000182885	s48198	GPR97	-1.085637351	adhesion G protein-coupled receptor G3	Among its related pathways are Innate Immune System. Gene Ontology (GO) annotations related to this gene include G-protein coupled receptor activity and transmembrane signaling receptor activity. An important paralog of this gene is ADGRG1.
ENSG00000123815	s36677	ADCK4	-1.087403515	coenzyme Q8B	Gene Ontology (GO) annotations related to this gene include DNA binding transcription factor activity. An important paralog of this gene is TSC22D1.
ENSG00000162337	s8293	LRP5	-1.087626427	LDL receptor related protein 5	Component of the Wnt-Fzd-LRP5-LRP6 complex that triggers beta-catenin signaling through inducing aggregation of receptor- ligand complexes into ribosome-sized signalsomes. Cell-surface coreceptor of Wnt/beta-catenin signaling, which plays a pivotal role in bone formation. Plays a role in norrin (NDP) signal transduction. The Wnt-induced Fzd/LRP6 coreceptor complex recruits DVL1 polymers to the plasma membrane which, in turn, recruits the AXIN1/GSK3B-complex to the cell surface promoting the formation of signalsomes and inhibiting AXIN1/GSK3-mediated phosphorylation and destruction of beta- catenin. Appears be required for postnatal control of vascular regression in the eye (By similarity). Required for posterior patterning of the epiblast during gastrulation (By similarity).
ENSG00000167261	s34535	DPEP2	-1.097855141	dipeptidase 2	Probable metalloprotease which hydrolyzes leukotriene D4 (LTD4) into leukotriene E4 (LTE4).

Ensembl ID (v. 92)	siRNA IDs	Targeted gene	Average PM score	Targeted gene name	Function of targeted gene
ENSG00000160349	s8109	LCN1	-1.104368438	lipocalin 1	Could play a role in taste reception. Could be necessary for the concentration and delivery of sapid molecules in the gustatory system. Can bind various ligands, with chemical structures ranging from lipids and retinoids to the macrocyclic antibiotic rifampicin and even to microbial siderophores. Exhibits an extremely wide ligand pocket.
ENSG00000153933	s16206	DGKE	-1.112979766	diacylglycerol kinase epsilon	Highly selective for arachidonate-containing species of diacylglycerol (DAG). May terminate signals transmitted through arachidonoyl-DAG or may contribute to the synthesis of phospholipids with defined fatty acid composition.
ENSG00000168653	s9399	NDUFS5	-1.115685883	NADH:ubiquinone oxidoreductase subunit S5	Accessory subunit of the mitochondrial membrane respiratory chain NADH dehydrogenase (Complex I), that is believed not to be involved in catalysis. Complex I functions in the transfer of electrons from NADH to the respiratory chain. The immediate electron acceptor for the enzyme is believed to be ubiquinone.
ENSG00000185483	s9756	ROR1	-1.135501341	receptor tyrosine kinase like orphan receptor 1	Has very low kinase activity in vitro and is unlikely to function as a tyrosine kinase in vivo. Receptor for ligand WNT5A which activate downstream NFkB signaling pathway and may result in the inhibition of WNT3A-mediated signaling. In inner ear, crucial for spiral ganglion neurons to innervate auditory hair cells.
ENSG00000069122	s48030	GPR116	-1.141801898	adhesion G protein-coupled receptor F5	Gene Ontology (GO) annotations related to this gene include DNA binding transcription factor activity. An important paralog of this gene is TSC22D1.
ENSG00000134817	s223458	APLNR	-1.157523739	apelin receptor	Receptor for apelin receptor early endogenous ligand (APELA) and apelin (APLN) hormones coupled to G proteins that inhibit adenylate cyclase activity. Plays a key role in early development such as gastrulation, blood vessels formation and heart morphogenesis by acting as a receptor for APELA hormone (By similarity). May promote angioblast migration toward the embryonic midline, i.e. the position of the future vessel formation, during vasculogenesis (By similarity). Promotes sinus venosus (SV)- derived endothelial cells migration into the developing heart to promote coronary blood vessel development (By similarity). Plays also a role in various processes in adults such as regulation of blood vessel formation, blood pressure, heart contractility and heart failure. (Microbial infection) Alternative coreceptor with CD4 for HIV-1 infection; may be involved in the development of AIDS dementia.
ENSG00000127472	s10595	PLA2G5	-1.185302669	phospholipase A2 group V	PA2 catalyzes the calcium-dependent hydrolysis of the 2- acyl groups in 3-sn-phosphoglycerides. This isozyme hydrolyzes more efficiently L-alpha-1-palmitoyl-2-oleoyl phosphatidylcholine than L-alpha-1-palmitoyl-2-arachidonyl phosphatidylcholine, L- alpha-1-palmitoyl-2-arachidonyl phosphatidylethanolamine, or L- alpha-1-stearoyl-2-arachidonyl phosphatidylinositol. May be involved in the production of lung surfactant, the remodeling or regulation of cardiac muscle.

Ensembl ID (v. 92)	siRNA IDs	Targeted gene	Average PM score	Targeted gene name	Function of targeted gene
ENSG00000005243	s27714	COPZ2	-1.209723533	coatomer protein complex subunit zeta 2	The coatomer is a cytosolic protein complex that binds to dilysine motifs and reversibly associates with Golgi non- clathrin-coated vesicles, which further mediate biosynthetic protein transport from the ER, via the Golgi up to the trans Golgi network. Coatomer complex is required for budding from Golgi membranes, and is essential for the retrograde Golgi-to-ER transport of dilysine-tagged proteins. The zeta subunit may be involved in regulating the coat assembly and, hence, the rate of biosynthetic protein transport due to its association-dissociation properties with the coatomer complex (By similarity).
ENSG00000183621	s47912	ZNF438	-1.213699218	zinc finger protein 438	Isoform 1 acts as a transcriptional repressor.
ENSG00000180016	s15919	OR1E1	-1.216403049	olfactory receptor family 1 subfamily E member 1	Odorant receptor.
ENSG00000165370	s38004	GPR101	-1.216532988	G protein-coupled receptor 101	Orphan receptor.
ENSG00000113231	s16401	PDE8B	-1.23287974	phosphodiesterase 8B	Hydrolyzes the second messenger cAMP, which is a key regulator of many important physiological processes. May be involved in specific signaling in the thyroid gland.
ENSG00000087586	s195	AURKA	-1.265358298	aurora kinase A	Mitotic serine/threonine kinase that contributes to the regulation of cell cycle progression. Associates with the centrosome and the spindle microtubules during mitosis and plays a critical role in various mitotic events including the establishment of mitotic spindle, centrosome duplication, centrosome separation as well as maturation, chromosomal alignment, spindle assembly checkpoint, and cytokinesis. Required for initial activation of CDK1 at centrosomes. Phosphorylates numerous target proteins, including ARHGEF2, BORA, BRCA1, CDC25B, DLGP5, HDAC6, KIF2A, LATS2, NDEL1, PARD3, PPP1R2, PLK1, RASSF1, TACC3, p53/TP53 and TPX2. Regulates KIF2A tubulin depolymerase activity. Required for normal axon formation. Plays a role in microtubule remodeling during neurite extension. Important for microtubule formation and/or stabilization. Also acts as a key regulatory component of the p53/TP53 pathway, and particularly the checkpoint-response pathways critical for oncogenic transformation of cells, by phosphorylating and stabilizing p53/TP53. Phosphorylates its own inhibitors, the protein phosphatase type 1 (PP1) isoforms, to inhibit their activity. Necessary for proper cilia disassembly prior to mitosis.
ENSG00000013441	s3162	CLK1	-1.278735492	CDC like kinase 1	Dual specificity kinase acting on both serine/threonine and tyrosine-containing substrates. Phosphorylates serine- and arginine-rich (SR) proteins of the spliceosomal complex and may be a constituent of a network of regulatory mechanisms that enable SR proteins to control RNA splicing. Phosphorylates: SRSF1, SRSF3 and PTPN1. Regulates the alternative splicing of tissue factor (F3) pre-mRNA in endothelial cells and adenovirus E1A pre-mRNA.

Ensembl ID (v. 92)	siRNA IDs	Targeted gene	Average PM score	Targeted gene name	Function of targeted gene
ENSG00000101197	s35797	BIRC7	-1.285008814	baculoviral IAP repeat containing 7	Apoptotic regulator capable of exerting proapoptotic and anti-apoptotic activities and plays crucial roles in apoptosis, cell proliferation, and cell cycle control. Its anti-apoptotic activity is mediated through the inhibition of CASP3, CASP7 and CASP9, as well as by its E3 ubiquitin-protein ligase activity. As it is a weak caspase inhibitor, its anti-apoptotic activity is thought to be due to its ability to ubiquitinate DIABLO/SMAC targeting it for degradation thereby promoting cell survival. May contribute to caspase inhibition, by blocking the ability of DIABLO/SMAC to disrupt XIAP/BIRC4-caspase interactions. Protects against apoptosis induced by TNF or by chemical agents such as adriamycin, etoposide or staurosporine. Suppression of apoptosis is mediated by activation of MAPK8/JNK1, and possibly also of MAPK9/JNK2. This activation depends on TAB1 and NR2C2/TAK1. In vitro, inhibits CASP3 and proteolytic activation of pro-CASP9. Isoform 1 blocks staurosporine-induced apoptosis. Isoform 2 blocks etoposide-induced apoptosis. Isoform 2 protects against natural killer (NK) cell killing whereas isoform 1 augments killing.
ENSG00000213024	s24248	NUP62	-1.299938496	nucleoporin 62	Essential component of the nuclear pore complex. The N-terminal is probably involved in nucleocytoplasmic transport. The C-terminal is involved in protein-protein interaction probably via coiled-coil formation, promotes its association with centrosomes and may function in anchorage of p62 to the pore complex. Plays a role in mitotic cell cycle progression by regulating centrosome segregation, centriole maturation and spindle orientation. It might be involved in protein recruitment to the centrosome after nuclear breakdown.
ENSG00000124939	s8729	SCGB2A1	-1.308368655	secretoglobin family 2A member 1	May bind androgens and other steroids, may also bind estramustine, a chemotherapeutic agent used for prostate cancer. May be under transcriptional regulation of steroid hormones.
ENSG00000170426	s42433	SDR9C7	-1.31989771	short chain dehydrogenase/reductase family 9C, member 7	Displays weak conversion of all-trans-retinal to all- trans-retinol in the presence of NADH. Has apparently no steroid dehydrogenase activity.
ENSG00000168412	s9047	MTNR1A	-1.330665621	melatonin receptor 1A	High affinity receptor for melatonin. Likely to mediate the reproductive and circadian actions of melatonin. The activity of this receptor is mediated by pertussis toxin sensitive G proteins that inhibit adenylate cyclase activity.

Ensembl ID (v. 92)	siRNA IDs	Targeted gene	Average PM score	Targeted gene name	Function of targeted gene
ENSG00000196083	s7275	IL1RAP	-1.335070021	interleukin 1 receptor accessory protein	Coreceptor for IL1RL2 in the IL-36 signaling system (By similarity). Coreceptor with IL1R1 in the IL-1 signaling system. Associates with IL1R1 bound to IL1B to form the high affinity interleukin-1 receptor complex which mediates interleukin-1- dependent activation of NF-kappa-B and other pathways. Signaling involves the recruitment of adapter molecules such as TOLLIP, MYD88, and IRAK1 or IRAK2 via the respective TIR domains of the receptor/coreceptor subunits. Recruits TOLLIP to the signaling complex. Does not bind to interleukin-1 alone; binding of IL1RN to IL1R1, prevents its association with IL1R1 to form a signaling complex. The cellular response is modulated through a non- signaling association with the membrane IL1R2 decoy receptor. Coreceptor for IL1RL1 in the IL-33 signaling system. Can bidirectionally induce pre- and postsynaptic differentiation of neurons by trans-synaptically binding to PTPRD (By similarity). Isoform 2: Associates with secreted ligand-bound IL1R2 and increases the affinity of secreted IL1R2 for IL1B; this complex formation may be the dominant mechanism for neutralization of IL1B by secreted/soluble receptors. Enhances the ability of secreted IL1R1 to inhibit IL-33 signaling (By similarity). Isoform 4: Unable to mediate canonical IL-1 signaling. Required for Src phosphorylation by IL1B. May be involved in IL1B-potentiated NMDA-induced calcium influx in neurons (By similarity).
ENSG00000169021	s14705	UQCRFS1	-1.340431178	ubiquinol-cytochrome c reductase, Rieske iron-sulfur polypeptide 1	Cytochrome b-c1 complex subunit Rieske, mitochondrial: Component of the mitochondrial ubiquinol-cytochrome c reductase complex dimer (complex III dimer), which is a respiratory chain that generates an electrochemical potential coupled to ATP synthesis. Incorporation of UQCRFS1 is the penultimate step in complex III assembly (By similarity). . Cytochrome b-c1 complex subunit 9: Possible component of the mitochondrial ubiquinol-cytochrome c reductase complex dimer (complex III dimer), which is a respiratory chain that generates an electrochemical potential coupled to ATP synthesis. UQCRFS1 undergoes proteolytic processing once it is incorporated in the complex III dimer, including this fragment, called subunit 9, which corresponds to the transit peptide. The proteolytic processing is necessary for the correct insertion of UQCRFS1 in the complex III dimer, but the persistence of UQCRFS1-derived fragments may prevent newly imported UQCRFS1 to be processed and assembled into complex III and is detrimental for the complex III structure and function. It is therefore unsure whether the UQCRFS1 fragments, including this fragment, are structural subunits.
ENSG00000139641	s23605; s23606	ESYT1	-1.347009741	extended synaptotagmin 1	Binds glycerophospholipids in a barrel-like domain and may play a role in cellular lipid transport (By similarity). Binds calcium (via the C2 domains) and translocates to sites of contact between the endoplasmic reticulum and the cell membrane in response to increased cytosolic calcium levels. Helps tether the endoplasmic reticulum to the cell membrane and promotes the formation of appositions between the endoplasmic reticulum and the cell membrane.

Ensembl ID (v. 92)	siRNA IDs	Targeted gene	Average PM score	Targeted gene name	Function of targeted gene
ENSG00000103266	s195026	STUB1	-1.349267454	STIP1 homology and U-box containing protein 1	E3 ubiquitin-protein ligase which targets misfolded chaperone substrates towards proteasomal degradation. Collaborates with ATXN3 in the degradation of misfolded chaperone substrates: ATXN3 restricting the length of ubiquitin chain attached to STUB1/CHIP substrates and preventing further chain extension. Ubiquitinates NOS1 in concert with Hsp70 and Hsp40. Modulates the activity of several chaperone complexes, including Hsp70, Hsc70 and Hsp90. Mediates transfer of non-canonical short ubiquitin chains to HSPA8 that have no effect on HSPA8 degradation. Mediates polyubiquitination of DNA polymerase beta (POLB) at 'Lys-41', 'Lys-61' and 'Lys-81', thereby playing a role in base-excision repair: catalyzes polyubiquitination by amplifying the HUWE1/ARF- BP1-dependent monoubiquitination and leading to POLB-degradation by the proteasome. Mediates polyubiquitination of CYP3A4. Ubiquitinates EPHA2 and may regulate the receptor stability and activity through proteasomal degradation. Acts as a co-chaperone for HSPA1A and HSPA1B chaperone proteins and promotes ubiquitin- mediated protein degradation. Negatively regulates the suppressive function of regulatory T-cells (Treg) during inflammation by mediating the ubiquitination and degradation of FOXP3 in a HSPA1A/B-dependent manner. Negatively regulates TGF-beta signaling by modulating the basal level of SMAD3 via ubiquitin-mediated degradation.
ENSG00000115758	s9822	ODC1	-1.37193972	ornithine decarboxylase 1	Catalyzes the first and rate-limiting step of polyamine biosynthesis that converts ornithine into putrescine, which is the precursor for the polyamines, spermidine and spermine. Polyamines are essential for cell proliferation and are implicated in cellular processes, ranging from DNA replication to apoptosis.
ENSG00000145348	s41177	TBCK	-1.386064108	TBC1 domain containing kinase	Involved in the modulation of mTOR signaling and expression of mTOR complex components. Involved in the regulation of cell proliferation and growth. Involved in the control of actin-cytoskeleton organization.
ENSG00000160683	s2004	CXCR5	-1.40272305	C-X-C motif chemokine receptor 5	Cytokine receptor that binds to B-lymphocyte chemoattractant (BLC). Involved in B-cell migration into B-cell follicles of spleen and Peyer patches but not into those of mesenteric or peripheral lymph nodes. May have a regulatory function in Burkitt lymphoma (BL) lymphomagenesis and/or B-cell differentiation.
ENSG00000175175	s22480	PPM1E	-1.404335636	protein phosphatase, Mg2+/Mn2+ dependent 1E	Protein phosphatase that inactivates multifunctional CaM kinases such as CAMK4 and CAMK2 (By similarity). Dephosphorylates and inactivates PAK. May play a role in the inhibition of actin fiber stress breakdown and in morphological changes driven by TNK2/CDC42. Dephosphorylates PRKAA2 (By similarity).
ENSG00000279486	s44606	OR2AG1	-1.432328476	olfactory receptor family 2 subfamily AG member 1 (gene/pseudogene)	Odorant receptor.
ENSG00000168830	s7036	HTR1E	-1.451747453	5-hydroxytryptamine receptor 1E	G-protein coupled receptor for 5-hydroxytryptamine (serotonin). Also functions as a receptor for various alkaloids and psychoactive substances. Ligand binding causes a conformation change that triggers signaling via guanine nucleotide-binding proteins (G proteins) and modulates the activity of down-stream effectors, such as adenylate cyclase. Signaling inhibits adenylate cyclase activity.

Ensembl ID (v. 92)	siRNA IDs	Targeted gene	Average PM score	Targeted gene name	Function of targeted gene
ENSG00000147262	s44243	GPR119	-1.531093956	G protein-coupled receptor 119	Receptor for the endogenous fatty-acid ethanolamide oleoylethanolamide (OEA) and lysophosphatidylcholine (LPC). Functions as a glucose-dependent insulinotropic receptor. The activity of this receptor is mediated by G proteins which activate adenylate cyclase. Seems to act through a G(s) mediated pathway.
ENSG00000163491	s45661	NEK10	-1.540167121	NIMA related kinase 10	Gene Ontology (GO) annotations related to this gene include DNA binding transcription factor activity. An important paralog of this gene is TSC22D1.
ENSG00000132589	s5285	FLOT2	-1.545194665	flotillin 2	May act as a scaffolding protein within caveolar membranes, functionally participating in formation of caveolae or caveolae-like vesicles. May be involved in epidermal cell adhesion and epidermal structure and function.
ENSG00000115170	s975	ACVR1	-1.56691109	activin A receptor type 1	On ligand binding, forms a receptor complex consisting of two type II and two type I transmembrane serine/threonine kinases. Type II receptors phosphorylate and activate type I receptors which autophosphorylate, then bind and activate SMAD transcriptional regulators. Receptor for activin. May be involved for left-right pattern formation during embryogenesis (By similarity).
ENSG00000131080	s34059	EDA2R	-1.585485067	ectodysplasin A2 receptor	Receptor for EDA isoform A2, but not for EDA isoform A1. Mediates the activation of the NF-kappa-B and JNK pathways. Activation seems to be mediated by binding to TRAF3 and TRAF6.
ENSG00000125772	s32104	GPCPD1	-1.604334833	glycerophosphocholine phosphodiesterase 1	May be involved in the negative regulation of skeletal muscle differentiation, independently of its glycerophosphocholine phosphodiesterase activity.
ENSG00000150938	s27728	CRIM1	-1.607233164	cysteine rich transmembrane BMP regulator 1	May play a role in CNS development by interacting with growth factors implicated in motor neuron differentiation and survival. May play a role in capillary formation and maintenance during angiogenesis. Modulates BMP activity by affecting its processing and delivery to the cell surface.
ENSG00000183479	s195094	TREX2	-1.609431924	three prime repair exonuclease 2	Exonuclease with a preference for double-stranded DNA with mismatched 3' termini. May play a role in DNA repair.
ENSG00000145675	s10536	PIK3R1	-1.621139968	phosphoinositide-3-kinase regulatory subunit 1	Binds to activated (phosphorylated) protein-Tyr kinases, through its SH2 domain, and acts as an adapter, mediating the association of the p110 catalytic unit to the plasma membrane. Necessary for the insulin-stimulated increase in glucose uptake and glycogen synthesis in insulin-sensitive tissues. Plays an important role in signaling in response to FGFR1, FGFR2, FGFR3, FGFR4, KITLG/SCF, KIT, PDGFRA and PDGFRB. Likewise, plays a role in ITGB2 signaling. Modulates the cellular response to ER stress by promoting nuclear translocation of XBP1 isoform 2 in a ER stress- and/or insulin-dependent manner during metabolic overloading in the liver and hence plays a role in glucose tolerance improvement.
ENSG00000112033	s10884	PPARD	-1.647281176	peroxisome proliferator activated receptor delta	Ligand-activated transcription factor. Receptor that binds peroxisome proliferators such as hypolipidemic drugs and fatty acids. Has a preference for poly-unsaturated fatty acids, such as gamma-linoleic acid and eicosapentanoic acid. Once activated by a ligand, the receptor binds to promoter elements of target genes. Regulates the peroxisomal beta-oxidation pathway of fatty acids. Functions as transcription activator for the acyl-CoA oxidase gene. Decreases expression of NPC1L1 once activated by a ligand.

Ensembl ID (v. 92)	siRNA IDs	Targeted gene	Average PM score	Targeted gene name	Function of targeted gene
ENSG00000171700	s20109	RGS19	-1.649528811	regulator of G-protein signaling 19	Inhibits signal transduction by increasing the GTPase activity of G protein alpha subunits thereby driving them into their inactive GDP-bound form. Binds to G-alpha subfamily 1 members, with the order G(i)a3 > G(i)a1 > G(o)a >> G(z)a/G(i)a2. Activity on G(z)-alpha is inhibited by phosphorylation and palmitoylation of the G-protein.
ENSG00000198838	s12399; s12400	RYR3	-1.666890657	ryanodine receptor 3	Calcium channel that mediates the release of Ca(2+) from the sarcoplasmic reticulum into the cytoplasm in muscle and thereby plays a role in triggering muscle contraction. May regulate Ca(2+) release by other calcium channels. Calcium channel that mediates Ca(2+)-induced Ca(2+) release from the endoplasmic reticulum in non-muscle cells. Contributes to cellular calcium ion homeostasis (By similarity). Plays a role in cellular calcium signaling.
ENSG00000148680	s7062	HTR7	-1.729182983	5-hydroxytryptamine receptor 7	This is one of the several different receptors for 5- hydroxytryptamine (serotonin), a biogenic hormone that functions as a neurotransmitter, a hormone, and a mitogen. The activity of this receptor is mediated by G proteins that stimulate adenylate cyclase.
ENSG00000105737	s6164	GRIK5	-1.736861834	glutamate ionotropic receptor kainate type subunit 5	Receptor for glutamate. L-glutamate acts as an excitatory neurotransmitter at many synapses in the central nervous system. The postsynaptic actions of Glu are mediated by a variety of receptors that are named according to their selective agonists. This receptor binds kainate > quisqualate > domoate > L- glutamate >> AMPA >> NMDA = 1S,3R-ACPD.
ENSG00000268089	s424	GABRQ	-1.773050967	gamma-aminobutyric acid type A receptor theta subunit	GABA, the major inhibitory neurotransmitter in the vertebrate brain, mediates neuronal inhibition by binding to the GABA/benzodiazepine receptor and opening an integral chloride channel.
ENSG00000102096	s21750	PIM2	-1.784005807	Pim-2 proto-oncogene, serine/threonine kinase	Proto-oncogene with serine/threonine kinase activity involved in cell survival and cell proliferation. Exerts its oncogenic activity through: the regulation of MYC transcriptional activity, the regulation of cell cycle progression, the regulation of cap-dependent protein translation and through survival signaling by phosphorylation of a pro-apoptotic protein, BAD. Phosphorylation of MYC leads to an increase of MYC protein stability and thereby an increase transcriptional activity. The stabilization of MYC exerted by PIM2 might explain partly the strong synergism between these 2 oncogenes in tumorigenesis. Regulates cap-dependent protein translation in a mammalian target of rapamycin complex 1 (mTORC1)-independent manner and in parallel to the PI3K-Akt pathway. Mediates survival signaling through phosphorylation of BAD, which induces release of the anti-apoptotic protein Bcl-X(L)/BCL2L1. Promotes cell survival in response to a variety of proliferative signals via positive regulation of the I-kappa-B kinase/NF-kappa-B cascade; this process requires phosphorylation of MAP3K8/COT. Promotes growth factor-independent proliferation by phosphorylation of cell cycle factors such as CDKN1A and CDKN1B. Involved in the positive regulation of chondrocyte survival and autophagy in the epiphyseal growth plate.
ENSG00000145863	s5487	GABRA6	-1.792962725	gamma-aminobutyric acid type A receptor alpha6 subunit	GABA, the major inhibitory neurotransmitter in the vertebrate brain, mediates neuronal inhibition by binding to the GABA/benzodiazepine receptor and opening an integral chloride channel.

Ensembl ID (v. 92)	siRNA IDs	Targeted gene	Average PM score	Targeted gene name	Function of targeted gene
ENSG00000142627	s4564	EPHA2	-1.822311578	EPH receptor A2	Receptor tyrosine kinase which binds promiscuously membrane-bound ephrin-A family ligands residing on adjacent cells, leading to contact-dependent bidirectional signaling into neighboring cells. The signaling pathway downstream of the receptor is referred to as forward signaling while the signaling pathway downstream of the ephrin ligand is referred to as reverse signaling. Activated by the ligand ephrin-A1/EFNA1 regulates migration, integrin-mediated adhesion, proliferation and differentiation of cells. Regulates cell adhesion and differentiation through DSG1/desmoglein-1 and inhibition of the ERK1/ERK2 (MAPK3/MAPK1, respectively) signaling pathway. May also participate in UV radiation-induced apoptosis and have a ligand- independent stimulatory effect on chemotactic cell migration. During development, may function in distinctive aspects of pattern formation and subsequently in development of several fetal tissues. Involved for instance in angiogenesis, in early hindbrain development and epithelial proliferation and branching morphogenesis during mammary gland development. Engaged by the ligand ephrin-A5/EFNA5 may regulate lens fiber cells shape and interactions and be important for lens transparency development and maintenance. With ephrin-A2/EFNA2 may play a role in bone remodeling through regulation of osteoclastogenesis and osteoblastogenesis. . (Microbial infection) Acts as a receptor for hepatitis C virus (HCV) in hepatocytes and facilitates its cell entry. Mediates HCV entry by promoting the formation of the CD81-CLDN1 receptor complexes that are essential for HCV entry and by enhancing membrane fusion of cells expressing HCV envelope glycoproteins.
ENSG00000173599	s10090	PC	-1.824260645	pyruvate carboxylase	Pyruvate carboxylase catalyzes a 2-step reaction, involving the ATP-dependent carboxylation of the covalently attached biotin in the first step and the transfer of the carboxyl group to pyruvate in the second. Catalyzes in a tissue specific manner, the initial reactions of glucose (liver, kidney) and lipid (adipose tissue, liver, brain) synthesis from pyruvate.
ENSG00000278195	s224690	SSTR3	-1.841549228	somatostatin receptor 3	Receptor for somatostatin-14 and -28. This receptor is coupled via pertussis toxin sensitive G proteins to inhibition of adenylyl cyclase.
ENSG00000110400	s11603	PVRL1	-1.849698494	nectin cell adhesion molecule 1	Gene Ontology (GO) annotations related to this gene include DNA binding transcription factor activity. An important paralog of this gene is TSC22D1.
ENSG00000186792	s15901	HYAL3	-1.889362431	hyaluronoglucosaminidase 3	Facilitates sperm penetration into the layer of cumulus cells surrounding the egg by digesting hyaluronic acid. Involved in induction of the acrosome reaction in the sperm. Involved in follicular atresia, the breakdown of immature ovarian follicles that are not selected to ovulate. Induces ovarian granulosa cell apoptosis, possibly via apoptotic signaling pathway involving CASP8 and CASP3 activation, and poly(ADP-ribose) polymerase (PARP) cleavage. Has no hyaluronidase activity in embryonic fibroblasts in vitro. Has no hyaluronidase activity in granulosa cells in vitro.
ENSG00000155111	s23030	CDK19	-2.039747674	cyclin dependent kinase 19	Gene Ontology (GO) annotations related to this gene include DNA binding transcription factor activity. An important paralog of this gene is TSC22D1.
ENSG00000221888	s25214	OR1C1	-2.204319064	olfactory receptor family 1 subfamily C member 1	Odorant receptor.

Ensembl ID (v. 92)	siRNA IDs	Targeted gene	Average PM score	Targeted gene name	Function of targeted gene
ENSG00000169918	s46286	OTUD7A	-2.242687777	OTU deubiquitinase 7A	Has deubiquitinating activity towards 'Lys-11'-linked polyubiquitin chains.
ENSG00000137673	s8857	MMP7	-2.422883957	matrix metallopeptidase 7	Degrades casein, gelatins of types I, III, IV, and V, and fibronectin. Activates procollagenase.
ENSG00000171631	s9971	P2RY6	-2.488175018	pyrimidinergic receptor P2Y6	Receptor for extracellular UDP > UTP > ATP. The activity of this receptor is mediated by G proteins which activate a phosphatidylinositol-calcium second messenger system.
ENSG00000153201	s11774	RANBP2	-2.610786842	RAN binding protein 2	E3 SUMO-protein ligase which facilitates SUMO1 and SUMO2 conjugation by UBE2I. Involved in transport factor (Ran-GTP, karyopherin)-mediated protein import via the F-G repeat-containing domain which acts as a docking site for substrates. Binds single-stranded RNA (in vitro). May bind DNA. Component of the nuclear export pathway. Specific docking site for the nuclear export factor exportin-1. Sumoylates PML at 'Lys-490' which is essential for the proper assembly of PML-NB. Recruits BICD2 to the nuclear envelope and cytoplasmic stacks of nuclear pore complex known as annulate lamellae during G2 phase of cell cycle.
ENSG00000164128	s9699	NPY1R	-2.755775647	neuropeptide Y receptor Y1	Receptor for neuropeptide Y and peptide YY. The rank order of affinity of this receptor for pancreatic polypeptides is NPY > [Pro-34] PYY, PYY and [Leu-31, Pro-34] NPY > NPY (2-36) > [Ile-31, Gln-34] PP and PYY (3-36) > PP > NPY free acid.
ENSG00000171522	s11455	PTGER4	-3.713913924	prostaglandin E receptor 4	Receptor for prostaglandin E2 (PGE2). The activity of this receptor is mediated by G(s) proteins that stimulate adenylate cyclase. Has a relaxing effect on smooth muscle. May play an important role in regulating renal hemodynamics, intestinal epithelial transport, adrenal aldosterone secretion, and uterine function.
ENSG00000198626	s12397	RYR2	-4.068621535	ryanodine receptor 2	Calcium channel that mediates the release of Ca(2+) from the sarcoplasmic reticulum into the cytoplasm and thereby plays a key role in triggering cardiac muscle contraction. Aberrant channel activation can lead to cardiac arrhythmia. In cardiac myocytes, calcium release is triggered by increased Ca(2+) levels due to activation of the L-type calcium channel CACNA1C. The calcium channel activity is modulated by formation of heterotetramers with RYR3. Required for cellular calcium ion homeostasis. Required for embryonic heart development.
ENSG00000070831	s2766	CDC42	-4.408475244	cell division cycle 42	Plasma membrane-associated small GTPase which cycles between an active GTP-bound and an inactive GDP-bound state. In active state binds to a variety of effector proteins to regulate cellular responses. Involved in epithelial cell polarization processes. Regulates the bipolar attachment of spindle microtubules to kinetochores before chromosome congression in metaphase. Plays a role in the extension and maintenance of the formation of thin, actin-rich surface projections called filopodia. Mediates CDC42-dependent cell migration. Required for DOCK10-mediated spine formation in Purkinje cells and hippocampal neurons. Facilitates filopodia formation upon DOCK11-activation (By similarity). Also plays a role in phagocytosis through organization of the F-actin cytoskeleton associated with forming phagocytic cups.

Table S 10 – TMEM16A function activator siRNAs.

Ensembl ID (v. 92)	siRNA IDs	Targeted gene	Average score	Targeted gene name
ENSG00000184160	s194275; s194276	ADRA2C	1.8378; 1.7558	adrenoceptor alpha 2C
ENSG00000112763	s21927; s223197	BTN2A1	1.1757; 3.4355	butyrophilin subfamily 2 member A1
ENSG00000186810	s6013; s6014	CXCR3	1.1505; 1.1576	C-X-C motif chemokine receptor 3
ENSG00000184845	s4281; s4282	DRD1	1.5401; 1.8359	dopamine receptor D1
ENSG00000179163	s5395; s5397	FUCA1	1.2647; 1.8569	fucosidase, alpha-L- 1, tissue
ENSG00000185803	s35852; s35853	GPR172A	1.9885; 1.0754	solute carrier family 52 member 2
ENSG00000132518	s6381; s6383	GUCY2D	3.7422; 2.2256	guanylate cyclase 2D, retinal
ENSG00000213903	s194337; s194338	LTB4R	2.0439; 1.0705	leukotriene B4 receptor
ENSG00000167306	s9209, s9210	MYO5B	2.4812; 2.0039	myosin VB
ENSG00000255095	s15913; s15914	OR1D4	1.6555; 1.1029	olfactory receptor family 1 subfamily D member 4 (gene/pseudogene)
ENSG00000114268	s10361; s10362	PFKFB4	4.1907; 1.1829	6-phosphofructo-2-kinase/fructose-2,6-biphosphatase 4
ENSG00000159527	s41579; s41580	PGLYRP3	1.1466; 2.1222	peptidoglycan recognition protein 3
ENSG00000142875	s11068; s11070	PRKACB	1.6376; 1.4141	protein kinase cAMP-activated catalytic subunit beta
ENSG00000100902	s626; s627	PSMA6	1.5553; 1.9468	proteasome subunit alpha 6
ENSG00000135597	s39846; s39848	REPS1	1.1952; 1.2326	RALBP1 associated Eps domain containing 1
ENSG00000143252	s55037; s55038	SDHC	1.2597; 1.8679	succinate dehydrogenase complex subunit C
ENSG00000126821	s37587; s37588	SGPP1	1.9694; 4.4168	sphingosine-1-phosphate phosphatase 1
ENSG00000136560	s19453; s19454	TANK	1.0566; 1.2319	TRAF family member associated NFKB activator
ENSG00000198033	s194841; s194842	TUBA3C	1.4252; 2.6644	tubulin alpha 3c
ENSG00000100749	s14820; s14821	VRK1	1.0319; 1.3698	vaccinia related kinase 1

Table S 11 – SLC26A9 traffic enhancer siRNAs.

Ensembl ID (v. 92)	siRNA IDs	Targeted gene	Average PM score	Targeted gene name	Function of targeted gene
ENSG00000174292	TNK1	s16595	32.39	Non-receptor tyrosine-protein kinase TNK1	Involved in negative regulation of cell growth. Has tumor suppressor properties. Could specifically be involved in phospholipid signal transduction.
ENSG00000175166	PSMD2	s11389	24.58	26S proteasome non-ATPase regulatory subunit 2	Component of the 26S proteasome, a multiprotein complex involved in the ATP-dependent degradation of ubiquitinated proteins.
ENSG00000165804	ZNF219	s27704	3.21	Zinc finger protein 219	Transcriptional regulator
ENSG00000175426	PCSK1	s10149	2.73	Neuroendocrine convertase 1	Involved in the processing of hormone and other protein precursors at sites comprised of pairs of basic amino acid residues.
ENSG00000185122	HSF1	s6951	1.9	Heat shock factor protein 1	Functions as a stress-inducible and DNA-binding transcription factor that plays a central role in the transcriptional activation of the heat shock response
ENSG00000137486	ARRB1	s1623	1.81	Beta-arrestin-1	Functions in regulating agonist-mediated G-protein coupled receptor (GPCR) signaling by mediating both receptor desensitization and resensitization processes.
ENSG00000127472	PLA2G5	s10595	1.69	Phospholipase A2 group V	Secretory calcium-dependent phospholipase A2 that primarily targets extracellular phospholipids
ENSG00000108654	DDX5	s4009	1.58	Probable ATP-dependent RNA helicase DDX5	Involved in the alternative regulation of pre-mRNA splicing
ENSG00000168830	HTR1E	s7035	1.53	5-hydroxytryptamine receptor 1E	G-protein coupled receptor for 5-hydroxytryptamine (serotonin).
ENSG00000185803	GPR172A	s35851	1.52	Solute carrier family 52, riboflavin transporter, member 2	Plasma membrane transporter mediating the uptake by cells of the water soluble vitamin B2/riboflavin that plays a key role in biochemical oxidation-reduction reactions of the carbohydrate, lipid, and amino acid metabolism
ENSG00000075151	EIF4G3	s16520	1.47	Eukaryotic translation initiation factor 4 gamma 3	Probable component of the protein complex eIF4F, which is involved in the recognition of the mRNA cap, ATP-dependent unwinding of 5'-terminal secondary structure and recruitment of mRNA to the ribosome
ENSG00000151929	BAG3	s18290	1.44	BAG family molecular chaperone regulator 3	Co-chaperone for HSP70 and HSC70 chaperone proteins.
ENSG00000151067	CACNA1C	s2283	1.41	Voltage-dependent L-type calcium channel subunit alpha-1C	Pore-forming, alpha-1C subunit of the voltage-gated calcium channel that gives rise to L-type calcium currents
ENSG00000140992	PDPK1	s10274	1.39	3-phosphoinositide-dependent protein kinase 1	Serine/threonine kinase which acts as a master kinase, phosphorylating and activating a subgroup of the AGC family of protein kinases.
ENSG00000152207	CYSLTR2	s32685	1.39	Cysteinyl leukotriene receptor 2	Receptor for cysteinyl leukotrienes. The response is mediated via a G-protein that activates a phosphatidylinositol-calcium second messenger system.
ENSG00000110011	DNAJC4	s7011	1.39	DnaJ homolog subfamily C member 4	Not known

Ensembl ID (v. 92)	siRNA IDs	Targeted gene	Average PM score	Targeted gene name	Function of targeted gene
ENSG00000112333	NR2E1	s14201	1.38	Nuclear receptor subfamily 2 group E member 1	Orphan receptor that binds DNA as a monomer to hormone response elements (HRE)
ENSG00000180251	SLC9A4	s52339	1.35	Sodium/hydrogen exchanger 4	Involved in pH regulation to eliminate acids generated by active metabolism or to counter adverse environmental conditions. In apical cell membrane may be involved in mediating sodium absorption.
ENSG00000078618	NRDC	s9719	1.33	Nardilysin	Cleaves peptide substrates on the N-terminus of arginine residues in dibasic pairs.
ENSG00000180530	NRIP1	s15703	1.32	Nuclear receptor-interacting protein 1	Modulates transcriptional activation by steroid receptors such as NR3C1, NR3C2 and ESR1.
ENSG00000132518	GUCY2D	s6381	1.29	Retinal guanylyl cyclase 1	Catalyzes the synthesis of cyclic GMP (cGMP) in rods and cones of photoreceptors. Plays an essential role in phototransduction, by mediating cGMP replenishment. May also participate in the trafficking of membrane-asociated proteins to the photoreceptor outer segment membrane
ENSG00000131771	PPP1R1B	s38573	1.26	Protein phosphatase 1 regulatory subunit 1B	Inhibitor of protein-phosphatase 1.
ENSG00000175832	ETV4	s4861	1.24	ETS translocation variant 4	Transcriptional activator
ENSG00000198160	MIER1	s33645	1.16	Mesoderm induction early response protein 1	Transcriptional repressor regulating the expression of a number of genes including SP1 target genes. Probably functions through recruitment of HDAC1 a histone deacetylase involved in chromatin silencing.
ENSG00000110243	APOA5	s42040	1.14	Apolipoprotein A-V	Minor apolipoprotein mainly associated with HDL and to a lesser extent with VLDL.
ENSG00000130348	QRSL1	s30620	1.13	Glutamyl-tRNA(Gln) amidotransferase subunit A, mitochondrial	Allows the formation of correctly charged Gln-tRNA(Gln) through the transamidation of misacylated Glu-tRNA(Gln) in the mitochondria.
ENSG00000175906	ARL4D	s1559	1.13	ADP-ribosylation factor-like protein 4D	Small GTP-binding protein which cycles between an inactive GDP-bound and an active GTP-bound form
ENSG00000090266	NDUFB2	s532	1.11	NADH dehydrogenase [ubiquinone] 1 beta subcomplex subunit 2, mitochondrial	Accessory subunit of the mitochondrial membrane respiratory chain NADH dehydrogenase
ENSG00000104419	NDRG1	s20335	1.07	Protein NDRG1	Stress-responsive protein involved in hormone responses, cell growth, and differentiation. Acts as a tumor suppressor in many cell types.
ENSG00000171570	RAB4B	s28802	1.07	Ras-related protein Rab-4B	Protein transport. Probably involved in vesicular traffic
ENSG00000109062	SLC9A3R1	s17920	1.06	Na(+)/H(+) exchange regulatory cofactor NHE-RF1	Scaffold protein that connects plasma membrane proteins with members of the ezrin/moesin/radixin family and thereby helps to link them to the actin cytoskeleton and to regulate their surface expression. May enhance Wnt signaling.

Ensembl ID (v. 92)	siRNA IDs	Targeted gene	Average PM score	Targeted gene name	Function of targeted gene
ENSG00000172939	OXSR1	s19304	1.06	Serine/threonine-protein kinase OSR1	Phosphorylates RELL1, RELL2 and RELT
ENSG00000033011	ALG1	s31867	1.05	Chitobiosyldiphosphodolichol beta-mannosyltransferase	Participates in the formation of the lipid-linked precursor oligosaccharide for N-glycosylation.
ENSG00000154237	LRRK1	s36138	1.03	Leucine-rich repeat serine/threonine-protein kinase 1	LRRK1 regulates EGFR transport from early to late endosomes and regulates the motility of EGF-containing early endosomes in a manner dependent on its kinase activity. It is thought to play a role in the regulation of bone mass.
ENSG00000084674	APOB	s1477	1.01	Apolipoprotein B receptor	Macrophage receptor that binds to the apolipoprotein B48 (APOB) of dietary triglyceride (TG)-rich lipoproteins (TRL) or to a like domain of APOB in hypertriglyceridemic very low density lipoprotein (HTG-VLDL).
ENSG00000138741	TRPC3	s14412	1.01	Short transient receptor potential channel 3	Thought to form a receptor-activated non-selective calcium permeant cation channel. Probably is operated by a phosphatidylinositol second messenger system activated by receptor tyrosine kinases or G-protein coupled receptors.